Enclosure 5

Response to NRC Supplemental Information Items

Enclosure 5

Response to NRC Supplemental Information Items

References:

1. Letter, John W. Crenshaw to NRC Document Control Desk, "STP Pilot Submittal and Request for Exemption for a Risk-Informed Approach to Resolve Generic Safety Issue (GSI)-191," January 31, 2013, NOC-AE-13002954 (ML13043A013)
2. Letter, Balwant K. Singal, NRC, Dennis L. Koehl, STPNOC, "South Texas Project, Units 1 and 2 – Supplemental Information Needed for Acceptance of Requested Licensing Action Re: Request for Exemption for a Risk-Informed Approach to Resolve Generic Safety Issue 191 (TAC Nos. MF0613 and MF0614)," April 1, 2013, AE-NOC-13002417 (ML13066A519)

In Reference 1, STP Nuclear Operating Company (STPNOC) requested an exemption from certain regulations affected by the risk-informed approach to resolution of GSI-191. In Reference 2, the NRC staff identified supplemental information needed for completion of the acceptance review. Reference 1 is superseded in its entirety by Reference 3 to the cover letter and this supplement.

In order to facilitate the staff completing its acceptance review of this submittal, responses to each of the supplemental information items identified in Reference 2 are provided. These responses also describe where and how supplemental information requested by the staff is addressed elsewhere in this submittal. Italicized text is as shown in Reference 2.

Changes to Enclosure 5:

1. Format change: Enclosure 5 was previously identified as Attachment in Reference 3 to the cover letter.
2. Format change: Responses are provided in document titled "Volume 6.2 - Responses to NRC Request for Supplemental Information on the 2013 Submittal"
3. Questions 2.1, 2.2, 2.3 and 2.4 responses have minor editorial differences from responses in Reference 3 of the cover letter.
4. Other changes are described in the change summary for Volume 6.2

South Texas Project Risk-Informed GSI-191 Evaluation

Volume 6.2

Responses to NRC Request for Supplemental Information on the 2013 Submittal

Document: STP-RIGSI191-V06.2
Revision: 1
Date: November 6, 2013

Prepared by:
Timothy D. Sande, Enercon Services, Inc.

Reviewed by:
Zahra Mohaghegh, University of Illinois at Urbana-Champaign
Seyed Reihani, University of Illinois at Urbana-Champaign

Approved by:
Ernie Kee, South Texas Project

REVISION HISTORY LOG

Revision	Date	Description
0	6/6/2013	Original document
1	See Cover Page	Several changes were made in this revision for consistency with the changes to Volume 3. The specific edits include the following: • Item 5: Updated table with references to Volume 3. • Item 5.a.1: Updated results. • Item 5.a.2: Updated results. • Item 5.a.3: Updated results. • Item 5.a.5: Updated assumptions and results. • Item 5.a.10: Updated assumptions. • Item 5.a.11: Updated results. • Item 5.a.12: Updated assumptions. • Item 5.a.13: Updated assumptions and results. • Item 5.a.15: Updated assumptions and results. • Item 5.a.16: Updated descriptions of LOCA frequency and fiberglass debris penetration. • Item 5.d: Updated input parameter summary table, added description for hot leg switchover time distribution, deleted pool erosion fraction distribution description, and replaced missing water mass probability curve. • Revised NRC Question and Response 2.1 and 2.4 for consistency with revised licensing application dated June 19, 2013, NO-AC-13002986. (Reference 3 of cover letter NOC-AE-13003043).

TABLE OF CONTENTS

1 INTRODUCTION

The purpose of this report is to provide supplemental information to the exemption request submittal transmitted to the NRC on January 31, 2013 (1). The NRC requested supplemental information as described in a letter to Mr. Dennis L. Koehl, President and CEO/CNO, STP Nuclear Operating Company, on April 1, 2013 (2).

This report contains the supplemental information in response to the specific issues identified by the NRC staff. The questions contained in the letter from the NRC (2) are written out and responses provided. Although much of the information is included directly in the engineering analysis, some is not. However, all of the information is used to form the basis for the methodology.

Also note that some of the information in Volumes 1 and 3 (Enclosures 4-1 and 4-3) is repeated in this supplementary document. The documentation set of Volumes 1, 2, and 3 (Enclosures 4-1,4-2, and 4-3) is intended to provide a comprehensive summary of the risk-informed GSI-191 analysis.

2 STP RESPONSES

2.1 NRC Staff Comment/Question 2.1

The NRC staff also concludes that the application does not provide adequate discussion of or justification for the requested exemptions. The licensee submittal requests exemption from Title 10 of the Code of Federal Regulations (10 CFR), Sections 50.46 and 50.67 and General Design Criterion 35, 38, 41 and 19. Each of these regulations require a justification for exemption. Please provide the following information in support of the exemption request for the NRC staff to start its review.

For each exemption request submitted under 10 CFR 50.12, the application should include a narrative as to why the licensee believes that the special circumstances provided in 10 CFR 50.12(a)(2) is present. The licensee in its application has stated that 10 CFR 50.10(a) (2) (ii) and (iii) apply. There appears to be a typographical error and the NRC staff believes licensee meant to invoke 10 CFR 50.12(a) (2) (ii) and (iii). Please confirm this and provide adequate technical basis in support of applicability of 10 CFR 50.12(a) (2) (ii) and (iii). Also, please describe in detail how the special circumstances address 10 CFR 50.12(a) (1).

Response

Separate requests for exemption are provided to address the following regulatory requirements:

Enclosure 2-1, 10 CFR 50.46(b)(5), *Long-term cooling*
Enclosure 2-2, General Design Criterion 35 – *Emergency core cooling*
Enclosure 2-3, General Design Criterion 38 – *Containment heat removal*
Enclosure 2-4, General Design Criterion 41 – *Containment atmosphere cleanup*

Each exemption request includes a discussion as to why special circumstances provided in 10 CFR 50.12(a)(2) apply, and specifically for 10 CFR 50.12(a)(2)(ii). Enclosure 2 provides a background and overview for the four exemption requests. STPNOC has determined that exemptions to 10 CFR 50.67 and General Design Criterion 19 are not required and that basis is discussed in the Enclosures identified above.

2.2 NRC Staff Comment/Question 2.2

The application describes a departure from the method of evaluation described in the Updated Final Safety Analysis Report (UFSAR) used in establishing the design bases in the plant's safety analysis, as defined in 10 CFR 50.59(a)(2) and proposes several draft modifications to the UFSAR. In accordance with 10 CFR 50.59(c)(2)(viii), these modifications would appear to be changes in the design and licensing basis and would require a license amendment in accordance 10 CFR 50.90. Please explain why an amendment is not proposed to accompany this exemption, with the associated draft no significant hazards consideration. The licensee should clearly state the scope and nature of the change to the design and licensing basis.

Response

In accordance with 10 CFR 50.59(c)(2)(viii), the proposed changes to the UFSAR constitute a departure from a method of evaluation described in the UFSAR used in establishing the design bases or in the plant's safety analyses, and has been evaluated to be a change to another method that has not been approved by the NRC for the intended application. On this basis, a license amendment request (LAR) is required pursuant to 10 CFR 50.90 and is included in Enclosure 3 with the proposed changes to the licensing basis for NRC review and approval. As required for the LAR submitted under 10 CFR 50.90, a no significant hazards consideration determination pursuant to 10 CFR 50.92(c) is also included.

The proposed risk-informed method of evaluation described in the LAR has been determined to require exemptions from certain regulatory requirements identified in Enclosure 2. Therefore, requests for specific exemptions pursuant to 10 CFR 50.12 are provided in Enclosures 2-1 through 2-4 to support the LAR and RG 1.174 submittal.

As a risk-informed approach to resolving GSI-191 with exemption requests in support of a RG 1.174 application, the STP method is intended to be consistent with previous NRC staff comments in the NRC staff safety evaluation on NEI-04-07 regarding Section 6, Alternate Evaluation, dated December 6, 2004 (ML043280007), and Enclosure 3, "Risk-Informed Approach to Address Generic Safety Issue-191, South Texas Project," to SECY-12-0093, "Closure Options for Generic Safety Issue – 191, Assessment of Debris Accumulation on Pressurized-Water Reactor Sump Performance," dated July 9, 2012 (ML121310659).

2.3 NRC Staff Comment/Question 2.3

To process the proposed exemption, the NRC staff will need to conduct an environmental review. Please provide the description that will address the special circumstances supporting this review in accordance with 10 CFR 51.41 and 10 CFR 51.45.

Response

In accordance with 10 CFR 51.41 and 10 CFR 51.21, for each exemption request provided in Enclosures 2-1 through 2-4, environmental considerations have been included to support the NRC staff's environmental review. Based on the guidance in RG 1.174 being met, justification is also provided for the actions to qualify for 10 CFR 51.22(c)(9) categorical exclusion. Therefore, an environmental report pursuant to 10 CFR 51.45 is not required.

2.4 NRC Staff Comment/Question 2.4

Please describe how the proposed change will affect the Technical Specifications (TSs). Please indicate whether changes are needed to the operability requirements for the affected systems and any changes to the existing TS Action Statements that may be needed.

Response

A description of how the proposed change will affect the technical specifications is provided in Regulatory Evaluation Section 4.1.3 in the LAR provided in Enclosure 3. As discussed in more detail in Enclosure 3, no changes to operability requirements for affected systems and no changes to the existing technical specification Action Statements are proposed. Proposed changes to the technical specification bases that conform to the changes in the licensing and design bases are included in Attachment 3 to Enclosure 3 for staff information.

2.5 NRC Staff Comment/Question 2.5

The basis for the proposed change is that the residual risk from the remaining GSI-191 issues (e.g., those not already addressed in a deterministic manner) satisfies the criteria in Regulatory Guide (RG) 1.174, Revision 2, "An Approach For Using Probabilistic Risk Assessment In Risk-Informed Decisions on Plant-Specific Changes to the Licensing Basis," May 2011 (ADAMS Accession No. ML100910006). However, the application does not appear to provide sufficient detail for the NRC staff to determine whether the criteria in RG 1.174 have been met. Please describe in detail how the principles of RG 1.174 criteria regarding safety margin, defense-in-depth (DID), and change in risk are met. In particular, please include the following:

a. *Regarding the technical evaluation that supports the risk metrics, the Project Summary (Enclosure 4 to the application) describes numerous areas where the technical evaluation deviates from the approved guidance for addressing GSI 191. However, the application provides little or no information on how the issues were addressed. Please provide a discussion in sufficient detail to permit NRC staff review of the methods, bases, assumptions, acceptance criteria, and results. If test results are used to develop probability distributions, please describe how these distributions were determined and used in the overall risk evaluation. Please also provide the basis for the acceptance criteria chosen. The NRC staff requires additional information in the following areas:*

    1) *Failure timing, failure amounts, and debris characteristics of unqualified coatings*
    2) *Capture of small and large pieces of debris on gratings and obstructions*
    3) *Washdown transport holdups*
    4) *Non-uniform debris distribution at the onset of recirculation*
    5) *Time dependent transport*
    6) *Chemical effects corrosion and dissolution models*
    7) *Basis for excluding any plant materials from chemical testing*
    8) *Chemical precipitation models – amount, type, head loss effect*
    9) *Disposition of chemical effects Phenomena Identification and Ranking Table open items*
    10) *Head loss model*
    11) *Chemical effects on head loss (bump-up factor) model*
    12) *Fiber bypass amounts and amounts reaching the core for various scenarios*
    13) *Fiber limits for in-vessel evaluations*
    14) *Thermal-hydraulic analysis for in-vessel evaluations*
    15) *Boric acid precipitation evaluations*
    16) *Methodology for determination and implementation of physical effects probability distributions*

b. *Regarding DID, please address how DID is maintained to account for scenarios that are predicted to lead to failure. One method of maintaining DID is to demonstrate that the operators can detect and mitigate inadequate flow through the recirculation strainer and inadequate core cooling. Please describe the supporting evaluations that demonstrate DID actions will be effective.*

c. *Please provide supporting evaluations that demonstrate that the barriers for the release of radioactivity will be maintained with sufficient safety margin.*

d. *Please provide sufficient detail necessary to assess the treatment of uncertainty. While several known categories of uncertainty are identified (zone of influence, chemical effects, debris transport, etc), the mechanistic models and associated parametric factors used in the analysis are not identified, nor are probability density functions for the parameters provided (Enclosure 4, Section 2.5). Please provide this information.*

Response

The table below lists sources of information for the responses to Items 5.a through 5.d provided in this Attachment. Volume 3 is included in the submittal as Enclosure 4-3, and the other specific calculations and reports are available for audit.

Table 2.5.1 – References for Responses to Items 5.a through 5.d

5.a Information Item	Reference Sources of Information
1) Failure timing, failure amounts, and debris characteristics of unqualified coatings	• Volume 3 Section 2.2.10 (Enclosure 4-3) • ALION-CAL-STP-8511-06 "STP Unqualified Coatings Debris Generation", Revision 2, November 26, 2012
2) Capture of small and large pieces of debris on gratings and obstructions	• Volume 3 Section 2.2.17 (Enclosure 4-3) • ALION-CAL-STP-8511-08, "Risk-Informed GSI-191 Debris Transport Calculation", Revision 2, January 21, 2013
3) Washdown transport holdups	• Volume 3 Section 2.2.18 (Enclosure 4-3) • ALION-CAL-STP-8511-08, "Risk-Informed GSI-191 Debris Transport Calculation", Revision 2, January 21, 2013
4) Non-uniform debris distribution at the onset of recirculation	• ALION-CAL-STP-8511-08, "Risk-Informed GSI-191 Debris Transport Calculation", Revision 2, January 21, 2013
5) Time dependent transport	• Volume 3 Section 5.5.8 (Enclosure 4-3) • ALION-CAL-STP-8511-08, "Risk-Informed GSI-191 Debris Transport Calculation", Revision 2, January 21, 2013

5.a Information Item	Reference Sources of Information
6) Chemical effects corrosion and dissolution models	• CHLE-016, "Calculated Material Release", Revision 1, January 10, 2013 • Texas A&M University Department of Nuclear Engineering, "Sump Temperature Sensitivity Analysis", Revision 2.0, January 2013 • CHLE-014, "T2 LBLOCA Test Report", Revision 1, January 12, 2013 • CHLE-019, "Test results for chemical effect tests stimulating corrosion and precipitation (T3 & T4)", Revision 1, August 27, 2013 • CHLE-020, "Test results for 10-day chemical effect test simulating LBLOCA condition (T5)" Revision 1, September 29, 2013
7) Basis for excluding any plant materials from chemical testing	• CHLE-006, "STP Materials Calculation", Revision 1, August 15, 2012. • ALION-CAL-STPEGS-2916-002, "GSI 191 Containment Recirculation Sump Evaluation: Debris Generation", Revision 3, October 20, 2008
8) Chemical precipitation models – amount, type, head loss effect	• Volume 3 Section 5.6.3 (Enclosure 4-3) • CHLE-016, "Calculated Material Release", Revision 1, January 10, 2013
9) Disposition of chemical effects Phenomena Identification and Ranking Table (PIRT) open items	• Volume 3 Section 5.6.3 (Enclosure 4-3) • CHLE-014, "T2 LBLOCA Test Report", Revision 1, January 12, 2013 • CHLE-012, "T1 MBLOCA Test Report", Revision 3, January 9, 2013 • CHLE-005, "Determination of the Initial Pool Chemistry for the CHLE Test", Revision 1, August 13, 2012 • CHLE-018, "Bench-Scale Test Results of Effect of pH and Temperature on Aluminum Corrosion and Silicon Dissolution", Revision 0, Draft • CHLE-011, "Test 2, Medium Break LOCA Tank Test Parameter Summary", Revision 1, October 30, 2012 • CHLE-013: "T2: Large Break LOCA Tank Test Parameter Summary", Revision 2, January 23, 2013 • ALION-CAL-STP-8511-07, "STP Crud Debris Generation", Revision 0, November 12, 2012 • ALION-SUM-WEST-2916-01, "CAD Model Summary: South Texas Reactor Building CAD Model for Use in GSI-191 Analyses", Revision 3, November 27, 2012 • ALION-CAL-STP-008511-02, "STP Cold Volume Analysis", Revision 0, May 17, 2012 • CHLE-015, "Summary of Chemical Effects Testing in 2012 for STP GSI-191 License Submittal", Revision 3, January 21, 2013

5.a Information Item	Reference Sources of Information
10) Head loss model	• Volume 3 Section 5.6.2 (Enclosure 4-3) • ALION-REP-STP-8511-02, "South Texas Vertical Loop Head Loss Testing Report", Revision 1, January 24, 2013
11) Chemical effects on head loss (bump-up factor) model	• Volume 3 Section 5.6.3 (Enclosure 4-3) • CHLE-012, "T1 MBLOCA Test Report", Revision 3, January 9, 2013 • CHLE-014, "T2 LBLOCA Test Report", Revision 1, January 12, 2013
12) Fiber bypass amounts and amounts reaching the core for various scenarios	• Volume 3 Sections 5.8 and 5.10 (Enclosure 4-3) • University of Texas at Austin, "Filtration as a Function of Debris Mass on the Strainer: Fitting a Parametric Physics Based Model", January 24, 2013 • ALION-REP-STP-8511-03, "South Texas Penetration Test Report", Revision 1, January 24, 2013
13) Fiber limits for in-vessel evaluations	• Volume 3 Sections 5.10 and 5.11 (Enclosure 4-3) • Texas A&M University, Department of Nuclear Engineering, "Core Blockage Thermal-Hydraulic Analysis", Revision 2.1, January 2013
14) Thermal-hydraulic analysis for in-vessel evaluations	• Volume 3 Section 5.10.2 (Enclosure 4-3) • Texas A&M University, Department of Nuclear Engineering, "Core Blockage Thermal-Hydraulic Analysis", Revision 2.1, January 2013 • Texas A&M University, Department of Nuclear Engineering, "RELAP5 Model Input Deck Certification", Revision 3.0, August 1, 2011
15) Boric acid precipitation evaluations	• Volume 3 Section 5.11 (Enclosure 4-3)
16) Methodology for determination and implementation of physical effects probability distributions	• Implementation is described in Volume 3 (Enclosure 4-3) Section 4 generically, and more specifically in Section 2 and other areas of the report. • UT Austin report, "A Framework for Uncertainty Quantification: Methods, Strategies, and an Illustrative Example", January 21, 2013.
5.b Defense-in-depth	• Volume 1 Section 2.1 and Appendix C (Enclosure 4-1)
5.c Barriers for release of reactivity safety margin	• Volume 1 Section 2.2 and Appendix C (Enclosure 4-1)
5.d Treatment of uncertainty	• Volume 1 Sections 5.2 through 5.5 (Enclosure 4-1) • UT Austin report, "A Framework for Uncertainty Quantification: Methods, Strategies, and an Illustrative Example", January 21, 2013.

Item 5.a: Technical Evaluation

The responses to the request for supplemental information on the 16 specific technical areas are provided below.

Item 5.a.1: Unqualified Coatings

Method: The basic methodology used for the STP unqualified coatings debris generation calculation is shown below:

1. Each component substrate with an unqualified coating was investigated for the coating type, substrate location, and total mass of the coating.
2. The failure fraction of each coating type was analyzed through a survey of applicable literature and test data. The probability of failure fraction was determined for each of the following coatings: IOZ, epoxy, alkyd, and baked enamel. The test data that was used includes testing performed by EPRI (3), GE (4), Comanche Peak (5), and Alion (6).
3. The failure timing of coatings was evaluated and the probability of the coating failing prior to containment spray termination was estimated based on test data. The test data that was used includes testing performed by EPRI (3), GE (4), Comanche Peak (5), and Alion (6).
4. The debris characteristics for each of the unqualified coatings were analyzed through a survey of previous literature. The type and size of debris was determined for IOZ, epoxy, alkyd, baked enamel, and intumescent coatings.

Basis: The following discussion provides a detailed description of how the methodology referred to above was used to develop the unqualified coatings input parameters (7).

Failure Fraction Analysis

Probability distributions were developed for the failure fractions of unqualified epoxy, IOZ, and alkyd coatings. The failure timing analysis was extrapolated from the 7 days of data to accurately represent the full 30-day mission time. As a consequence of this extrapolation, a 152.5% increase of probability statistics was introduced to the failure timing relative frequency analysis (See Failure Timing Analysis). This increase in the failure timing analysis will affect the failure fraction probability. To account for this, the probability of 100% failure for each of the coating types is increased by 152.5%, and the rest of the distribution is fit to this correction with an attempt to keep prior inflection points. This is a significant conservatism because this skews the distribution towards 100% failure, despite the fact that the data shows this is unlikely. For each of the unqualified coatings, the probability distribution based on the data from the Carboline and EPRI testing is provided in contrast to the corrected probability distribution that will be used in the risk-informed analysis.

The statistics for the failure fraction of unqualified epoxy coatings, based on the EPRI and Carboline analysis, is summarized in the following table:

Table 2.5.2 – Epoxy Failure Fraction Probability Statistics

% Failure	Probability
0	0.0088
1	0.0088
5	0.0352
10	0.0088
20	0.0088
100	0.0088

The following figure illustrates the probability distribution of the failure fraction for the epoxy coatings based on the available data:

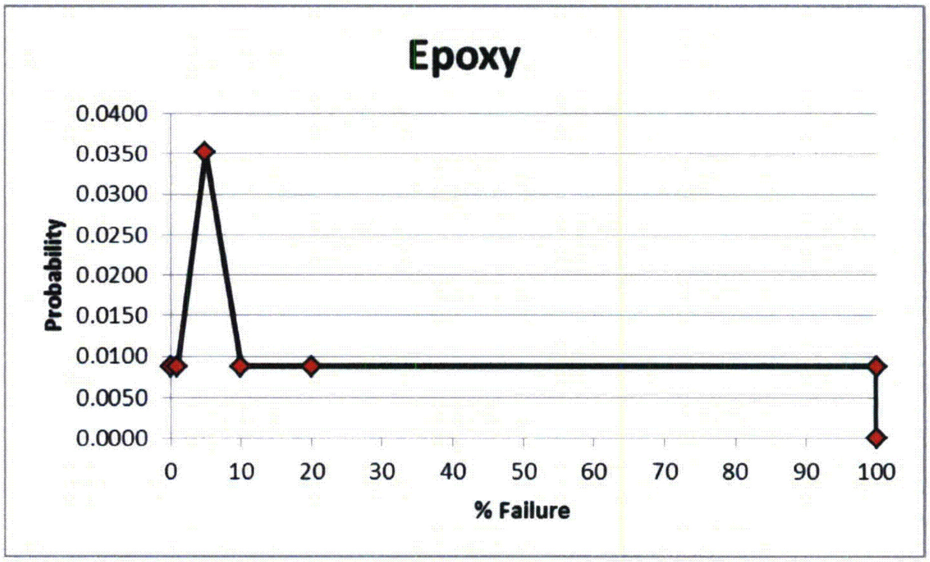

Figure 2.5.1 – Raw Epoxy Failure Fraction Probability Distribution

The data supports the probability of 100% failure as 0.0088. Applying the 152.5% increase to correct for the failure timing extrapolation yields the probability of 100% failure as 0.0222. The rest of the probability distribution is fit to the 100% failure probability. The area under the probability distribution must be equal to 100%: this yields 0% probability of any failure fraction below 10.1%. The following table illustrates the corrected probability statistics that accounts for the failure timing extrapolation:

Table 2.5.3 – Corrected Epoxy Failure Fraction Probability Statistics

% Failure	Probability
0.0	0.0000
10.1	0.0000
100.0	0.0222

These statistics yield the following corrected probability distribution for the failure fraction of unqualified epoxy coatings:

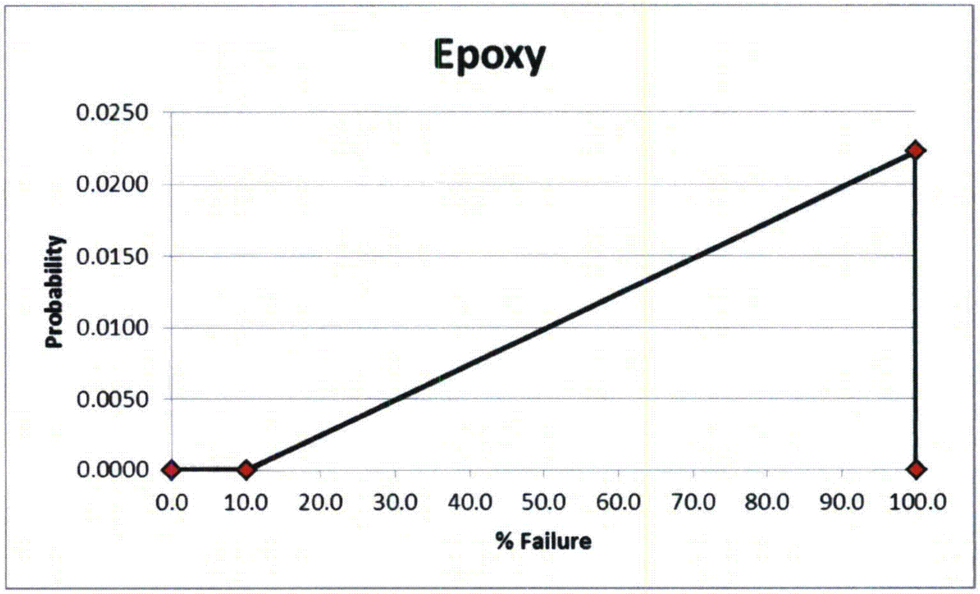

Figure 2.5.2 – Epoxy failure fraction probability distribution

The probability statistics for the failure fraction of unqualified alkyd coatings based on the test data supplied by EPRI and Carboline is summarized in the following table:

Table 2.5.4 – Alkyd Failure Fraction Probability Statistics

% Failure	Probability
0	0.0000
1	0.0127
5	0.0317
20	0.0063
50	0.0127
55	0.0063
80	0.0063
95	0.0063
100	0.0063

The following figure illustrates the probability distribution of the failure fraction for the alkyd coatings based on the available data:

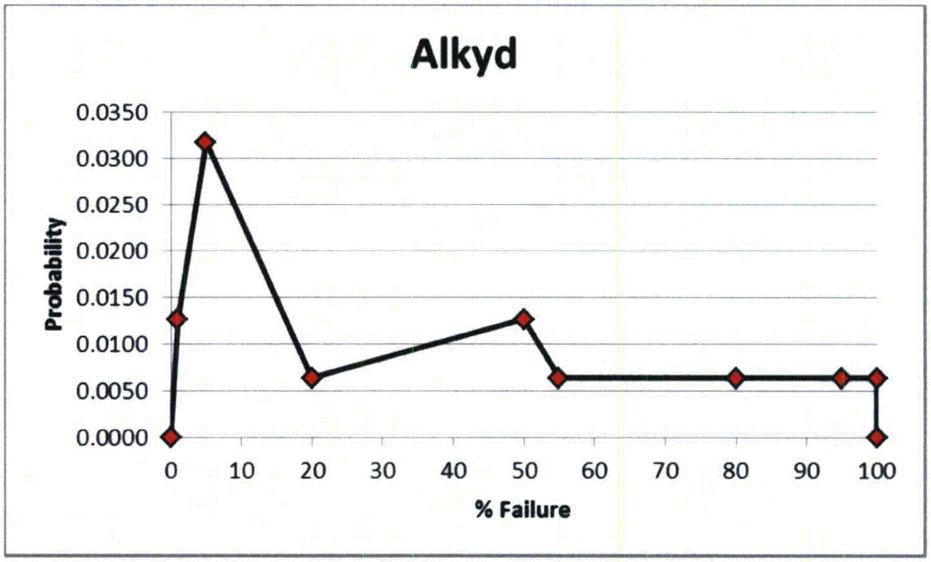

Figure 2.5.3 – Raw Alkyd Failure Probability Distribution

This probability distribution was formulated with the current data available for the failure fraction of unqualified alkyd coatings. However, the two peaks in the distribution are not likely to occur in the natural failure of alkyd coatings. Therefore, the probability distribution was altered to provide a more reasonable distribution (without the two peaks). This was done by keeping the proportional probability between the 5%, 50%, and 100% failure data points, yielding the following probability statistics:

Table 2.5.5 – Altered Alkyd Probability Statistics

% Failure	Probability
0	0
5	0.02054
50	0.008229
100	0.004082

This yields the following probability distribution for the unqualified Alkyd coatings:

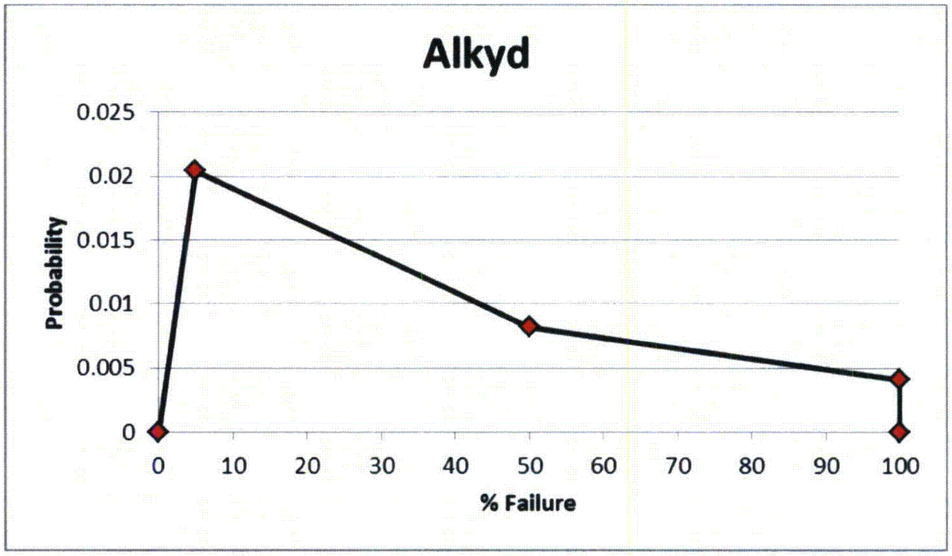

Figure 2.5.4 – Altered Alkyd Failure Fraction Probability Distribution

The following table illustrates the corrected probability statistics that accounts for the failure timing extrapolation:

Table 2.5.6 – Corrected Alkyd Failure Fraction Probability Statistics

% Failure	Probability
0	0.0000
5	0.0102
100	0.0103

These statistics yield the following corrected probability distribution for the failure fraction of unqualified alkyd coatings:

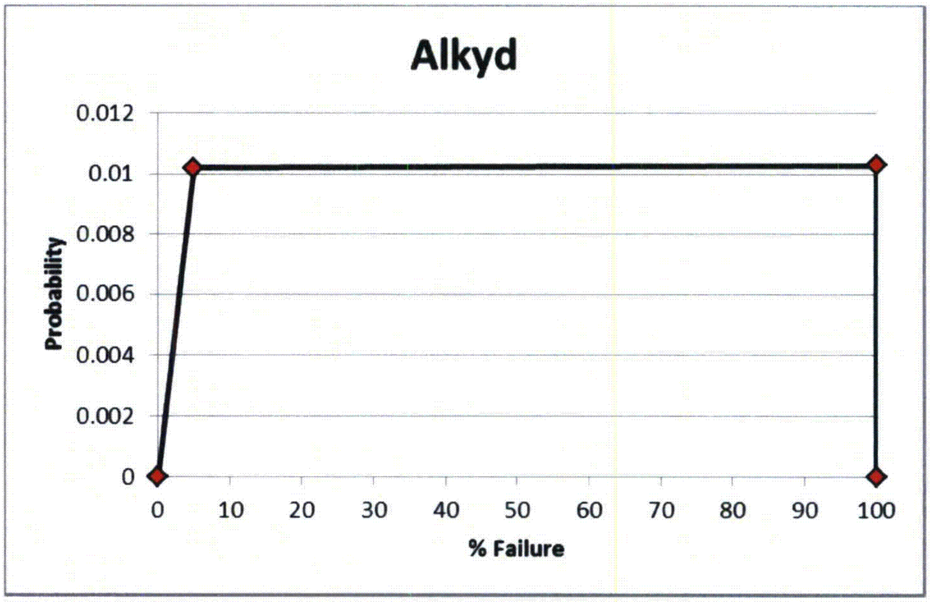

Figure 2.5.5 – Alkyd and baked enamel failure fraction probability distribution

There is not sufficient data for the IOZ failure fracture to perform the same statistical analysis as for alkyds and epoxy. The EPRI sponsored testing shows that the IOZ failure fraction ranges from 1 to 95%. The Carboline testing also supports a similar range of failure: from 0 to 100%. Therefore, the data supports the assertion that the failure fraction probability will be the same over the complete range from 0 to 100%. This yields the following probability distribution for the IOZ failure fraction:

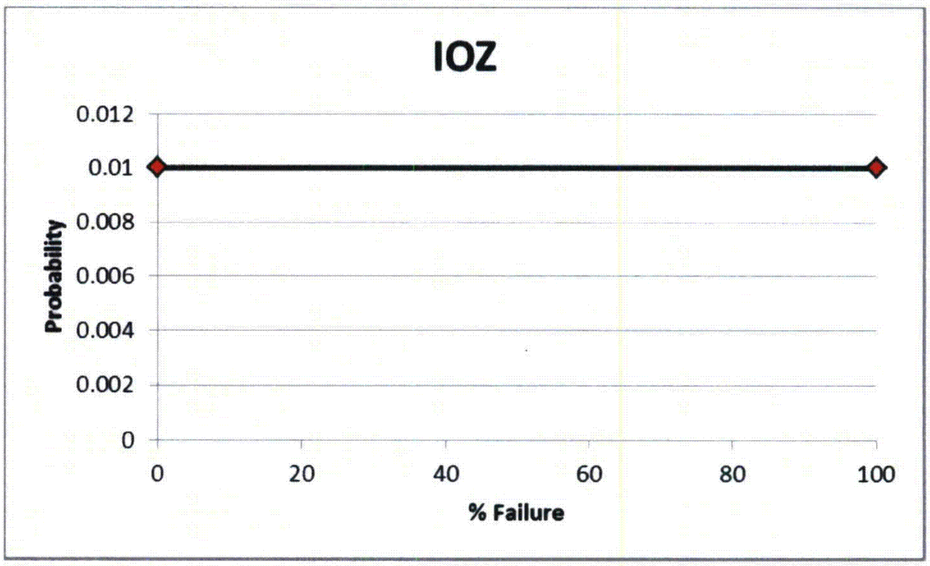

Figure 2.5.6 – Raw IOZ Failure Fraction Probability Distribution

The following table illustrates the corrected probability statistics that accounts for the failure timing extrapolation:

Table 2.5.7 – Corrected IOZ Failure Fraction Probability Statistics

% Failure	Probability
0	0.0000
21	0.0000
100	0.0253

Applying the correction to the 100% failure statistic yields the following corrected probability distribution for the failure fraction of unqualified IOZ coatings:

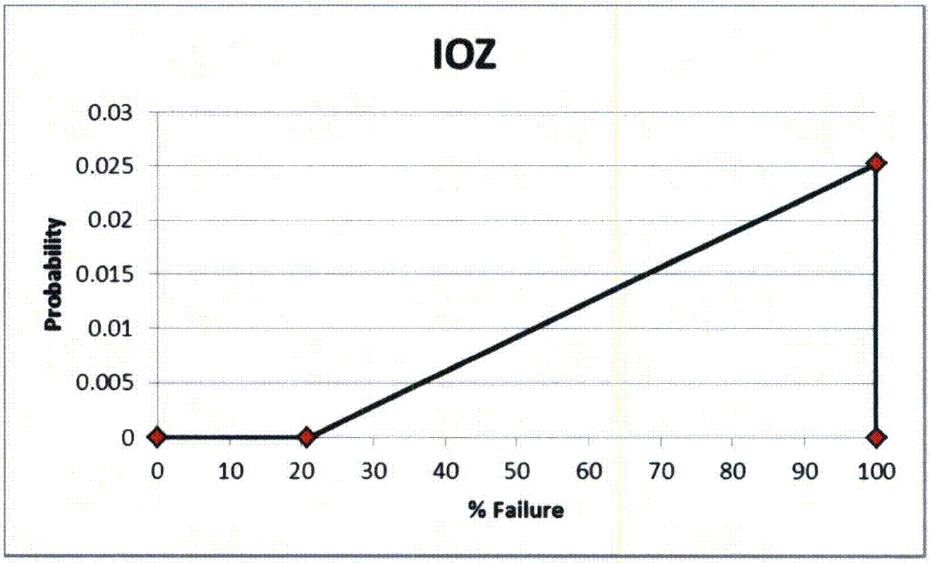

Figure 2.5.7 – IOZ failure fraction probability distribution

Failure Timing Analysis

The other item in the evaluation of unqualified coatings that required probability statistics was the failure timing analysis. In the EPRI sponsored design basis accident (DBA) testing of OEM unqualified coatings (including a combination of epoxy, IOZ, and alkyds), a means of determining the timing of failure was present. The filters used in the autoclave to capture the failed debris were replaced over fifteen times in uneven time increments over the 172 hour test. The time at which these filters were replaced were at 3 hours, 4 hours, 5 hours, 6 hours, 24 hours, 48 hours, 72 hours, 96 hours, 97 hours, 98 hours, 99 hours, 100 hours, 124 hours, 148 hours, and 172 hours. These discarded filters provide a visual timetable of coatings failure. The following figure illustrates the filters that were removed from the autoclave: the filter removal time increases from left to right:

Figure 2.5.8 – EPRI Testing Removed Filters

Test 1 from the previous figure illustrates the filters that captured unqualified coatings debris from the panels that were subjected to irradiation. This test is more prototypical of containment conditions, as the coated surfaces in containment have been subjected to radiation for tens of years. Therefore, the filters from Test 1 will be used to qualitatively determine the timing of failure.

As can be seen from the figure, significant failure of the unqualified OEM coatings starts with the sixth filter from the left: time between 24 and 48 hours. The qualitative estimate of the failure frequency based on visual examination is illustrated in the following figure:

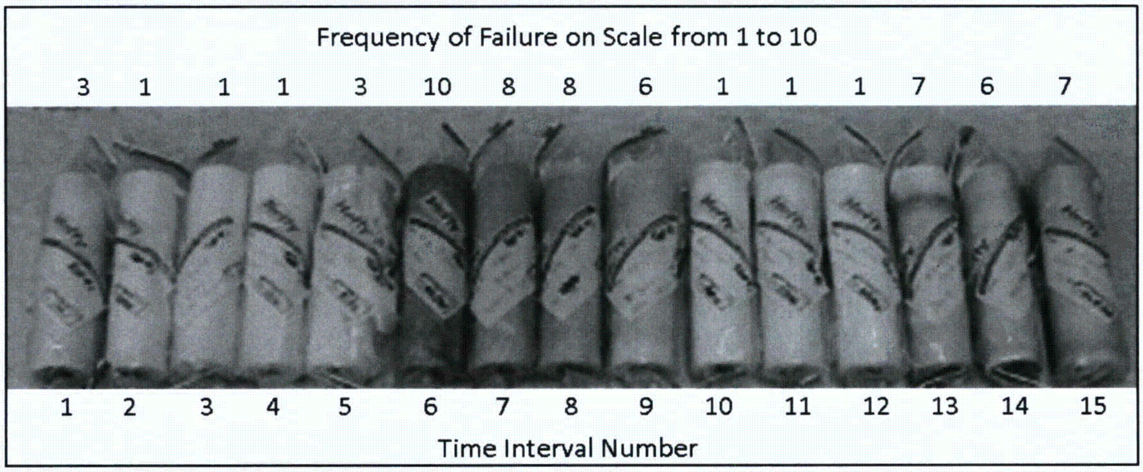

Figure 2.5.9 – Qualitative Frequency of Failure

The most significant failure happens after the 5th time interval (after 24 hours). The following table contains the time interval and its relative frequency of failure:

Table 2.5.8 – Relative Frequency of Failure

Time Interval (#)	**Time Interval (hours)**	**Relative Frequency of Failure**
1	0-3	0.047
2	3-4	0.016
3	4-5	0.016
4	5-6	0.016
5	6-24	0.047
6	24-48	0.156
7	48-72	0.125
8	72-96	0.125
9	96-97	0.094
10	97-98	0.016
11	98-99	0.016
12	99-100	0.016
13	100-124	0.109
14	124-148	0.094
15	148-172	0.109

The following histogram shows the coatings failure per time interval as determined by visual inspection:

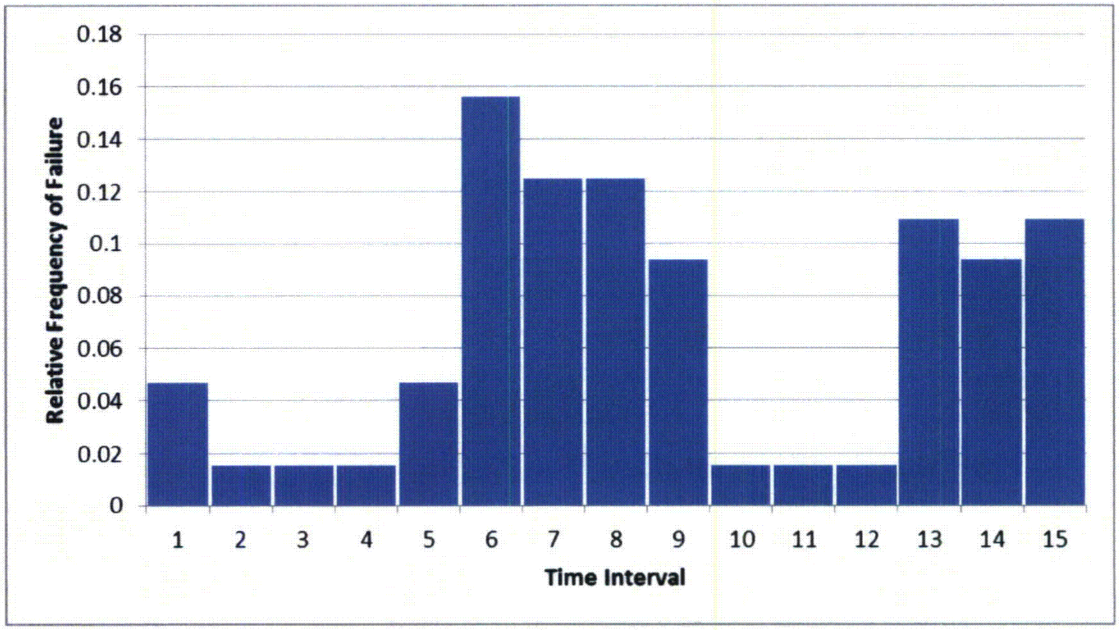

Figure 2.5.10 – Failure Timing Histogram

The time intervals are composed of different time steps. In order to gain a better understanding of the relative frequency of failure timing, the following figure provides an illustration of the normalized failure frequency over the entire 172 hour test (with time interval 9 outlier removed):

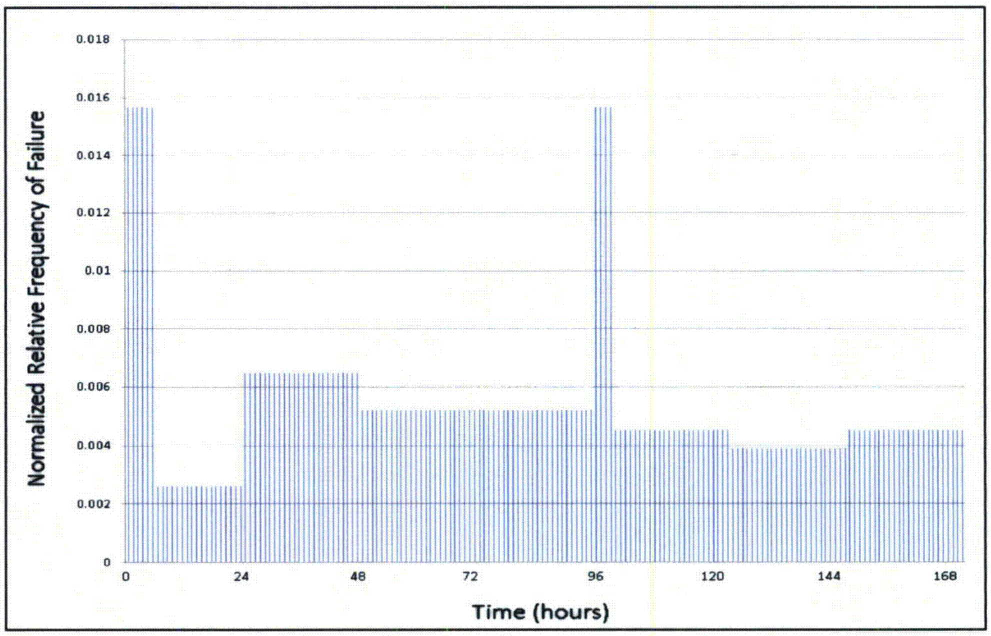

Figure 2.5.11 – Figure Normalized Failure Timing Histogram

This figure shows that although the failure seems to be decreasing, it does not taper off to 0% failure at the end of the 7 days. Therefore, this data has been extrapolated to include the entire 30-day mission time. As can be seen from Figure 2.5.11, there is a slightly declining slope to the failure as time increases. These results have been extrapolated to represent the entire 30-day mission time. The following table illustrates the probability statistics for the extrapolation:

Table 2.5.9 – Failure Timing Statistics

Time (hours)	Probability
1	0.00671
2	0.00671
3	0.00671
4	0.00671
5	0.00671
6	0.00671
7	0.00112
8	0.00112
9	0.00112
10	0.00112
11	0.00112
12	0.00112
13	0.00112
14	0.00112
15	0.00112
16	0.00112
17	0.00112
18	0.00112
19	0.00112
20	0.00112
21	0.00112
22	0.00112
23	0.00112
24	0.00112
25	0.00280
26	0.00280
27	0.00280
28	0.00280
29	0.00280
30	0.00280
31	0.00280
32	0.00280
33	0.00280
34	0.00280
35	0.00280
36	0.00280

Time (hours)	Probability
37	0.00280
38	0.00280
39	0.00280
40	0.00280
41	0.00280
42	0.00280
43	0.00280
44	0.00280
45	0.00280
46	0.00280
47	0.00280
48	0.00280
49	0.00224
50	0.00224
51	0.00224
52	0.00224
53	0.00224
54	0.00224
55	0.00224
56	0.00224
57	0.00224
58	0.00224
59	0.00224
60	0.00224
61	0.00224
62	0.00224
63	0.00224
64	0.00224
65	0.00224
66	0.00224
67	0.00224
68	0.00224
69	0.00224
70	0.00224
71	0.00224
72	0.00224
73	0.00224
74	0.00224

Time (hours)	Probability
75	0.00224
76	0.00224
77	0.00224
78	0.00224
79	0.00224
80	0.00224
81	0.00224
82	0.00224
83	0.00224
84	0.00224
85	0.00224
86	0.00224
87	0.00224
88	0.00224
89	0.00224
90	0.00224
91	0.00224
92	0.00224
93	0.00224
94	0.00224
95	0.00224
96	0.00224
97	0.00671
98	0.00671
99	0.00671
100	0.00671
101	0.00196
102	0.00196
103	0.00196
104	0.00196
105	0.00196
106	0.00196
107	0.00196
108	0.00196
109	0.00196
110	0.00196
111	0.00196
112	0.00196

Time (hours)	Probability
113	0.00196
114	0.00196
115	0.00196
116	0.00196
117	0.00196
118	0.00196
119	0.00196
120	0.00196
121	0.00196
122	0.00196
123	0.00196
124	0.00196
125	0.00168
126	0.00168
127	0.00168
128	0.00168
129	0.00168
130	0.00168
131	0.00168
132	0.00168
133	0.00168
134	0.00168
135	0.00168
136	0.00168
137	0.00168
138	0.00168
139	0.00168
140	0.00168
141	0.00168
142	0.00168
143	0.00168
144	0.00168
145	0.00168
146	0.00168
147	0.00168
148	0.00168
149	0.00196
150	0.00196

Time (hours)	Probability
151	0.00196
152	0.00196
153	0.00196
154	0.00196
155	0.00196
156	0.00196
157	0.00196
158	0.00196
159	0.00196
160	0.00196
161	0.00196
162	0.00196
163	0.00196
164	0.00196
165	0.00196
166	0.00196
167	0.00196
168	0.00196
169	0.00196
170	0.00196
171	0.00196
172	0.00196
173	0.00201
174	0.00201
175	0.00201
176	0.00201
177	0.00201
178	0.00201
179	0.00201
180	0.00201
181	0.00201
182	0.00201
183	0.00201
184	0.00201
185	0.00201
186	0.00201
187	0.00201
188	0.00201

Time (hours)	Probability
189	0.00201
190	0.00201
191	0.00201
192	0.00201
193	0.00168
194	0.00168
195	0.00168
196	0.00168
197	0.00168
198	0.00168
199	0.00168
200	0.00168
201	0.00168
202	0.00168
203	0.00168
204	0.00168
205	0.00168
206	0.00168
207	0.00168
208	0.00168
209	0.00168
210	0.00168
211	0.00168
212	0.00168
213	0.00168
214	0.00168
215	0.00168
216	0.00168
217	0.00168
218	0.00168
219	0.00168
220	0.00168
221	0.00168
222	0.00168
223	0.00168
224	0.00168
225	0.00168
226	0.00168

Time (hours)	Probability
227	0.00168
228	0.00168
229	0.00168
230	0.00168
231	0.00168
232	0.00168
233	0.00168
234	0.00168
235	0.00168
236	0.00168
237	0.00168
238	0.00168
239	0.00168
240	0.00168
241	0.00140
242	0.00140
243	0.00140
244	0.00140
245	0.00140
246	0.00140
247	0.00140
248	0.00140
249	0.00140
250	0.00140
251	0.00140
252	0.00140
253	0.00140
254	0.00140
255	0.00140
256	0.00140
257	0.00140
258	0.00140
259	0.00140
260	0.00140
261	0.00140
262	0.00140
263	0.00140
264	0.00140

Time (hours)	Probability
265	0.00140
266	0.00140
267	0.00140
268	0.00140
269	0.00140
270	0.00140
271	0.00140
272	0.00140
273	0.00140
274	0.00140
275	0.00140
276	0.00140
277	0.00140
278	0.00140
279	0.00140
280	0.00140
281	0.00140
282	0.00140
283	0.00140
284	0.00140
285	0.00140
286	0.00140
287	0.00140
288	0.00140
289	0.00140
290	0.00140
291	0.00140
292	0.00140
293	0.00140
294	0.00140
295	0.00140
296	0.00140
297	0.00140
298	0.00140
299	0.00140
300	0.00140
301	0.00140
302	0.00140

Time (hours)	Probability
303	0.00140
304	0.00140
305	0.00140
306	0.00140
307	0.00140
308	0.00140
309	0.00140
310	0.00140
311	0.00140
312	0.00140
313	0.00140
314	0.00140
315	0.00140
316	0.00140
317	0.00140
318	0.00140
319	0.00140
320	0.00140
321	0.00140
322	0.00140
323	0.00140
324	0.00140
325	0.00140
326	0.00140
327	0.00140
328	0.00140
329	0.00140
330	0.00140
331	0.00140
332	0.00140
333	0.00140
334	0.00140
335	0.00140
336	0.00140
337	0.00112
338	0.00112
339	0.00112
340	0.00112

Time (hours)	Probability
341	0.00112
342	0.00112
343	0.00112
344	0.00112
345	0.00112
346	0.00112
347	0.00112
348	0.00112
349	0.00112
350	0.00112
351	0.00112
352	0.00112
353	0.00112
354	0.00112
355	0.00112
356	0.00112
357	0.00112
358	0.00112
359	0.00112
360	0.00112
361	0.00112
362	0.00112
363	0.00112
364	0.00112
365	0.00112
366	0.00112
367	0.00112
368	0.00112
369	0.00112
370	0.00112
371	0.00112
372	0.00112
373	0.00112
374	0.00112
375	0.00112
376	0.00112
377	0.00112
378	0.00112

Time (hours)	Probability
379	0.00112
380	0.00112
381	0.00112
382	0.00112
383	0.00112
384	0.00112
385	0.00112
386	0.00112
387	0.00112
388	0.00112
389	0.00112
390	0.00112
391	0.00112
392	0.00112
393	0.00112
394	0.00112
395	0.00112
396	0.00112
397	0.00112
398	0.00112
399	0.00112
400	0.00112
401	0.00112
402	0.00112
403	0.00112
404	0.00112
405	0.00112
406	0.00112
407	0.00112
408	0.00112
409	0.00112
410	0.00112
411	0.00112
412	0.00112
413	0.00112
414	0.00112
415	0.00112
416	0.00112

Time (hours)	Probability
417	0.00112
418	0.00112
419	0.00112
420	0.00112
421	0.00112
422	0.00112
423	0.00112
424	0.00112
425	0.00112
426	0.00112
427	0.00112
428	0.00112
429	0.00112
430	0.00112
431	0.00112
432	0.00112
433	0.00112
434	0.00112
435	0.00112
436	0.00112
437	0.00112
438	0.00112
439	0.00112
440	0.00112
441	0.00112
442	0.00112
443	0.00112
444	0.00112
445	0.00112
446	0.00112
447	0.00112
448	0.00112
449	0.00112
450	0.00112
451	0.00112
452	0.00112
453	0.00112
454	0.00112

Time (hours)	Probability
455	0.00112
456	0.00112
457	0.00084
458	0.00084
459	0.00084
460	0.00084
461	0.00084
462	0.00084
463	0.00084
464	0.00084
465	0.00084
466	0.00084
467	0.00084
468	0.00084
469	0.00084
470	0.00084
471	0.00084
472	0.00084
473	0.00084
474	0.00084
475	0.00084
476	0.00084
477	0.00084
478	0.00084
479	0.00084
480	0.00084
481	0.00084
482	0.00084
483	0.00084
484	0.00084
485	0.00084
486	0.00084
487	0.00084
488	0.00084
489	0.00084
490	0.00084
491	0.00084
492	0.00084

Time (hours)	Probability
493	0.00084
494	0.00084
495	0.00084
496	0.00084
497	0.00084
498	0.00084
499	0.00084
500	0.00084
501	0.00084
502	0.00084
503	0.00084
504	0.00084
505	0.00084
506	0.00084
507	0.00084
508	0.00084
509	0.00084
510	0.00084
511	0.00084
512	0.00084
513	0.00084
514	0.00084
515	0.00084
516	0.00084
517	0.00084
518	0.00084
519	0.00084
520	0.00084
521	0.00084
522	0.00084
523	0.00084
524	0.00084
525	0.00084
526	0.00084
527	0.00084
528	0.00084
529	0.00084
530	0.00084

Time (hours)	Probability
531	0.00084
532	0.00084
533	0.00084
534	0.00084
535	0.00084
536	0.00084
537	0.00084
538	0.00084
539	0.00084
540	0.00084
541	0.00084
542	0.00084
543	0.00084
544	0.00084
545	0.00084
546	0.00084
547	0.00084
548	0.00084
549	0.00084
550	0.00084
551	0.00084
552	0.00084
553	0.00084
554	0.00084
555	0.00084
556	0.00084
557	0.00084
558	0.00084
559	0.00084
560	0.00084
561	0.00084
562	0.00084
563	0.00084
564	0.00084
565	0.00084
566	0.00084
567	0.00084
568	0.00084

Time (hours)	Probability
569	0.00084
570	0.00084
571	0.00084
572	0.00084
573	0.00084
574	0.00084
575	0.00084
576	0.00084
577	0.00056
578	0.00056
579	0.00056
580	0.00056
581	0.00056
582	0.00056
583	0.00056
584	0.00056
585	0.00056
586	0.00056
587	0.00056
588	0.00056
589	0.00056
590	0.00056
591	0.00056
592	0.00056
593	0.00056
594	0.00056
595	0.00056
596	0.00056
597	0.00056
598	0.00056
599	0.00056
600	0.00056
601	0.00056
602	0.00056
603	0.00056
604	0.00056
605	0.00056
606	0.00056

Time (hours)	Probability
607	0.00056
608	0.00056
609	0.00056
610	0.00056
611	0.00056
612	0.00056
613	0.00056
614	0.00056
615	0.00056
616	0.00056
617	0.00056
618	0.00056
619	0.00056
620	0.00056
621	0.00056
622	0.00056
623	0.00056
624	0.00056
625	0.00056
626	0.00056
627	0.00056
628	0.00056
629	0.00056
630	0.00056
631	0.00056
632	0.00056
633	0.00056
634	0.00056
635	0.00056
636	0.00056
637	0.00056
638	0.00056
639	0.00056
640	0.00056
641	0.00056
642	0.00056
643	0.00056
644	0.00056

Time (hours)	Probability
645	0.00056
646	0.00056
647	0.00056
648	0.00056
649	0.00056
650	0.00056
651	0.00056
652	0.00056
653	0.00056
654	0.00056
655	0.00056
656	0.00056
657	0.00056
658	0.00056
659	0.00056
660	0.00056
661	0.00056
662	0.00056
663	0.00056
664	0.00056
665	0.00056
666	0.00056
667	0.00056
668	0.00056
669	0.00056
670	0.00056
671	0.00056
672	0.00056
673	0.00056
674	0.00056
675	0.00056
676	0.00056
677	0.00056
678	0.00056
679	0.00056
680	0.00056
681	0.00056
682	0.00056

Time (hours)	Probability
683	0.00056
684	0.00056
685	0.00056
686	0.00056
687	0.00056
688	0.00056
689	0.00056
690	0.00056
691	0.00056
692	0.00056
693	0.00056
694	0.00056
695	0.00056
696	0.00056
697	0.00056
698	0.00056
699	0.00056
700	0.00056
701	0.00056
702	0.00056
703	0.00056
704	0.00056
705	0.00056
706	0.00056
707	0.00056
708	0.00056
709	0.00056
710	0.00056
711	0.00056
712	0.00056
713	0.00056
714	0.00056
715	0.00056
716	0.00056
717	0.00056
718	0.00056
719	0.00056
720	0.00056

These statistics yield the following extrapolated probability of failure timing:

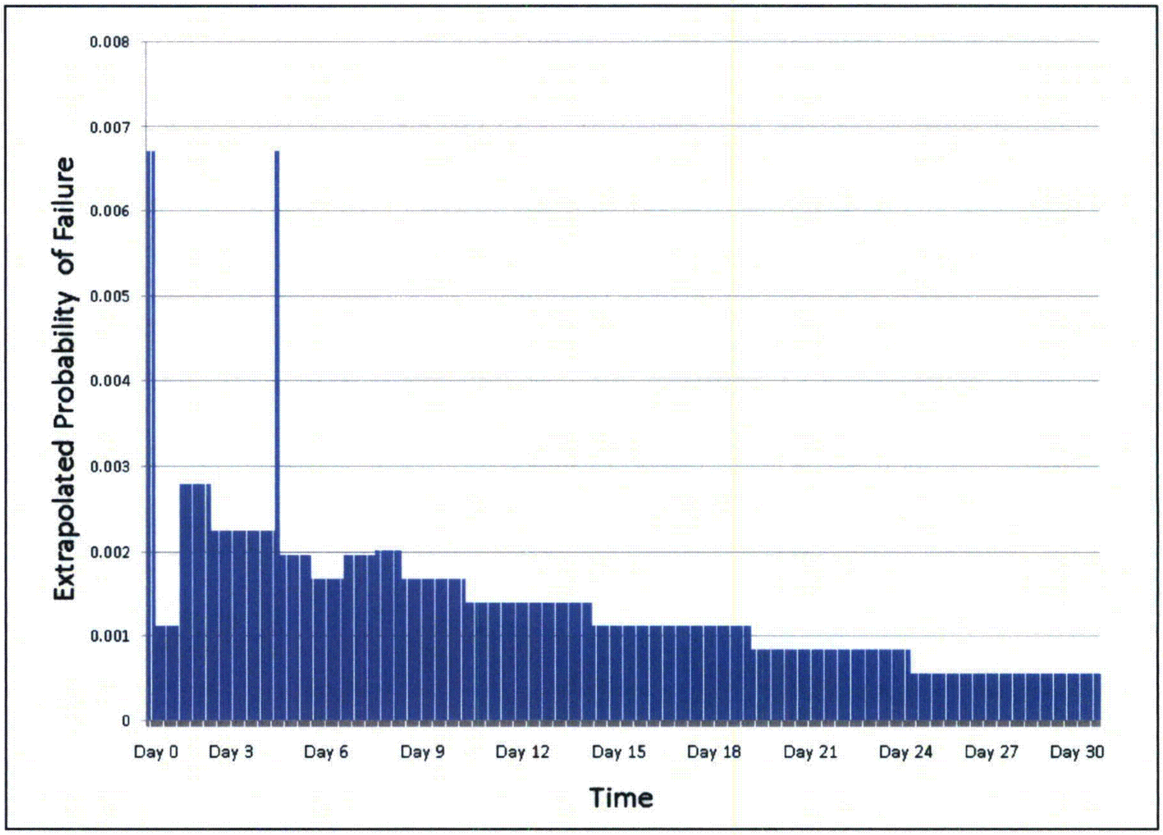

Figure 2.5.12 – Extrapolated Probability of Failure

As a result of this extrapolation, the probability of failure at a time before seven days is 39.6% of the total probability. Therefore, there is a 152.5% increase in probability statistics due to the extrapolation to the 30-day mission time. This increase in probability is applied to the 100% failure statistic of the failure fraction analysis to correct for the extrapolation (See Failure Fraction Analysis). This results in a significant increase in the quantity of failed coatings. Additionally, all of the failed unqualified coatings in upper containment are assumed to be exposed to containment sprays. Therefore, all of the coatings in upper containment that fail when containment sprays are on will transport to the pool. This is conservative since some of the failed coatings in upper containment may be in locations that are shielded from containment sprays. These conservative factors minimize the inherent risk of extrapolation.

Debris Characteristics

The debris characteristics of the failed unqualified coatings in STP are defined in this section. Different types of coating have different failure characteristics. Epoxy coatings are expected to fail as chips while

IOZ and Alkyd coatings fail as particulate. The failure mode of each coating determines the debris transportability when exposed to containment sprays.

The IOZ unqualified coatings are expected to fail as particulate. Several studies have shown that the unqualified IOZ fails as powder on the order of 10 microns. The BWROG supported testing that indicated the size range of the IOZ failed coating debris is between 1 and 20 micron (8); with 80% less than 10 micron, and 50% less than 5 micron. Other testing supports these conclusions. The BWR utility resolution guide gives the size range of the failed IOZ coating between 4-20 micron (9). The density of a common IOZ coating (Carbozinc 11) is 208 lbm/ft^3 (10). The weight-averaged density of the unqualified IOZ coatings found at STP is calculated in the following table (11):

Table 2.5.10 – Unqualified IOZ Weight-Averaged Density

Substrate number	Mass (lbm)	Dry Film Density (lbm/ft^3)
6	5.3	256.6
12a	4.3	121
13	29.1	256.6
16a	1.1	150.1
21	601.3	256.6
23a	37.2	256.6
26a	66.6	150.1
30a	3.5	150.1
31	16.9	150.1
37	8.7	256.6
38a	1.3	256.6
Weighted Average		**243.7**

The epoxy unqualified coatings are expected to fail as chips. There have been several studies to determine the failure mode and size of the epoxy debris. The BWROG supported generic testing that indicated that the thickness of these chips on average is 275 micron (11 mil) (8). Generally, the chip thickness is assumed to be the same as the applied dry film thickness (DFT). The weighted average of DFT for the unqualified epoxy coatings at STP is calculated from information in the unqualified coatings log (11):

Table 2.5.11 – Weight Average of Unqualified Epoxy DFT

Substrate #	Mass (lbm)	DFT (mils)
1a	381.15	10
1b	959.86	22
1c	233.42	5
12b	9.9	11
16b	1.74	8
18b	54.2	8
20	9.57	14
23b	42.23	8
24	2.05	7
26b	110.01	8
27	0.57	6
28	6.55	6
29	0.57	6
30b	4.81	8
32	2.29	12
33	10.4	7
38b	1.56	8
39b	0.42	6.5
Weighted Average		**15**

The Carboline unqualified coatings testing indicated that epoxy chips disbonded at lengths of up to 1" long (4). Moreover, the BWR utility resolution guide states that IOZ with an epoxy topcoat will fail as follows: the epoxy chips with be in the size range of 0.125 to 2.0 inches, while the IOZ will both adhere to the back of the chips and separate as small particulate (9). In addition to this general testing, plant specific testing has been conducted to determine the size distribution of the epoxy chips. Alion characterized samples from Comanche Peak that indicated the length of the failed epoxy chips range from around 6 mils to 2 inches (5). The following table illustrates these results:

Table 2.5.12 – Epoxy Debris Size Distribution by Mass

Size Range of Coating	Mass (g)	Percentage of Total Mass
1-2 inch	3.4657	32.03%
0.5-1 inch	0.9784	9.04%
0.25-0.5 inch	0.4774	4.41%
0.125-0.25 inch	0.5434	5.02%
< 0.125 inch	5.3561	49.50%
Total	10.821	100.00%

The less than 0.125 inch size range includes fines and fine chips. Of the 49.50% of this size range, 12.275% are assumed to be 6 mil particles (fines) and 37.225% are assumed to be 1/64 inch (fine chips) (10). Additionally, 50% of the chips above 0.5 inches are assumed to be curled (5). The following size distributions will be used in the risk-informed analysis:

Table 2.5.13 – Epoxy Debris Size Distribution

Size Designation	Size Range (inch)	Percentage of Total Mass
Fines (particles)	0.006	12.28%
Flat Fine Chips	0.0156	37.23%
Flat Small Chips	0.125-0.5	9.43%
Flat Large Chips	0.5-2.0	20.53%
Curled Chips	0.5-2.0	20.53%

The weight-averaged density of the unqualified epoxy coatings found at STP is calculated based on information from the unqualified coatings log (11):

Table 2.5.14 – Unqualified Epoxy Weight-Averaged Density

Substrate Number	Mass (lbm)	Dry Film Density (lbm/ft^3)
1a	381.2	113.0
1b	959.9	129.4
1c	233.4	138.5
12b	9.9	138.5
16b	1.7	108.5
18b	54.2	84.1
20	9.6	109.4
23b	42.2	109.4
24	2.1	109.4
26b	110.0	108.5
27	0.6	109.4
28	6.6	109.4
29	0.6	109.4
30b	4.8	102.5
32	2.3	109.4
33	10.4	109.4
38b	1.6	109.4
39b	0.4	93.5
Weighted Average		**123.7**

The alkyd coatings are expected to fail as particulate. The debris characteristics of the alkyd coating are shown to be soft pliable pieces and particulate in the BWR utility resolution guide (9). In addition, unqualified alkyd coatings bench top testing conducted by Alion determined that the failure mode was potential delamination and release of particles into solution (6). This testing program showed that the particles were on the order of 10 micron. Due to the similar particle size of the alkyd coatings to IOZ coatings, the size distribution of the particles will be assumed to be the same as IOZ. The weight-averaged density of the specific unqualified alkyd coatings found at STP is calculated based on information from the unqualified coatings log (11):

Table 2.5.15 – Unqualified Alkyd Weight-Averaged Density

Substrate number	**Mass (lbm)**	**Dry Film Density (lbm/ft^3)**
2a	13.5	120.4
2b	54.6	97.2
4	25	228.5
8 (zinc rich alkyd)	133.8	268.5
18a	12.3	102.3
22(zinc rich alkyd)	23.7	228.8
35a	1.5	120.4
35b	2.5	97.2
39a	4	120.4
Weighted Average		**207.3**

Baked enamels are assumed to have the same debris characteristics as an alkyd. This is because baked enamel is the common alkyd coating sold for metal finished products (6). The average density of the specific unqualified baked enamel coatings found at STP is calculated based on information in the unqualified coatings log (11):

Table 2.5.16 – Unqualified Baked Enamel Weight-Averaged Density

Substrate number	**Mass (lbm)**	**Dry Film Density (lbm/ft^3)**
3	260	93.8
7	7.2	69.5
Weighted Average		**93.1**

There is currently no information on the debris characteristics of intumescent coatings. Therefore, it will be assumed to have the same debris characteristics as epoxy. The weight-averaged density of the intumescent coatings found at STP is calculated based on the unqualified coating logs (11):

Table 2.5.17 – Unqualified Intumescent Weight-Averaged Density

Substrate Number	Mass (lbm)	Dry Film Density (lbm/ft^3)
5a	0.5	83.8
5b	1.8	97.2
19a	10.7	134.0
19b	19.5	75.3
19c	5.0	96.8
Weighted Average		**96.0**

Assumptions: Several assumptions were made in the development of the unqualified coatings calculation (7). The more significant assumptions are listed below:

- For any component substrate location that was indeterminate, it was assumed that the location was at the pool level allowing direct transport to the pool. This is the most conservative alternative.
- The debris characteristics and failure fraction of baked enamel is assumed to be the same as that for the unqualified alkyd coatings. This is a reasonable assumption because baked enamel is a common type of alkyd coating (6).
- It was assumed that the total mass quantities formulated in this calculation are applicable to both STP units. This is a reasonable assumption because the containment buildings for STP Units 1 and 2 are essentially identical.
- The debris characteristics of intumescent coatings are assumed to be the same as epoxy. This is a reasonable assumption because many commercially available intumescent coatings are partially composed of epoxy.

Acceptance Criteria: No acceptance criteria were used for the unqualified coatings evaluation.

Results: The results of the unqualified coatings calculation (7) are used as an input to the overall GSI-191 evaluation (12). These results are described in detail below.

The total quantity and locations of potentially transportable unqualified coatings are shown in Table 2.5.18, and the debris characteristics are shown in Table 2.5.19. Since unqualified coatings can fail outside the zone of influence, these quantities are applicable for all break scenarios.

Table 2.5.18 – Quantity and location of potentially transportable unqualified coatings debris

Coatings Type	Upper Containment Quantity (lb_m)	Lower Containment Quantity (lb_m)	Reactor Cavity Quantity (lb_m)	Total Quantity (lb_m)
Unqualified Epoxy	295 (15%)	36 (2%)	1,574 (83%)	1,905
Unqualified IOZ	305 (83%)	64 (17%)	0 (0%)	369
Unqualified Alkyd	146 (54%)	125 (46%)	0 (0%)	271
Unqualified Baked Enamel	0 (0%)	267 (100%)	0 (0%)	267
Unqualified Intumescent	0 (0%)	2 (100%)	0 (0%)	2

Table 2.5.19 – Material properties of unqualified coatings debris

Debris Type	Debris Size	Macroscopic Density	Microscopic Density
Unqualified Epoxy	Fines: 6 mil particles	-	124 lb_m/ft^3
	Fine Chips: 0.0156"×15 mil		
	Small Chips: 0.125"-0.5"×15 mil		
	Large Chips: 0.5"-2.0"×15 mil		
	Curled Chips: 0.5"-2.0"×15 mil		
Unqualified Alkyd	Fines: 4 - 20 μm particles	-	207 lb_m/ft^3
Unqualified IOZ	Fines: 4 - 20 μm particles	-	244 lb_m/ft^3
Unqualified Baked Enamel	Fines: 4 - 20 μm particles	-	93 lb_m/ft^3

A failure fraction of 100% was used for all cases. The washdown transport fraction for unqualified coatings in upper containment was based on the failure timing graph that showed that approximately 6% of the unqualified coatings would fail in the first 24 hours (7). Although containment sprays would be secured after approximately 6.5 hours (12), all coatings that failed in upper containment in the first 24 hours were assumed to be washed down to the pool. The transportable coatings were introduced to the containment pool at a constant rate of approximately 2.8% per hour for the first 36 hours (12).

Additional details on the basis for the unqualified coatings quantities, locations, failure fractions, and failure timing are provided in the STP unqualified coatings debris generation calculation (7).

In a typical deterministic GSI-191 evaluation, the time-dependence is not considered (i.e. the unqualified coatings are normally assumed to fail at the beginning of the event). The unqualified coatings are often assumed to fail as 10 micron particulate, although some plants have credited a range of chip sizes for unqualified epoxy coatings. The results from the debris characteristics evaluation of unqualified coatings at STP are documented in the following table:

Table 2.5.20 – Debris Characteristics Summary

Coating Type	Debris Type	Size Range	Density
IOZ	Particulate	4-20 micron	244 lbm/ft^3
Epoxy	Chips	10 mils-2 inches	124 lbm/ft^3
Alkyd	Particulate	4-20 micron	207 lbm/ft^3
Baked Enamel	Particulate	4-20 micron	93 lbm/ft^3
Intumescents	Chips	6 mils-2 inches	96 lbm/ft^3

For the STP risk-informed evaluation, the location, failure timing, and debris characteristics are important for several reasons:

- Unqualified coatings in upper containment that fail after containment sprays are secured would not be transported to the containment pool.
- Unqualified coatings in lower containment were assumed to fall directly in the pool and be available for transport. However, delays in the failure timing result in delayed arrival at the strainer and a delayed impact on head loss.
- Unqualified coatings in the reactor cavity would only be available for transport to the strainers if the break is in the reactor cavity.
- Although the unqualified coatings fines would essentially all transport to the strainer, the transport for the chips would be significantly reduced.

Additional details on how the unqualified coatings debris was treated in the overall GSI-191 evaluation are provided in Volume 3 (12).

<u>Item 5.a.2: Debris Capture</u>

<u>Method</u>: The methodology for debris capture on gratings and obstructions during the blowdown phase is documented in an engineering calculation based on plant-specific features (locations of grating, etc.) and applicable test data (13). The test data that was used is documented in the drywell debris transport study (DDTS) (14). The full range of break scenarios were grouped into the following break categories:

- Breaks in the steam generator compartments
- Breaks in the reactor cavity
- Breaks inside secondary shield wall beneath steam generator compartments
- Breaks in the pressurizer compartment
- Breaks outside secondary shield wall in the pressurizer surge line
- Breaks outside secondary shield wall in the RHR compartments
- Breaks outside secondary shield wall in the annulus

For each of these break locations, the fraction of debris blown up toward upper containment or down toward the containment floor was determined based on the relative containment volumes. The fine debris generated inside the zone of influence (ZOI) was assumed to fully transport with the blowdown flow. For small and large pieces of debris, the effects of debris capture were taken into account for miscellaneous structures, grating, and 90° turns in the flow path based on test data from the DDTS.

For each of these break locations, the fraction of debris blown up toward upper containment or down toward the containment floor was determined based on the relative containment volumes. The volume of upper containment (including areas above the operating deck) was calculated to be 2,320,079 ft^3, and the total volume in containment was calculated to be 3,322,040 ft^3. The fine debris generated inside the zone of influence (ZOI) was assumed to fully transport with the blowdown flow. Therefore, the transport fraction for the total fine debris from all areas would be 70% to upper containment. For small and large pieces of debris, the effects of debris capture were taken into account for miscellaneous structures, grating, and 90° turns in the flow path based on test data from the DDTS. The results of the DDTS testing showed that in a wetted, highly congested area, approximately 0% to 13% of small fiberglass debris would be trapped by miscellaneous structures, 15% to 29% would be trapped by grating, and 3% to 29% would be captured at 90° turns in flow path. The amount of small piece debris that gets blown to upper containment can be calculated as shown in the following equation:

$$F_{BD} = \left(\frac{V_{upper}}{V_{total}} \right)(1.00 - F_{misc})(1.00 - F_{90^\circ turns} \cdot N_{turns})(1.00 - F_{grating} \cdot N_{gratings})$$

where:

F_{BD} = fraction of debris blown to upper containment
V_{upper} = volume of upper containment
V_{total} = total volume in containment
F_{misc} = fraction of debris trapped by miscellaneous structures
$F_{90^\circ turns}$ = fraction of debris trapped by changes in flow direction
N_{turns} = number of turns or changes in flow direction debris would pass through
$F_{grating}$ = fraction of debris trapped by grating
$N_{gratings}$ = number of gratings debris would pass through

Large piece debris would be blown away from the break similar to the small piece debris. However, this debris would not pass through grating.

Each break location was analyzed separately to determine the average number of turns and gratings applicable to each location.

Breaks in the Steam Generator Compartments

For breaks in the Steam Generator Compartments, it was determined that the small piece debris blown to upper containment would have to pass through 78% coverage of grating above these compartments, an average of one 90° turn, and a variety of miscellaneous structures. As shown in the following equations, it was determined that the range for small fiberglass debris blown to upper containment is 33% to 60%.

$$F_{blowdown\ (small\ fiber)} = (0.70)(1.00-0.00)(1.00-0.03)(1.00-0.15\cdot 0.78) = 0.60$$

$$F_{blowdown\ (small\ fiber)} = (0.70)(1.00-0.13)(1.00-0.29)(1.00-0.29\cdot 0.78) = 0.33$$

For the small piece debris blown to lower containment from these compartments, it was determined that debris would have to pass through 1 level of grating at the bottom of the compartments, an average of one 90° turn, and a variety of miscellaneous structures. As shown in the following equations, it was determined that 13% to 25% of small piece debris would be blown to lower containment.

$$F_{blowdown\ SG\ comps.\ (small\ fiber)} = (0.30)(1.00-0.00)(1.00-0.03)(1.00-0.15\cdot 1.00) = 0.25$$

$$F_{blowdown\ SG\ comps.\ (small\ fiber)} = (0.30)(1.00-0.13)(1.00-0.29)(1.00-0.29\cdot 1.00) = 0.13$$

Since the large piece debris would not pass through the floor grating toward lower containment, and a negligible quantity would be blown past miscellaneous structures and the 78% effective grating toward upper containment, it is estimated that 0% to 22% would be blown to upper containment.

Breaks in the Reactor Cavity

For breaks inside the reactor cavity, the transport fractions for small and large fiberglass debris was determined to be the same as for a break in the Steam Generator Compartments, since this debris would essentially follow the same path towards upper containment. Therefore, 33% to 60% of small fiberglass debris would be in upper containment, 13% to 25% in the containment pool, and 15% to 54% remaining in the steam generator compartments. For small and large RMI generated in the reactor cavity, it was estimated that all of this debris would be blown to the containment pool since the RMI debris would be caught up in the reactor cavity and miscellaneous structures more easily. Since Microtherm is in the secondary shield wall penetrations, there wouldn't be any of this type of debris destroyed for a reactor cavity break.

Breaks below the Steam Generator Compartment Floor

For breaks below the Steam Generator Compartment Floor, it was determined that debris would have to pass through one level of grating between the compartments, and the 78% coverage of grating above the steam generator compartments. As shown in the following equations, it was determined that the range of small fiber blown to upper containment would be 21% to 50% based on an average of one 90° turn, and a variety of miscellaneous structures.

$$F_{blowdown\ (small\ fiber)} = (0.70)(1.00-0.00)(1.00-0.03)(1.00-0.15\cdot 1.78) = 0.50$$

$$F_{blowdown\ (small\ fiber)} = (0.70)(1.00-0.13)(1.00-0.29)(1.00-0.29\cdot 1.78) = 0.21$$

The remaining small fiberglass not blown to upper containment would be blown to the containment pool. The large fiberglass would be captured by the grating; therefore, 0% would be transported to upper containment.

Breaks in the Pressurizer Compartment

For breaks in the pressurizer compartment, it was estimated that small piece debris blown to upper containment would have to pass through an average of two 90° turns and a variety of miscellaneous structures. Therefore, as shown in the following equations, the range of small piece debris blown to upper containment would be 26% to 66%.

$$F_{blowdown\ (small\ fiber)} = (0.70)(1.00 - 0.00)(1.00 - 0.03 \cdot 2.00) = 0.66$$

$$F_{blowdown\ (small\ fiber)} = (0.70)(1.00 - 0.13)(1.00 - 0.29 \cdot 2.00) = 0.26$$

The small piece debris blown to lower containment was also estimated to pass through an average of two 90° turns and a variety of miscellaneous structures. Therefore, the range of small piece debris blown to the containment floor would be 11% to 28%, as shown in the following equations.

$$F_{blowdown\ PRZR\ comp.\ (small\ fiber)} = (0.30)(1.00 - 0.00)(1.00 - 0.03 \cdot 2.00) = 0.28$$

$$F_{blowdown\ PRZR\ comp.\ (small\ fiber)} = (0.30)(1.00 - 0.13)(1.00 - 0.29 \cdot 2.00) = 0.11$$

The large piece debris would be blown away from the break similar to the small piece debris. However, the transport fraction for this debris would be on the lower end of the range of transport values for the small pieces, since this debris would be more easily held up on structures and the 90° turns in flow path. It was estimated that 16% to 26% would be in upper containment, 1% to 11% in the containment pool, and 63% to 83% remaining in the compartment.

Breaks in the Pressurizer Surge Line

It was estimated that debris blown to upper containment would have to pass through the grating at the 19'-0" elevation or the 37'-3" elevation, and at least two additional levels of grating above these gratings. Therefore, the range of the small piece debris blown to upper containment would be 3% to 36% as shown in the following equations based on debris passing through an average of two 90° turns, 3 levels of effective grating, and miscellaneous structures.

$$F_{blowdown\ (small\ fiber)} = (0.70)(1.00 - 0.00)(1.00 - 0.03 \cdot 2.00)(1 - 0.15 \cdot 3.00) = 0.36$$

$$F_{blowdown\ (small\ fiber)} = (0.70)(1.00 - 0.13)(1.00 - 0.29 \cdot 2.00)(1.00 - 0.29 \cdot 3.00) = 0.03$$

Since there is no grating between the pressurizer surge line break and lower containment, it was estimated that the remaining small piece debris would be blown to the containment pool.

The large fiberglass debris would be blown away in the same manner as the small debris. However, since this debris would not pass through grating, it was estimated that 100% would be blown to the containment pool.

Microtherm is present in the surge line penetration in the secondary shield wall. Seventy percent of the Microtherm fines would be blown towards upper containment.

Breaks in the RHR Compartments

The RHR compartments are highly compartmentalized, and debris would be blown down and then back up to upper containment. It was estimated that the range of the percentage of small piece debris blown to upper containment in the RHR compartments would be 3% to 45% as shown in the following equations based on a fraction of debris passing through an average of three 90° turns, 2 levels of effective grating, and a variety of miscellaneous structures.

$$F_{blowdown\,(small\ fiber)} = (0.70)(1.00-0.00)(1.00-0.03\cdot 3.00)(1-0.15\cdot 2.00) = 0.45$$

$$F_{blowdown\,(small\ fiber)} = (0.70)(1.00-0.13)(1.00-0.29\cdot 3.00)(1-0.29\cdot 2.00) = 0.03$$

Thirty percent of small piece debris would get blown to the containment floor. Some of this debris would be captured at significant flow turns and by miscellaneous structures. Therefore, the range of small piece debris blown to the containment floor would be 1% to 19% as shown in the following equations:

$$F_{blowdown\,(small\ fiber)} = (0.30)(1.00-0.00)(1.00-0.03\cdot 3.00)(1-0.15\cdot 2.00) = 0.19$$

$$F_{blowdown\,(small\ fiber)} = (0.30)(1.00-0.13)(1.00-0.29\cdot 3.00)(1-0.29\cdot 2.00) = 0.01$$

The large piece debris would be blown away from the break similar to the small piece debris. However, since this debris would not pass through grating, the transport fraction to upper containment would be 0%. Some large piece debris could be transported to lower containment, however, since there are locations in the compartment that are located below the lowest level of grating. It is estimated that about 0% to 10% would be in lower containment, and 90% to 100% remaining in the compartments.

Breaks in the Annulus

The break locations in the annulus are between the 19′ elevation grating and the 37′-3″ elevation grating. Therefore, in order for debris to reach upper containment, it would have to pass through three levels of grating. The range of the transport fractions for small debris blown to upper containment would be 6% to 37% as shown in the following equations, based on debris passing through an average of one 90° turn, three levels of grating, and miscellaneous structures.

$$F_{blowdown\ (small\ fiber)} = (0.70)(1.00 - 0.00)(1.00 - 0.03 \cdot 1.00)(1 - 0.15 \cdot 3.00) = 0.37$$

$$F_{blowdown\ (small\ fiber)} = (0.70)(1.00 - 0.13)(1.00 - 0.29 \cdot 1.00)(1.00 - 0.29 \cdot 3.00) = 0.06$$

Thirty percent of small piece debris would get blown to the containment floor. Some of the debris would get trapped on grating and miscellaneous structures. Therefore, the range of debris that would be blown to lower containment would be 13% to 25% as shown in the following equations, based on an average of one 90° turn, one level of grating, and miscellaneous structures.

$$F_{blowdown\ (small\ fiber)} = (0.30)(1.00 - 0.00)(1.00 - 0.03 \cdot 1.00)(1.00 - 0.15 \cdot 1.00) = 0.25$$

$$F_{blowdown\ (small\ fiber)} = (0.30)(1.00 - 0.13)(1.00 - 0.29 \cdot 1.00)(1.00 - 0.29 \cdot 1.00) = 0.13$$

The large piece debris would be blown away in the same manner as the small debris. However, since this debris would not pass through grating, 100% would remain in the annulus above the pool elevation.

Basis: The methodology used for debris capture during the blowdown phase is based on refined deterministic debris transport methods that have been previously accepted by the NRC (15). The primary difference in the risk-informed evaluation is that several additional break locations are considered, and the retention fractions on grating and other structures is based on the range of values provided in the DDTS rather than a simple bounding value.

Assumptions: The assumptions made in the risk-informed debris transport calculation with respect to blowdown debris capture include the following (13):

- It was assumed that the fines generated by the LOCA blast would be transported to upper containment in proportion to the volume of upper containment compared to the entire volume. This is a reasonable assumption since fine debris generated by the LOCA jet would be easily entrained and carried with the blowdown flow.
- It was assumed that a fraction of small piece debris would also be transported to upper containment in proportion to the relative volume. Each compartment/area where breaks may occur was individually analyzed to determine the percentage of small and large piece debris that would get transported to upper containment.

Acceptance Criteria: No acceptance criteria were used for the blowdown debris capture analysis.

Results: The analysis of debris capture during the blowdown phase is one aspect of the debris transport evaluation. The blowdown transport fractions as well as the transport fractions during other phases of the event (washdown, pool fill, and recirculation) (13) are used as an input for the overall GSI-191 evaluation (12). The results of the blowdown transport analysis are shown in Table 2.5.21.

Table 2.5.21 – Blowdown transport fractions according to break location

Break Location	Debris Type and Size	Blowdown Transport Fractions		
		Upper Containment	Lower Containment	Remaining in Compartments
1. Steam Generator Compartments	Fines	70%	30%	0%
	Small LDFG	33-60%	13-25%	15-54%
	Large LDFG	0-22%	0%	78-100%
2. Reactor Cavity	Fines	70%	30%	0%
	Small LDFG	33-60%	13-25%	15-54%
	Large LDFG	0-22%	0%	78-100%
3. Below Steam Generator Compartments	Fines	70%	30%	NA
	Small LDFG	21-50%	50-79%	NA
	Large LDFG	0%	100%	NA
4. Pressurizer Compartment	Fines	70%	30%	0%
	Small LDFG	26-66%	11-28%	6-63%
	Large LDFG	16-26%	1-11%	63-83%
5. Pressurizer Surge Line	Fines	70%	30%	NA
	Small LDFG	3-36%	64-97%	NA
	Large LDFG	0%	100%	NA
6. RHR Compartments	Fines	70%	30%	0%
	Small LDFG	3-45%	1-19%	36-96%
	Large LDFG	0%	0-10%	90-100%
7. Annulus	Fines	70%	30%	0%
	Small LDFG	6-37%	13-25%	38-81%
	Large LDFG	0%	0%	100%

The types of debris that would be subject to the blowdown forces include Nukon, Microtherm, qualified coatings, and crud. The Nukon debris would fail as fines, small pieces, large pieces, and intact blankets. The Microtherm, qualified coatings, and crud debris would all fail as fine debris and would transport similar to the Nukon fines. Because the intact blankets would not transport readily, this debris was not included in the transport analysis.

It was assumed that the overall transport fractions for each type of debris can be represented by the bounding transport fractions for an LBLOCA in the steam generator compartments (12). Therefore, only the blowdown transport fractions shown in the table below were implemented in CASA Grande.

Table 2.5.22 – Blowdown transport fractions used in CASA Grande

Debris Type	Blowdown Transport Fractions		
	Upper Containment	Upper Containment	Remaining in Compartments
Fines	70%	30%	0%
Small LDFG	60%	25%	15%
Large LDFG	22%	0%	78%

Additional details on how the blowdown transport was incorporated in the overall GSI-191 evaluation are provided in Volume 3 (12).

<u>Item 5.a.3: Washdown Transport</u>

<u>Method</u>: The methodology for calculating debris holdup during the washdown phase is documented in an engineering calculation based on plant-specific features (locations of grating, etc.) and applicable test data (13). The test data that was used is documented in the DDTS (14).

During the washdown phase of a LOCA, debris would be transported down to the containment pool by operation of the containment spray system. Significant amounts of debris could, however, be captured on the concrete floors and grated areas above the containment floor as containment spray water transporting the debris drains through grating to reach the pool.

The debris remaining inside the steam generator compartments would also be washed toward lower containment by the spray flow as well as the break flow. However, some small piece debris and all of the large piece debris would be held up on grating.

The debris blown to upper containment would be scattered around. Therefore, a reasonable approximation of the washdown locations can be made based on the spray flow split in upper containment. As shown in Figure 2.5.13, 25% of the containment sprays were estimated to flow directly into the steam generator compartments, 28% were estimated to flow into the steam generator compartments via the refueling canal (21%) and cable tray chase (7%), and the remaining 47% of the sprays were estimated to flow into the annulus.

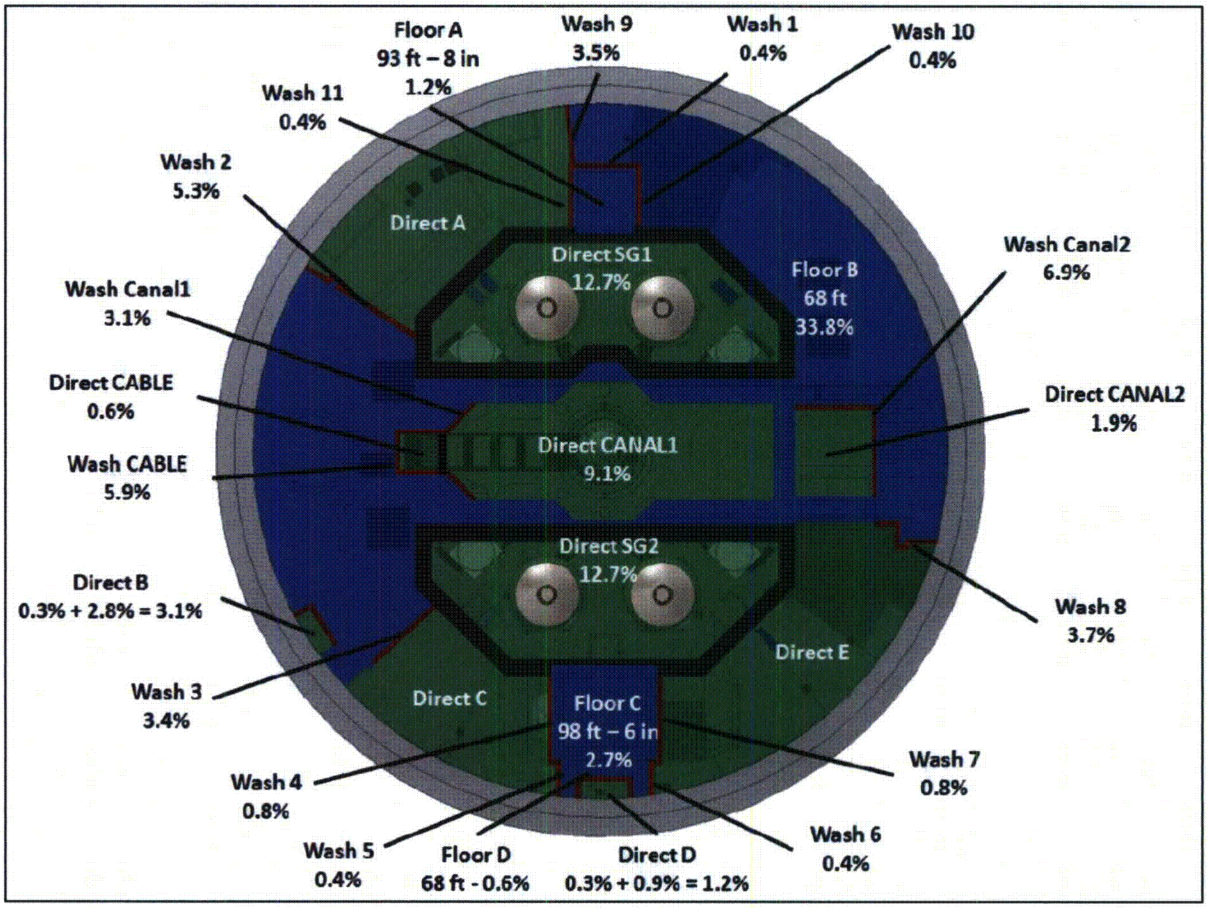

Figure 2.5.13 – 68' Elevation Spray Flow Distribution

The results of the DDTS testing showed that approximately 40-50% of small fiberglass debris landing on grating would be washed through the grating due to spray flows (16). Due to the fact that many of the flow paths to the containment pool would pass through multiple levels of grating, it was assumed that 0-25% of small pieces would be held up on each additional grating level as shown in the following equation. It was conservatively assumed that 100% of fines would transport to the pool. Retention of debris on concrete floors was considered, but was not credited in the final analysis.

$$F_{wash} = F_{CS} \cdot F_{WG} \cdot (1 - F_{AG})^{(N_{gratings} - 1)}$$

where:

F_{wash} = fraction of debris washed down to lower containment
F_{CS} = fraction of debris washed down by containment sprays
F_{WG} = fraction of debris held up when washed through first level of grating
F_{AG} = fraction of debris held up when washed through additional grating
$N_{gratings}$ = total number of gratings debris would pass through

The small piece debris that is present on the operating deck was conservatively assumed to be washed down to lower containment without any retention on grating or structures, since the flow of water over the edge would be concentrated and may be strong enough to push the debris to lower containment through the grating. The small debris washed down in the annulus would pass through a maximum of 5 levels of grating, and a minimum of 1 level. Therefore, the transport fraction for small pieces of fiber washed down in the annulus would be 7% to 19% as shown in the following equations:

$$F_{wash\ annulus\ small\ fiber\ max} = 0.47 \cdot 0.40 \cdot (1.00 - 0.00)^{(1-1)} = 0.19$$
$$F_{wash\ annulus\ small\ fiber\ min} = 0.47 \cdot 0.50 \cdot (1.00 - 0.25)^{(5-1)} = 0.07$$

The small piece debris that is present in the steam generator compartment would have to pass through only one level of grating to reach the pool, so the transport fraction for this debris would be 21% to 27% as shown in the following equations:

$$F_{wash\ SG\ comp\ small\ fiber\ max} = (0.25 + 0.28) \cdot (0.40)(1.00 - 0.00)^{(1-1)} = 0.21$$
$$F_{wash\ SG\ comp\ small\ fiber\ min} = (0.25 + 0.28) \cdot (0.50)(1.00 - 0.25)^{(1-1)} = 0.27$$

The large fiber debris would be washed down in the same locations as the small debris. However, since this debris would not pass through grating, the washdown fraction from upper containment through the annulus and inside the secondary shield wall would be 0%.

Containment sprays would not wash down any debris in the pressurizer compartment or RHR compartments, since the top of these compartments is blocked with a concrete roof or equipment hatches. Therefore, all of the debris remaining in these compartments at the end of blowdown will remain in the compartments during washdown.

Basis: The methodology used for the washdown analysis is similar to refined deterministic debris transport methods that have been used in the past. The retention fraction for the first level of grating is based on the DDTS results, and the retention fraction for each additional level of grating is based on engineering judgment (i.e., if a piece of debris passes through one level of grating, it is more likely to pass through a second level of grating, but still has a non-zero probability of being captured).

Assumptions: The following assumption was made in the risk-informed debris transport calculation with respect to washdown debris holdup (13):

- It was assumed that all debris blown upward would be subsequently washed back down by the containment spray flow with the exception of pieces of debris held up on grating. The fraction of debris washed down to various locations was calculated based on the spray flow split.

Acceptance Criteria: No acceptance criteria were used for the washdown debris holdup analysis.

Results: The analysis of debris holdup during the washdown phase is one aspect of the debris transport evaluation. The washdown transport fractions as well as the transport fractions during other phases of the event (blowdown, pool fill, and recirculation) (13) are used as an input for the overall GSI-191 evaluation (12). The results of the washdown transport analysis are shown in Table 2.5.23.

Table 2.5.23 – Washdown transport fractions according to spray initiation

Sprays Initiated?	Debris Type	Washdown Transport Fraction	
		Washed Down in Annulus	Washed Down inside Secondary Shield Wall
Yes	Fines	47%	53%
	Small LDFG	7-19%	21-27%
	Large LDFG	0%	0%
No	All	0%	0%

The washdown transport fractions do not depend on the location of the break, but only whether sprays are initiated. Since unqualified coatings debris may fail later in the event, this debris would only be washed down to the pool if the sprays are initiated and the coatings fail before the sprays are secured. The bounding washdown transport fractions (assuming sprays are always initiated) were used for all breaks (12). Therefore, only the blowdown transport fractions shown in the table below were implemented in CASA Grande.

Table 2.5.24 – Washdown transport fractions used in CASA Grande

Debris Type	Washdown Transport Fractions	
	Washed Down in Annulus	Washed Down inside Secondary Shield Wall
Fines	47%	53%
Small LDFG	19%	27%
Large LDFG	0%	0%

Additional details on how the washdown transport was incorporated in the overall GSI-191 evaluation are provided in Volume 3 (12).

Item 5.a.4: Debris Distribution

Method: The methodology for determining the non-uniform debris distribution at the start of recirculation is documented in an engineering calculation based on plant-specific features and careful consideration of break locations, flow paths, and debris types and sizes (13).

Since the various types and sizes of debris transport differently during the blowdown, washdown, and pool fill-up phases, the initial distribution of this debris at the start of recirculation could vary widely. Insulation debris on the pool floor would be scattered around by the break flow as the pool fills, and debris in upper containment would be washed down at various locations by the spray flow. Due to the fact that the containment pool does not flow preferentially in any given direction after the inactive and sump cavities have been filled and before recirculation begins, it was assumed that the debris washed down by containment sprays would remain in the general vicinity of the washdown locations until recirculation starts.

Basis: The methodology used for determining the initial debris distribution is very similar to the refined deterministic debris transport methods that have been previously approved by the NRC (17). The primary difference is that a more realistic distribution was used for pieces of debris blown to lower containment rather than automatically assuming that these pieces would be preferentially distributed toward the sump strainers.

Assumptions: The following assumptions were made in the risk-informed debris transport calculation with respect to the debris distribution at the beginning of recirculation (13):

- With the exception of latent debris washed to the sump and inactive cavities during pool fill-up, it was conservatively assumed that all latent debris is in lower containment, and would be uniformly distributed in the containment pool at the beginning of recirculation. This is a conservative assumption since no credit is taken for debris remaining on structures and equipment above the pool water level.
- It was assumed that the unqualified coatings outside the reactor cavity would be uniformly distributed in the recirculation pool. This is a reasonable assumption since the unqualified coatings are scattered around containment in small quantities (7).
- It was assumed that the debris washed down inside the secondary shield wall by the break and spray flow would be initially distributed inside the secondary shield wall. It was also assumed that the debris washed down outside the secondary shield wall would be initially distributed in the annulus. These are reasonable assumptions since the debris would be spread out to a certain extent, but there is no preferential pool flow direction during pool fill-up after the inactive and sump cavities have been filled.
- With the exception of debris washed directly to the sump strainers or to inactive areas, it was assumed that the fine debris that is not blown to upper containment would be uniformly distributed in the recirculation pool at the beginning of recirculation. This is a reasonable assumption, since the initial shallow flow at the beginning of pool fill-up would carry the fine debris to all regions of the pool.
- It was assumed that small pieces and large pieces of debris that are blown to the containment pool would be uniformly distributed inside the secondary shield wall for breaks inside the secondary shield wall. For breaks outside the secondary shield wall, it was assumed that small pieces of debris that are blown to the containment pool would be uniformly distributed outside the secondary shield wall, and large pieces would be distributed in the vicinity of the break location. This is a reasonable assumption since the small piece debris would be transported easily with the blowdown and pool fill flows, and since the large piece debris is less readily transported, this debris is likely to remain in the proximity of the break location.

Acceptance Criteria: No acceptance criteria were used for the initial debris distribution.

Results: The initial debris distribution at the start of recirculation is used to determine the recirculation transport. The recirculation transport fractions as well as the transport fractions during other phases of the event (blowdown, washdown, and pool fill) (13) are used as an input for the overall GSI-191 evaluation (12). The initial debris distributions that were used to determine the recirculation transport fractions are shown in Figure 2.5.14 through Figure 2.5.19.

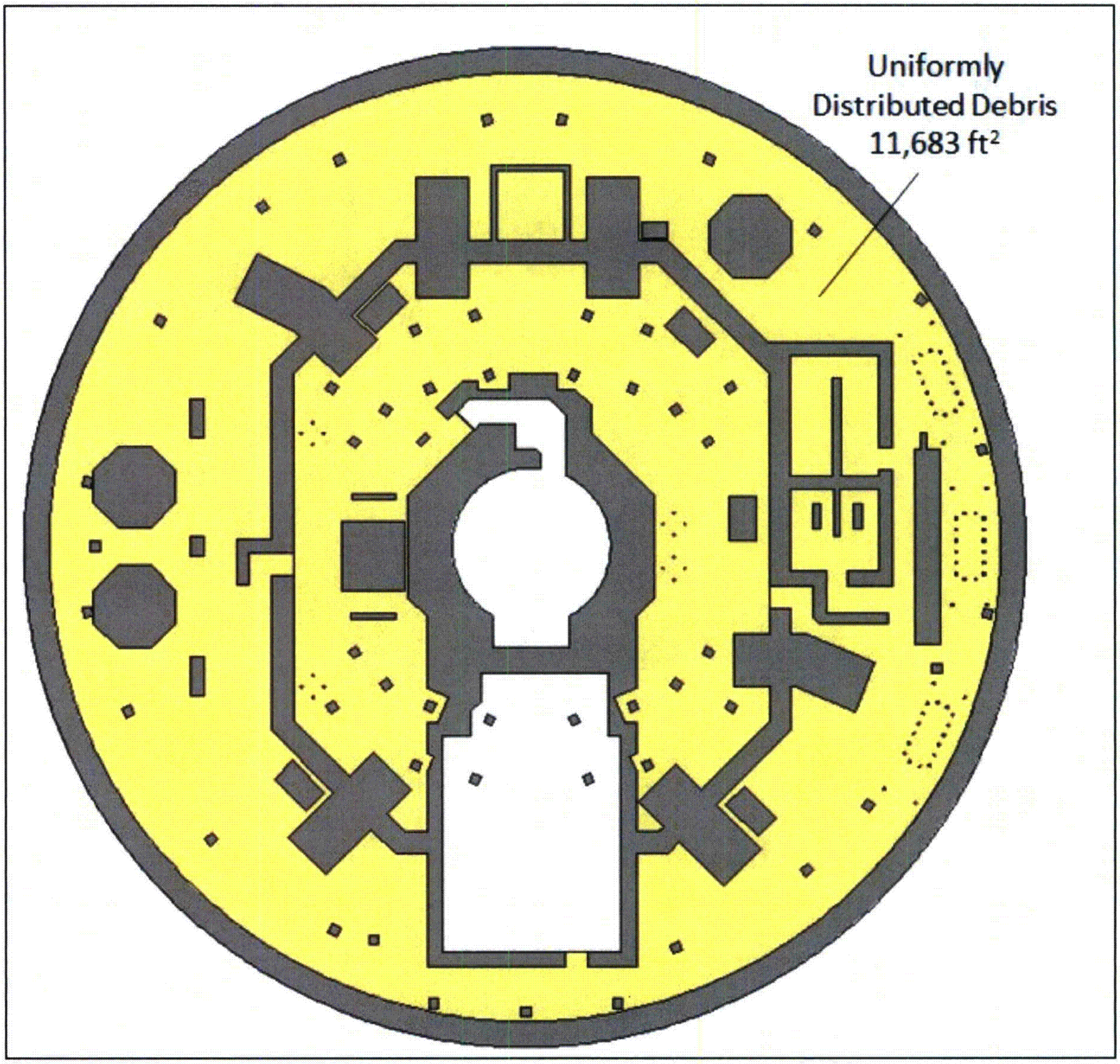

Figure 2.5.14 – Distribution of latent debris, unqualified coatings, and fines in lower containment

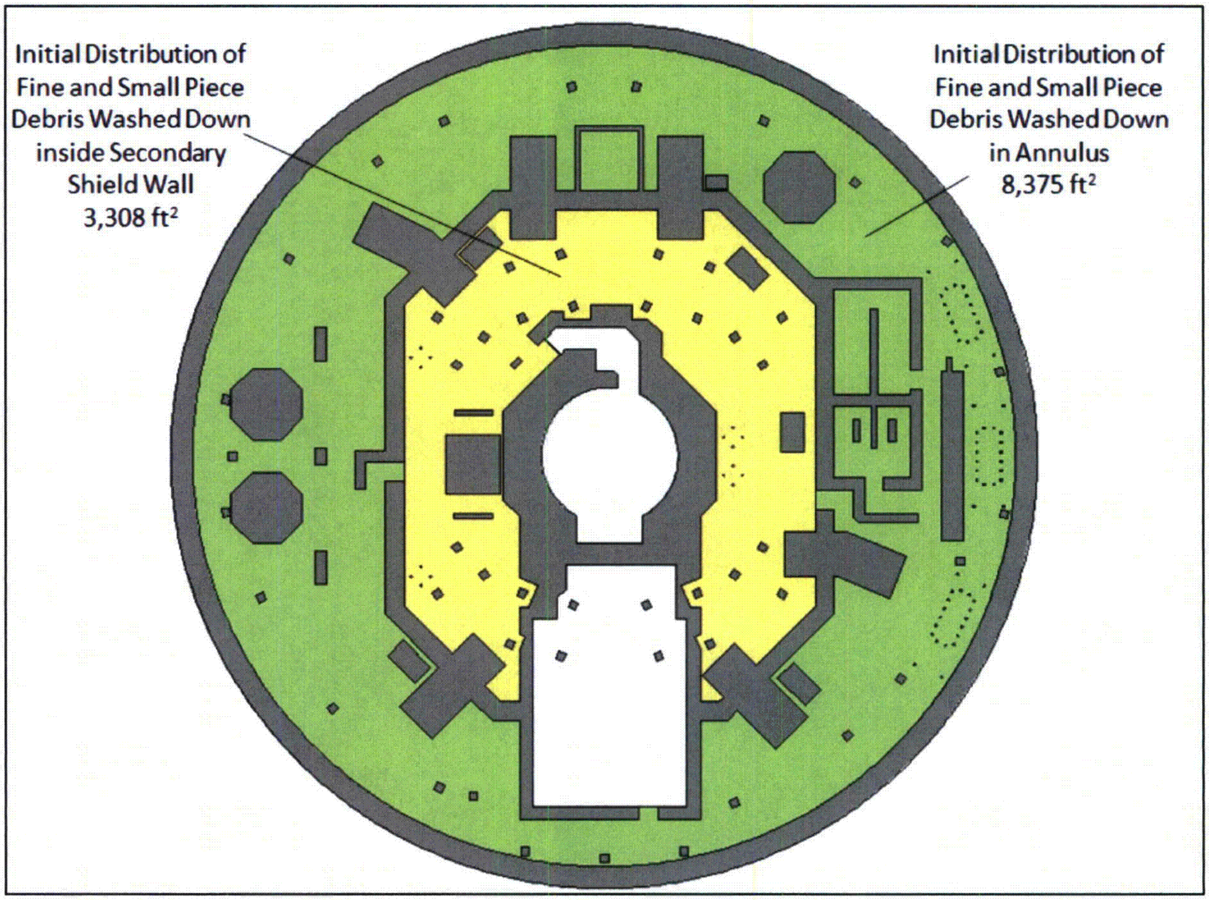

Figure 2.5.15 – Distribution of fines and small piece debris washed down from upper containment and the steam generator compartments

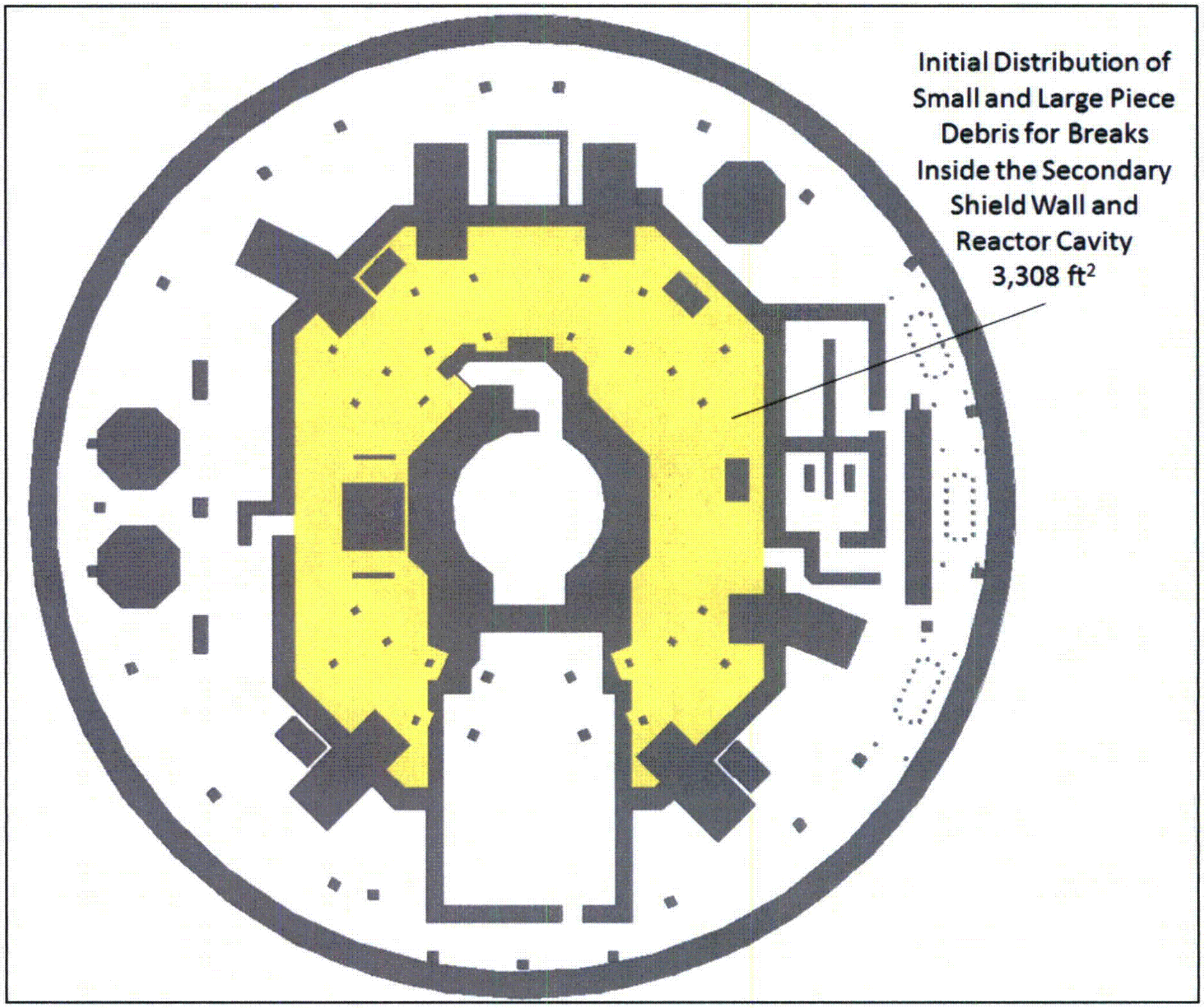

Figure 2.5.16 – Distribution of small & large piece debris in lower containment (breaks inside the secondary shield wall)

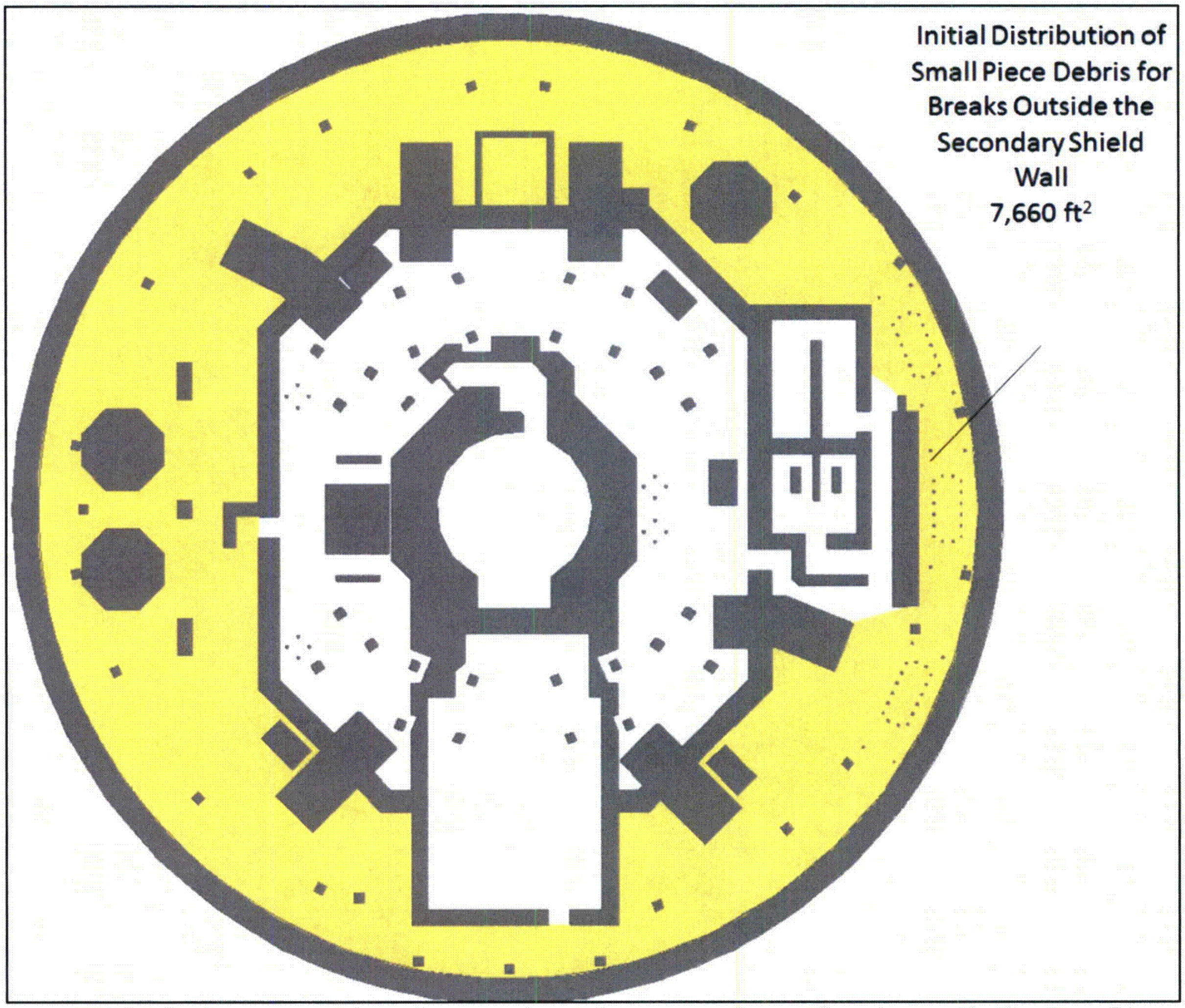

Figure 2.5.17 – Distribution of small piece debris in lower containment (breaks outside the secondary shield wall)

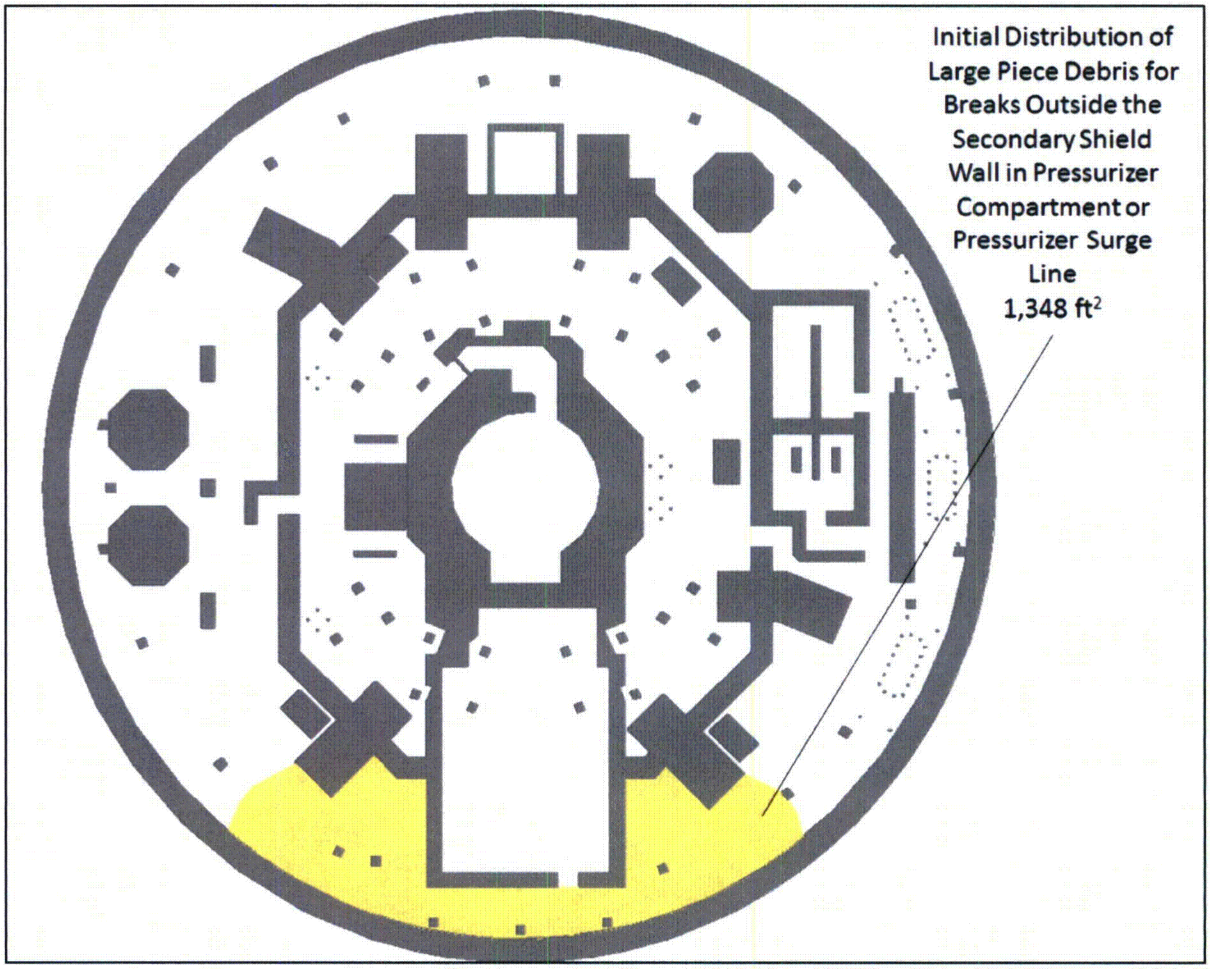

Figure 2.5.18 – Distribution of large piece debris in lower containment (breaks outside the secondary shield in pressurizer compartment and pressurizer surge line)

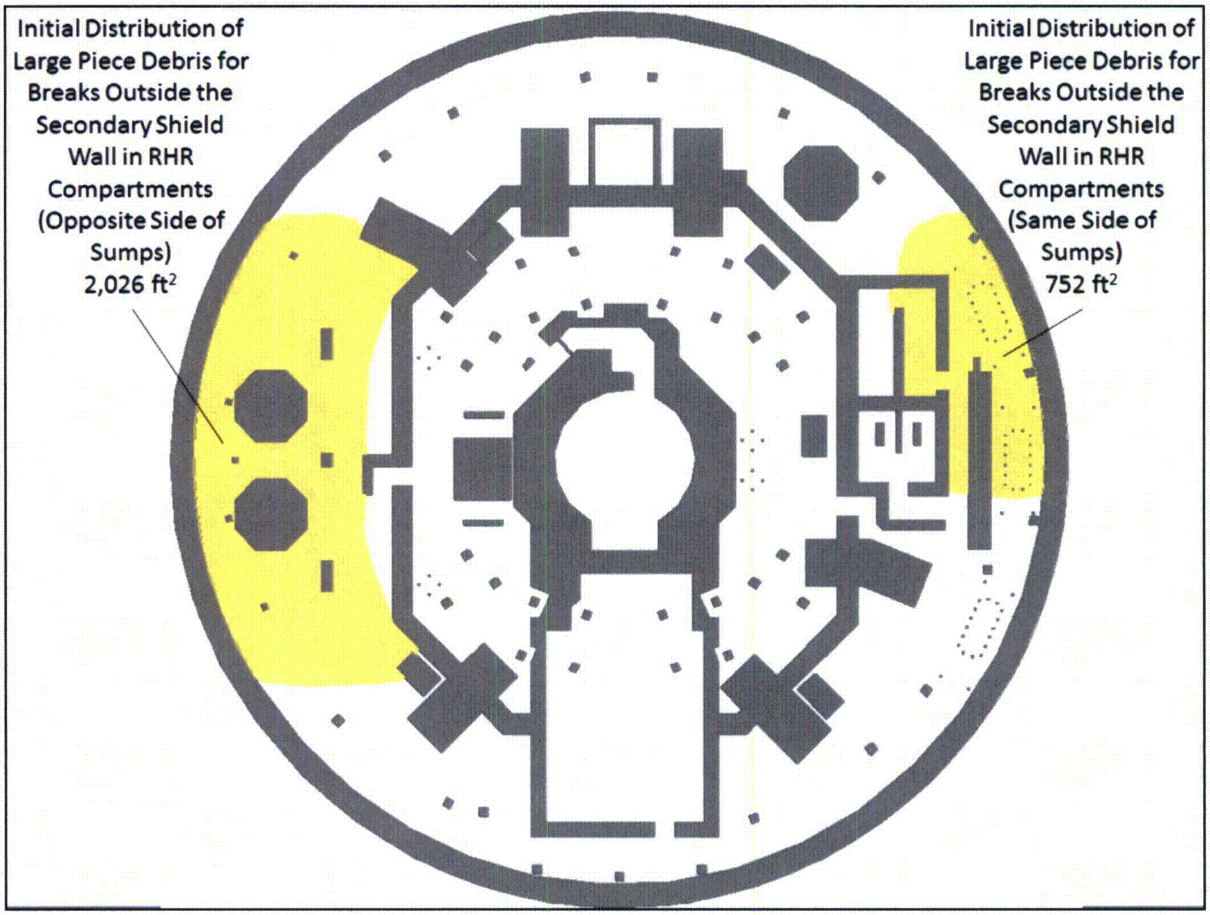

Figure 2.5.19 – Distribution of large piece debris in lower containment (breaks outside the secondary shield in RHR compartments)

Additional details on how the distributions are used to calculate the recirculation transport fractions are provided in the risk-informed debris transport calculation (13).

Additional details on how the recirculation transport fractions were incorporated in the overall GSI-191 evaluation are provided in Volume 3 (12).

Item 5.a.5: Time-Dependent Transport

Method: The methodology for determining time-dependent debris transport is documented in an engineering calculation based on plant-specific features and test data (13). The test data that was used for the time-dependent transport analysis includes the DDTS (14) and Alion erosion testing (18). The methodology includes the following steps:

1. The spray flow path of containment sprays to the pool was determined through the CAD model.

2. The areas and perimeters of each floor that the containment sprays came in contact with were calculated to determine how long containment spray flow would remain on a specific floor level, and if the velocities over the edge would be significant enough to transport debris from the operating deck to the pool level.
3. For each flow path, the number of gratings that flow would have to pass through was used to determine the fraction of debris that would reach the pool during washdown.

Basis: The following discussion provides a detailed description of how the methodology referred to above was used to develop the time-dependent transport (13).

The spray flow paths were determined in the CAD model, and are shown in Figure 2.5.20 through Figure 2.5.27.

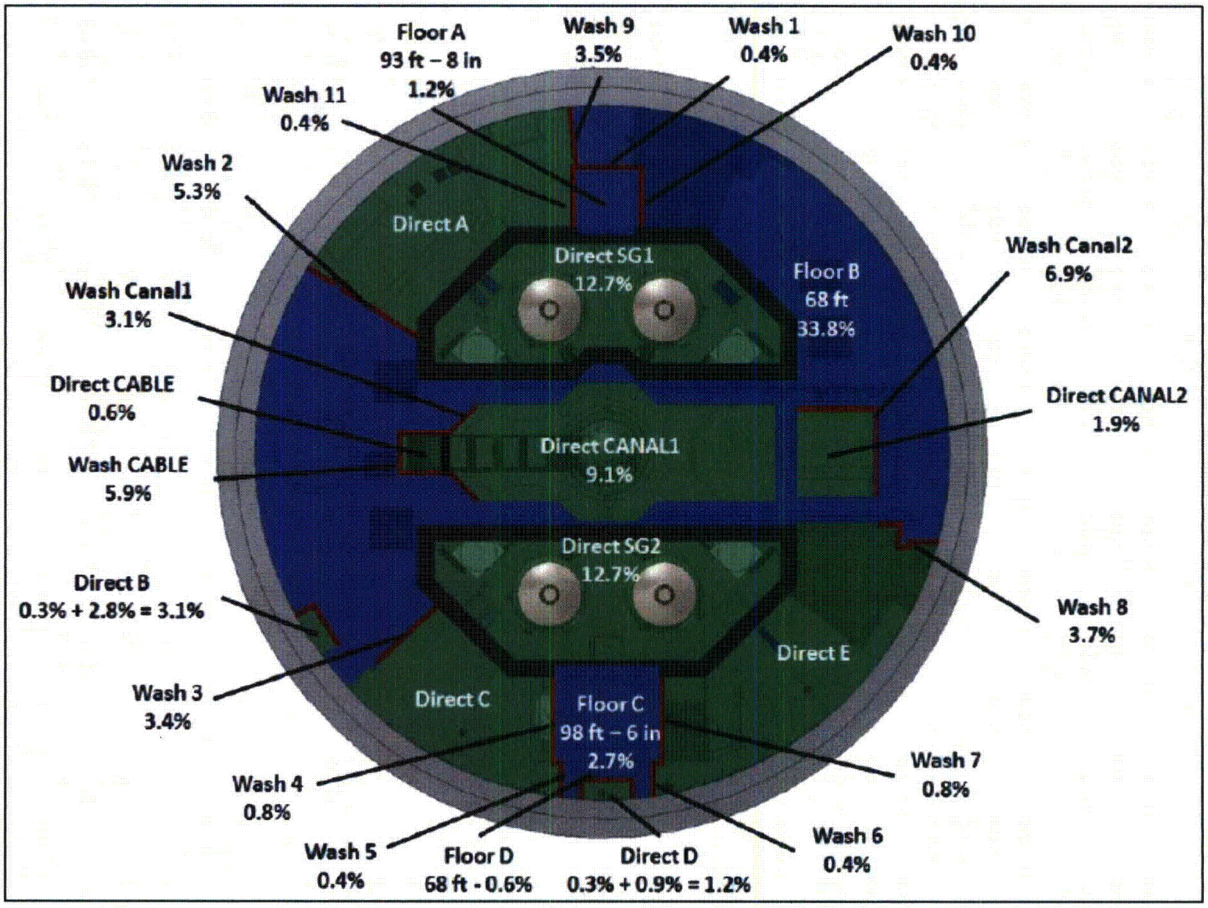

Figure 2.5.20 – 68' elevation spray flow distribution

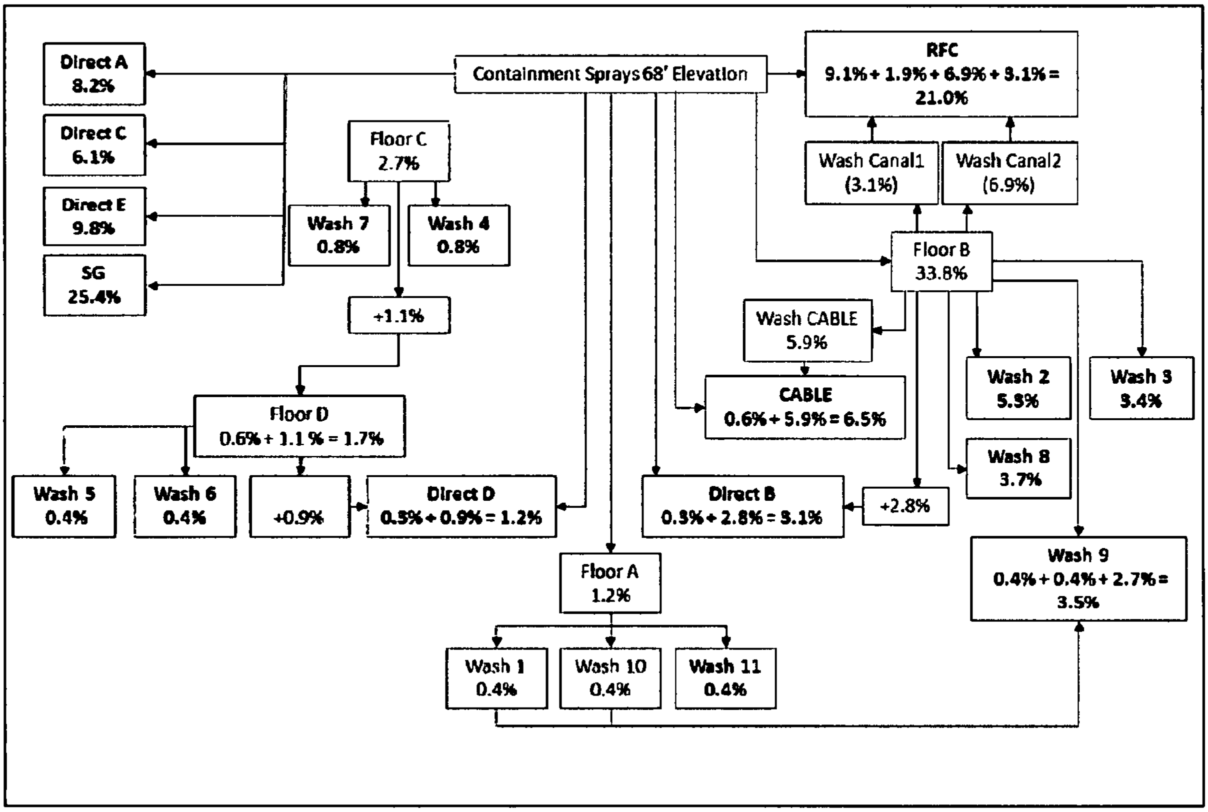

Figure 2.5.21 – 68' elevation spray flow flowchart

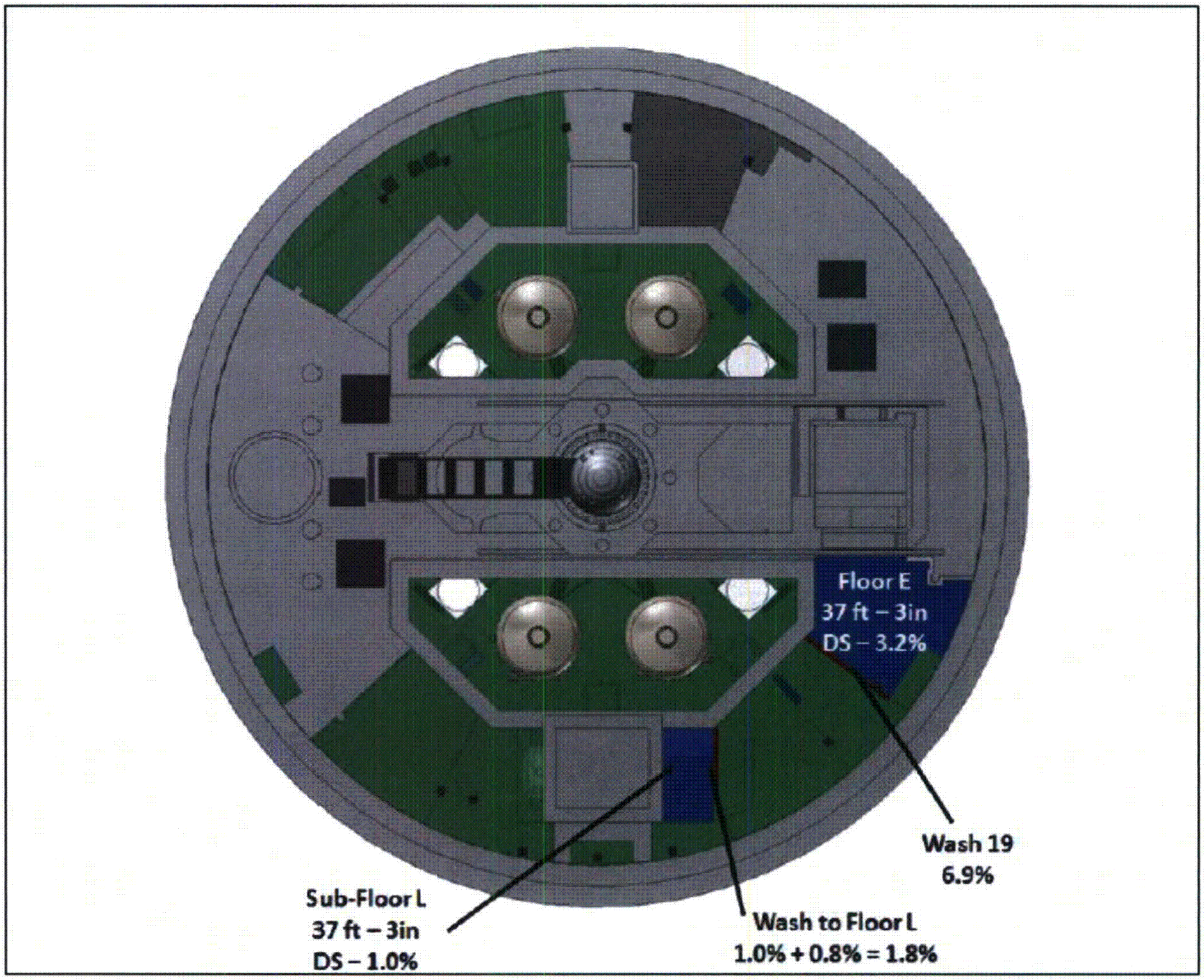

Figure 2.5.22 – 37'-3" elevation spray flow distribution

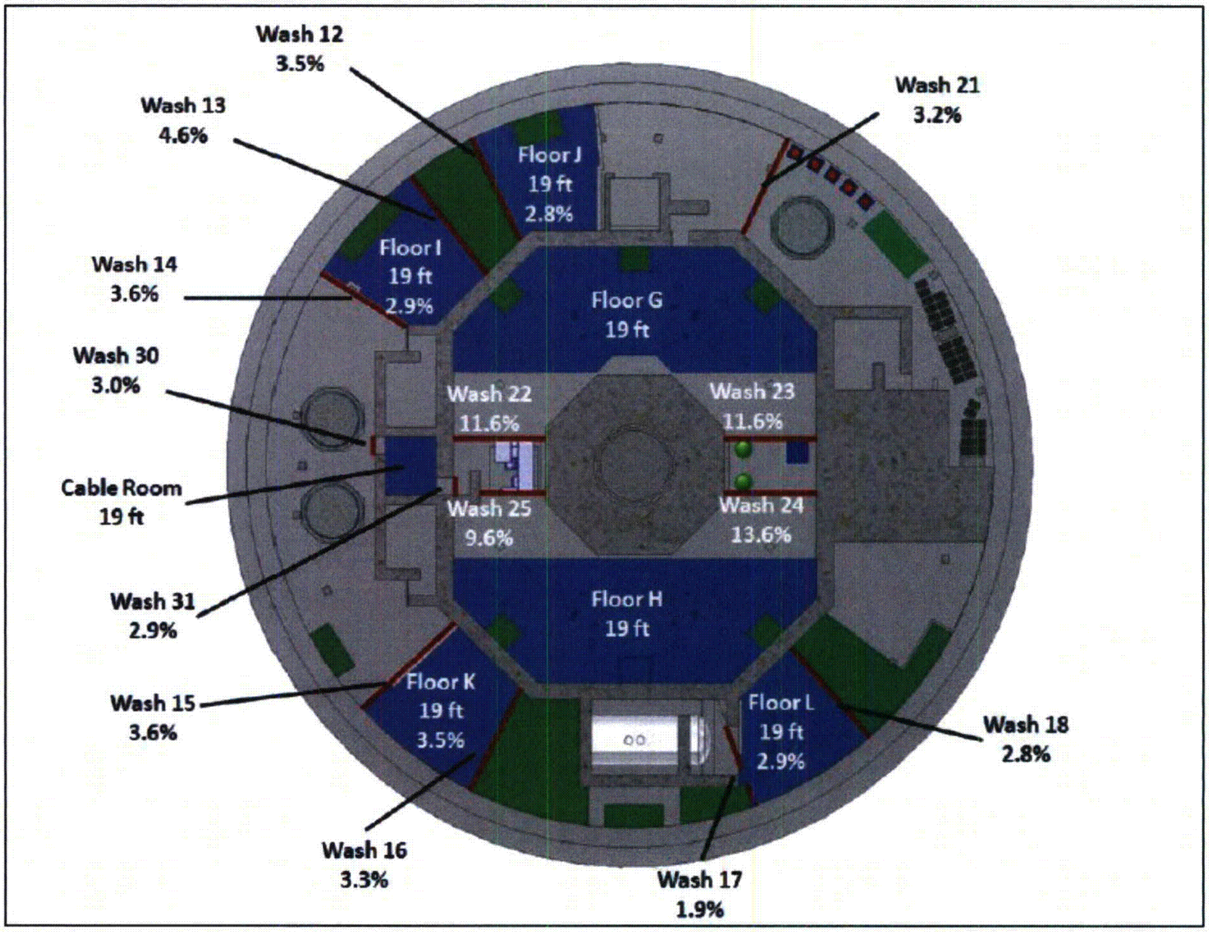

Figure 2.5.23 – 19' elevation spray flow distribution

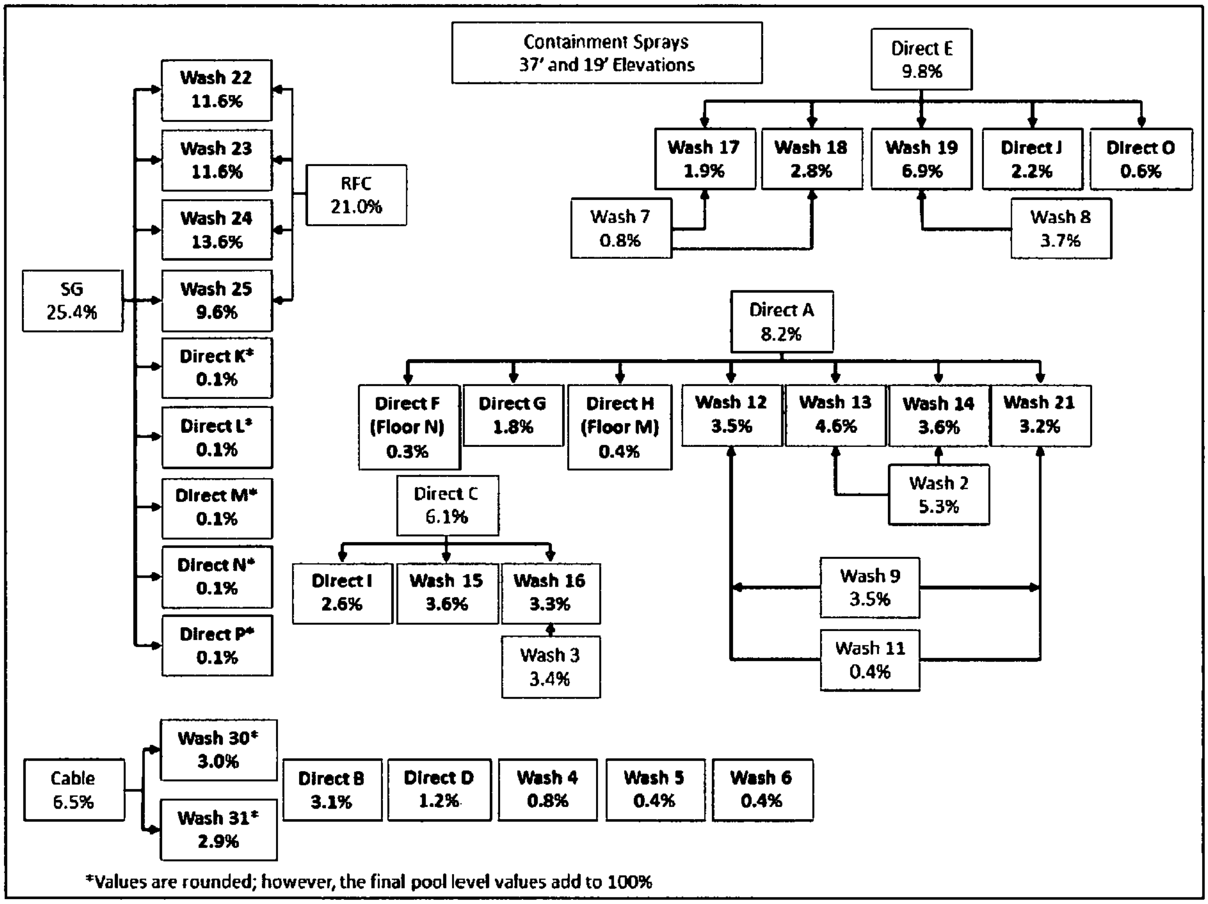

Figure 2.5.24 – 37'-3" and 19' elevation spray flow flowchart

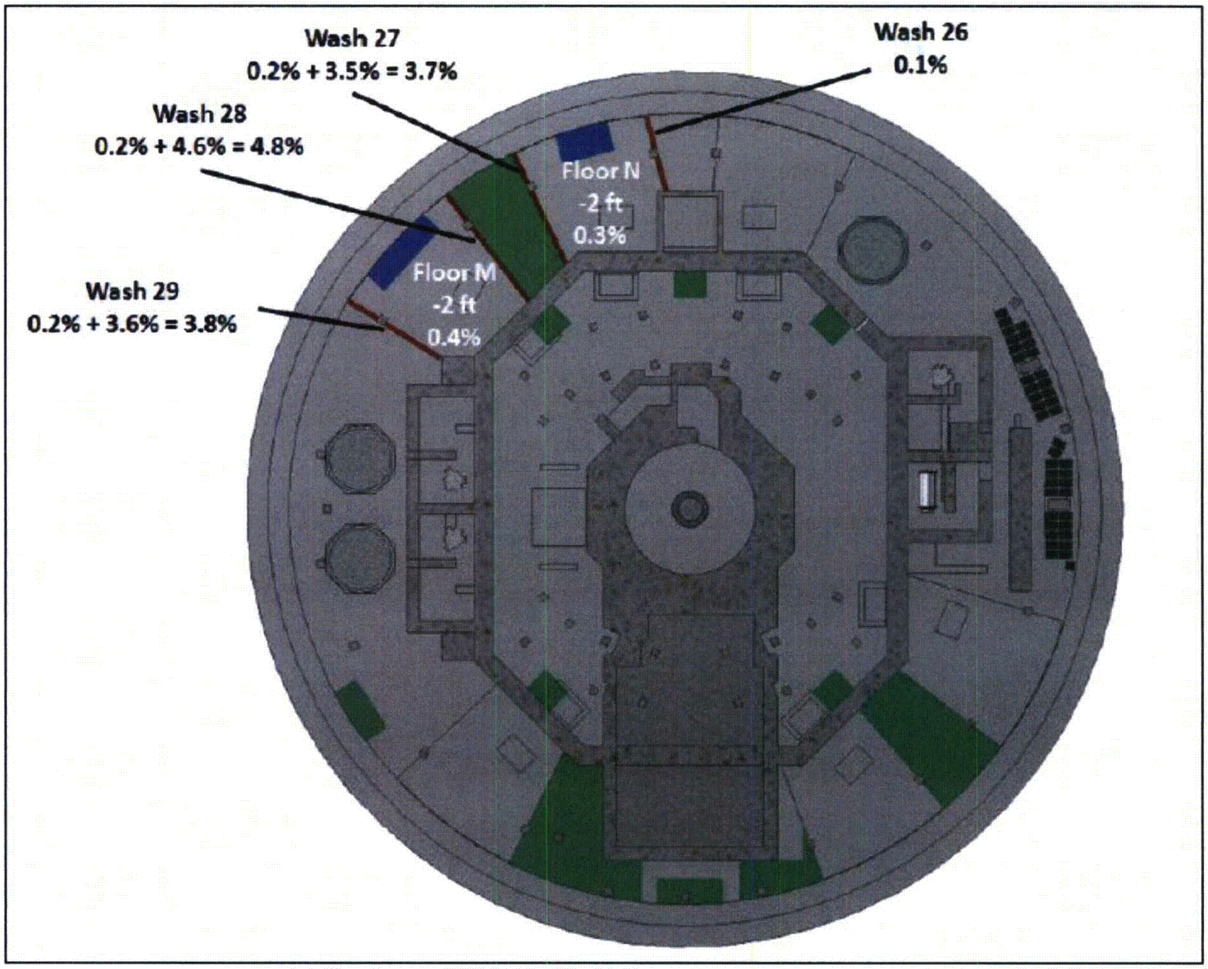

Figure 2.5.25 – (-)2' elevation spray flow distribution

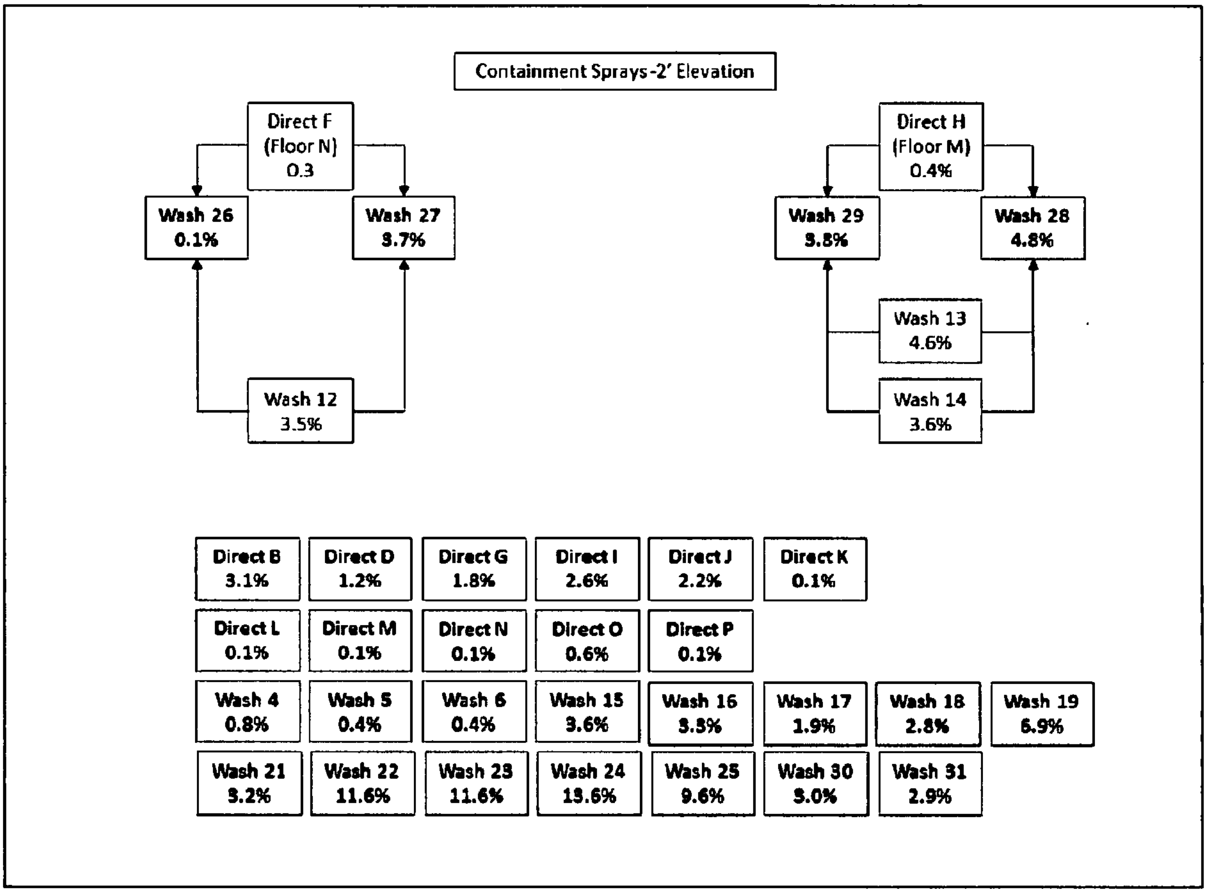

Figure 2.5.26 – (-)2' elevation spray flow flowchart

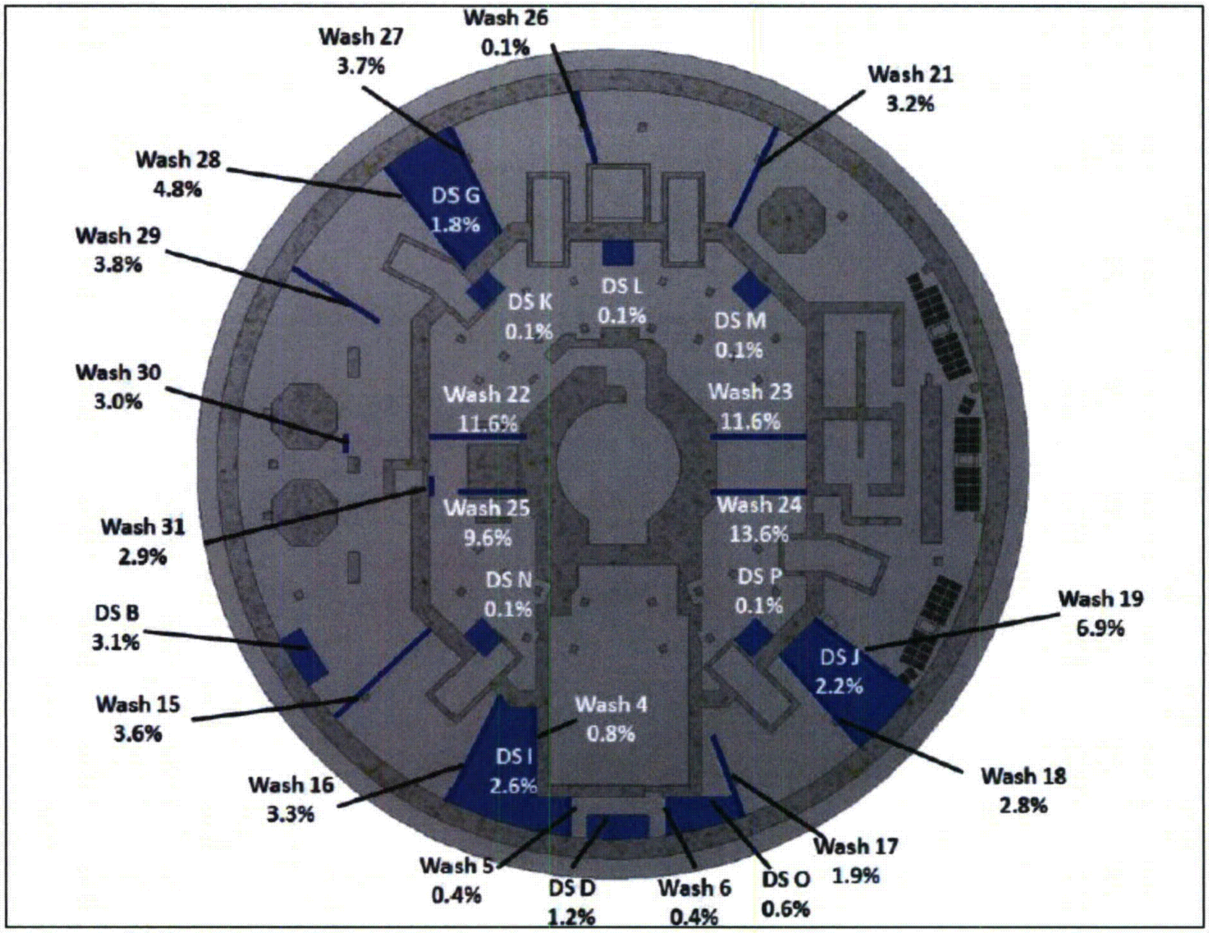

Figure 2.5.27 – Floor elevation spray flow distribution

During the washdown phase of a LOCA, debris would be transported down to the containment pool by operation of the containment spray system. Significant amounts of debris could, however, be captured on the concrete floors and grated areas above the containment floor as containment spray water transporting the debris drains through grating to reach the pool.

The containment sprays would drain to the pool via several flow paths over concrete decks and through grating at elevations 98'-6", 93'-8", 68', 52', 37'-3", 19', and (-)2'. The major flow split through the operating deck elevation (68') would be 24.3% to the refueling cavity, 74.5% off of the concrete operating deck into the annulus through grated openings, and 1.2% directly to the annulus through an opening without grating.

Since a percentage of the debris would land directly on concrete, it was necessary to determine whether it would be transported to the pool. The depth of water on the operating deck and subsequent concrete floors can be approximated as weir flow over a weir opening where the opening length is equal to the open perimeters. The following equation describes weir flow (19).

$$Q = 3.33 \cdot L \cdot H^{1.5}$$

Where Q is the flow rate, L is the perimeter of the floor, H is the height of water on the concrete, 3.33 is an experimentally obtained value with units of $ft^{1/2}/s$. The total perimeter around the operating deck (Floor B) is 198.05 ft. Since the total runoff flow to the operating deck for 3 train operation is 1,835 gpm (4.09 ft^3/s), the water height can be calculated as follows:

$$H = \left(\frac{Q}{3.33 \cdot L}\right)^{2/3} = \left(\frac{4.09\,ft^3/s}{3.33 \cdot 198.05\,ft}\right)^{2/3} = 0.034\,ft = 0.41\,in$$

Taking this depth, along with the flow perimeters and flow rate for 3 train operation, the average velocity on the operating deck would be approximately 0.61 ft/s.

The incipient tumbling velocity for small pieces of fiberglass is 0.12 ft/s (20). However, since this tumbling velocity is for 1" clumps of fiberglass completely submerged in water, the velocity required to tumble clumps of fiberglass sitting on the STP operating deck would be somewhat different since the depth of the water is not sufficient to fully submerge the debris pieces. Assuming that the small pieces of fiberglass on the operating deck are 1 inch clumps with dimensions of approximately 1" × 1" × ½", the clumps would be approximately 82% submerged in the 0.41" water level. As shown in the following calculations, the difference in the submergence level has a significant impact on the transportability of the fiberglass pieces.

The bulk density of Nukon is 2.4 lb_m/ft^3; the material density is 159 lb_m/ft^3 (21). Using the following porosity equation (22), along with an air density of 0.075 lb_m/ft^3 (23) gives the following porosity for Nukon:

$$\phi = \left(\frac{159\,lb_m/ft^3 - 2.4\,lb_m/ft^3}{159\,lb_m/ft^3 - 0.075\,lb_m/ft^3}\right) = 0.985$$

When saturated with water at 272 °F (density of 58.2 lb_m/ft^3), the bulk density of the fiberglass would be:

$$\rho_b = 159\,lb_m/ft^3 - 0.985\left(159\,lb_m/ft^3 - 58.2\,lb_m/ft^3\right) = 59.7\,lb_m/ft^3$$

The horizontal forces acting on the piece of fiberglass include the drag from the water flow (a function of the water velocity and the cross-sectional area of fiberglass), and the friction force between the fiberglass and concrete. The friction force is directly proportional to the normal force which is equal to the weight of the piece of fiberglass minus the buoyancy.

$$\sum F_{horizontal} = F\{velocity, area\} - F_{friction} = 0$$

$$F_{friction} = \mu \cdot N$$

$$N = Weight - Bouyancy$$

$$Weight = V \cdot \rho_b \cdot g$$

$$Bouyancy = V_{submerged} \cdot \rho_{water} \cdot g$$

Since the pieces of fiberglass on the STP operating deck would only be 82% submerged:

$$V_{submerged} = 82\% \cdot V$$

$$N_{submerged} = V \cdot \rho_b \cdot g - 82\% \cdot V \cdot \rho_{water} \cdot g = V \cdot g(\rho_b - 82\% \cdot \rho_{water})$$

And the ratio of the normal forces on a 82% submerged piece of fiberglass versus a fully submerged piece would be:

$$\frac{N_{Partially\ Submerged}}{N_{Fully\ Submerged}} = \frac{V \cdot g(\rho_b - 82\% \cdot \rho_{water})}{V \cdot g(\rho_b - \rho_{water})} = \frac{59.7\ lb_m / ft^3 - 82\% \cdot 58.2\ lb_m / ft^3}{59.7\ lb_m / ft^3 - 58.2\ lb_m / ft^3} = 8$$

Therefore, since the coefficient of friction between fiberglass and concrete would be constant, and the reduced cross-sectional area for a partially submerged piece of fiberglass can be conservatively neglected, an 8 times higher flow velocity would be required to tumble a piece of fiberglass that is 82% submerged compared to a piece of fiberglass that is fully submerged. Given that the incipient tumbling velocity for a fully submerged piece of fiberglass is 0.12 ft/s, a velocity of approximately 0.96 ft/s would be required to tumble the small pieces of fiberglass on the STP operating deck. Since this is more than 50% higher than the actual water velocity on the operating deck, the small fiberglass debris would not transport to the grated openings. This method can be applied to the other concrete floors between the operating deck and the containment floor as shown in Table 2.5.25.

Table 2.5.25 – Velocities and transportability for various floor levels

		1 TRAIN MAX		2 TRAIN MIN		2 TRAIN MAX		3 TRAIN MIN		3 TRAIN MAX	
FLOOR	ELEVATION	VELOCITY ft/s	TRANSPORT yes/no	VELOCITY ft/s	TRANSPORT yes/no	VELOCITY ft/s	TRANSPORT yes/no	VELOCITY ft/s	TRANSPORT yes/no	VELOCITY ft/s	TRANSPORT yes/no
A	93'-8"	0.27	NO	0.30	NO	0.33	NO	0.33	NO	0.36	NO
B	68'	0.49	NO	0.56	NO	0.60	NO	0.61	NO	0.66	NO
C	98'-6"	0.31	NO	0.35	NO	0.37	NO	0.38	NO	0.41	NO
D	68'	0.21	NO	0.25	NO	0.26	NO	0.27	NO	0.29	NO
E	37'-3"	0.61	NO	0.70	YES	0.74	YES	0.76	YES	0.82	YES
G	19'	0.73	YES	0.84	YES	0.89	YES	0.91	YES	0.98	YES
H	19'	0.77	YES	0.88	YES	0.94	YES	0.96	YES	1.03	YES
I	19'	0.49	NO	0.55	NO	0.59	NO	0.60	NO	0.65	NO
J	19'	0.46	NO	0.52	NO	0.56	NO	0.57	NO	0.61	NO
K	19'	0.45	NO	0.51	NO	0.55	NO	0.55	NO	0.60	NO
Sub Floor L	37'-3"	0.33	NO	0.38	NO	0.39	NO	0.41	NO	0.44	NO
L	19'	0.41	NO	0.47	NO	0.51	NO	0.52	NO	0.56	NO
M	(-)2'	0.17	NO	0.19	NO	0.21	NO	0.21	NO	0.24	NO
N	(-)2'	0.18	NO	0.20	NO	0.20	NO	0.20	NO	0.23	NO
CABLE	19'	0.84	YES	0.96	YES	1.02	YES	1.05	YES	1.13	YES

It is possible to approximate the time it takes for debris to transport from various floors to the pool level. It is simplest to split this time into two categories: the time it takes the debris to flow over concrete floors, and the time it takes to fall between floor levels.

The time it takes for water to drop between floor levels can be determined using the kinematic equations of motion with uniform acceleration, in conjunction with the terminal velocity of a water droplet (24). These times are not dependent upon flow rate and are listed in Table 2.5.26. Most notably, it takes 5.8 seconds for direct sprays to reach the pool level.

Table 2.5.26 – Falling times for containment sprays (s)

		Falling Elevation						
		143 ft	**98 ft 8 in**	**93 ft 8 in**	**68 ft**	**37 ft 3 in**	**19 ft**	**(-) 2 ft**
	98.67 ft	2.0						
	93.67 ft	2.2						
Landing	**68 ft**	3.0	1.5					
Elevation	**37 ft 3 in**	4.1	2.6	2.4	1.5			
	19 ft	4.7		3.0	2.1	1.1		
	(-) 2 ft	5.5						
	(-) 11 ft 3 in	5.8	4.2		3.2	2.1	1.5	0.8

The refueling canal and cavity have areas of hold-up that need to fill before sprays can wash through the canal drains to the 19' elevation. As these cavities are fairly large, the time to fill them would be considerably longer than the time it takes for sprays to follow the other flow paths, and since there are multiple flow sources to these areas, it is reasonable to estimate the fill times using the aggregate flow rates and cavity volumes. Table 2.5.27 shows the hold-up times for different containment spray rates.

Table 2.5.27 – Cavity fill times

			1 TRAIN MAX		2 TRAIN MIN		2 TRAIN MAX		3 TRAIN MIN		3 TRAIN MAX	
	Hold-up Volume ft^3	**% CS Flow**	**Flow Rate (ft^3/s)**	**Fill Time (min)**	**Flow Rate (ft^3/s)**	**Fill Time (min)**	**Flow Rate (ft^3/s)**	**Fill Time (min)**	**Flow Rate (ft^3/s)**	**Fill Time (min)**	**Flow Rate (ft^3/s)**	**Fill Time (min)**
Lower Internals	605	11.50%	0.67	15.0	0.99	10.2	1.20	8.4	1.27	7.9	1.58	6.4
Refueling Cavity	5545	7.50%	0.43	214.9	0.65	142.2	0.79	117.0	0.83	111.3	1.03	89.7

A steady state volume for each floor can be determined using the floor area and the water depth previously calculated. The time it takes to wash fines from a concrete floor can be estimated by doubling the time it takes to fill this steady state volume. That time is doubled so that there is time to fill the floor with enough water to spill over the edge, and then enough time for that entire volume of water to be replaced once. These times are tabulated in Table 2.5.28 for fine debris and in Table 2.5.29 for small piece debris. It should be noted that the spray flow from the reactor cavity was not included in the flow to Floors G & H, as the time of holdup in the cavity was much longer than the direct spray.

Table 2.5.28 – Time for fine debris to wash from specific concrete floors

			1 TRAIN MAX		2 TRAIN MIN		2 TRAIN MAX		3 TRAIN MIN		3 TRAIN MAX	
	Percent CS	Concrete Area (ft^2)	Flow Rate (ft^3/s)	Average Time (s)	Flow Rate (ft^3/s)	Average Time (s)	Flow Rate (ft^3/s)	Average Time (s)	Flow Rate (ft^3/s)	Average Time (s)	Flow Rate (ft^3/s)	Average Time (s)
Floor A	1.20%	197	0.07	37.1	0.10	33.0	0.13	30.3	0.13	30.3	0.17	27.5
Floor B	33.80%	6004	1.96	134.8	2.91	118.0	3.54	110.6	3.74	108.8	4.65	101.2
Floor C	2.70%	472	0.16	51.4	0.23	45.6	0.28	42.8	0.30	41.9	0.37	39.0
Floor D	0.60%	98	0.03	25.3	0.05	21.2	0.06	20.0	0.07	19.1	0.08	18.3
Floor E	6.90%	594	0.40	100.1	0.59	88.0	0.72	82.3	0.76	80.8	0.95	75.0
Floor G	23.20%	2184	1.34	157.1	2.00	137.6	2.43	128.9	2.57	126.5	3.19	117.8
Floor H	23.20%	2146	1.34	171.4	2.00	150.0	2.43	140.6	2.57	137.9	3.19	128.4
Floor I	8.20%	512	0.48	45.9	0.71	40.2	0.86	37.6	0.91	37.0	1.13	34.4
Floor J	6.70%	1082	0.39	105.4	0.58	92.5	0.70	86.9	0.74	85.1	0.92	79.3
Floor K	6.90%	614	0.40	55.6	0.59	48.7	0.72	45.5	0.76	44.8	0.95	41.6
Sub Floor L	1.00%	179	0.06	59.7	0.09	52.0	0.10	50.4	0.11	48.9	0.14	45.0
Floor L	4.70%	505	0.27	58.4	0.40	51.0	0.49	47.8	0.52	46.8	0.65	43.5
Floor M	0.40%	563	0.02	146.0	0.03	127.3	0.04	115.5	0.04	115.5	0.06	101.3
Floor N	0.30%	540	0.02	157.0	0.03	140.7	0.03	140.7	0.03	140.7	0.04	127.0
Cable Room	6.50%	146	0.38	49.4	0.56	43.4	0.56	40.7	0.72	39.9	0.9	37.0

Table 2.5.29 – Total time for small debris to transport to the pool

	Total Time to Pool		
Wash	**1 TRAIN (min)**	**2 TRAIN (min)**	**3 TRAIN (min)**
19	NA	1.8-10.5	1.7-9.7
22	8.1-56.4	6.9-49.5	6.3-45.6
23	8.1-56.5	6.9-49.6	6.3-45.7
24	8.9-57.2	7.4-50.2	6.8-46.1
25	8.9-57.2	7.4-50.2	6.8-46.1
30	2.8	2.3-2.5	2.2-2.3
31	2.8	2.3-2.5	2.2-2.3

Based on the DDTS testing, approximately 40-50% of small pieces of debris would pass through one level of grating (16). Due to the fact that many of the flow paths to the containment pool would pass through multiple levels of grating, it was assumed that 0-25% of small pieces would be held up on each additional grating level as shown in the following equation. It was conservatively assumed that 100% of fines would transport to the pool. For the purposes of calculating the transport fractions, it was assumed that the small pieces of debris passing through grating would be in the middle of the range, 45%.

$$F_{wash} = F_{CS} \cdot F_{WG} \cdot (1 - F_{AG})^{(N_{gratings} - 1)}$$

Where:

F_{CS} = fraction of debris washed down by containment sprays
F_{WG} = fraction of debris washed through first level of grating
F_{AG} = fraction of debris held up when washed through additional grating
$N_{gratings}$ = total number of gratings debris would pass through

Table 2.5.30 and Table 2.5.31 show the transport fractions of washdown to the pool for specific washes, and is separated into transport to the area inside the secondary shield wall and transport to the annulus.

Table 2.5.30 – Number of gratings and transport fractions for individual washes

Wash	Number of Gratings	Transport Fraction
19	5	0.94%
22	1	4.99%
23	1	4.99%
24	1	5.85%
25	1	4.13%
30	1	1.29%
31	1	1.25%
Total Inside SSW		21.21%
Total In Annulus		2.23%

Table 2.5.31 – Number of gratings and transport fractions for direct sprays

Direct Spray	Number of Gratings	Transport Fraction
B	4	0.56%
D	0	1.20%
G	5	0.24%
I	4	0.47%
J	5	0.30%
K	1	0.04%
L	1	0.04%
M	1	0.04%
N	1	0.04%
O	4	0.11%
P	1	0.04%
Total Inside SSW		0.20%
Total In Annulus		2.88%

Table 2.5.32 shows the ranges for the fraction of debris in upper containment and the steam generator compartments that would be expected to transport to the pool floor inside and outside the secondary shield wall during 1, 2, and 3 Train operation. Note that washdown transport fractions for the latent debris and degraded qualified coatings outside the ZOI were not quantified.

Table 2.5.32 – Total washdown transport fractions

Debris Type	Fines	Small Pieces			Unjacketed Large Pieces	Jacketed Large Pieces
		1 Train	2 Train	3 Train		
LDFG	100%	26%	26%	25%-26%	0%	0%
Microtherm	100%	26%	26%	25%-26%	NA	NA
Qualified Coatings (inside ZOI)	100%	26%	26%	25%-26%	NA	NA
Unqualified Miscellaneous Coatings (outside ZOI)	NA	NA	NA	NA	NA	NA
Unqualified Epoxy in Reactor Cavity (outside ZOI)	NA	NA	NA	NA	NA	NA
Dirt/Dust	NA	NA	NA	NA	NA	NA
Latent Fiber	NA	NA	NA	NA	NA	NA

For time-dependent washdown, Figure 2.5.28 through Figure 2.5.31 summarize the time it takes for containment sprays to reach the pool.

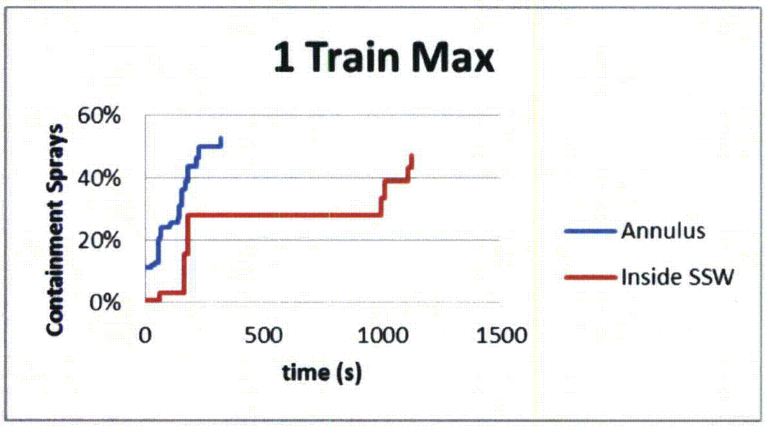

Figure 2.5.28 – Time for containment sprays to wash to pool for 1 train max operation

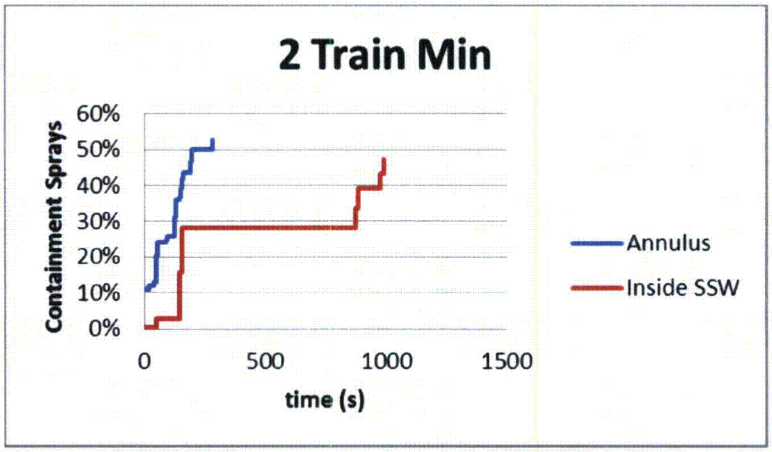

Figure 2.5.29 – Time for containment sprays to wash to pool for 2 train min operation

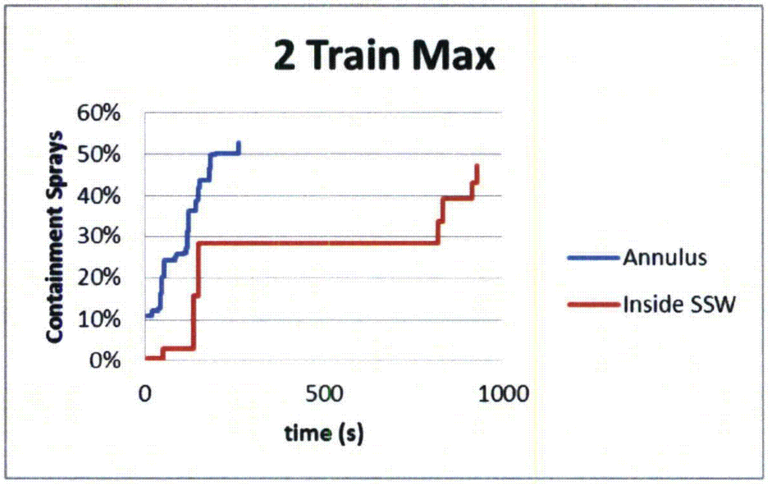

Figure 2.5.30 – Time for containment sprays to wash to pool for 2 train max operation

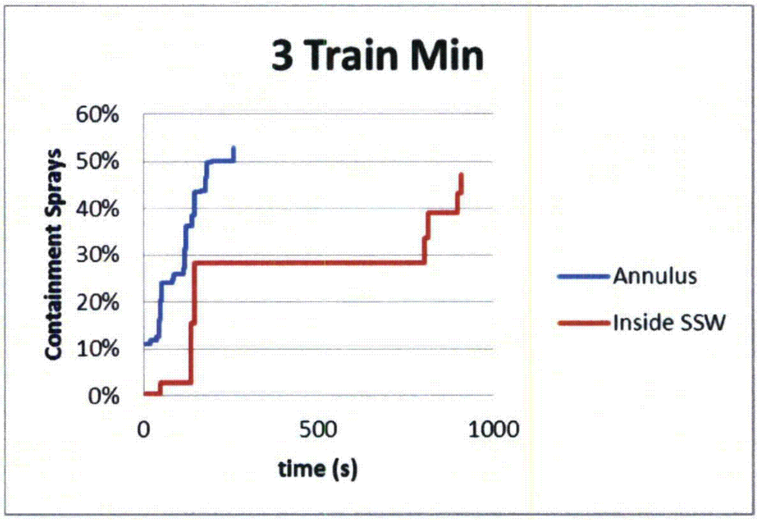

Figure 2.5.31 – Time for containment sprays to wash to pool for 3 train min operation

Assumptions: The following assumptions related to time-dependent transport were made in Volume 3 (12):

- It was assumed that debris washed down from upper containment reaches the pool after the inactive and sump cavities are filled, but before recirculation is initiated. This is a conservative assumption since it neglects transport of any washdown debris to inactive cavities during pool fill, but accelerates the time that debris would reach the strainer during the recirculation phase.
- It was assumed that the fine debris that is initially in the pool at the start of recirculation as well as the fine debris that transports to the pool during recirculation would be uniformly distributed in the pool. This is a reasonable assumption since the fine debris in lower containment prior to the start of recirculation would be well mixed in the pool as it fills, and the fine debris washed down from upper containment during recirculation would be well mixed due to the dispersed locations where containment sprays enter the pool.
- It was assumed that fiberglass debris erosion caused by flow in the pool or by containment sprays would occur prior to the start of recirculation. This is a conservative assumption since it accelerates the time that erosion fines would reach the strainers.
- It was assumed that all debris that penetrates the strainer and bypasses the core (either through the containment sprays or directly out the break) would immediately be transported back to the containment pool. This is a conservative assumption since it neglects potential hold-up of debris in various locations and neglects the time that it would take for debris to transport through the systems and wash back to the pool.

Acceptance Criteria: No acceptance criteria were used for the time-dependent transport analysis.

Results: Evaluating time-dependent transport requires an analysis of several different factors. The results of the analysis are summarized in Table 2.5.33 and Figure 2.5.32.

Table 2.5.33 – Time-dependent transport

Source	Time or Equation	Comments
Inactive Cavity Fill	t = ~0 s (no curbs around inactive cavity entrances)	Assume only applies for debris blown to pool and latent debris
Sump Strainer Fill	t ~ 425 s (based on a flow rate of 14,040 gpm and a pool volume of 13,325 ft^3)	Assume only applies to debris blown to pool and latent debris
Total Fill (Switchover)	t ~ 20 min (LBLOCA)	
Initial Washdown	6 s – 1000 s (fines); 2 min – 50 min (small pieces)	Assume washdown occurs after inactive and sump cavities are filled, but before recirculation is initiated
Unqualified Coatings Failure	0 min – 30 days	Conservatively introduced at a constant rate from 10 minutes to 36 hours
Recirculated Spray Flow Debris Washdown	t ~ 300s	Assume instant washdown
Recirculated Break Flow Debris Washdown	t < 300s	Assume instant washdown
Spray Erosion Washdown	t < 15 min	Assume during pool fill
Pool Erosion Recirculation	0-30 days	Assume during pool fill
Initial Debris in Pool at start of recirculation (x_i)	x_i = blowdown + initial washdown - pool fill	Total debris in pool from blowdown and initial washdown minus the debris transported to inactive cavities or the strainer during pool fill
Debris Recirculation Time (x(t))	Described in Section 5.8 of Volume 3	Based on arrival time, flow rate, pool volume, debris penetration, and core bypass.

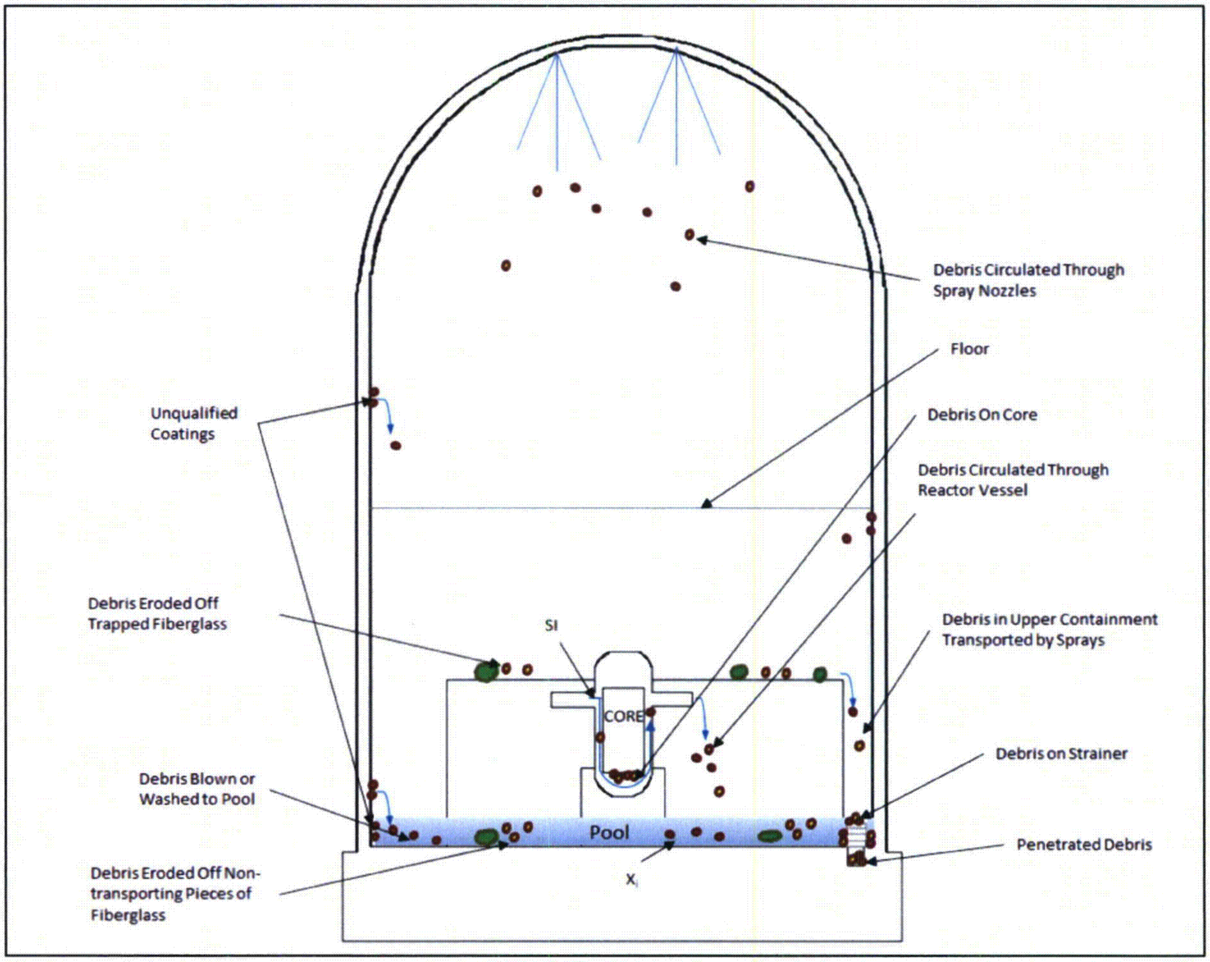

Figure 2.5.32 – Illustration of time-dependent transport

Additional details on how the time-dependent transport was incorporated in the overall GSI-191 evaluation are provided in Volume 3 (12).

Item 5.a.6: Corrosion and Dissolution Model

Method: One of the goals of the STP chemical effects test program was to develop a new corrosion and dissolution release model specific to STP conditions. However, this model was not fully developed for the submittal. Instead, the material release for aluminum, silicon, and calcium was calculated for a series of scenarios and documented in an engineering calculation based on plant-specific conditions (25). The scenarios that were evaluated included small, medium, and large breaks ranging from 1.5 inches to 27.5 inches, a range of fiberglass debris quantities from 0 ft^3 to 2,385 ft^3, and a range of water volumes from 1,775,000 L to 2,255,000 L. The analysis also looked at a range of pH profiles from minimum to maximum conditions and a range of temperature profiles from nominal to maximum conditions. The total quantity of Al, Si, and Ca released for each scenario was determined based on the release equations developed through bench-top testing as documented in WCAP-16530-NP (26). The solubility limit for aluminum and calcium products was estimated for specific conditions based on limited thermodynamic modeling. These solubility limits were compared to the release quantities to determine which scenarios would result in a chemical product. The way this information was used to address chemical effects in the overall analysis is described in more detail in Volume 3 (12).

Basis: The approach for calculating the release of aluminum, silicon, and calcium is based on the standard deterministic methodology in WCAP-16530-NP, which has been approved by the NRC (27). The determination of whether a chemical product would form was based on a combination of engineering judgment and limited thermodynamic modeling. The total quantity of material released was not assumed to fully precipitate into chemical products. Instead, solubility limits of chemical products expected to form (28) were calculated as a function of temperature and pH using Visual MINTEQ to determine the lowest concentration of metal required for product formation from the range of selected conditions. Sodium aluminum silicate and aluminum oxyhydroxide are the aluminum products described as possible precipitates in WCAP-16530-NP; however only the aluminum hydroxide solubility limit (Log K of 10.8 (29)) was considered in this analysis since it was determined as a suitable substitute for sodium aluminum silicate in head loss testing (28). Calcium phosphate (Log K of -28.25 (29)) solubility limits were also evaluated.

The lowest concentration of metals required to form these chemical products were determined by identifying the lowest solubility over the pH range of 7.0 to 7.3 at a defined temperature. Different temperature bounds were required for this evaluation because a decrease in temperature results in a decrease of aluminum product solubility over the given pH range as seen in Figure 2.5.33; while it produces an increase in calcium product solubility over the same pH range as seen in Figure 2.5.34. The temperature bound for aluminum product solubility was set at 140 °F (60°C) since this temperature has been used by U.S. nuclear power plants in past analyses. The temperature bound for the calcium product solubility was set at 185°F (85°C). The chosen bound was lower than the LOCA peak temperatures because these peaks occur over a very short duration (minutes) of a 30-day event and return to temperatures ≤185°F (85°C) for appreciable durations before declining (30; 31). Using this approach, the concentration of aluminum expected to result in formation of a chemical product is approximately 4.9 mg/L. The calcium concentration expected to result in the formation of a chemical product was 0.8 mg/L. These values were used to assess the presence of chemical product formation from the calculated material release.

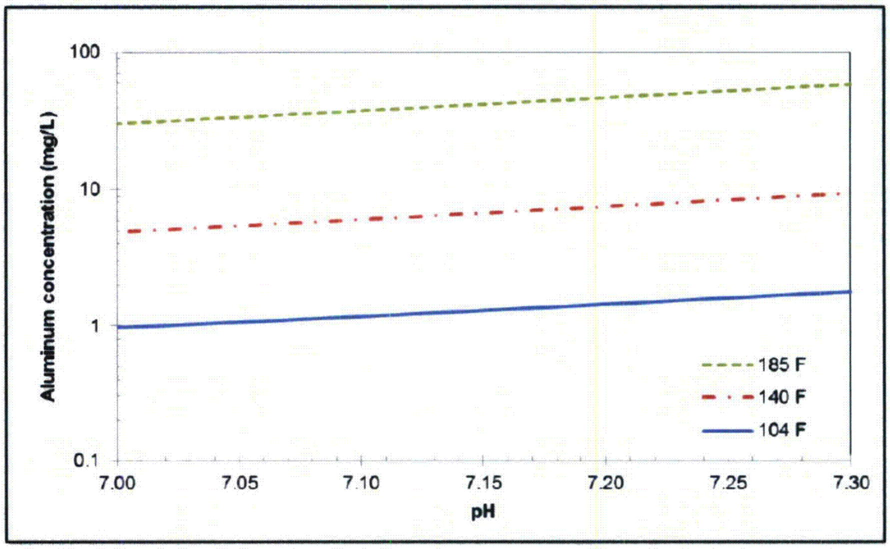

Figure 2.5.33 – Aluminum Hydroxide Solubility in Borated-TSP Solution

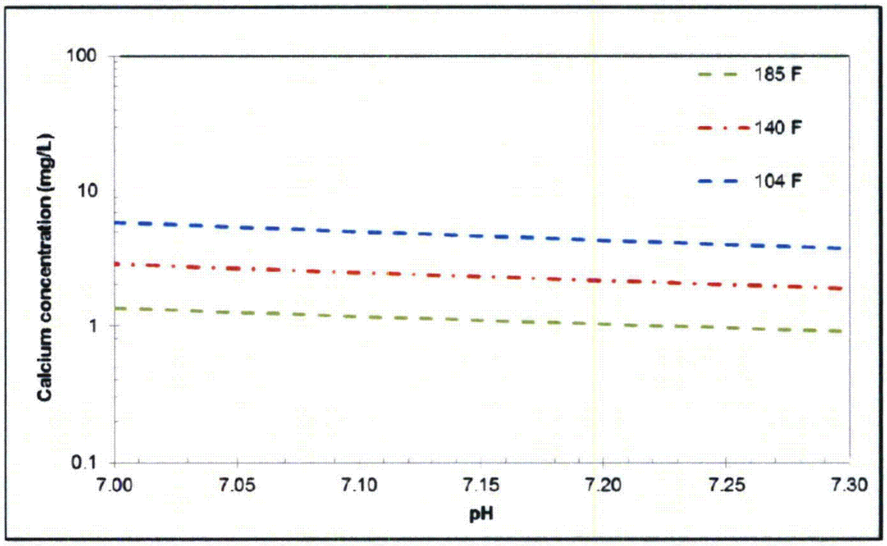

Figure 2.5.34 – Calcium Hydroxide Solubility in Borated-TSP Solution

Assumptions: The following assumptions were made as part of the chemical release analysis (25):

- The nominal temperature profiles, which were generated for the first 10 hours from the thermal-hydraulic analysis (32), were estimated from 10 hours to 30 days by linearly interpolating between the final simulation temperatures at 10 hours to a temperature of 110 °F at 30 days. This gives a conservatively high temperature profile for the majority of the event, which maximizes the total release quantities.

- Although a zinc (Zn) product was observed to form under STP LOCA test conditions, it was not included in this analysis since the product was determined to be crystalline and mainly adhere to structures within containment as opposed to readily travel with solution (33).

Acceptance Criteria: A chemical product was judged to form for scenarios where the aluminum concentration is greater than 4.9 mg/l or the calcium concentration is greater than 0.8 mg/l (25).

Results: For nominal temperature profiles, chemical products (aluminum and calcium precipitates) were not predicted to form for any of the small breaks evaluated. However, some of the medium and large break cases evaluated had total aluminum concentrations that were approximately equal to or slightly higher than the estimated solubility limits (25). The calcium concentration was relatively high for cases where a maximum fiberglass quantity of 2,385 ft^3 was assumed. However, for cases with 60 ft^3 of fiber or less, the calcium concentration was approximately equal to the solubility limit (25). As discussed in Volume 3, the quantity of fiberglass insulation debris generated was less than 10 ft^3 for 99.9% of the scenarios evaluated (12). This indicates that even if chemical products form for the nominal scenarios, the effects on strainer head loss would be relatively benign. An evaluation of the chemical concentrations for a maximum temperature profile, however, indicated that the concentration of aluminum would be significantly higher (on the order of 20 times greater than the nominal scenarios). It is possible that these scenarios could result in significant chemical head loss. However, the maximum temperature profiles were developed based on a highly unlikely scenario where the CCW temperature is at the maximum level, four out of six fan coolers fail to operate, and all of the RHR heat exchangers fail (32). Extreme temperature profiles like this have not been fully evaluated yet, so the current limited testing does not completely preclude the possibility that chemical products may form and arrive at a debris-laden strainer in sufficient quantity to cause unacceptable head loss. The detailed results of the chemical release analysis are shown in Table 2.5.34 for the nominal temperature profiles.

Table 2.5.34 – Nominal temperature profile material release results

Case	pH	Fiber Quantity	Water Volume	Break Size (in)	Ca (mg/l)	Si (mg/l)	Al (mg/l)	Product
1	Min	Min	Min	1.5	0.2	1.7	1.3	-
				2	0.2	1.7	3.5	-
				4	0.3	2.8	4.3	-
				6	0.3	2.8	1.7	-
				8	0.9	8.4	1.3	Ca only
				15	0.9	7.2	1.1	Ca only
				27.5	0.9	7.7	1.1	Ca only
2	Min	Min	Max	1.5	0.1	1.4	1.1	-
				2	0.1	1.4	2.9	-
				4	0.2	2.3	3.6	-
				6	0.2	2.3	1.5	-
				8	0.8	7.0	1.1	-
				15	0.8	6.2	0.9	-
				27.5	0.8	6.6	0.9	-

Case	pH	Fiber Quantity	Water Volume	Break Size (in)	Ca (mg/l)	Si (mg/l)	Al (mg/l)	Product
3	Min	Max	Min	1.5	0.3	2.9	1.4	-
				2	0.3	2.9	3.6	-
				4	0.9	8.4	4.5	Ca only
				6	0.9	8.4	1.8	Ca only
				8	30.0	161.5	2.6	Ca only
				15	25.0	41.6	1.5	Ca only
				27.5	30.0	72.4	1.7	Ca only
4	Min	Max	Max	1.5	0.3	2.4	1.1	-
				2	0.3	2.4	2.9	-
				4	0.8	7.0	3.8	-
				6	0.8	7.0	1.5	-
				8	25.0	154.5	2.3	Ca only
				15	25.0	37.5	1.3	Ca only
				27.5	25.0	65.9	1.5	Ca only
5	Max	Min	Min	1.5	0.2	1.7	1.6	-
				2	0.2	1.7	4.1	-
				4	0.3	2.8	5.0	Al only
				6	0.3	2.8	2.1	-
				8	0.9	8.4	1.5	Ca only
				15	0.9	8.0	1.3	Ca only
				27.5	0.9	8.4	1.3	Ca only
6	Max	Min	Max	1.5	0.1	1.4	1.3	-
				2	0.1	1.4	3.4	-
				4	0.2	2.3	4.2	-
				6	0.2	2.3	1.7	-
				8	0.8	7.0	1.3	-
				15	0.8	6.9	1.1	-
				27.5	0.8	7.0	1.1	-
7	Max	Max	Min	1.5	0.3	2.9	1.6	-
				2	0.3	2.9	4.1	-
				4	0.9	8.4	5.3	Ca and Al
				6	0.9	8.4	2.2	Ca only
				8	30.0	173.1	2.9	Ca only
				15	26.4	45.4	1.7	Ca only
				27.5	30.0	78.6	2.0	Ca only
8	Max	Max	Max	1.5	0.3	2.4	1.3	-
				2	0.3	2.4	3.4	-
				4	0.8	7.0	4.4	-
				6	0.8	7.0	1.8	-
				8	25.0	167.3	2.6	Ca only
				15	25.0	41.2	1.5	Ca only
				27.5	25.0	72.0	1.7	Ca only

The analysis was repeated using the maximum temperature profile for 6-inch breaks. As shown in Table 2.5.35, the release quantities were significantly larger for the higher temperature conditions based on the higher release rates.

Table 2.5.35 – Maximum temperature profile material release results

Case	pH	Fiber Quantity	Water Volume	Break Size (in)	Ca (mg/l)	Si (mg/l)	Al (mg/l)	Product
1	Min	Min	Min	6	0.3	2.8	37.0	Al only
2	Min	Min	Max	6	0.3	2.3	30.8	Al only
3	Min	Max	Min	6	0.9	8.4	37.6	Ca and Al
4	Min	Max	Max	6	0.8	7.0	31.3	Al only
5	Max	Min	Min	6	0.3	2.8	41.8	Al only
6	Max	Min	Max	6	0.3	2.3	34.9	Al only
7	Max	Max	Min	6	0.9	8.4	42.4	Ca and Al
8	Max	Max	Max	6	0.8	7.0	35.4	Al only

Additional details on the methodology and basis for the chemical release and product formation analysis are provided in the material release calculation (25).

Additional details on how this analysis was incorporated in the overall GSI-191 evaluation are provided in Volume 3 (12).

Item 5.a.7: Basis for Excluding any Plant Materials from Chemical Testing

The potentially relevant materials not included in the large break LOCA integrated chemical effects test (33) include copper, lead, carbon steel, Microtherm, alkyd coatings, and epoxy coatings. The basis for excluding these plant materials from the chemical effects testing is described below.

Copper: Various sources of copper are found in containment at STP. These sources include wiring, cables, and tubes of the fan coolers (34). While copper is present in STP containment, none of it will be submerged during a LOCA. In addition, significant quantities of the unsubmerged copper will be protected from spray impingement. Copper cable and wiring will not be subjected to spray as long as some insulation is in place. As a result of all these factors, copper was excluded from the long-term CHLE tests.

Lead: Lead exists in STP containment in two forms: (1) lead blankets in storage containers and (2) permanently installed lead blankets on piping. There are approximately 500 lead blankets (1 ft x 3 ft) in storage containers (45% are submerged and 55% not submerged) (34). The equivalent thickness for a lead sheet in the blanket is 3/16" (34). These lead blankets are stored in drums with holes to prevent them from floating if containment floods, but the sources of lead are sealed within vinyl-laminated nylon covers which provide a protection barrier between the material and pool solution.

The permanently installed lead blankets are sparsely present on only three pipes in containment. The probability that these blankets will be in the zone of influence is relatively low (34). Since the contribution of lead from the pipe insulation is not a likely occurrence in a LOCA, the probable contribution from this material to the pool solution was neglected.

Carbon Steel: Uncoated carbon steel is generally present in containment as structural supports. While there is a significant amount of carbon steel in containment, previous research found that carbon steel corrosion occurred in insignificant amounts (35). The ICET tests contained 0.15 ft^2/ft^3 of carbon steel, with 34 percent of the material submerged and 66 percent in the vapor space. The unsubmerged uncoated steel coupons had very little change in weight, with changes ranging from +1.3 to -0.4 g, compared to a mean pre-test weight of 1025 g. The submerged uncoated steel coupons in Test #1 (high pH) had a weight change of -23.3 g, but had very little weight change in the remainder of the tests (ranging from +1.4 to -1.1 g). In ICET Test #2, which corresponded most closely to the STP conditions, the unsubmerged coupons gained 1.3 g and the submerged coupons gained 1.4 g of weight. Iron concentrations remained nearly undetectable throughout the full duration of all the ICET tests. The highest concentrations of iron were less than 0.1 mg/L, during the first few days of ICET Test #3. Iron was undetectable during the entire ICET Test #2. Based on these results, uncoated carbon steel was not included in the CHLE tank tests.

Microtherm: Microtherm was excluded from the CHLE tank tests due to the relatively insignificant quantity in containment (36).

Alkyd Coatings: Alkyd coatings were excluded from the CHLE tank tests based on testing that indicated that the coatings would not play a significant role in the creation of chemical precipitates (6).

Epoxy Coatings: Similar to the alkyd coatings, epoxy coatings were excluded from the CHLE tank tests based on testing that indicated that the coatings would not play a significant role in the creation of chemical precipitates (26; 37; 38).

Item 5.a.8: Chemical Precipitation Model

The methodology, basis, and results for the chemical precipitation model are described in the response to Item 5.a.6.

Item 5.a.9: Chemical Effects Phenomena Identification and Ranking Table

The following discussion provides details of the specific PIRT issues and how they were addressed. The italicized text was copied directly from the NRC's March 2011 report describing each of the issues (39).

PIRT Item 1.1: RCS coolant chemistry conditions at break

The reactor coolant system (RCS) coolant chemistry varies over the fuel cycle. Boron concentrations vary from approximately 2,000 to 4,000 parts per million (ppm) at the beginning of the fuel cycle to approximately 50 ppm at the end of the fuel cycle. Therefore, the initial reactor water chemistry spewing out of the break and forming the containment pool will have variable boron concentration while the ratio of lithium to boron is approximately constant. The two-phase jet emanating from the break is initially at 315 degrees Celsius (C) (599 degrees Fahrenheit (F)) and then cools to 120 degrees C (248 degrees F). The main concern raised by the peer reviewers relates to how variations in the initial RCS chemistry will affect the interaction with containment materials and whether these variations have been appropriately *addressed. Variations may influence corrosion rates of metals, leaching of species from nonmetallic materials, formation of chemical precipitates, and ultimately, plant-specific chemical effects.*

The following root issues are contained in this item:

1. The break jet impacts different materials, and chemistry variations may have different effects.
2. Boron concentration in the RCS fluid varies over the fuel cycle.
3. Lithium concentration in the RCS fluid varies over the fuel cycle.
4. The temperature of the water exiting the break varies over the duration of the event.

The blowdown phase is brief (less than a minute for large break conditions), so chemical effects issues associated with impact by the break jet are negligible. After the blowdown phase ends, the water from the break would simply spill into the pool with minimal contact of containment materials.

Boron concentration is an important factor for chemical effects—partly due to potential chemical reactions, and partly due to its effect on pH. Therefore, a realistic boron concentration should be used to determine a realistic pH level, and an appropriate concentration should be added at the start of an integrated test.

Lithium is not likely to be a major contributor to chemical effects since the concentration is generally low (ranging from negligible quantities to a few ppm). However, since it is relatively easy to include, a representative concentration of lithium should be added at the start of an integrated test.

Temperature is an important factor since it has a direct effect on corrosion rates and solubility limits. Therefore, a realistic analysis should take into consideration temperature variations over the duration of the event.

<u>STP Resolution</u>: Long-term (30-day) tests were run representing medium and large LOCA scenarios (31; 33). The quantities of materials in each test were determined from the quantities of materials present in STP containment that are impacted by each size break, as determined by break modeling.

The boron and lithium concentrations for each test were selected by determining the concentrations in the RCS, RWST, and accumulators at STP and calculating the concentration based on the contribution from each source for each LOCA scenario (40). The boron and lithium contributions from the RCS were based on time-averaged concentrations. The impact of higher and lower concentrations of boron and lithium on the pH of the system was evaluated using chemical equilibrium modeling (Visual MINTEQ). Based on the ranges observed over two operating cycles (fall 2009 through summer 2012), the pH would not be significantly affected by the variation in boron and lithium concentrations. The results of this evaluation showed that pH is controlled tightly within a range of approximately 7.1 – 7.3 (40).

The temperature for the two long-term tests was varied over the 30-day duration to match the temperature profile of the selected break scenarios (31; 33).

PIRT Item 1.2: pH Variability

The normal operating pH of the RCS is typically in the range of 6.9–7.4. The pH adjusted to 25 degrees C (77 degrees F) changes during the course of the fuel cycle from acidic at the beginning of the cycle to closer to neutral by the end of a fuel cycle. There are implications similar to those discussed in Section 1.1 of this report with respect to how pH variations may affect the interactions between containment materials and the post-LOCA environment. These variations may influence corrosion rates of metals, leaching of species from nonmetallic materials, formation of chemical precipitates, and ultimately plant-specific chemical effects.

The following root issue is contained in this item:

1. pH level in the RCS fluid varies over the fuel cycle.

pH is an important factor since it has a direct effect on corrosion rates and solubility limits. Therefore, a realistic analysis should take into consideration pH variations in the RCS fluid and the resulting impact on the overall pH in the pool.

STP Resolution: The issue of pH variability over the fuel cycle is addressed by the selection of boron and lithium concentrations in PIRT Item 1.1. Bench tests were run at pH values of 6.0, 7.2, and 7.7 to investigate the effects of pH variability (41).

PIRT Item 1.3: Hydrogen Sources within Containment

Dissolved hydrogen may play a significant role in the containment pool water chemistry. Hydrogen sources within the containment include the RCS inventory; the corrosion of metallic materials, including the reactor fuel cladding; and the Schikorr reaction. Containment pool reduction-oxidation (redox) potential is a function of the dissolved hydrogen resulting from these sources. Higher H_2 concentrations may decrease the redox potential. However, containment conditions are expected to foster H_2 evaporation, which could raise the redox potential. This issue could be important if H_2 concentrations have a significant effect on the redox potential in the post-LOCA containment water. The redox potential determines which materials will corrode or dissolve within the pool. A higher redox potential (i.e., more oxidizing) promotes metallic corrosion. As the concentration of dissolved constituents increases, so does the potential for solid species precipitation that could affect ECCS performance. The NRC or industry testing has not attempted to accurately simulate post-LOCA H_2 concentrations. However, the Schikorr reaction, by itself, may be beneficial by converting compounds that could form gelatinous-type chemical species into the mineral magnetite.

The following root issue is contained in this item:

1. Dissolved hydrogen may increase corrosion or dissolution of materials in the containment pool.

As discussed in the March 2011 review (39), H_2 is considered insignificant since there will be limited amounts of H_2 in solution, and higher concentrations could actually reduce potential corrosion.

STP Resolution: No action required.

PIRT Item 1.4: Containment spray CO_2 scavenging and CO_2/O_2 air exchange

Air entrainment within the containment pool beginning soon after the LOCA will cause carbon dioxide (CO_2) absorption within the containment pool. This entrainment increases the amount of CO_2, which could produce higher carbonate precipitate concentrations than would otherwise be present. These precipitates could also enhance nucleation and precipitation of other chemical species. Consequently, the air/liquid interactions within containment may increase the amount of chemical precipitates and degrade ECCS performance more than if these interactions were not considered.

The following root issue is contained in this item:

1. Dissolved carbon dioxide may result in carbonate precipitates such as $CaCO_3$.

This is more of an issue for plants that do not use TSP as a buffer since dissolved calcium can react with the TSP to form calcium phosphate precipitates. As discussed in the March 2011 review (39), tests that are open to the atmosphere would generally have a higher concentration of dissolved CO_2 than an air-tight containment. Therefore, although this is a potentially significant issue that should be considered for air-tight tests, no additional analysis is required for tests that are not air-tight.

STP Resolution: The STP containment contains sufficient air space that the pool solution will be in equilibrium with the CO_2 and O_2 in the atmosphere (chemically, the solution behaves as an open system). The CHLE loop is not air tight, and the lid will periodically be removed during sampling, so the tests will have sufficient opportunity for air to interact with the solution and will also behave as an open system. Calculations were performed to determine the dissolved gas concentrations that would be present in the solution in the STP containment, and it was determined that the concentration of carbonate in the CHLE tank would be slightly higher than it would be in the post-LOCA pool (40). No special provisions were performed to control the dissolved CO_2 and O_2 concentrations during the tests.

PIRT Item 1.5: Emergency Core Cooling System Injection of Boron

After a pipe break, RWST inventory with a boron concentration of approximately 2,800 ppm is injected into the RCS to cool the reactor core. This provides for a large boron source, which may affect chemical reaction products in the containment pool. Specifically, the boron source will serve as a pH buffer. This may influence corrosion rates of metals, leaching of species from nonmetallics, and ultimately formation of chemical precipitates.

The following root issue is contained in this item:

1. Boron concentration in the RWST will affect the pH in the pool.

Boron concentration is an important factor for chemical effects—partly due to potential chemical reactions, and partly due to its effect on pH. Therefore, a realistic boron concentration should be used to determine a realistic pH level, and an appropriate concentration should be added at the start of an integrated test.

STP Resolution: The concentration of boron used for the testing is addressed in PIRT Item 1.1.

PIRT Item 2.1: Radiolytic Environment

Radiolysis is the dissociation of molecular chemical bonds by a high energy radiation flux. The largest source of this radiation flux is the gamma radioactive decay of the reactor fuel. When the ECCS fluid passes through the reactor core, it is subjected to this radiation flux. Radiolysis reactions may change the pH of the ECCS containment pool, the fluid's redox potential, or both. Hence, chemical species which differ from those evaluated may form or the fluid may be more corrosive than that evaluated in all previous chemical effects testing.

The following root issues are contained in this item:

1. Radiolysis can affect pool pH through the creation of H_2O_2 and OH radicals.
2. Radiolysis can break down electrical cable insulation or dissolved nitrogen to form strong acids.

As discussed in the March 2011 report, the formation of H_2O_2 and OH radicals is not considered to be a significant issue based on previous analyses (39). The formation of strong acids due to the breakdown of cables may have a non-negligible impact on the long-term pH, and therefore should be considered. As discussed in the March 2011 report, one licensee determined that acid formation would reduce the pH by 0.2 (39).

STP Resolution: The quantity of acid formation due to radiolysis at STP has been calculated to be 0.8 mM of hydrochloric acid and 0.25 mM of nitric acid over a 30-day LOCA duration. This quantity of acid has been calculated to depress the pH by approximately 0.15 pH units based on the chemical system and buffers in STP during a LOCA (40). While 0.15 pH units may not be significant, a decrease in pH decreases the solubility of aluminum hydroxide precipitates, and may cause precipitation if the solution in the CHLE tests is near the precipitation threshold. Therefore, the quantity of acid as projected by calculations for STP was included over time in the CHLE tests (42; 43).

PIRT Item 2.2: Radiological Effects: Corrosion Rate Changes

Radiolysis of water bearing the chloride ion (Cl^-) can elevate the post-LOCA corrosion rate through formation of hypochlorite (ClO^-) or hypochlorous (HOCl) acid. The presence of these acids could increase the corrosion rate of metallic and nonmetallic species in containment, which in turn could alter the chemical byproducts formed. Hence, the chemical precipitates that form could differ from those previously evaluated. These different precipitates could subsequently affect ECCS performance in a manner that has not been considered previously.

The following root issue is contained in this item:

1. Radiolysis of water with chloride ions can create strong acids.

Chloride ions may be in solution primarily due to the breakdown of electrical cable insulation, but also due to potential leaching from coatings. As discussed for Item 2.1, the formation of strong acids may have a non-negligible impact on long-term pH, and therefore should be considered.

STP Resolution: The addition of acid to the tests to simulate radiolysis is addressed in PIRT Item 2.1.

PIRT Item 2.3: Hydrolysis

Nickel oxide (NiO), as well as other oxides, resulting from the corrosion of stainless steel and Alloy 600 metals can become a catalyst for producing H_2 from radiolysis of water. This process occurs more readily at higher water temperatures (i.e., hydrothermal environments). The hydrothermal hydrolysis of various organic/inorganic coating and insulation materials could partially depolymerize polymeric materials, producing materials ranging from small molecules to colloids. The colloids could subsequently aggregate into larger particles and gels. If this were to occur, the aggregated depolymerized materials may be more likely to transport to the sump strainer and affect pump performance or create chemical precipitates with different characteristics than those evaluated.

The following root issue is contained in this item:

1. Hydrolysis may cause H_2 formation.

As discussed in the March 2011 report (39), hydrolysis is a chemical reaction that causes water molecules to split into hydrogen and hydroxide ions. Hydrolysis is more significant at higher temperatures (generally above boiling). Since the containment pool temperature would only be above 200°F for a few hours, and the formation of H_2 due to hydrolysis is a gradual process, this is an insignificant issue.

STP Resolution: No action required.

PIRT Item 2.4: Conversion of N_2 to HNO_3

One panelist was concerned about the effects of nitric acid (HNO_3) formed in the containment pool due to radiolysis of dissolved nitrogen (N_2). This panelist was mostly concerned that the HNO_3 concentration may overwhelm the buffering capacity and cause the containment pool pH to drop precipitously to a range within 1–3. If the containment pool pH were this acidic, the redox potential becomes strongly oxidizing and corrosive and would lead to significant metallic corrosion and leaching of inorganic ions from other materials (e.g., concrete). Most previous NRC and industry-sponsored research has evaluated the chemical effects and their implications associated within the neutral-to-alkaline pH range (i.e., 7–10) that is expected within the buffered post-LOCA containment pool. Therefore, if the containment pool pH were highly acidic (i.e., 1–3), the chemical effects that would occur may differ significantly from those previously evaluated. The implications of these effects on ECCS performance would also be largely unknown.

The following root issues are contained in this item:

1. Radiolysis of dissolved N_2 may result in the formation of nitric acid.
2. Nitric acid may cause the pool pH to become strongly acidic.

As discussed in the March 2011 report (39), the formation of nitric acid due to radiolysis is expected to be relatively low due to the low solubility of N_2 in water. The assumption that the pool could become strongly acidic did not take into account the presence of the buffers. Therefore, the pool is not expected to become strongly acidic. However, similar to the other issues regarding the formation of strong acids, the effects on long-term pH due to the formation of nitric acid should be considered.

STP Resolution: The addition of acid to the tests to simulate radiolysis is addressed in PIRT Item 2.1.

PIRT Item 2.5: Additional Debris Bed Chemical Reactions

The concentration of radionuclides, postulated to be hundreds of Curies, available within the sump strainer fiber bed acts as a "resin bed" or chemical reactor potentially altering the local chemical conditions, such as pH. A number of possible radiolytic reactions could occur which may directly alter the chemical byproducts formed. This effect may lead to the formation of different, or a larger quantity of, chemical products than those evaluated, which could have a different impact on head loss than that considered.

The following root issues are contained in this item:

1. Radionuclides trapped in the debris bed may change the local chemistry and cause precipitation.
2. Radionuclides trapped in the debris bed may cause the bed to break down.

As discussed in the March 2011 report (39), local changes in the chemistry (i.e. the formation of H_2O_2 due to radiolysis) will not have a significant effect since the constant flow through the debris bed will effectively flush it out. Also, the concern that the fiber bed may break down due to the radionuclides is not considered to be significant since materials similar to fiberglass insulation are routinely used as a filtration media for high activity particulate.

During the chemical effects summit, the NRC questioned whether other types of insulation or coatings debris besides fiberglass may break down in the debris bed due to the radionuclides (44).

STP Resolution: The non-fiberglass debris at STP includes Microtherm and coatings debris. Coatings have been extensively tested in DBA conditions including high radiation. Although unqualified coatings can break down due to the heat, humidity, and radiation in a post-LOCA environment, the size distribution for unqualified coatings already takes these effects into consideration. The Microtherm debris quantity at STP is minor compared to the quantity of fiberglass debris. Therefore, even if radiolysis did have an effect on Microtherm particulate, it would not significantly change the structure of the overall debris bed at STP. Therefore, no additional evaluation is required.

PIRT Item 3.1: Crud Release

A PIRT panelist postulated that iron and nickel corrosion oxides up to 125 microns thick may exist on the interior of the RCS piping, fuel, and components. These oxides could be released by the hydraulic shock of the LOCA event. After release, the reduced Fe and Ni ions can be dissolved in the RCS (aided by radiolysis) and, when combined with air, can form oxides of hematite, maghemite, and magnetite. The crud release can create a localized radiolytic environment on materials caught on the sump screens, which could affect subsequent chemical reactions. The crud particles would also add to the debris concentration within the containment pool.

The following root issues are contained in this item:

1. The crud may influence the localized radiolytic environment.

2. A significant quantity of crud could be released as another source of particulate debris.

As discussed in the March 2011 report (39), the radiolytic effects of crud are insignificant compared to other sources. The March 2011 report estimated that the total quantity of crud in the RCS could be on the order of 400 kg (39). This is a potentially significant source of particulate debris, but it is not likely that 100% of the crud would be released by the oxidation effects and hydraulic shock of a LOCA. The March 2011 report concluded based on transport considerations that this is not a significant issue (39).

At the chemical effects summit, the NRC questioned whether the RCS crud could transport and have a significant impact on head loss (44).

STP Resolution: This item was not addressed in the 30-day CHLE tests. The crud is a source term for particulate debris and is not expected to affect the chemical environment. Crud release was addressed by considering it as a potential additional source term for particulate debris that can contribute to head loss. The total quantity of crud debris released was calculated to be within a range of 5 – 24 lb_m (45).

PIRT Item 3.2: Jet Impingement

The two-phase jet, and fine debris within the jet, will impact surfaces and could chip coatings, cause metallic erosion, or ablate materials like concrete. This phenomenon will govern the contributions of these materials in the early post-LOCA time period, before corrosion and leaching become important. Jet impingement could also initiate pitting corrosion, which could accelerate the corrosion of normally passivated materials like stainless steel. Most of the discussion from the peer review panel describes the jet interaction with materials as the primary source for post-LOCA debris. Jet impingement could result in a potential chemical effects debris source term that is greater than currently anticipated.

The following root issues are contained in this item:

1. Debris can be generated by the jet blast.
2. Pitting due to jet impingement could accelerate corrosion.

The generation of debris and subsequent effects of that debris in terms of both debris bed head loss and chemical effects is an important issue that should be considered.

As discussed in the March 2011 report (39), jet impingement during blowdown has a very short duration, and any pitting that occurs would be localized and have a minimal effect on the overall quantity of corrosion products.

STP Resolution: The approach for determining the quantity of materials during each test takes debris generation into account and is addressed in PIRT Item 1.1.

PIRT Item 3.3: Debris Mix Particulate/Fiber Ratio

Breaks in different locations will create different debris characteristics with respect to the total mass of debris, debris constituents, and the ratio of particulates to fiber. Depending on the specific break location, significantly different types and quantities of debris (e.g., Cal-Sil and fiberglass insulations) can *alter the type and quantity of chemical effects. Ultimately, the debris bed characteristics determine the chemical product capture efficiency and the total pressure drop across the sump screen strainer.*

The following root issues are contained in this item:

1. Different mixtures of debris can have a different impact on chemical effects.
2. Variations in the particulate/fiber ratio impact the chemical precipitate capture efficiency.
3. Variations in the particulate/fiber ratio impact the debris bed head loss.

In an integrated environment, the presence of some materials may inhibit the corrosion or dissolution of other materials. For example, silicon that is released into solution from the dissolution of fiberglass may inhibit the corrosion of aluminum. In some cases, therefore, scenarios with lower quantities of certain types of debris could potentially result in more severe chemical effects.

Fiber beds act as very effective filters and can capture small particles. As the particulate to fiber ratio increases, the debris bed is compacted and the filtration efficiency increases (along with the head loss). Therefore, the particulate to fiber ratio is a significant parameter.

STP Resolution: The mixture of debris to be used in each test is addressed in PIRT Item 1.1. The long-term tests used a fiber-only debris bed to assess the relative impact of chemical effects under a standardized condition (31; 33). The impact of variations in the particle/fiber ratio on chemical precipitate capture efficiency was not evaluated during the test program. The method used to address chemical effects head loss is described in Volume 3 (12).

PIRT Item 3.4: Effects of Dissolved Silica from Reactor Coolant System and Refueling Water Storage Tank

Dissolved silica is present in the water storage systems and the RCS during normal operation. This silica can react with other chemical constituents (most prominently magnesium, calcium, and aluminum) that form as a result of material dissolution or corrosion, or both, within the containment pool after the LOCA occurs. This reaction may result in a greater concentration of the chemical precipitates than would otherwise exist. The reaction may also alter the nature of the chemical precipitates by creating amorphous materials or gels or precipitates with retrograde solubility (i.e., they become more insoluble as temperature increases). The creation of additional chemical precipitates, amorphous materials, and retrograde soluble species could degrade ECCS performance by increasing head loss at the sump strainer or decreasing in the heat transfer rate from the reactor fuel if significant quantities of silica-containing precipitates are formed.

The following root issue is contained in this item:

1. The dissolved silica initially in the water may precipitate with other materials later in the event.

Silicon is an important factor for chemical effects. In some cases, it may help inhibit corrosion of aluminum, and also can contribute to precipitate formation. Therefore, the initial concentration of dissolved silica in the RCS, RWST, and accumulators should be considered.

STP Resolution: The quantity of silica present in the RCS, RWST, and accumulators at STP was evaluated along with the boron and lithium as described in PIRT Item 1.1. The concentration of silica in the RWST was determined to be between 1 and 6 mg/l based on operating history (40). However, it was decided not to include silica in the integrated tests since silicon can passivate aluminum and reduce the corrosion rate (40). The effects of the ratio of aluminum to silicon on corrosion were investigated in bench-scale tests (41).

PIRT Item 3.5: Containment Spray Transport

Following a LOCA, the containment spray will tend to wash latent debris, corrosion products, insulation materials, and coating debris into the containment pool. This changes the containment debris sources (types, amounts, compositions) and chemical species reaching the containment pool environment which could affect the sump strainer debris bed and the formation of chemical precipitates.

The following root issues are contained in this item:

1. Corrosion products generated above the pool could be washed down into the pool.
2. Debris above the pool could be washed into the pool.

Both of these items are potentially significant and should be considered.

STP Resolution: The debris quantities used for the CHLE tests (42; 43) took into account debris transport due to containment sprays for each accident scenario. The amount of material transported to the pool versus the debris held up above the pool surface was evaluated as part of the larger risk-informed approach (12).

PIRT Item 3.6: Initial Debris Dissolution

Typical debris generated by the LOCA (within the first 20 minutes) includes Cal-Sil insulation, cement dust, organic fiberglass binders, and protective coatings. Initial debris dissolution could indicate potential important contributors to the chemical containment pool environment. It is possible that the dissolved, ionic species could react and precipitate to form new, solid phases that were not originally in the containment pool.

The following root issue is contained in this item:

1. Dissolution of debris can form chemical precipitates.

This is the chemical effects issue and should be appropriately modeled in realistic chemical effects tests.

STP Resolution: The relevant materials and debris determined to be present at STP and contribute to chemical effects in each of the LOCA scenarios were included in the CHLE loop at the beginning of each test (42; 43). Determination of the quantities of debris is addressed in PIRT Item 1.1.

PIRT Item 3.7: Submerged Source Terms: Lead Shielding

Acetates present in the containment pool will corrode any submerged lead existing in containment, which could lead to formation of lead carbonate particulate or dissolved lead within the containment pool. Lead blanketing or lead wool is used to shield radiation hot spots during refueling outages and may *remain in the containment building during the fuel cycle. In addition, several plants may still use small quantities of lead wool for insulation.*

Lead carbonate contributions would provide additional particulate loading within the containment pool that could contribute to head loss at the sump strainer screen. Dissolved lead could also lead to cracking of submerged stainless steel structural components within containment. Neither the testing conducted to date nor do the licensee evaluations of ECCS performance consider these contributions. These omissions are potentially non-conservative if significant quantities of lead carbonate or dissolved lead are formed.

The following root issues are contained in this item:

1. Lead could dissolve and precipitate with other materials.
2. Dissolved lead may lead to cracking of submerged stainless steel components.

Generally, the quantity of lead exposed to the pool or sprays would be low. However, the dissolution of lead and subsequent precipitation is a potentially significant issue that should be considered.

As discussed in the March 2011 report (39), relatively low lead concentrations will not induce cracking in stainless steel components within the 30-day mission time.

STP Resolution: The lead in containment at STP includes lead blankets in storage barrels and lead blankets that are permanently installed on a few pipes. The lead blankets in the storage barrels are at different elevations including the containment floor. The storage barrels have holes in them so that they would be filled with water during a LOCA event. However, the lead blankets are sealed within vinyl-laminated nylon covers that provide a protective barrier between the material and pool solution. The lead blankets are inspected both before and after use, and blankets that exhibit signs of wear (such as cracking of the blanket material, damaged or corroded grommets, or other signs of physical damage) are removed from service (46). The jacketing material would not be damaged during a break, and the water in the barrels would be relatively stagnant, so it is reasonable to assume that this source of lead will not have an impact on chemical effects. The other source of lead is lead blankets installed on three pipes in the steam generator compartments (47). The lead blankets are robust and would only be damaged by larger breaks in the near vicinity of the blankets. Also, even for the cases where the lead blankets could be damaged, the pieces of lead wool would not be easily transported to lower containment. Therefore, lead was not included in the 30-day CHLE tests.

PIRT Item 3.8: Submerged Source Terms: Copper

Copper present in containment can accelerate or inhibit corrosion of other metals. One way in which Cu can alter the corrosion rate of other materials is by forming a galvanic couple. Galvanic effects can accelerate corrosion of less noble material while inhibiting corrosion of more noble materials. Dissolved copper can also enhance the rate of corrosion of other metals within an oxygenated environment. Different corrosion rates can impact the amount of corrosion products formed and therefore could have different effects on ECCS sump head loss.

The following root issues are contained in this item:

1. Galvanic couples can accelerate or inhibit corrosion of other metals.

2. Dissolved copper can enhance the corrosion rate of other metals by forming local galvanic cells.
3. Copper can inhibit corrosion of other metals by depositing and creating a passivation layer.

As discussed in the March 2011 report (39), the potential effect of galvanic couples in containment is insignificant. Local galvanic cells may enhance corrosion of aluminum, but this would only apply to the submerged aluminum. Also, as discussed in the March 2011 report, copper deposits were observed on aluminum samples in some of the ICET tests, which may have helped inhibit aluminum corrosion since the tests had negligible aluminum concentrations (39). Copper corrosion is expected to be relatively minor, but is a potentially significant issue that should be considered.

As discussed at the chemical effects summit (44), only the second root issue is important for chemical effects—potential enhancement of metal corrosion due to a local galvanic cell. The NRC also stated that the corrosion of zinc (from galvanized steel or other sources), and subsequent formation of zinc precipitates is a potentially significant issue that should be evaluated.

<u>STP Resolution</u>: The sources of copper at STP include copper in the fan coolers and copper wiring in the electrical cables. The fan coolers are above the containment pool elevation and the copper would be shielded from containment sprays. The copper in the electrical cables would only be exposed if the cables are damaged by the break jet. The cable insulation is robust and the cable trays would help protect the cables from damage, so the exposed surface area of copper wiring would be negligible.

The ICET tests had significant quantities of copper in both the submerged and unsubmerged portion of the tank. The copper coupons in the ICET tests exhibited very little change in weight: the mean change in weight ranged from +0.2 to -0.3 g for the submerged copper coupons and from +0.3 to -0.2 g for the unsubmerged copper coupons in all tests, compared to a mean pre-test weight of 1318 g. In ICET Test #2, which is most representative of the STP chemical conditions, the mean change in weight of both submerged and unsubmerged coupons was <0.1 g (48). Throughout all ICET tests, the copper concentration in solution was below about 1 mg/L. In ICET Test #2, the copper concentration was below the limit of detection for the entire 30 day duration of the test (48). Since the exposure of copper in a LOCA at STP would be substantially less than the copper included in the ICET tests, copper was not included in the CHLE tests.

Galvanized steel and zinc granules (representing inorganic zinc coatings debris) were included in the large break test to evaluate the effects (43).

<u>PIRT Item 3.9: Concrete Material Aging</u>

The PIRT panelists raised questions about the effect of aging on the leaching process for nonmetallic materials such as concrete. Neither the exposed concrete faces nor concrete dust in the containment building is likely to be fresh. After 30 years of exposure to the atmosphere, a substantial fraction of both the exposed calcium silicate hydrate (C-S-H) gel and the portlandite ($Ca(OH)_2$) constituents of the concrete would have been carbonated. Carbonation or other aging processes of concrete could affect the leaching rates and dissolved species as compared to relatively fresh concrete samples used in the ICET experiments and other research programs.

The following root issue is contained in this item:

1. Aged concrete may release a larger quantity of calcium.

Concrete surfaces in containment are generally coated, which would prevent carbonation due to aging. However, this may be a significant issue for plants with large uncoated concrete surfaces; especially if the plant uses a TSP buffer. Therefore, this issue should be addressed for realistic testing.

During the chemical effects summit, the NRC stated that the difference in dissolution between aged and fresh concrete is not significant and it is not necessary to use aged samples for chemical effects testing.

<u>STP Resolution</u>: No action required.

<u>PIRT Item 3.10: Alloying Effects</u>

Another issue raised by the PIRT is the effect of different alloys on the quantity of corrosion products. Corrosion rate data exhibit wide variability depending on the specific corrosion conditions and the nature of the alloy being subject to corrosion. Alloying could affect dissolution and corrosion rates, thereby affecting the solid species precipitates that are formed.

The following root issue is contained in this item:

1. Differences in alloys may affect dissolution and corrosion rates.

As discussed in the March 2011 report (39), alloys would generally exhibit lower corrosion rates than pure metals. In realistic testing, it may be beneficial to use the actual alloys that exist in containment. Regardless, it is important to appropriately justify all surrogate materials (including metal coupons) that are used in chemical effects tests.

At the chemical effects summit, the NRC stated that there is not a large difference between corrosion rates for pure materials and alloys. However, it is appropriate to use materials that are representative of what is in containment.

<u>STP Resolution</u>: Pieces of aluminum scaffolding from STP were used in the CHLE tests to represent the aluminum sources (42; 43). Galvanized steel coupons were not included in the medium break test, but were included in the large break test (43).

<u>PIRT Item 3.11: Advanced Metallic Corrosion Understanding</u>

The PIRT panel raised several other issues related to the understanding of metallic corrosion in the post-LOCA environment. These issues include enhanced Al corrosion caused by hypochlorite or other catalytic effects (e.g., jet impingement), synergistic effects on corrosion, and corrosion inhibition. These effects could substantially affect corrosion rates and therefore could have different effects on ECCS sump head loss.

The following root issues are contained in this item:

1. Enhanced corrosion due to acid formation.

2. Enhanced corrosion due to pitting from jet impingement.
3. Synergistic effects on corrosion.
4. Corrosion inhibition.

As discussed previously, the long-term effects on pH due to acid formation may be an important factor that should be considered. Also as discussed previously, pitting from jet impingement is considered to be an insignificant factor due to the localized impact of the jet. Generally, synergistic effects tend to inhibit corrosion, but both synergistic effects and corrosion inhibition are inherently considered in integrated testing.

STP Resolution: Synergistic effects and corrosion inhibition are address due to the selection of materials in the proper proportions relative to the STP containment, as described in PIRT Item 1.1. Acid formation is addressed in PIRT Item 2.1.

PIRT Item 3.12: Submerged Source Terms: Biological Growth in Debris Beds

The PIRT considered the propensity for bacteria or other biota to grow in preexisting debris beds located on the sump strainer screen or elsewhere within the ECCS system. Significant bacterial growth may be important if it creates additional debris that contributes to sump screen clogging or detrimental performance of downstream components like pumps and valves.

The following root issue is contained in this item:

1. Biological growth in the post-LOCA environment may contribute to clogging issues.

As discussed in the March 2011 report (39), most microorganisms cannot survive under high temperature, low or no light, and high radiation conditions. Any microorganisms that do survive would be highly unlikely to experience significant growth under the harsh post-LOCA conditions. Therefore, biological effects can be reasonably neglected for a realistic chemical-effects analysis.

During a public conference call on September 6, 2012, the NRC stated that STP should examine any wet sumps in containment to determine whether there is a significant source of existing biological material (49).

STP Resolution: A review of the corrective action records was made to determine whether there were ever any problems with biological debris in the secondary sump. Two issues were identified for Unit 2. In the first case, a sensor was caked with "sludge" (50), and in the second case a sensor was covered with "rusty slime" (51). There was no indication that the foreign material was biological, and in both cases it was cleaned up at the time of discovery. Note also, that the secondary sump is flushed with hydrogen peroxide during refueling outages, which is very effective in killing any bacteria that could be present.

PIRT Item 3.13: Reactor Core: Fuel Deposition Spall

Spall of reactor fuel cladding oxides (ZrO_2) and deposited chemical products could be a potential source of activated materials that could affect chemical reactions in the post-LOCA containment pool. Also, precipitates of post-LOCA chemical products (organics, Al, B, Ni, Fe, Zn, Ca, Mg, silicates (SiO_3^{2-} and SiO_4^{4-}

), and CO_3^{2-}-based products) could deposit on the fuel clad and spall, contributing either to clogging within the reactor core, or head loss across the sump strainer.

The following root issues are contained in this item:

1. Spall of activated fuel cladding oxides could affect chemical reactions in the containment pool.
2. Precipitation and spall of chemical products on the fuel could contribute to fuel or strainer clogging.

As discussed previously, the effect of activated particles on chemical effects due to radiolysis is considered to be insignificant. However, this debris could contribute to the source term for particulate debris with an effect on the overall head loss across the strainer or fuel channels. This issue is addressed in PIRT Item 3.1.

Some precipitates, particularly certain calcium precipitates, exhibit retrograde solubility. As water flows through the reactor vessel, the high temperature in the vicinity of the fuel rods may cause some of these materials to precipitate. The precipitates may form on the fuel rods themselves, or in solution where they can be swept out of the reactor vessel and potentially contribute to strainer clogging. This is a potentially significant issue that needs to be addressed for materials that exhibit retrograde solubility.

STP Resolution: The effects of chemical precipitation on the fuel rods have been previously addressed in a conservative manner for STP using the LOCADM software (52). Calcium phosphate and other calcium products demonstrate retrograde solubility characteristics. Although they could potentially form under STP conditions, there was no observation of any calcium products in the CHLE tests (31; 33). A detailed evaluation of these or other products that may exhibit retrograde solubility was not performed. However, the methodology used to address strainer head loss and in-vessel head loss (12) is believed to encompass the potential effects from chemical products formed due to retrograde solubility.

PIRT Item 4.1: Polymerization

The PIRT panelists expect polymerization to occur after molecular precipitation as a precursor to solid species agglomeration in post-LOCA environments. Molecular precipitation refers to the formation of bonds between metallic species and oxygen to form monomers. Polymerization is the ripening of these bonds to form covalent bonds and the growth of the monomers through one of many types of polymerization reactions. Chain polymerization, which is the most common, consists of initiation and propagation reactions and may include termination and chain transfer reactions. Step-growth and condensation polymerization are two additional mechanisms. Polymerization occurs until approximately nanometer-sized particles have formed. These particles can then continue to grow to larger sizes through agglomeration mechanisms.

The PIRT panelists expect polymerization is needed to form large enough particles to tangibly affect ECCS performance. The fact that chemical precipitates have formed during testing to simulate post-LOCA conditions provides evidence that polymerization is likely occurring. The issue is important only if the differences in polymerization mechanisms in the simulated and actual post-LOCA environments are significant enough to alter head loss or downstream effects associated with the chemical precipitates.

The following root issue is contained in this item:

1. Polymerization processes may cause initial precipitate growth.

As discussed in the March 2011 report (39), polymerization is expected to be an important process in the formation of precipitates, but is appropriately represented in testing and does not need to be further evaluated.

STP Resolution: No action required.

PIRT Item 4.2: Heat Exchanger: Solid Species Formation

Chemical species having normal solubility profiles may be dissolved in the containment pool at higher temperatures. However, these chemical species may precipitate in the heat exchanger because of a drop in temperature of approximately 30 degrees F. Some possible solid species that could form include $Al(OH)_3$, FeOOH, and amorphous SiO_2. The lower temperature at the heat exchanger outlet could also facilitate the development of macroscale coatings or suspended particulates, or both, that can continue to transport in the circulating fluid. Possible implications of this scenario include (1) species remain insoluble at higher reactor temperatures and affect the ability to cool the reactor core, (2) solid species formed may clog the reactor core and degrade heat transfer from the fuel, (3) species remain insoluble at higher containment pool temperatures and cause additional head loss upon recirculation, and (4) particulates act as nucleation sites for other compounds to precipitate.

The following root issue is contained in this item:

1. The temperature drop at the heat exchanger may reduce the solubility limit sufficiently to cause precipitate formation.

This is a potentially significant issue that should be evaluated in realistic testing. Timing is an important factor here. Early in the event while the pool temperatures are hot, the temperature drop across the heat exchangers may be significantly higher than 30°F. Since it takes time for containment materials to corrode and dissolve, precipitation may not be possible until much later in the event when the concentration in the pool starts to approach the solubility limit. Timing may also be important with respect to the kinetics of precipitate formation since the duration that coolant flow is exposed to lower temperatures downstream of the heat exchangers is relatively brief.

STP Resolution: At STP, only the LHSI flow passes through a heat exchanger. The LHSI flow rate ranges from 0 gpm for an SBLOCA to a maximum of 2,800 gpm per pump for an LBLOCA (12). The HHSI flow (1,620 gpm per pump) mixes with the LHSI flow downstream of the heat exchangers prior to reaching the cold or hot leg pipes. Based on the maximum flow rates and the volume of the piping and reactor vessel lower plenum and downcomers (53), the water would be at the cold heat exchanger discharge temperature for approximately 4 seconds and at the cool LHSI and HHSI mixture temperature for approximately a minute before reaching the core.

The CHLE testing included a loop in which the temperature of the solution was decreased, passed through an analytical system to detect whether precipitation occurred, and then increased back to the tank temperature. The turbidity measurements and membrane filters both before and after the heat exchanger were used to identify whether any precipitates formed due to the temperature drop. No significant differences were observed in the filters or turbidity measurements (31; 33).

PIRT Item 4.3: Reactor Core: Precipitation

The increased temperature in the reactor vessel (i.e., 70 degrees C higher than the containment pool) and retrograde solubility of some species (e.g., Ca silicate, Ca carbonate, zeolite, sodium calcium aluminate) causes precipitation and additional chemical product formation. This could result in the following: (1) additional precipitate could be created and transported to the sump screen that would then contribute to head loss and (2) precipitate or spall (see Section 3.13 of this report) passing through the sump screen may degrade the performance of ECCS components downstream from the screen.

The following root issue is contained in this item:

1. High localized temperatures in the reactor vessel may cause precipitation of materials with retrograde solubility.

This is a potentially significant issue that should be evaluated in realistic testing. It should be noted, however, that the bulk flow temperature in the reactor vessel would generally not be 70°C (158°F) higher than the pool temperature. It is possible for local temperatures within the core (i.e. next to the fuel cladding) to be significantly hotter than the pool, which could result in localized precipitation. Also, under certain scenarios (such as a cold leg break during cold leg injection), it is possible for the water in the core to boil. Even under these conditions, however, the maximum bulk temperature in the core would be limited to the saturation temperature, which would never approach a level that is 158°F hotter than the pool. Therefore, the focus of this issue should be on localized high temperatures in the reactor vessel rather than overall high temperatures in the bulk flow.

STP Resolution: This issue is addressed in the response to PIRT Item 3.13.

PIRT Item 4.4: Particulate Nucleation Sites

Particles within containment create the nucleation sites required for chemical precipitation. Examples of particles that could serve as nucleation sites include irradiated particles, dirt particles, coating debris, insulation debris, biological debris, and other materials within the post-LOCA containment pool. These particles then grow through polymerization (see Section 4.1 of this report) and agglomeration (see Sections 5.1 and 6.2 of this report) into solid species that are large enough to possibly degrade ECCS performance.

This issue identifies a fundamental aspect of the formation of solid species. Implications only arise if the nucleation sites in the post-LOCA environment are not appropriately simulated in testing. That is, the quantities and types of nucleation sites used in testing should be representative of the post-LOCA environment to ensure that solid species formation is not suppressed.

The following root issue is contained in this item:

1. Heterogeneous nucleation sites are required for precipitation to occur.

As discussed in the March 2011 report (39), both containment and test conditions contain numerous nucleation sites. Therefore, this is not a significant issue.

STP Resolution: No action required.

PIRT Item 4.5: Coprecipitation

Coprecipitation occurs when a normally soluble ion becomes either included or occluded into the crystalline structure of a particle of insoluble material. Precipitation of one species could lead to increased precipitation of another species (which, if taken separately, are each below their solubility limit). Thus, more solid species could form, which could lead to a greater concentration of chemical precipitates at the sump strainers or downstream of the strainers. Additionally, the species that form could differ in size from those observed in the ICET tests (i.e., 1 to 100 microns) such that they affect the head loss at the sump strainer more significantly.

The following root issue is contained in this item:

1. Precipitation of one material may result in precipitation of another material that would not otherwise have precipitated.

Coprecipitation does not reduce the solubility limit of precipitates, and therefore would not cause precipitation of two materials that are both below their solubility limit as suggested above. Although it is a potentially significant issue, in an integrated test environment, the various reactive materials are present together and coprecipitation can occur naturally. Therefore, this issue is inherently included in an integrated test.

STP Resolution: The issue of coprecipitation is addressed by inclusion of all materials that participate in chemical reactions in the same proportions that they are present at STP, as described in PIRT Item 1.1.

PIRT Item 5.1: Inorganic Agglomeration

Inorganic agglomeration is the formation of larger clumps of smaller particulates. This phenomenon depends upon the pH of the point of zero charge (PZC) of the species and the ionic strength (the higher the ionic strength, the smaller the distance for agglomeration) of the fluid. This phenomenon is sensitive to many factors, including particle shape factors, and maximum particle size. Inorganic agglomeration of small particles into larger sized particulates could degrade strainer performance.

The following root issue is contained in this item:

1. Agglomeration of chemical precipitates, insulation particulate, and/or latent particulate may form larger particles that would be more easily captured in a debris bed.

In general, agglomeration of particles will make the debris less transportable. Also, as shown in NUREG/CR-6224 (54), smaller particles have a larger impact on head loss due to the larger surface-to-volume ratio. Since head loss testing has shown that fiber beds can very effectively capture 10 micron particles, and the majority of insulation, latent, and coatings particulate debris would be larger than 10 microns, agglomeration of this material with each other or chemical precipitates is not a significant issue.

STP Resolution: No attempt to either stimulate or prevent agglomeration of particles was incorporated in the CHLE tests.

PIRT Item 5.2: Deposition and Settling

Chemical products formed in the post-LOCA containment environment could either settle within the containment pool or be deposited on other surfaces. Chemical species which attach to or coat particulate debris may enhance settling. Examples are aluminum coating on NUKON® fiber shifting the PZC or formation of a hydrophobic organic coating. This could result in less particulate debris and chemical product transporting to the sump screen and either accumulating on or passing through it. The possible implications of this issue are that the chemical precipitates added to the plant-specific chemical effects tests could result in increased settling during the tests compared to actual plant conditions.

The following root issue is contained in this item:

1. Chemical precipitates may settle or enhance settling of other particulate in the containment pool.

Given their small size, chemical precipitates can readily transport under relatively low flow conditions, and it is not expected that significant settling would occur. Therefore, this is not considered to be a significant issue.

STP Resolution: No action required.

PIRT Item 5.3: Quiescent Settling of Precipitate

Quiescent flow regions within the containment pool promote settling. The low flow rate within most of the containment pool also allows larger size, more stable particles and precipitates to form, which promotes settling. Settling of nonchemical debris and precipitate could be beneficial with respect to the pressure drop across the sump strainer.

The following root issue is contained in this item:

1. Chemical precipitates may settle or enhance settling of other particulate in the containment pool.

As discussed above, this is not considered to be a significant issue.

STP Resolution: No action required.

PIRT Item 5.4: Transport Phenomena: Precipitation and Coprecipitation

Precipitation or coprecipitation and ripening of solid species within the containment pool would create solid species which are less likely to transport. Decreased transportability will result in less product migrating to or through the sump screen.

The following root issue is contained in this item:

1. Chemical precipitates may settle in the containment pool.

As discussed above, this is not considered to be a significant issue.

STP Resolution: No action required.

PIRT Item 6.1: Break Proximity to Organic Sources

The pipe break location plays an important role in debris generation. If the break occurs in close proximity to organic sources, it could introduce a significant amount of organic materials into the containment pool. Organic sources could then affect the nature, properties, and quantities of chemical byproducts that form in the post-LOCA containment environment. The scenario evaluated by the PIRT considered failure or leakage of oil and other organics from either the RCP oil collection tanks or lube oil systems resulting from LOCA-induced damage. If the pipe break occurs in close proximity to the organic sources, up to approximately 250 gallons of oil may be released to the containment pool. If this should occur, head loss and downstream effects may be altered, either beneficially or negatively, by these organic materials.

The following root issues are contained in this item:

1. Certain breaks may result in a significant quantity of oil being released into the containment pool.
2. Other organic materials may be present due to failure of coatings and the organic binders in insulation debris.

As discussed in the March 2011 report (39), one licensee added a large quantity of oil (representative of the quantity from one RCP motor) to an integrated chemical effects head loss test. The oil addition had no impact on the head loss, and is not considered to be a significant factor.

Similarly, the presence of smaller quantities of organic material from other sources is not expected to have a significant effect on the pool chemistry conditions.

During the chemical effects summit, the NRC stated that although the issue of RCP motor oil does not appear to be a significant concern, the results of the integrated chemical effects test where oil was added were not clear since there was no differential test to compare against (44). They also stated that in general, qualified and unqualified coatings particulate debris could be important for chemical effects, although intact qualified coatings and failed epoxy paint chips do not need to be considered for leaching.

STP Resolution: The cases where a significant quantity of oil would be introduced to the containment pool would be limited to a few larger breaks in the vicinity of one of the RCP motors. Since the majority of break cases would not have significant quantities of oil, it was not included in the 30-day CHLE tests. Additional analysis of the effects of oil was not performed. However, the methodology used to address strainer head loss and in-vessel head loss (12) is believed to encompass the potential effects of oil for the limited scenarios where a significant quantity of oil could be released into the containment pool. The issue of organic materials from coatings failure is addressed in PIRT Item 6.4.

PIRT Item 6.2: Organic Agglomeration

Organic agglomeration is the process of small organic colloidal particles (1 to 100 nanometers in size) joining together, or coagulating, to form larger particles and precipitates. Coagulated particles can collect on sump strainers, decreasing ECCS flow; they could also collect on other wetted surfaces, such as walls or structural steel, and decrease the debris loading on the sump screen. Hence, head losses and downstream effects could differ from those evaluated during plant-specific testing.

The following root issue is contained in this item:

1. Organic agglomeration may form larger particles that would be more easily captured in a debris bed.

As discussed in the March 2011 report (39), this issue is similar to the issue of inorganic agglomeration. During the chemical effects summit, the NRC agreed that organic agglomeration is probably not an issue, but could be important if chemical precipitates are amorphous (44).

STP Resolution: Amorphous precipitates were not observed in either the medium or large break CHLE tests (31; 33). However, the method used to address chemical head loss encompassed the extreme effects of head loss increases due to full capture of amorphous chemical precipitates. This is described in detail in Volume 3 (12).

PIRT Item 6.3: Organic Complexation

Organic complexing agents act to inhibit agglomeration either by adsorption onto solid surfaces or by interaction in solution with metal ions. Organic surface complexation occurs if organic molecules (i.e., amines, acids, and heterocycles) adsorb on surfaces of ions or solids and inhibit the subsequent precipitation or growth of those species. The implications of organic complexation are counter to those associated with organic agglomeration. Organic complexation could reduce the effects associated with chemical precipitates and therefore may be beneficial to ECCS performance if this phenomenon is not credited or addressed during plant-specific testing.

The following root issue is contained in this item:

1. Organic complexation may inhibit agglomeration.

Since both inorganic and organic agglomeration are not considered to be significant issues, organic complexation would be an insignificant factor also.

STP Resolution: No action required.

PIRT Item 6.4: Coating Dissolution and Leaching

Coatings existing within containment represent possible additional physical debris sources. Generally conservative guidance for considering the effects of physical coating debris is provided for the evaluation of ECCS performance. However, dissolution and leaching of coatings can impact the chemical effects that occur within, or are transported to, the ECCS cooling water. Both inorganic (e.g., zinc-based) and organic (e.g., epoxy-based) coatings exist within containment. One concern is that these coatings leach chemicals as a result of being submerged in the containment pool environment after the LOCA. Coatings may create additional chemical species (e.g., chlorides or organics) within the containment pool that could potentially increase sump screen head loss or promote more deleterious downstream effects.

The following root issue is contained in this item:

1. Materials may leach from coatings affecting the overall pool chemistry.

As discussed in the March 2011 report (39), the amount of material that dissolves or leaches from coatings is expected to be relatively low. However, this is a potentially significant issue and should be appropriately addressed in realistic testing.

STP Resolution: Existing literature was reviewed to assess the effects of leaching from coated surfaces. Alkyd coatings were excluded from the CHLE tank tests based on testing that indicated that the coatings would not play a significant role in the creation of chemical precipitates (6). Similar to the alkyd coatings, epoxy coatings were excluded from the CHLE tank tests based on testing that indicated that the coatings would not play a significant role in the creation of chemical precipitates (26; 37; 38). Zinc particles were included in the CHLE tests to address potential concerns regarding the effects of inorganic zinc coatings on the formation of zinc products (42; 43).

PIRT Item 7.1: Emergency Core Cooling System Pump: Seal Abrasion and Erosion or Corrosion

Abrasive wearing of pump seals (e.g., magnetite—high volume or concentration of mild abrasive) creates additional materials that contribute to containment pool chemistry. In addition, chemical byproducts cause erosion or corrosion of pump internals, especially close-clearance components (e.g., bearings, wear rings, impellers). The possible implications of these phenomena are (1) additional particles could contribute to reactor core clogging, (2) particles could add additional sump screen loading, (3) particles could affect chemical species formation, and (4) pump performance degrades, possibly to the point of being inoperable.

The following root issue is contained in this item:

1. Particulate debris generated by abrasive wearing of pump seals may cause additional downstream problems.

As discussed in the March 2011 report (39), the quantity of particulate material generated by wearing of the pump seals is insignificant compared to other particulate sources. Also, the pump materials are not unique, and the surface area of similar metals and materials in containment are large enough that the impact of the pump internals on chemical effects is considered to be negligible. Therefore, this issue is insignificant.

STP Resolution: No action required.

PIRT Item 7.2: Heat Exchanger: Deposition and Clogging

Solid species which form in the heat exchanger lead to surface deposition or clogging, or both, within close-packed heat exchanger tubes (5/8-inch in diameter). This could cause decreased flow through the heat exchanger core or diminished heat transfer between the ECCS and heat exchanger cooling water, or both. Diminished cooling of the ECCS water could ultimately decrease the capacity of the ECCS water to remove heat from the reactor core.

The following root issue is contained in this item:

1. Precipitation within the heat exchanger may affect the heat exchanger performance.

As discussed in the March 2011 report (39), chemical precipitates would not have enough shear strength to block flow through the heat exchanger tubes. It's possible that some precipitates could create a thin coat on the tube walls. However, since the precipitates would generally form later in the event when the heat exchangers have ample margin, any slight degradation in performance due to the precipitates is negligible.

During the chemical effects summit, the NRC agreed that clogging of the heat exchanger is not likely to be a significant issue. However, they suggested that a post-test inspection of the heat exchanger would be a good idea (44).

STP Resolution: The efficiency of heat exchange and performance of the heat exchanger was not monitored during the CHLE tests. Based on the diagnostic methods used during the CHLE tests (turbidity measurements and membrane filters both upstream and downstream of the heat exchanger), there was no reason to suspect formation of precipitates within the heat exchanger (31; 33). The ends of the heat exchanger tubes were also examined, with no indication of any chemical products on the tube surfaces.

PIRT Item 7.3: Reactor Core: Fuel Deposition and Precipitation

The increased temperature (+70 degrees C from containment pool) and retrograde solubility of some species (e.g., Ca silicate, Ca carbonate, zeolite, sodium calcium aluminate) causes scale buildup on the reactor core. Zn, Ca, Mg, and CO_2-based deposits, films, and precipitates may form at higher temperatures within the reactor core. This may lead to (1) a decrease in heat transfer from the reactor fuel, (2) localized boiling due to insufficient heat removal, and (3) spallation of deposits, creating additional debris sources which could clog the reactor core or contribute to sump screen head loss.

The following root issue is contained in this item:

1. High localized temperatures in the reactor vessel may cause precipitation of materials with retrograde solubility.

As discussed previously, precipitation of materials with retrograde solubility on the fuel surfaces or in solution within the core is a significant issue that needs to be addressed.

STP Resolution: This issue is addressed in the response to PIRT Item 3.13.

PIRT Item 7.4: Reactor Core: Diminished Heat Transfer

Physical and chemical solid debris within the ECCS coolant water could diminish the fluid's heat transfer capacity and degrade the ability of the coolant to remove heat from the core.

The following root issue is contained in this item:

1. Concentrated materials in the reactor vessel may reduce the water's heat removal capacity.

The highest debris concentrations would occur under cold leg break conditions during cold leg injection since the water entering the core would boil off raising the concentration of boron, other dissolved materials, and suspended solids. As discussed in the March 2011 report (39), the relatively dilute concentration of dissolved solids would not significantly affect the rate of boiling and rate of heat removal. The effects of high boron concentration on heat removal are not fully understood, but a PWROG program investigating this issue is currently in progress and is expected to be completed by 2015. Although the outcome of the PWROG research may change the acceptable limit for boron concentration in the reactor vessel, it would not affect the physical processes that must be evaluated in realistic chemical effects testing. Therefore, the PWROG progress should be monitored for potential plant modifications that may be required (i.e. timing for switchover from cold leg to hot leg injection), but is not a significant issue for realistic chemical effects testing.

At the chemical effects summit, the NRC announced that the boron precipitation issue must now be addressed as part of the overall resolution of GSI-191 (44).

STP Resolution: The resolution of the boron precipitation issue was addressed as part of the larger risk-informed approach (12).

PIRT Item 7.5: Reactor Core: Blocking of Flow Passages

Fuel deposition products and precipitated retrograde soluble chemical species spall and settle within the reactor vessel. Settling can be potentially deleterious if flow passages to the fuel elements are either globally or locally impeded. Reduced flow within the RPV, if significant, has the potential to diminish heat transfer from the fuel.

The following root issue is contained in this item:

1. Debris may spall and settle within the reactor vessel causing blockage.

As discussed previously, precipitates that form due to retrograde solubility within the reactor vessel must be properly addressed. This item raises an additional issue of the potential settling of precipitates or other debris spall under low flow conditions within the reactor vessel. During cold leg injection, the flow would move upward through the core and would tend to lift the debris and transport it out of the reactor vessel. If the settling velocity is high enough for the debris to settle, it would not be expected to create any significant head loss since the flow would simply have to overcome the "weight" of the debris to continue injecting into the core. During hot leg injection, the flow would move downward through the core in the same direction that settling debris would be moving. The debris could accumulate in various locations where it could form a bed and cause higher head losses. However, this issue would occur regardless of debris settling. Therefore, debris settling concerns are insignificant for realistic chemical effects testing.

STP Resolution: No action required.

PIRT Item 7.6: Reactor Core: Particulate Settling

Relatively low, upwards flow (for cold leg injection) within the reactor causes particulates to settle. Compacted deposits form and may impede heat transfer and water flow, especially for lower portions of reactor fuel.

The following root issue is contained in this item:

1. Particulate debris may settle during cold leg injection causing flow path blockage or inhibiting heat transfer.

As discussed previously, debris that settles during cold leg injection would not result in significant head loss. Also, as discussed in the March 2011 report (39), the higher flow through the core for a hot leg break, and the turbulence due to boiling for a cold leg break would be expected to keep the particulate debris from blocking heat transfer to the lower portions of the fuel. Therefore, debris settling concerns are insignificant for realistic chemical effects testing.

STP Resolution: No action required.

Item 5.a.10: Conventional Head Loss Model

Method: The methodology for determining the conventional debris head loss as a function of time-dependent parameters is based directly on the NUREG/CR-6224 head loss correlation (54). Limited testing was conducted to ensure that the correlation provided a reasonable prediction of head loss under STP-specific conditions (55).

These tests were conducted in a high temperature vertical loop (HTVL) which circulated water down through a vertical section of 6-inch transparent piping where an installed screen was used to entrap debris introduced from above. An installed heat exchanger was used to control the water temperature, which was also measured and recorded. Additives were used to control the water chemistry. The debris was introduced at the open top of the loop and was uniformly distributed on the horizontal screen located in the middle section of the vertical pipe. Water was circulated at prescribed flow rates while the temperature and the differential pressure were measured. The test screen was a perforated plate that supports the debris bed while imparting minimal clean screen head loss. The test loop instrumentation included three temperature thermocouples, two flow meters, and three differential pressure sensors. The temperature thermocouples were located upstream of the debris screen, downstream of the debris screen, and the room environment. Instrumentation was calibrated before the first test in each test series and rechecked before the last test in each series.

A total of eleven tests were conducted. The HTVL tests were performed with the same water chemistry as determined for the CHLE tank tests. The strainer area, the size of the screen holes, and the screen orientation necessarily remained constant for all of the tests. The varied parameters included the flow velocity, the water temperature, and the masses of the fiber and particulate debris.

Due to previously raised concerns regarding the NUREG/CR-6224 correlation, however, a bump-up factor of 5x was used to account for uncertainties in the head loss predictions.

Basis: The correlation is based on theoretical and experimental research for head loss across a variety of porous and fibrous media carried out since the 1940s. The NUREG/CR-6224 head loss correlation was developed in support of the NRC evaluation of the strainer clogging issue in BWRs and has been extensively validated for a variety of flow conditions, water temperatures, experimental facilities, types and quantities of fibrous insulation debris, and types and quantities of particulate matter debris. The types of fibrous insulation material tested include Nukon, Temp-Mat, and mineral wool. The particulate matter debris tested includes iron oxide particles from 1 to 300 μm in characteristic size, inorganic zinc, and paint chips. In all of these cases, the NUREG/CR-6224 head loss correlation has bounded the experimental results. Due to the semi-empirical nature of the correlation, STP performed confirmatory head loss tests to demonstrate the applicability of the correlation to STP conditions (55). Table 2.5.36 illustrates the debris loads and objectives for the STP conventional head loss tests:

Table 2.5.36 – Basic Test Parameters

Test No.	Nukon Bed	Particulates	Mass Ratio	Specific Objectives
1	NEI Protocol 13.4 g Nominal 2" (at 0.9 lbm/ft^3)	67 g F600 SiC introduced after testing with the fiber alone	5	(1) Establish uniform fiber bed using standard NEI protocol. (2) obtain data for fiber without particulates, & (3) assess the filterability of the fine F600 SiC particulates.
2	NEI Protocol 13.4 g Nominal 2" (at 0.9 lbm/ft^3)	(1) 67 g F400 SiC mixed in with fiber (2) Follow on addition of 30 g F500 SiC (3) Follow on addition of 67 g F320 SiC	(1)5.0 (2)7.2 (3)12	(1) Improve NEI protocol fiber bed uniformity by introducing particulate mixed in with the fiber and assess the filterability of the F400 SiC particulates 2) follow on addition of F500 SiC. (3) follow on addition of easily filtered coarse F320 SiC to enhance bed compaction and subsequent effect on head loss. (SiC consistently did not result in a characteristic head loss.)

Test No.	Nukon Bed	Particulates	Mass Ratio	Specific Objectives
3	NEI Protocol 4.5 g Nominal 1/4" thin-bed (at 2.4 lbm/ft^3)	(1) 88 g SiC (before fiber) (a) 20% F320 (b) 30% F400 (c) 30% F500 (d) 20% F600 (2) Follow on addition of 30 g F320 SiC	(1) 20 (2) 26	(1) Develop a procedure for establishing a uniform thin layer of fiber and establish thin-bed of SiC particulates, (2) follow on addition of easily filtered coarse F320 SiC to force further head loss and bed compression. (SiC consistently did not result in a characteristic head loss.)
4	NEI Protocol 18 g Nominal 1" (at 2.4 lbm/ft^3)	88 g SiC (mixed in with fiber) (a) 20% F320 (b) 30% F400 (c) 30% F500 (d) 20% F600	4.9	Establish a thick bed of fiber replicating successful procedure developed in Test 3 and further assess the ability of SiC to generate head loss. (SiC consistently did not result in a characteristic head loss.)
5	NEI Protocol 18 g Nominal 1" (at 2.4 lbm/ft^3)	138 g Iron Oxide (BWR Specific Distribution) (mixed in with fiber)	7.7	Using successful fiber bed procedure from Test 4, assess the head loss for alternate type of particulate for direct comparison with SiC in Test 4.
6	NEI Protocol 18 g Nominal 1" (at 2.4 lbm/ft^3)	44 g Pulverized Acrylic Coatings (mixed in with fiber)	2.4	Using same fiber bed procedure used in Test 4 and 5, assess the head loss of pulverized acrylic coatings particulate.
7	NEI Protocol 18 g Nominal 1" (at 2.4 lbm/ft^3)	180 g Tin Particulate (mixed in with fiber)	10	Using same fiber bed procedure used in Test 4, 5, and 6, assess the head loss of tin particulate
8	NEI Protocol 4.0 g Nominal 0.22" thin bed (at 2.4 lbm/ft^3)	(a) 33.5 g tin (b) 14.9 g acrylic (c) 0.92 g Microtherm (d) 4.5 g Marinate	16	Replicate the August 2008 ARL prototype test
9	NEI Protocol 2.8 g Nominal 0.15" thin bed (at 2.4 lbm/ft^3)	(a) 28 g acrylic (b) 33.5 g tin (c) 20 g Microtherm	(a) 10 (b) 12 (c) 7.1	(1) Additional acrylic particulate data (2) Additional tin particulate data (3) Fist Microtherm data

Test No.	Nukon Bed	Particulates	Mass Ratio	Specific Objectives
10	NEI Protocol 9 g Nominal 0.5" (at 2.4 lbm/ft^3)	44 g Pulverized Acrylic Coatings (mixed in with fiber)	4.9	Additional acrylic particulate data
11	NEI Protocol 9 g Nominal 0.5" (at 2.4 lbm/ft^3)	44 g Pulverized Acrylic Coatings (mixed in with fiber)	4.9	Repeat of Test 10

Assumptions: The following assumptions related to debris bed head loss were made in Volume 3 (12):

- It was assumed that miscellaneous debris would partially overlap and would fully block strainer flow over an area equivalent to 75% of the miscellaneous debris surface area. This assumption is consistent with the guidance in NEI 04-07 (56).
- It was assumed that all coatings materials would have a packing fraction similar to acrylic coatings. It was also assumed that non-coatings particulate debris would have a packing fraction similar to iron oxide sludge. These assumptions are based on engineering judgment due to limited data.
- It was assumed that a fiber bed of at least 1/16th of an inch is necessary to capture chemical precipitates. This is a reasonable assumption since a thinner debris bed would not fully cover the strainer and would not support appreciable head losses due to chemical debris.
- It was assumed that 100% of the transported particulate debris would be captured on the strainer at the time of arrival. This assumption does not imply that no particulate would penetrate the strainer. However, since the in-vessel effects acceptance criteria that were implemented in CASA are independent of the particulate quantity, this assumption is conservative.
- It was assumed that the debris on the strainers would be homogenously mixed. This is a reasonable assumption since much of the debris would arrive at the strainer simultaneously.
- It was assumed that fiberglass debris would accumulate uniformly on the strainers with a density of 2.4 lb_m/ft^3. This is consistent with the assumptions used in NUREG/CR-6224 (54). For the purposes of developing the strainer loading table, the pool height was assumed to always be sufficient to allow debris to accumulate on the top of the strainer, but debris accumulation on the bottom of the strainer was limited to 2 inches to account for the height of the strainer above the floor. Assuming that the pool height is greater than the debris accumulation on the top of the strainer is not necessarily accurate for cases where the water level is relatively low and the debris load is large. However, for the majority of cases, the debris load would not be large enough to accumulate a fiber bed that exceeds the submergence level.

Acceptance Criteria: The time-dependent total strainer head loss (the combination of clean strainer, conventional debris, and chemical debris head losses) was compared to the strainer structural margin and the time-dependent NPSH margin. If the strainer head loss exceeded either of these values, the ECCS was assumed to completely fail.

Results: Discussion of the calculated total strainer head losses is provided in the response to Item 5.a.11.

The application of a head loss correlation to head loss data requires the measurements of head loss, water temperature, and flow velocity for a relatively uniform and homogeneous fibrous/particulate debris bed of known composition at relatively stable conditions. Turbidity measurements, as well as water clarity, are used to judge the completeness of the filtration process.

The correlation validation process depends on knowing the input hydraulic characteristics of each type and size category of debris introduced into the test. Debris size characterization can be used to approximate the hydraulic characteristics of simple forms of debris, such as Nukon fibers, but not for complex particulates. A typical particulate consists of roughly shaped particles of varied sizes making the analytical assessment of the specific surface area, S_v, somewhat difficult and uncertain. Some insulation materials such as calcium silicate, Microtherm, Min-K, and amorphous chemical precipitates have complex forms that simply cannot be assessed analytically, and their impact on head loss has to be addressed experimentally. The solid density of a particle is based on the material properties and the particulate bulk density can be deduced by weighing a known volume of the particulate. The S_v value is deduced by applying a head loss correlation to head loss test data where all parameters are known except the S_v value for the material in question. As such, inaccuracies in the form of the correlation become inherent in the experimentally deduced input parameters. Therefore, the correlation and the hydraulic characteristics become somewhat interdependent.

A total of eleven exploratory head loss tests were performed (57). All testing was done using fibers from a single-side baked Nukon blanket, which was processed using the NEI debris preparation process. All testing was conducted starting at 200 °F at the STP buffered and borated water conditions. The particulate types tested were green silicon carbide, iron oxide (the BWR sludge simulant used in the development of the NUREG/CR-6224 head loss correlation), tin, and ground acrylic paint. Flow and temperature sweeps were performed at the end of some of the experiments to examine the impact of different flow conditions and temperatures.

The NUREG/CR-6224 head loss correlation was used to replicate the measured head loss of the test conducted with iron oxide and a debris bed thickness similar to the test parameters used in the development of the NUREG/CR-6224 head loss correlation (57). The iron oxide S_v value was adjusted until the calculated head loss matched the measured head loss. The final S_v value was in reasonable agreement with the specifications of the size distribution of the sludge simulant indicating that the NUREG/CR-6224 head loss correlation was a reasonable predictor of head losses at STP water and temperature conditions. The iron oxide test, however, was limited to the lowest approach velocity of 0.02 ft/s due to equipment limitations. The NUREG/CR-6224 head loss correlation also generated reasonable estimates of the head loss experiments conducted with ground acrylic paint and extended the approach velocity down to the STP strainer approach velocity of 0.0086 ft/s.

The NUREG/CR-6224 head loss correlation, however, could not replicate the low head losses observed in the tests with tin and/or green silicon carbide. The test report provides a hypothesis for this behavior based on observations of the difference in smooth surfaces noted on SEMs of green silicon carbide and tin as compared to the rough surfaces of iron oxide and ground acrylic paint (57). Further experiments would need to be conducted to confirm this hypothesis. This lack of agreement between the NUREG/CR-6224 head loss correlation and testing with green silicon carbide and tin does not impact the STP head loss calculations since there is no green silicon carbide or tin in the STP debris mixture. The green silicon carbide has been used in the past as a simulant of paint, and the tin has been used as a simulant of IOZ coatings. Most of the STP particulate debris comes from coatings, either from qualified coatings in the ZOI or from unqualified coatings elsewhere.

Another anomaly observed in the STP head loss tests was the absence of a direct correlation of the head losses observed in the temperature sweeps with the water viscosity. The test report provides a hypothesis that the temperature also impacts the compression of the fiber debris bed due to the temperature impact on the malleability of the fibers (57). An analytical model was developed to couple the compression to temperature that showed good agreement with the experimentally determined temperature sweep data. The compression algorithm implemented in the NUREG/CR-6224 head loss correlation used in CASA was not modified to incorporate the temperature dependence suggested by the tests. The experiments showed that the measured head losses at lower temperature were lower than the head losses calculated by the NUREG/CR-6224 head loss correlation, hence the CASA calculated head losses are conservative. Additional experiments and analysis need to be performed to validate the temperature dependent compression algorithm prior to its implementation in CASA.

One of the tests conducted (Test 8) was designed to replicate the August 2008 ARL STP prototype test (57; 58). However, this test completely failed to replicate the head losses observed in the previous testing. Both tests used the same primary surrogates of Nukon fibers along with tin and acrylic particulates. Three differences in the tests are: 1) Test 8 had a greater thickness of fiber than was reported in the ARL test, 2) Test 8 used Alion supplied Microtherm and Marinate board particulate instead of the same materials used at ARL, and 3) the ARL fiber debris preparation protocol used a food processor whereas Test 8 used the NEI debris preparation protocol. Based on the experience of the CHLE tests (59), fiber beds with food processor prepared fiber tended to exhibit higher head losses than fiber beds prepared in accordance with the NEI debris preparation protocol. Comparisons of the beds prepared with food processor prepared debris and the NEI debris protocol revealed that the NEI protocol fibers tended to bridge the perforated plate holes and form a debris bed over the perforated plate, while the food processor fibers tended to form low porosity "dimples" at the perforated plate holes. The higher head losses observed with food processor beds was attributed to the formation of the low porosity "dimples". The food processor prepared fibers used in the ARL test could have also formed low porosity "dimples", and allowed the particulate to pack tighter in the ARL test than in Test 8 resulting in a lower porosity bed with higher head losses. The formation of "dimples" in the strainer holes instead of a fiber bed over the perforated plate could also explain the very thin bed observed in the ARL test. The lack of reproducibility of the head losses observed in the Alion vertical loop test compared with the ARL test does not impact the applicability of the NUREG/CR-6224 in calculating the CASA head losses since the differences in the results are attributable to different debris preparation methods. The NUREG/CR-6224 head loss correlation assumes the formation of a debris bed over a perforated plate as was observed with the debris beds prepared in accordance with the NEI debris preparation protocol. Therefore, the NUREG/CR-6224 head loss correlation is considered to be applicable to the debris beds formed with STP prototypical debris.

The test report also addresses the impact of the three main ACRS comments of the NUREG/CR-6224 head loss correlation (57). These ACRS comments were mainly directed at debris beds containing calcium silicate, a known problematic insulation. The test report provides suggested modifications to the NUREG/CR-6224 head correlation to address the three main ACRS concerns (57). Note that all Marinite (similar to calcium silicate) has been removed from containment at STP. Therefore, as shown in the test report, the three main ACRS comments are not significant for STP conditions (57).

Overall, these tests demonstrated that the NUREG/CR-6224 head loss correlation provided reasonable predictions of head loss for the prototypical STP debris types and loads, water chemistry, temperature, and strainer approach velocities. However, due to the generic concerns regarding the NUREG/CR-6224 correlation, the head loss calculated using the correlation was increased by a factor of five in CASA Grande to account for uncertainties in the head loss predictions.

Additional details on the STP conventional debris head loss testing are provided in the head loss test report (55).

Additional details on how the test results were used to justify use of the NUREG/CR-6224 correlation and how the correlation was incorporated in the overall GSI-191 evaluation are provided in Volume 3 (12).

Item 5.a.11: Chemical Effects Head Loss Model

Method: As discussed in the response to Item 5.a.6, there are a relatively limited number of scenarios where significant chemical effects would be observed. However, since the corrosion and dissolution release model and the solubility model were not directly implemented in CASA Grande, a set of chemical effects bump-up factor probability distributions were developed and applied for all breaks. To account for the presence of extreme conditions in the scenario sample space, exponential probability distributions were defined and applied as direct multipliers to the estimated conventional head loss. The probability distributions were developed based on the current results from the CHLE testing (31; 33), WCAP-16530-NP calculations (25), and reasonable engineering judgment.

Basis: The magnitude and probability distributions for the chemical effects bump-up were developed using engineering judgment. In chemical effects testing, a wide range of effects have been observed. In some cases, there are no chemical products, or chemical products form but have a negligible impact on head loss. In other cases, chemical products have been observed to cause head loss to spike dramatically. For STP, the actual formation and effect of chemical products based on realistic conditions has been relatively minor. However, since not all scenarios have been fully evaluated, the probability distributions included conservative extremes as discussed below.

Assumptions: The following assumptions related to chemical head loss were made in Volume 3 (12):

- It was assumed that chemical products would not form before the pool temperature drops below 140 °F. This is a reasonable assumption for the purposes of this evaluation since the solubility limit for aluminum precipitates increases significantly at higher temperatures, and calcium precipitates are not expected to form in large quantities for most of the scenarios evaluated (25). Note that the temperature profiles used in the CASA Grande evaluation conservatively minimize the temperature and therefore minimize the time that it would take for chemical products to form.

Acceptance Criteria: The time-dependent total strainer head loss (the combination of clean strainer, conventional debris, and chemical debris head losses) was compared to the strainer structural margin and the time-dependent NPSH margin. If the strainer head loss exceeded either of these values, the ECCS was assumed to completely fail.

Results: The chemical effects model that was implemented in CASA Grande is described below:

- No bump-up factor is applied if the fiber quantity on a given strainer is less than 1/16 of an inch.
- No bump-up factor is applied prior to the temperature dropping below 140 °F. Note that since only two temperature profiles were implemented in CASA Grande, the increase in head loss would occur approximately 5 hr after the start of the event for large breaks, and approximately 16 hr after the start of the event for small and medium breaks.
- As shown in Table 2.5.37 and Figure 2.5.35 through Figure 2.5.37, the probability distributions for the chemical effects bump-up factors were developed with mean bump-up factors of approximately 2x for small breaks, 3x for medium breaks, and 3x for large breaks, and maximum bump-up factors of approximately 15x for small breaks, 18x for medium breaks, and 24x for large breaks.

Table 2.5.37 – Exponential probability distribution parameters applied to chemical effects bump-up factors for each LOCA category

Parameters		SBLOCA	MBLOCA	LBLOCA	Tail Probability
Formal	Min	0	0	0	~1e-5
	Mean	1.25	1.5	2.0	~1e-5
	Max	14.3	17.2	23	~1e-5
Shifted	Min	1	1	1	~1e-5
	Mean	2.25	2.5	3.0	~1e-5
	Max	15.3	18.2	24	~1e-5

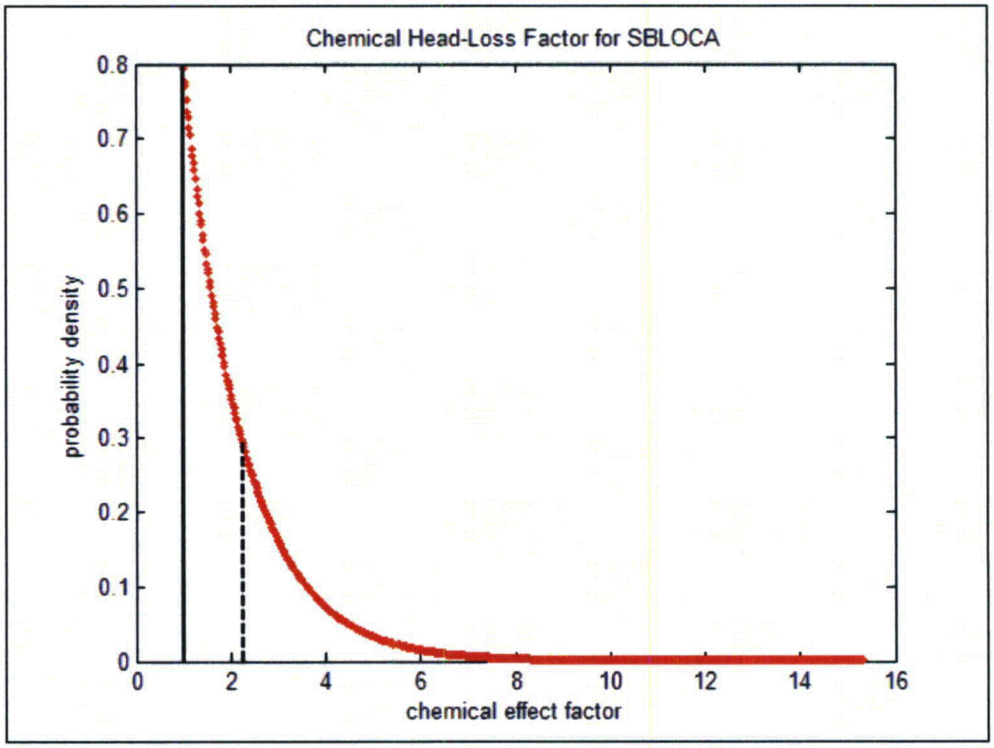

Figure 2.5.35 – Exponential probability density function for chemical effects bump-up factors applied to SBLOCAs

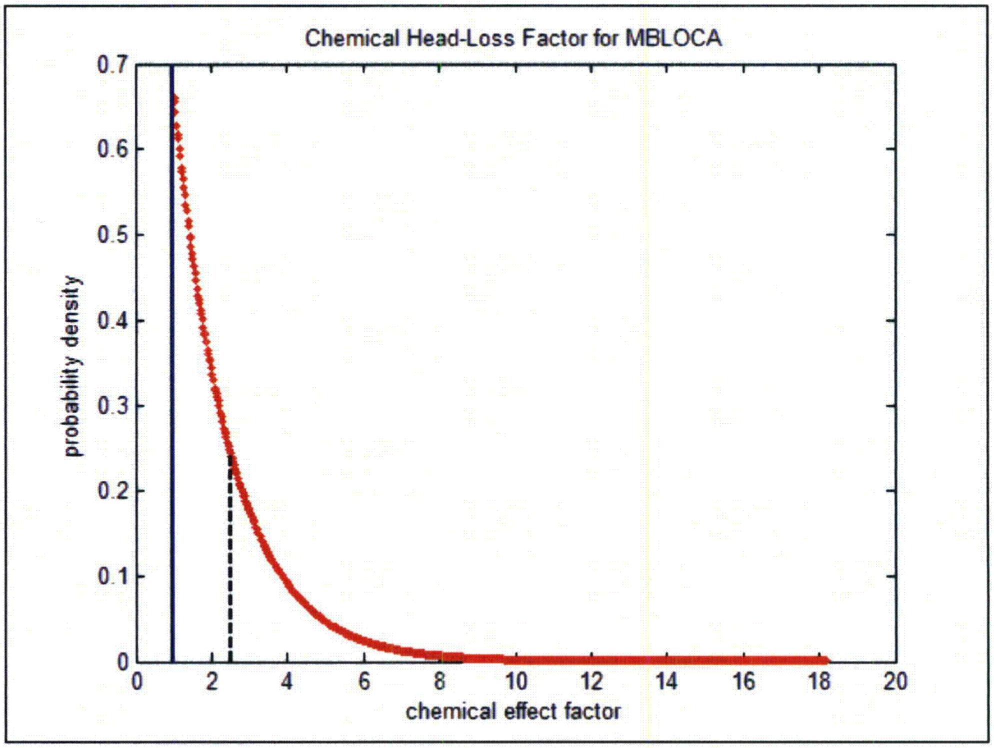

Figure 2.5.36 – Exponential probability density function for chemical effects bump-up factors applied to MBLOCAs

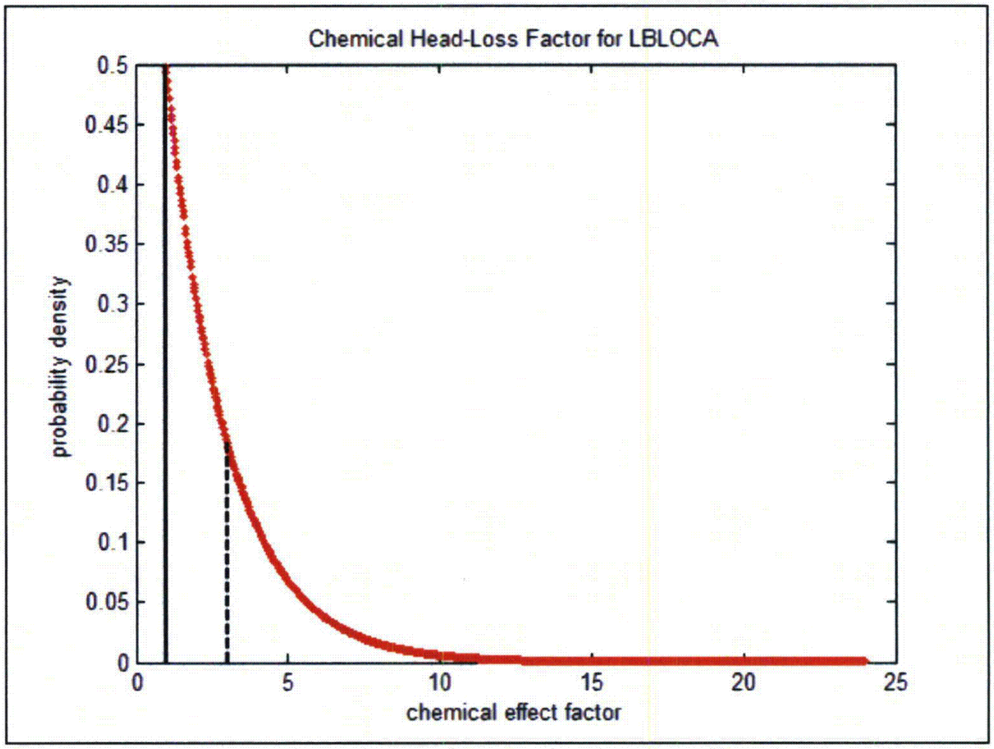

Figure 2.5.37 – Exponential probability density function for chemical effects bump-up factors applied to LBLOCAs

Figure 2.5.38 shows an example of the time-dependent total strainer head losses calculated for various random scenarios. In the final evaluation, strainer failure was not predicted for any of the small or medium breaks. The conditional probability of strainer failure given a large break scenario was only 3.41E-03 for the baseline case where all trains of ECCS are operating.

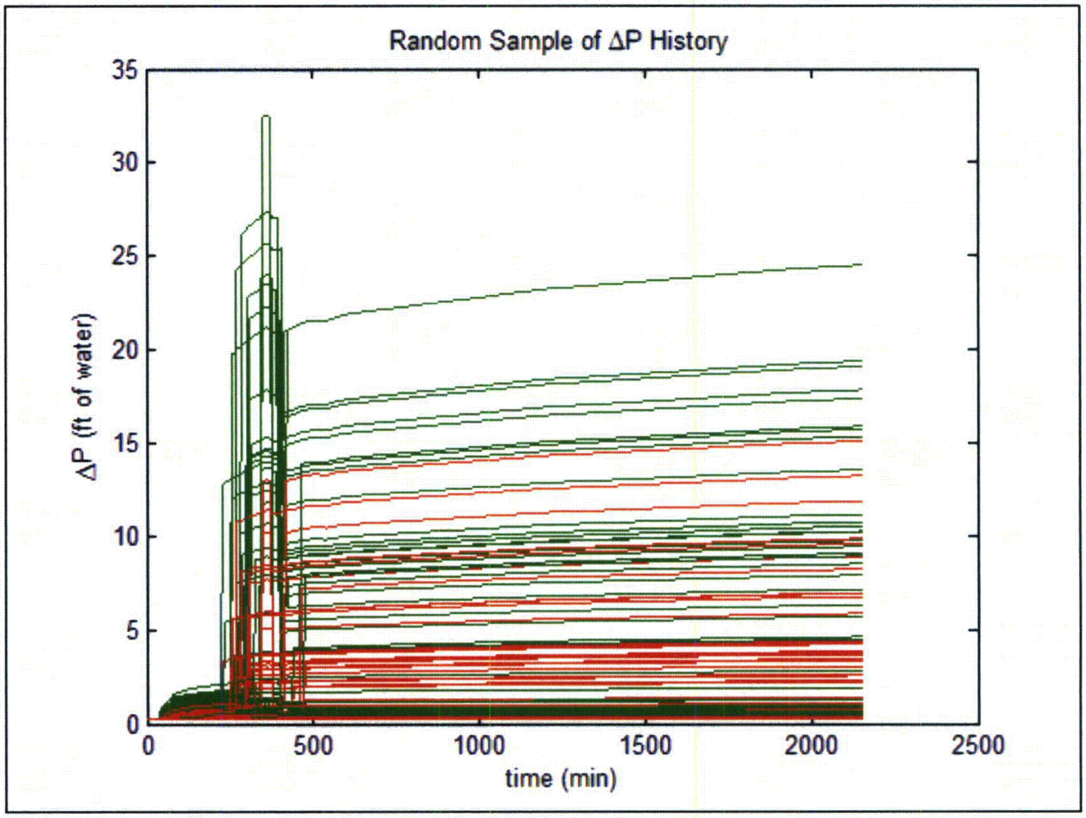

Figure 2.5.38 – Typical sample of sump-strainer head loss histories generated under the assumption of exponential chemical effects factor and artificial head-loss inflation

Additional details on the chemical effects bump-up factor probability distributions and the impact on the overall GSI-191 evaluation are provided in Volume 3 (12).

Item 5.a.12: Fiber Bypass

Method: Debris penetration is a function of two mechanisms. The first mechanism is direct passage of debris as it arrives on the strainer. A portion of the debris that initially arrives at the strainer will pass through, and the remainder of the debris will be captured by the strainers. The direct passage penetration is inversely proportional to the combined filtration efficiency of the strainer and the initial debris bed that forms. The second mechanism is shedding, which is the process of debris working its way through an existing bed and passing through the strainer. By definition, the fraction of debris that passes through the strainer by direct penetration will go to zero after the strainer has been fully covered with a fiberglass debris bed. Shedding, however, is a longer term phenomenon since particulate and small fiber debris may continue to work its way through the debris bed for the duration of the event.

Debris that penetrates the strainer can cause both ex-vessel and in-vessel problems. The most significant downstream effects concern is related to the quantity of fiberglass debris that accumulates in the core. This is a highly time-dependent process due to the following time-dependent parameters:

- Initiation of recirculation with cold leg injection
- Switchover to hot leg recirculation
- Arrival of debris at the strainer
- Accumulation of debris on the strainer
- Direct passage
- Debris shedding
- Flow changes when pumps are secured
- Decay heat boil-off

The various parameters associated with time-dependent debris accumulation on the strainer and core are illustrated in Figure 2.5.39, where $S_n(t)$ is the source rate for initial introduction of debris type n, V(t) is the pool volume, $m_n(t)$ is the mass of debris n in the pool, $f_n(t)$ is the filtration efficiency for debris n at the strainer, $s_n(t)$ is the shedding rate for debris n from the existing debris bed, Q(t) is the volumetric flow rate passing through the strainers, γ is the fraction of SI flow compared to the total flow, λ is the fraction of flow passing through the core compared to the total SI flow, and $g_n(t)$ is the filtration efficiency for debris n at the core.

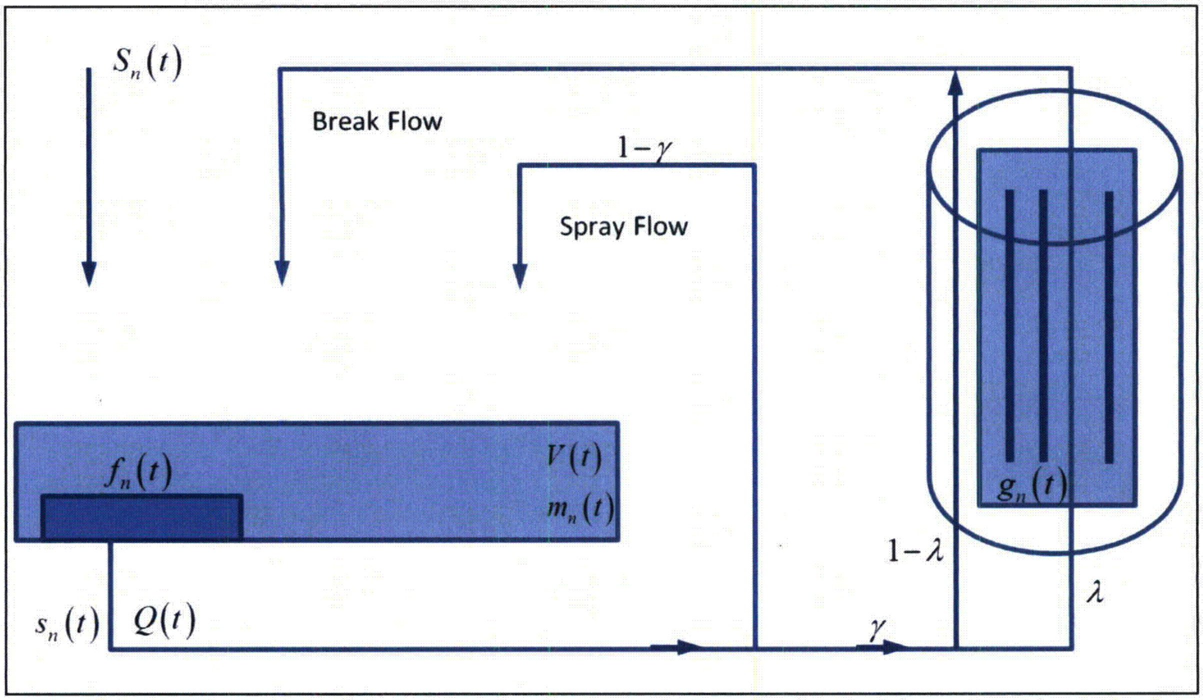

Figure 2.5.39 – Illustration of time-dependent parameters associated with debris accumulation on the strainer and core

As illustrated by Figure 2.5.39, debris that passes through the strainer will not necessarily end up on the core. A portion of the debris could pass through the containment spray pumps, and a portion could either bypass or pass directly through the core and spill out the break. The debris that doesn't accumulate in the core may end up back in the pool where it could transport and potentially pass through the strainer again.

The methodology for determining the coefficients associated with the direct penetration and shedding terms is described in an evaluation (60) based on STP-specific testing (61). The methodology for calculating the time-dependent arrival of debris at the strainer, time-dependent penetration through the strainer, and time-dependent accumulation of debris on the core is described in Volume 3 (12). Additional discussion is also provided in the responses to Item 5.a.2 through Item 5.a.5 and Item 5.a.16.

Basis: The bases for the penetration correlation and the time-dependent accumulation on the core are described in detail in Volume 3 (12).

Assumptions: The following assumptions related to debris penetration and core accumulation were made in Volume 3 (12):

- It was assumed that the debris beds on the strainers would not be disrupted after the debris initially accumulates. This is a reasonable assumption since the strainers are not located in the immediate vicinity of any potential breaks where the break flow could impinge the strainers and shear off a portion of the debris.
- It was assumed that debris that penetrates the strainers would be uniformly distributed in the flow and would transport proportional to the flow split to the SI pumps vs. CS pumps (γ) and the flow split to the core vs. bypass paths (λ). This is a reasonable assumption since the fiber that penetrates the strainer would be very fine and would easily transport with the flow.
- It was assumed that all debris that penetrates the strainer and transports through the core would be trapped on the core (i.e., 100% filtration efficiency). This is a conservative assumption since it maximizes the debris load on the core.
- It was assumed that all debris that penetrates the strainer and bypasses the core (either through the containment sprays or directly out the break) would immediately be transported back to the containment pool. This is a conservative assumption since it neglects potential hold-up of debris in various locations and neglects the time that it would take for debris to transport through the systems and wash back to the pool.

Acceptance Criteria: The acceptance criteria for debris accumulation on the core are described in the response to Item 5.a.13.

Results: Discussion of the calculated debris accumulation on the core is provided in the response to Item 5.a.13.

Additional details on the STP penetration testing and statistical analysis are provided in the test report (61) and data analysis report (60). This is also discussed in response to Item 5.a.16.

Additional details on how the penetration correlation was implemented in the overall GSI-191 evaluation are provided in Volume 3 (12).

<u>Item 5.a.13: In-Vessel Fiber Limits</u>

<u>Method</u>: In-vessel fiber limits were selected based on an evaluation of the realistic phenomena associated with the core blockage and boron precipitation for the various scenarios (cold and hot leg breaks during the cold and hot leg injection phases). Thermal-hydraulic modeling was used to determine the potential for core damage to occur given full blockage at the bottom of the core at the start of recirculation for small, medium, and large cold leg and hot leg breaks (62). For the cases that could lead to core damage, the core blockage acceptance criteria in WCAP-16793-NP was used (63). In addition, a more stringent boron precipitation fiber limit criterion was used for medium and large cold leg breaks based on the draft NRC safety evaluation on WCAP-16793-NP (64).

<u>Basis</u>: The basis for the in-vessel acceptance criteria is a combination of STP-specific thermal-hydraulic model results, generic PWROG fuel blockage test results, and boron precipitation considerations. This is described in more detail in Volume 3 (12).

<u>Assumptions</u>: The following assumptions related to core blockage were made in Volume 3 (12). Additional assumptions related to boron precipitation are provided in the response to Item 5.a.15.

- It was assumed that a debris bed would not form at the top of the core (blocking flow to the core) during the hot leg injection phase. This is a reasonable assumption since debris blockage would result in boiling in the core, which would disrupt the debris bed.
- To calculate the boil-off flow rate for a cold leg break during cold leg injection, it was assumed that the RCS pressure is 14.7 psia, and the SI flow entering the reactor vessel is saturated liquid (i.e., 212 °F). This assumption conservatively maximizes the boil-off flow rate since a lower inlet temperature and/or a higher RCS pressure would increase the enthalpy required to boil the water.

<u>Acceptance Criteria</u>: The acceptance criteria for debris loads on the core were defined based on the break location, injection flow path, and fiberglass debris loads that could potentially cause issues for debris blockage. Based on the thermal-hydraulic modeling, which showed that full blockage at the bottom of the core would not result in core damage for hot leg breaks, the acceptance criterion was set to essentially an infinite fiber quantity. For cold leg breaks, an acceptance criterion of 15 g/FA was used based on the conservative results of testing by the PWROG (63). Note, however, that the core blockage acceptance criteria are bounded by the boron precipitation acceptance criteria. As discussed in the response to Item 5.a.15, boron precipitation was not considered to be an issue for hot leg breaks. For medium and large cold leg breaks, the acceptance criterion for boron precipitation was assumed to be 7.5 g/FA of fiber debris on the core.

<u>Results</u>: In the final evaluation, failure due to core blockage or boron precipitation was not predicted for any of the small or medium breaks. The conditional probability of in-vessel failure given a large break scenario was only 1.25E-03 for the baseline case where all trains of ECCS are operating.

Additional details on the STP thermal-hydraulic analysis are provided in the core blockage calculation (62).

Additional details on how the in-vessel fiber acceptance criteria were defined for the overall GSI-191 evaluation are provided in Volume 3 (12).

Item 5.a.14: In-Vessel Thermal Hydraulic Analysis

Method: RELAP5-3D was selected to perform the simulation of the reactor system. The reactor containment response was simulated using MELCOR.

As described in the response to Item 5.a.13, a series of simulations were run to investigate worst case scenarios with full core blockage at the start of the ECCS recirculation phase. Two RELAP5-3D models were developed and used to conduct the simulations. The *3D Vessel – 1D Core* model was selected to run the basic simulations of the LOCA transients under a hypothesized full core and core bypass blockage. This model was selected because it combines the detailed nodalization of the vessel (using multi-dimensional components available in RELAP5-3D) accounting for more realistic injection flow paths, with the one-dimensional core and core bypass to minimize the simulation time. The following basic scenarios were simulated using the *3D Vessel – 1D Core* model:

- Small Break (2") in Cold Leg.
- Small Break (2") in Hot Leg.
- Medium Break (6") in Cold Leg.
- Medium Break (6) in Hot Leg.
- Double-Ended Guillotine Break (27.5") in Cold Leg.
- Double-Ended Guillotine Break (29") in Hot Leg.

Additional simulations were conducted to study the thermal-hydraulic behavior of the core under partial core blockage for a selected case (medium cold leg break), using the *3D Vessel – 3D Core* model. This model simulates the reactor core with multi-dimensional components, allowing partial core blockage (by fuel channel) with a relatively larger simulation time. The additional cases that were run include:

- Full core blockage and full core bypass blockage (confirmation of *3D Vessel – 1D Core* model results)
- Full core blockage with open core bypass
- Core bypass blockage and core blockage except for one fuel channel (center)
- Core bypass blockage and core blockage except for one fuel channel (periphery)

Both models used for these simulation sets were originated from a *Full 1D* model, which is described in detail in the input certification report (65).

Basis: The basis for the RELAP5 simulations are described in the core blockage calculation and input certification report (62; 65).

Reactor System Response

A set of RELAP5-3D models were developed to perform the analysis of the STP reactor system during LOCA scenarios of different break size and locations.

Full 1D model

This model uses one-dimensional components such as single-volumes, branches, and pipes to simulate the regions of the reactor system. The primary cooling loops were simulated independently to account for the expected flow asymmetry during the phases of the injection. The power plant was modeled using a total of 283 nodes. The total number of junctions defined in the model was 293. The reactor core was modeled using two one-dimensional pipe components. One pipe component was used to simulate the average channels, where 192 assemblies were lumped together, and one pipe component was used to simulate the hot channel. Heat structures were defined and connected to the hot and average channels to simulate the fuel pins, including the fuel, gap, and cladding regions. Radial and axial peaking factors were defined to distribute the total power of the reactor within the average channels and the hot channel (hot rod and average rods in hot channel). The model nodalization diagram is shown in Figure 2.5.40 (65).

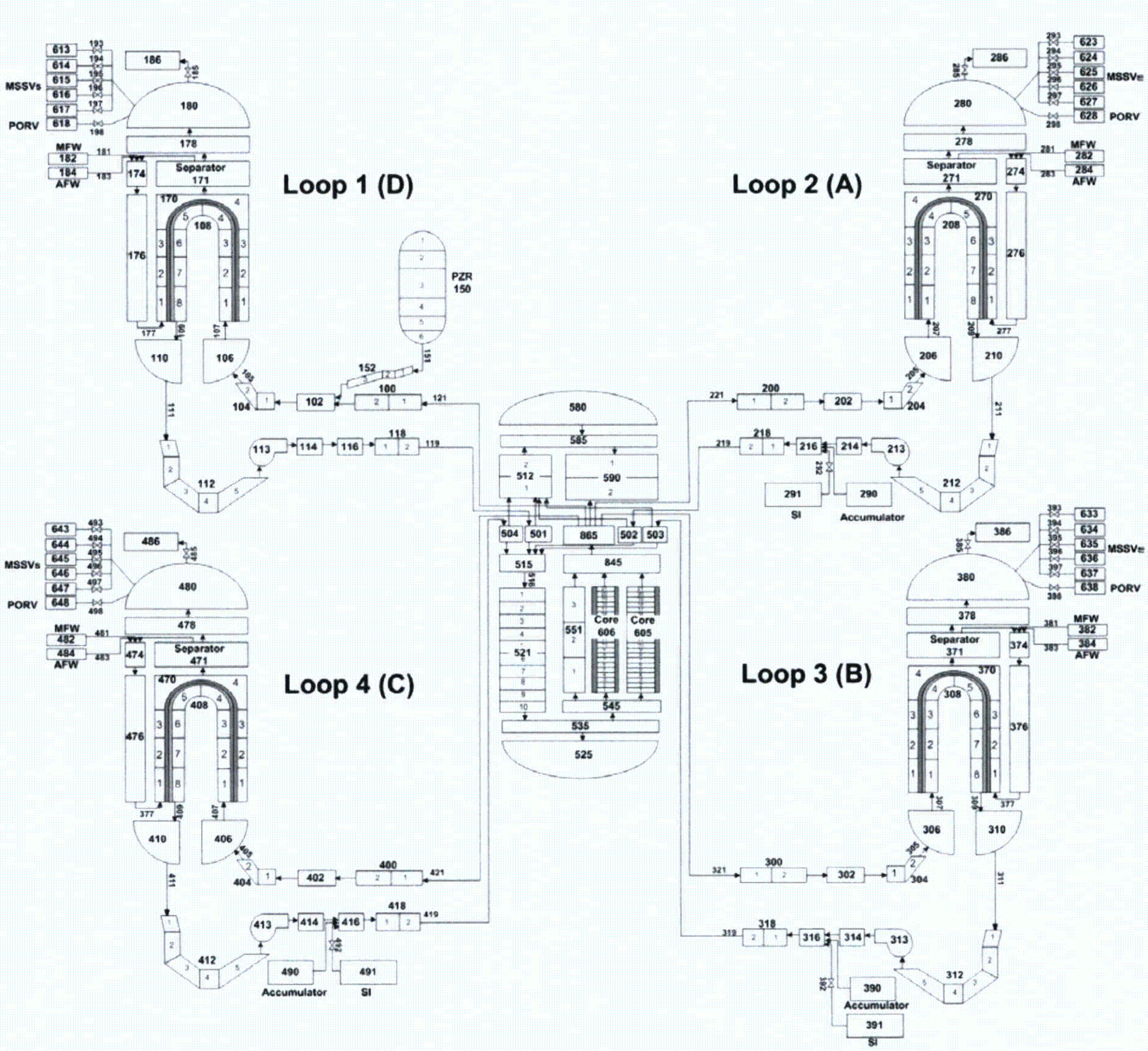

Figure 2.5.40 – RELAP5-3D - 1D Model Nodalization Diagram

The Safety Injection system of the power plant consists of three independent trains, which were simulated according to the realistic geometry. Each train contains:

- One Accumulator simulated using the accumulator component available in RELAP5-3D. A control variable was defined in order to isolate the accumulator during special LOCA manual operation procedures.
- One HPSI modeled with a time-dependent junction, where a table of the velocity of the liquid to be injected as a function of the pressure of the primary system injection location was defined.
- One LPSI modeled with a time-dependent junction, where the same approach applied to the HPSI was used.
- One RHR connected downstream the LPSI pump simulated.

- The RWST and sump, modeled using a common time-dependent volume, where the condition of the thermal-hydraulic conditions of the water before and after the sump switchover were defined using a table controlled by a trip function (defined true at sump switchover and false otherwise).
- A set of two trip valves to control the injection location (cold or hot leg).

The nodalization adopted for the injection system is shown in Figure 2.5.41.

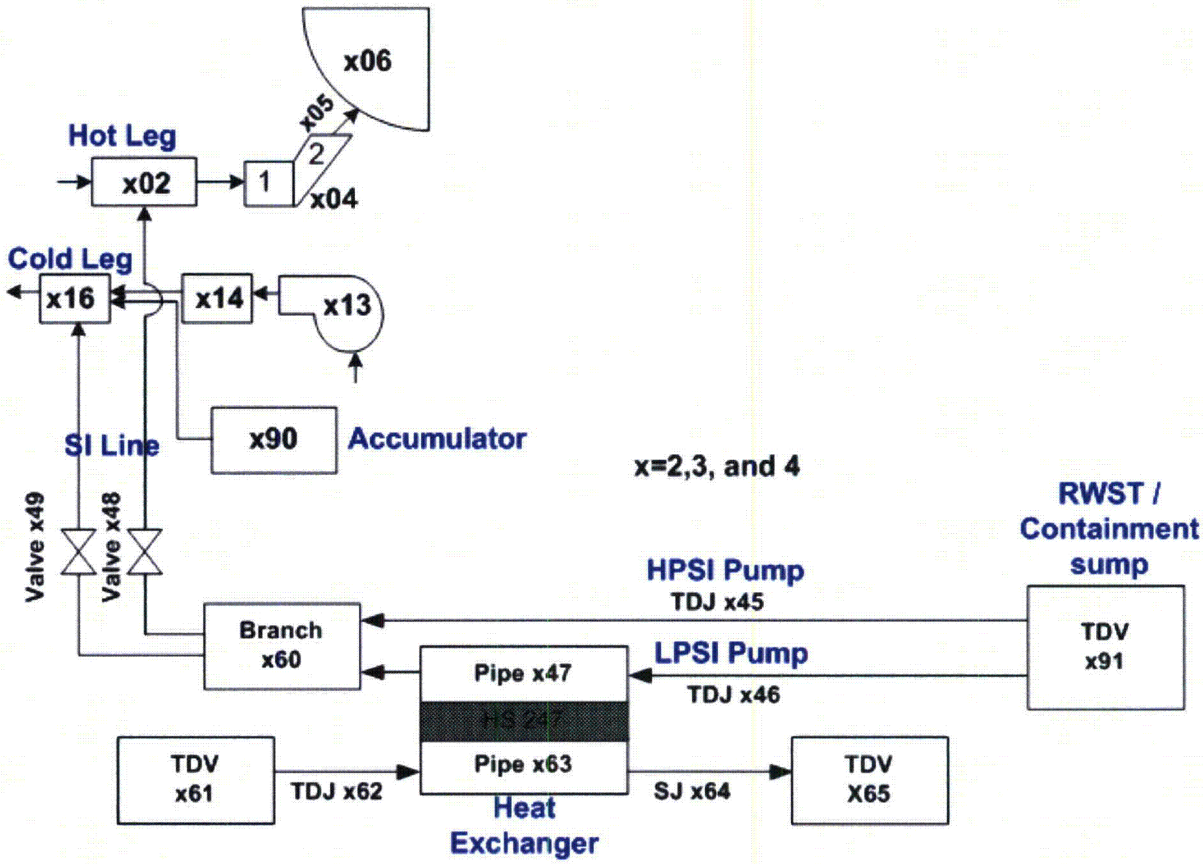

Figure 2.5.41 – SI System Nodalization Diagram

3D models

Two 3D models (3D Vessel – 1D Core and 3D Vessel – 3D Core) were prepared to perform selected simulations of LOCA scenarios, to achieve a more realistic representation of selected regions of the vessel and the core. In particular, multi-dimensional Cartesian components were used to simulate 193 fuel channels with cross-flow. The regions outside the vessel (loops, steam generators, and SI system was simulated with one-dimensional components as described for the 1D Model. This specific model was used to perform selected simulation of LOCA scenarios under hypothetical core blockage. The total number of nodes defined in the 3D Vessel – 3D Core model is 4235. The number of junctions is 11627. The nodalization diagram for these models is shown in Figure 2.5.42.

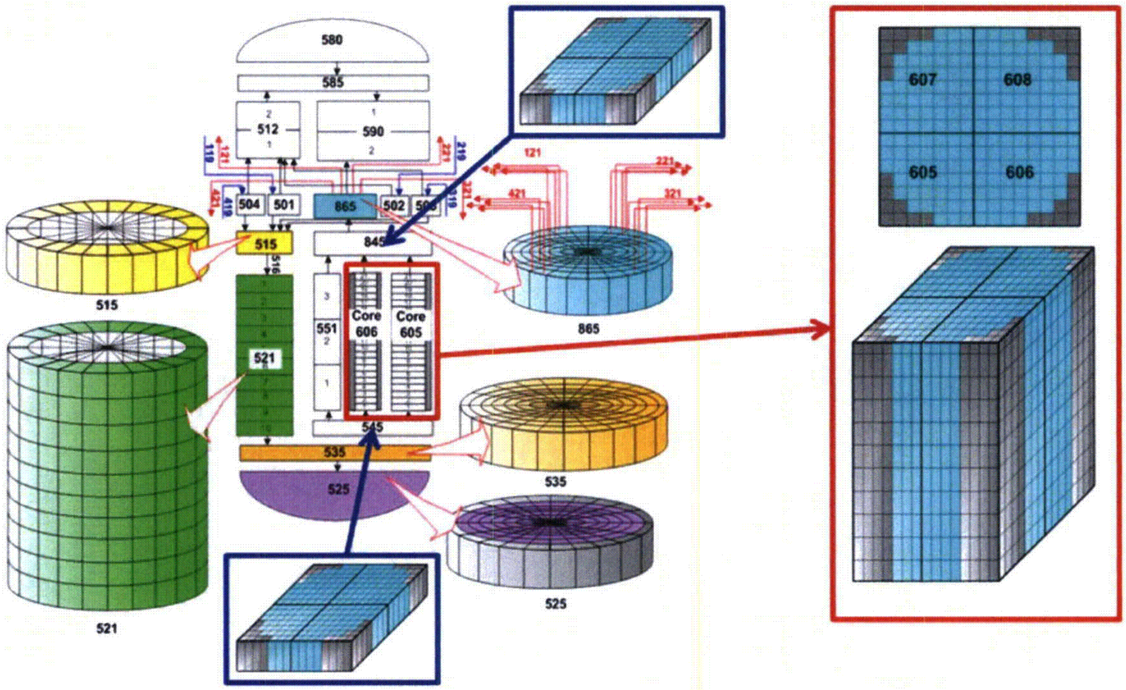

Figure 2.5.42 – RELAP5-3D - 3D Models Nodalization Diagrams (Left: 1D Core; Right: 3D Core)

Containment Response

The MELCOR containment model of the STP PWR large, dry containment was prepared to run the simulations of the containment response during the LOCA scenarios. The model consists of six control volumes, eleven flow paths, and forty-nine heat structures that represent ceilings, walls, and floors among other condensing surfaces. Cavity compartment, lower compartment, steam-generator compartment (where the break in the primary system is assumed to discharge), upper compartment, annular compartment (where the sump is located), and pressurizer compartment were created in the containment model. Each compartment is a single control volume with geometry defined by volume/altitude tables. Additional flow paths were included in the model to represent drainage pathways from the refueling canal (lower portion of the upper compartment) to the steam generator compartment. Heat structures were defined to simulate walls, floor and other structures in the reactor containment. Pressure suppression features (engineered safety features) such as six fan coolers and three containment sprays were included in the model and behaved realistically according to actuation set-points, delays, ramp-ups, coast-downs, etc. Control functions were defined to control the fan coolers and sprays actuation and manual operations (sprays shutoff). Figure 2.5.43 shows the MELCOR nodalization diagram adopted (66).

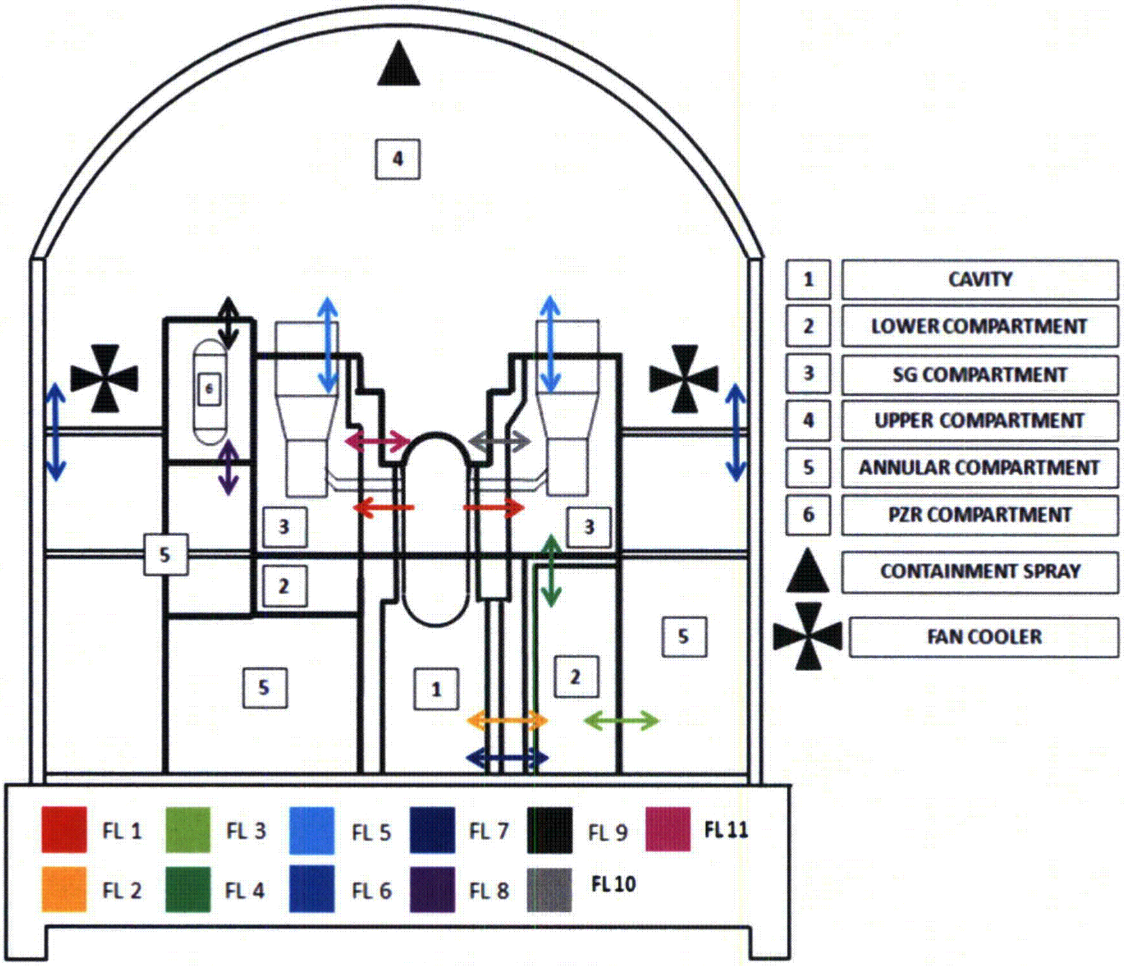

Figure 2.5.43 – MELCOR Nodalization Diagram

Validation Approach

The RELAP5 and MELCOR models were based on existing certified input files of the reactor system and containment.

The RELAP5-3D model was created starting from the RETRAN input file of the reactor system (65). All the geometrical information of the regions of the system were extracted from the RETRAN input file and specified in the RELAP input deck. Additional information was extracted from the MAAP input file for selected components (Steam Generators, SI system). The validation of the model was conducted by:

- Comparing the steady-state results for selected parameters with the plant normal operating conditions.
- Comparing the simulation results for selected LOCA scenarios with the plant simulator results.

The MELCOR model of the reactor containment was based on the existing MAAP input file (66). The model was modified to account for additional details retrieved from the CAD drawings and other plant-specific information.

Assumptions: The assumptions associated with the thermal-hydraulic simulations include the following (62):

- In all the cases, the break orientation was imposed at the bottom of the leg. In all the models used for the simulations, all the safety systems were assumed to be available throughout the transient.
- For the blowdown phase, it was assumed that the break would open instantaneously.
- For the six cases run with the *3D Vessel – 1D Core* model, it was assumed that the bottom of the core and baffle bypass flow paths would be fully blocked just after the start of ECCS recirculation. This is a conservative assumption because of the time-dependence associated with debris transport and accumulation. Also, significant quantities of debris would be required to reach the point where the core could be considered fully blocked (in most cases, full blockage would never occur).
- For the three additional cases run with open flow through the core bypass channel, center fuel assembly channel, or periphery fuel assembly channel, it was assumed that blockage of the other channels would occur just after the start of ECCS recirculation similar to the initial six cases.
- All the cases which produced a peak cladding temperature increase due to the core blockage which did not exceed 800 °F were assumed to be successful cases which may not lead to core damage.

Acceptance Criteria: The acceptance criterion for the thermal-hydraulic simulations was a peak cladding temperature of 800 °F.

Results: The models prepared were used to perform selected simulations of the reactor system and containment response under specific conditions. Three sets of simulations were performed:

1) Core Blockage Simulations to Support the In-Vessel Effects Analysis (62)
2) Sump Temperature Sensitivity Analysis to Support CASA Grande Calculations (32)
3) Sump Temperature Analysis for and Medium (6") and Large (DEG) LOCA to Support the CHLE Tests (67; 68)

Core Blockage Simulations to Support the In-Vessel Effects Analysis

The simulations were conducted using the RELAP5 model (3D Vessel – 1D core and 3D Vessel – 3D Core) to analyze the reactor system response under hypothetical core blockage scenarios during selected Loss of Coolant Accident (LOCA). The purpose of these calculations was to:

1) Identify the scenarios which may produce an increase in the peak cladding temperature and, subsequently, a potential core damage among selected LOCAs of different break sizes and locations under full core and core bypass blockage.
2) For the cases identified in 1), analyze the system response under a partial core blockage hypothesis.

The simulations performed for this task are listed below:

- Small Break (2") in Cold Leg.
- Small Break (2") in Hot Leg.
- Medium Break (6") in Cold Leg.
- Medium Break (6) in Hot Leg.
- Double-Ended Guillotine (DEG) Break in Cold Leg.
- Double-Ended Guillotine (DEG) Break in Hot Leg.

Table 2.5.38 summarized the basic assumptions and boundary conditions for the simulations:

Table 2.5.38 – Boundary Conditions

Parameter	Simulation Condition
ECCS	3 Trains Running (A, B, C)
Break Location	Cold Leg B, bottom
Core Blockage Methodology	Istantaneous Increase of the k-loss after Sump Switchover
Reactor Core Power (MWt)	3853
Axial Power Shape	Double Peak (0.15 and 0.8 Core Height)
Actinides	RELAP5-3D Default Actinide Model
Decay Heat Model	ANS73 +0%
RWST Temperature	85 F
ECCS Flow	Realistic

The blockage of the core was assumed to be instantaneous after the sump switchover. Both core and core bypass (baffle flow) were assumed to be blocked at the bottom. The peaking cladding temperature was used as figure of merit to determine the success of failure of the scenario simulated. All the cases which produced a peak cladding temperature after the core blockage which did not exceed 800 °F were assumed to be successful cases, which may not lead to core damage. The cases where the maximum peak cladding temperature was found to diverge after the core blockage time (exceeding the limiting temperature of 800 °F) were considered failing cases, which may lead to core damage. The peak cladding temperature for the scenarios analyzed is plotted in Figure 2.5.44 (small breaks), Figure 2.5.45 (medium breaks), and Figure 2.5.46 (DEG breaks).

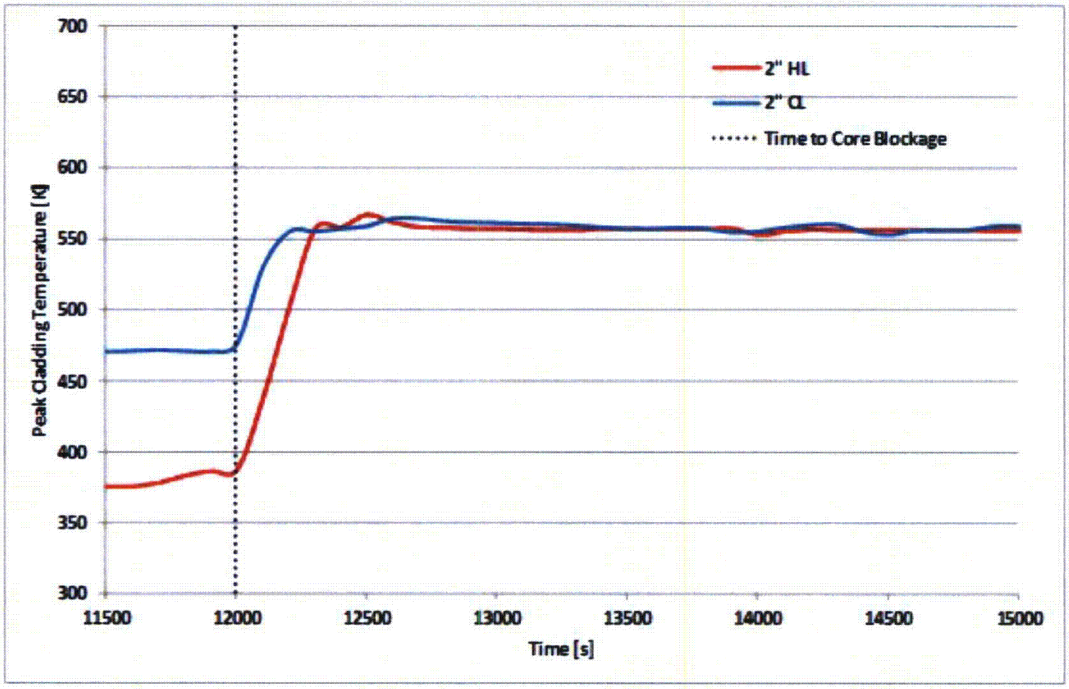

Figure 2.5.44 – Small break LOCA peak cladding temperature

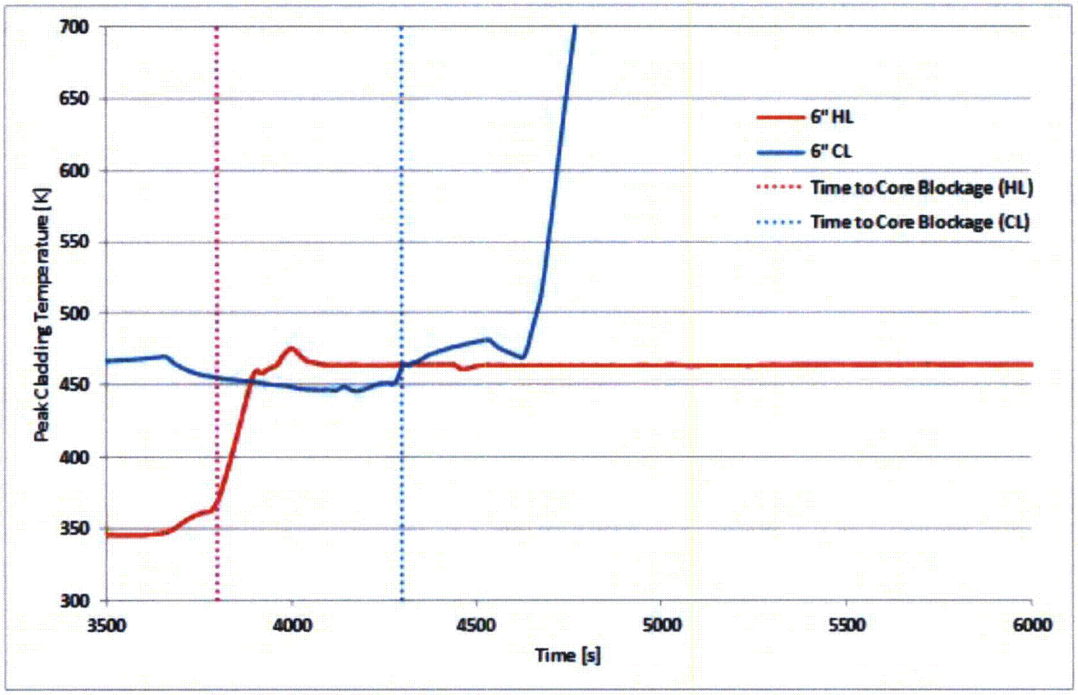

Figure 2.5.45 – Medium break LOCA peak cladding temperature

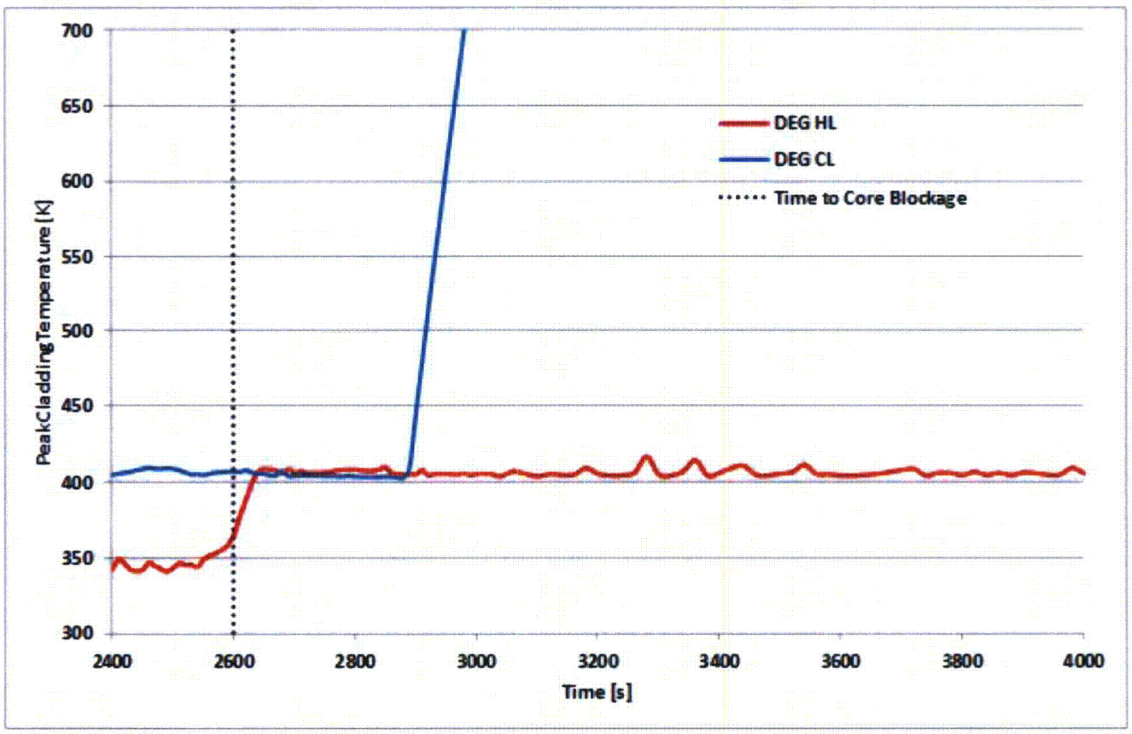

Figure 2.5.46 – DEG break LOCA peak cladding temperature

Table 2.5.39 summarizes the results obtained.

Table 2.5.39 – Core Blockage Scenarios - Summary

	Break Location	
Break Size	**Cold Leg**	**Hot Leg**
Small (2")	Pass	Pass
Medium (6")	Fail	Pass
Large (DEG)	Fail	Pass

Cold Leg Break Scenarios

For smaller breaks (2"), the injection system was found to be able to refill the steam generators with liquid water so that, at the time of core blockage, an alternative flow path was already available for the cooling water to reach to top of the core (from the cold leg injection point, through the steam generators tubes, and to the top of the core via the hot legs).

For larger break sizes (6" and DEG), the break flow takes most of the cooling water coming from the two intact injection loops. The water injected through the cold leg preferentially moved in the downcomer toward the broken cold leg. The steam generators were found to be empty at the time of core blockage so no available alternative flow paths were observed for these cases. The core peak cladding temperature was found to diverge starting from the core blockage time. The simulations were stopped when the maximum limit of 800 °F was reached.

Hot Leg Break Scenarios

Due to the break location compared to the loop injection location (cold leg) at the time to core blockage, the injected cooling water was forced to flow through the steam generators and reach the upper plenum before leaving the vessel through the broken hot leg.

Additional Simulations

Assuming the maximum peak cladding temperature as figure of merit, the scheme presented in Figure 2.5.47 summarizes the results of the simulations performed with the *3D Vessel – 3D Core* model (pass/fail).

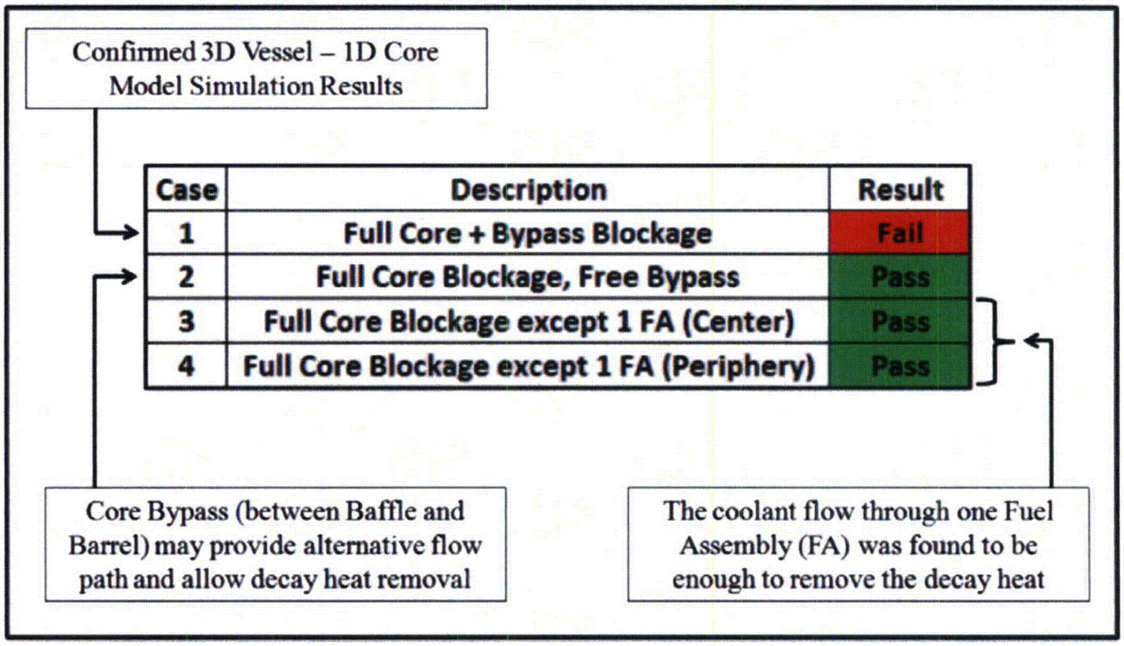

Figure 2.5.47 – Summary of thermal-hydraulic simulations for partial blockage

Case 1 showed what was previously found using the *3D Vessel – 1D Core* model: the peak cladding temperature steadily increases reaching the maximum limit, confirming that the full core and core bypass blockage assumption imposed in this case may lead to core damage. Case 2 showed that the flow through the core bypass is sufficient to provide the required coolant flow at the top of the core and minimize the peak cladding temperature, even if the core is assumed to be fully blocked. Cases 3 and 4 predicted a sufficient flow through only one free fuel assembly to supply the required coolant flow and maintain the peak cladding temperature under the limit.

Sump Temperature Sensitivity Analysis to Support CASA Grande Calculations

Simulations were conducted to study the effects of selected thermal-hydraulic parameters on the containment water temperature during the phases of Loss of Coolant Accidents (LOCA). LOCA scenarios of different break sizes (very small, small, medium, and large) were analyzed. Different conditions were also considered in the analysis to investigate the behavior of the reactor containment response. This included engineering features unavailability (fan coolers and containment sprays) or other operating conditions such as Component Cooling Water temperature and Residual Heat Removal heat exchanger's availability. RELAP5-3D was used to perform the simulations of the primary system (1D Model). The containment response was simulated using MELCOR.

The independent parameters selected for this analysis were:

- Break Size
- Number of Operating Containment Fan Coolers (2 or 6 in operation)
- Number of Operating Containment Sprays (3 trains or no trains available)

- Number of Operating Residual Heat Removal (RHR) Heat Exchangers (3 or no exchangers available)
- Component Cooling Water (CCW) Temperature (60 °F, 85.84 °F or 150 °F)

From the same sets of simulations, selected thermal-hydraulic parameters related to the primary system were also analyzed, such as:

- Time to Sump Switchover
- Total Safety Injection (SI) Flow Rate

Table 2.5.40 summarizes the cases simulated. All the cases assumed the break to be in cold leg. The maximum sump temperature (Column "Maximum" in Table 2.5.40) was achieved by minimizing the system heat removal capabilities (only two operating fan coolers, no containment sprays and RHR heat exchangers available, maximum CCW temperature). The minimum sump temperature (Column "Minimum" in Table 2.5.40) was achieved by maximizing the system heat removal capabilities (all the engineering features available, minimum CCW temperature). Complete engineering features availability and nominal CCW temperature were assumed to simulate the nominal (Column "Nominal" in Table 2.5.40) conditions.

Table 2.5.40 – Simulation matrix

	Operating Conditions (see Table 1.)		
Break Size	**Minimum**	**Nominal**	**Maximum**
1.5"		X	
2"	X	X	X
4"		X	X
6"	X	X	X
8"		X	X
15"		X	X
DEG (27.5")		X	X

Results were summarized in terms of containment pressure and sump temperature profiles as a function of the break size and implemented into CASA Grande. Figure 2.5.48 shows an example of the sump temperature profiles for the nominal case (by break size) used for the CASA Grande calculations. Examples of additional parameters extracted, such as sump switchover time and total SI flow rate, are shown in Table 2.5.41.

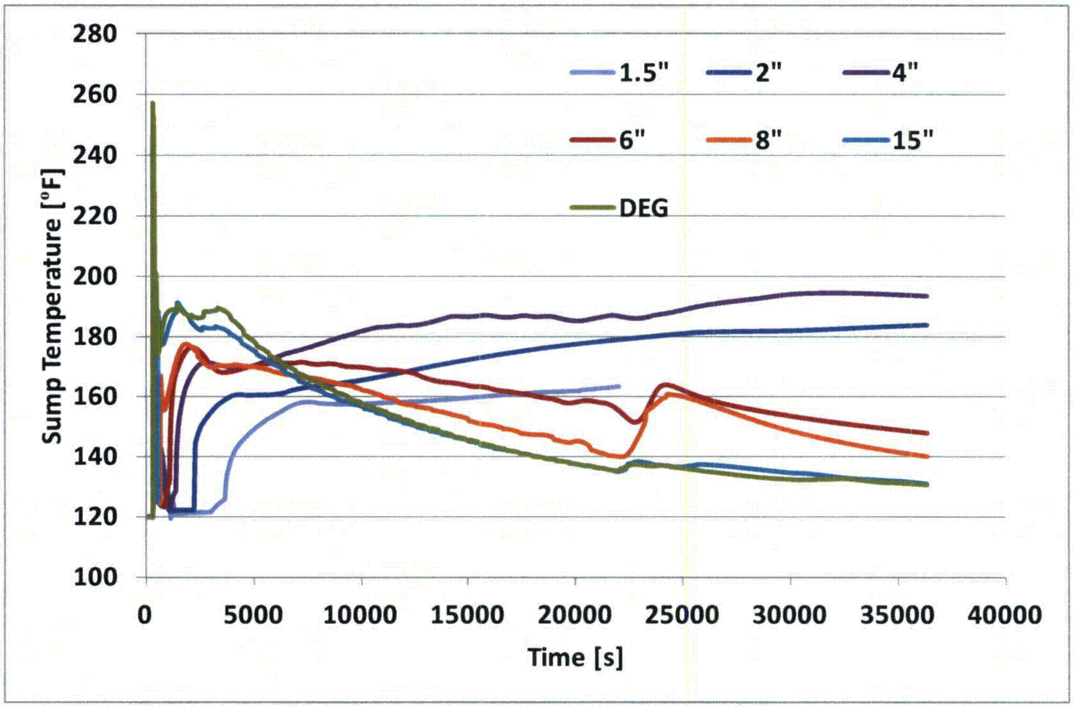

Figure 2.5.48 – Example of the sump sensitivity results (nominal cases)

Table 2.5.41 – Results summary (nominal cases)

Break Size	1.5"	2"	4"	6"	8"	15"	DEG
Sump Switchover Time	5.6h	1.3h	55.9m	44.2m	37.8m	31.2m	29.5m
Total SI (US gal/min)	1230.686	2075.797	4119.646	7950.749	10285.35	11779.73	11988.22

Sump Temperature Analysis for a Medium (6") and Large (DEG) LOCA to Support the CHLE Tests

The simulation of the containment response during a medium (6") and large (DEG) break Loss of Coolant Accident (LOCA) scenario in the cold leg was performed in order to predict the sump water temperature profile during a period of 30 days from the break event, to support the CHLE tests. The MELCOR model was used to perform the calculations of the reactor containment response. The boundary conditions for the MELCOR simulations were calculated with the RELAP5-3D (1D Model) model. The simulation approach was similar to the one described for the nominal cases for the sump temperature sensitivity analysis. Selected thermal-hydraulic parameters of reactor containment and primary system were provided to the CHLE test team, such as:

- Sump Compartment Water Temperature
- Water Temperature Variation through the Residual Heat Removal (RHR) Heat Exchangers

The simulations were extended to comprehend:

a) A 300s *Steady-State* Phase

b) The *Safety Injection* phase (from break opening at t = 300s to the sump switchover time)
c) The *Long-Term Cooling* phase with *Cold Leg Injection* (from the sump switchover time to the Hot Leg switchover time)
d) The *Long-Term Cooling* phase with the *Hot Leg Injection* (from the Hot Leg switchover time up to t_{end} = 30 days)

Figure 2.5.49 and Figure 2.5.50 show the sump pool temperature profile calculated with MELCOR for the 6" cold leg break scenarios. The temperature profile for the 15" cold leg break scenario is shown in Figure 2.5.51 and Figure 2.5.52.

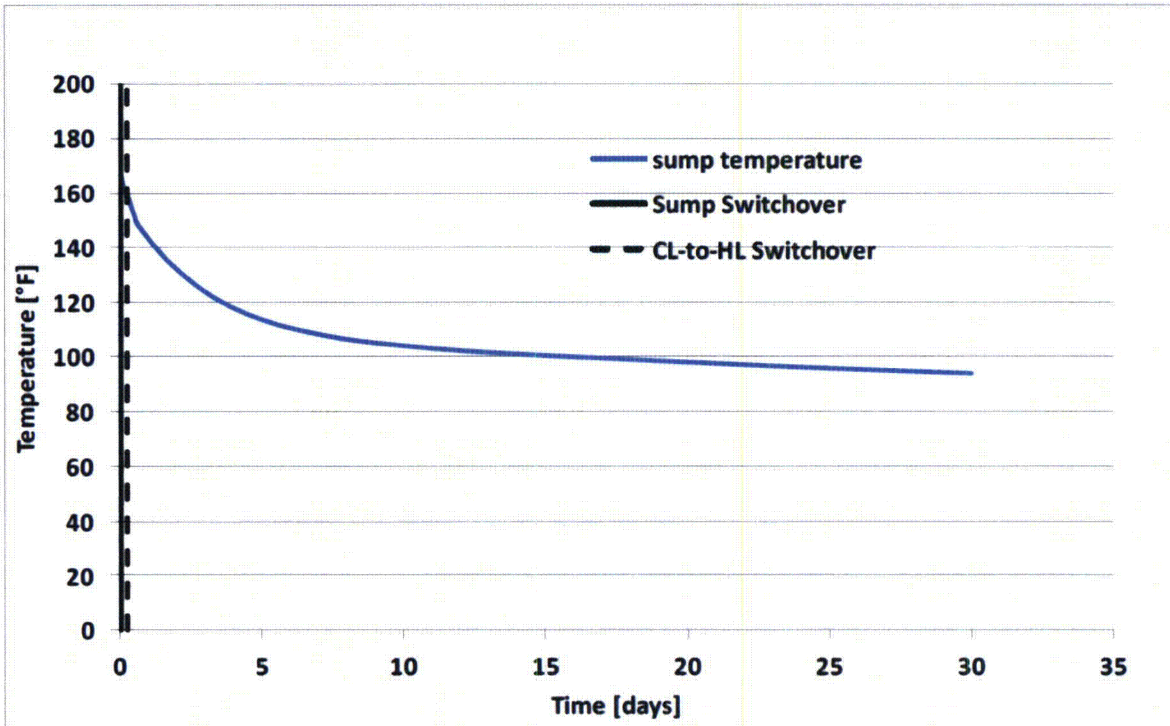

Figure 2.5.49 – 6" break sump temperature profile (30-day overview)

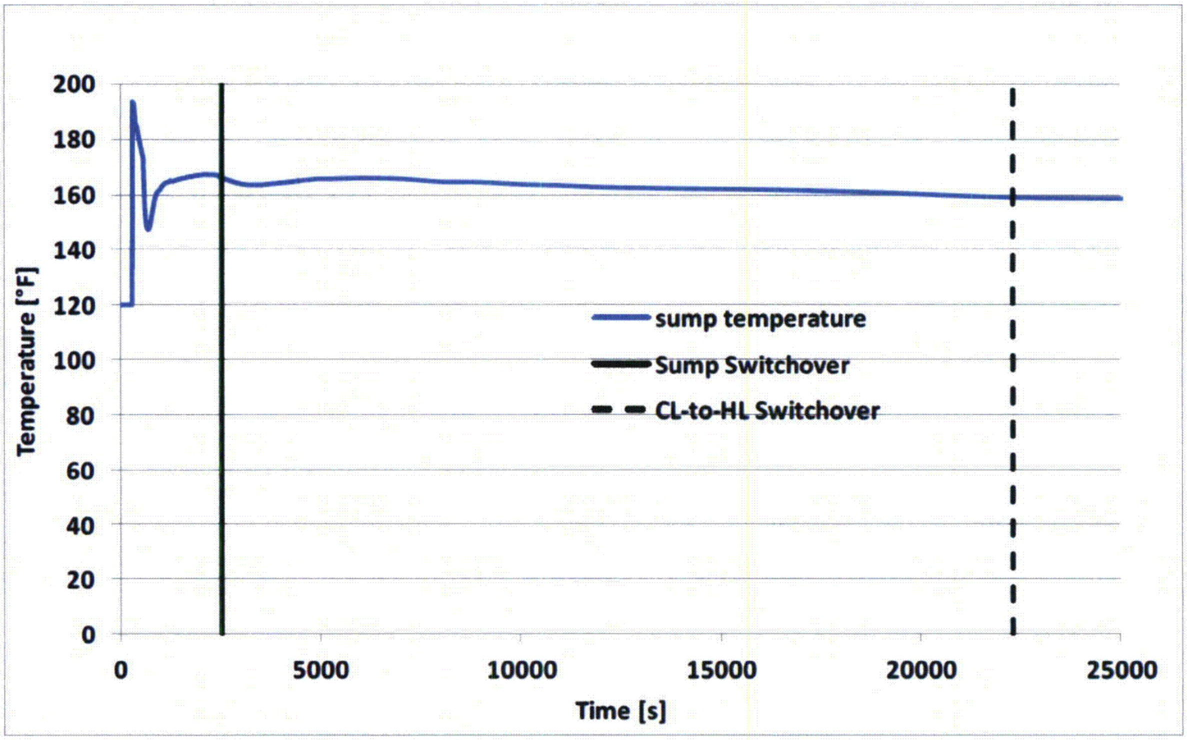

Figure 2.5.50 – 6" break sump temperature profile (zoom)

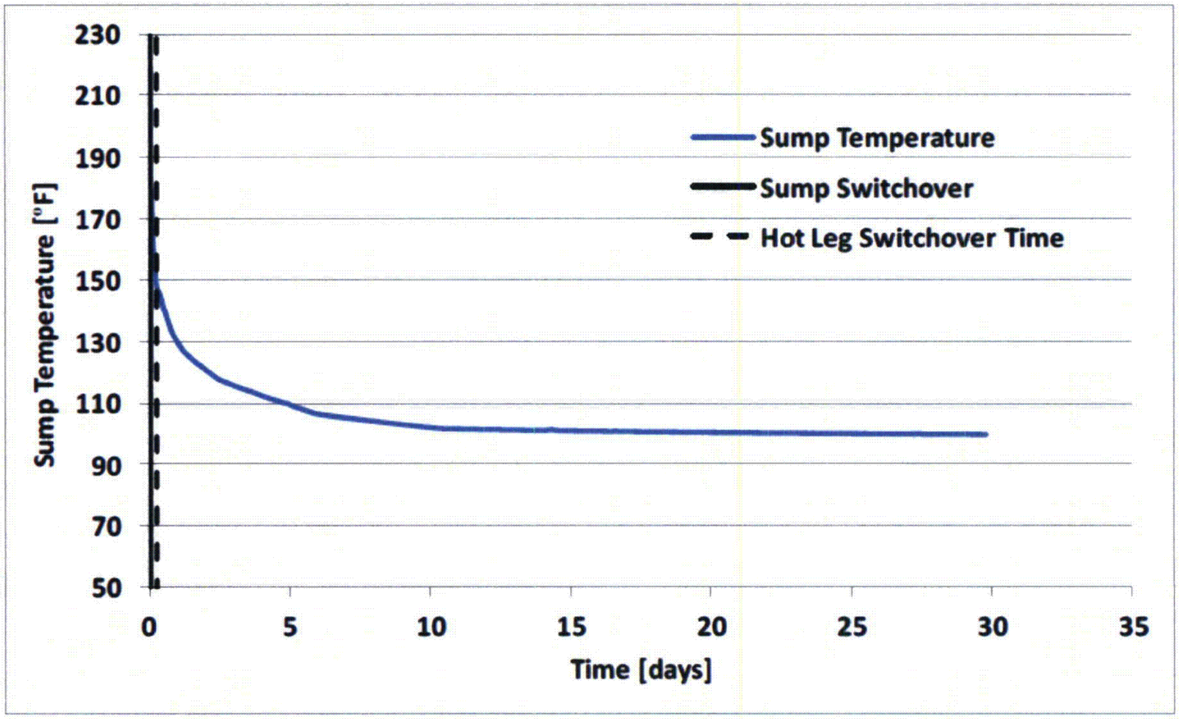

Figure 2.5.51 – 15" break sump temperature profile (30-day overview)

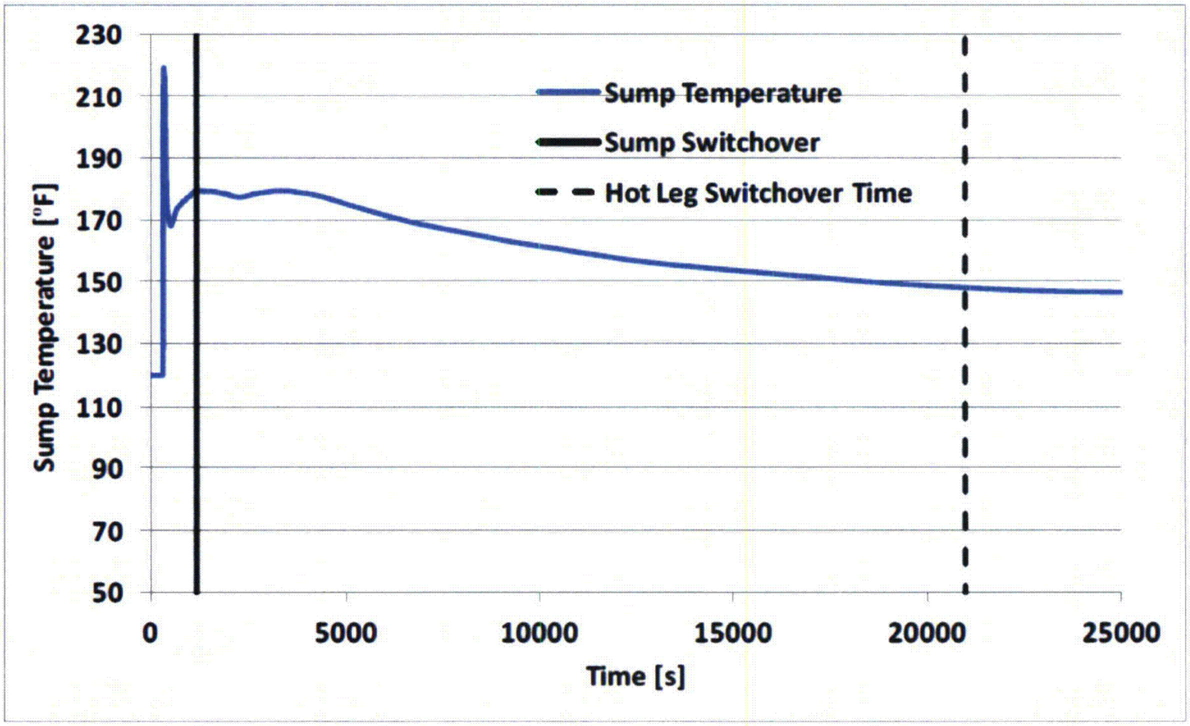

Figure 2.5.52 – 15" break sump temperature profile (zoom)

Additional details on how the thermal-hydraulic results were used in the overall GSI-191 evaluation are provided in Volume 3 (12).

Item 5.a.15: Boric Acid Precipitation

Method: Significant boron precipitation is most likely to occur for a medium or large cold leg break during cold leg injection. In this scenario the water in the core would be boiling and the net flow entering the core would be equivalent to the decay heat boil-off rate. To prevent boron precipitation in these scenarios, the SI flow is switched from cold leg injection to hot leg injection. The required switchover timing is dependent on the concentration of boron in the RCS/RWST/accumulators, the decay heat level, and natural mixing processes within the reactor vessel based on temperature and/or density gradients. The generic methodology used for evaluating boron precipitation has been questioned by the NRC (69), and the PWROG is currently addressing these concerns to determine whether the physical phenomena associated with temperature or density driven mixing have been appropriately modeled. The reason that boron precipitation was included in the overall GSI-191 issue, however, is that even if the physical phenomena for temperature and density driven mixing was appropriately modeled previously, the formation of a debris bed at the bottom of the core may interrupt these natural mixing processes and accelerate the onset of boron precipitation.

Based on an STP-specific evaluation using the old methodology, it was determined that boron precipitation would not occur until at least 7.0 hours after the initiation of the event (70). For the risk-informed GSI-191 evaluation, it was assumed that the previous methodology was appropriate, and that boron precipitation would not occur unless a significant debris bed builds up on the bottom of the core that could disrupt the natural mixing processes that were credited.

Basis: The basis for the current switchover time is documented in the hot leg switchover calculation (70). The basis for the fiber acceptance criteria of 7.5 g/FA is documented in the SER on WCAP-16793-NP (71).

Assumptions: The following assumptions related to boron precipitation were made in Volume 3 (12).

- It was assumed that the current STP design basis evaluation methodology used to calculate the required hot leg switchover timing is appropriate with the exception of GSI-191 related phenomenon (i.e., formation of a debris bed on the core). This is an appropriate assumption since the generic boron precipitation issues not related to GSI-191 are being separately addressed by the PWROG and do not need to be evaluated for GSI-191 closure.
- It was assumed that for a medium or large cold leg break during cold leg injection, a fiber debris load of at least 7.5 g/FA would form a debris bed that would prevent the natural mixing processes credited in the design basis hot leg switchover calculation resulting in boron precipitation prior to switchover. This is a conservative assumption since a debris bed of 15 g/FA was necessary to capture chemical precipitates and cause significant blockage concerns.
- It was assumed that boron precipitation would not be an issue for small breaks. This is a reasonable assumption since natural circulation would maintain a relatively steady concentration of boron in the core. Boron precipitation failures were not explicitly precluded for

small breaks (i.e., the same acceptance criteria were used for all break sizes). However, no boron precipitation failures were observed to occur for small breaks.

- It was assumed that boron precipitation would not be an issue for medium and large hot leg breaks. This is a reasonable assumption since at least one train would be injecting in the cold leg throughout the event. This flow would pass through the core and maintain a relatively steady concentration of boron. Even if significant core blockage occurs, some flow would still pass through the debris bed and flush through the core.

Acceptance Criteria: For medium and large cold leg breaks, the acceptance criterion for boron precipitation was assumed to be 7.5 g/FA of fiber debris on the core.

Results: Due to the more stringent acceptance criterion, all in-vessel failures were attributed to boron precipitation. In the final evaluation, failure due to boron precipitation was not predicted for any of the small or medium breaks. The conditional probability of in-vessel failure given a large break scenario was only 1.25E-03 for the baseline case where all trains of ECCS are operating.

Additional details on how the boron precipitation issue was addressed in the overall GSI-191 evaluation are provided in Volume 3 (72).

Item 5.a.16: Probability Distributions

The computer simulation model, CASA Grande, has numerous input variables detailed in Volume 3; see Figure 1.1 of Section 1 in (12) for an overview. Some of these input parameters are treated as deterministic parameters while others are treated as random variables with specified probability distributions. The manner in which these probability distributions were determined depends on the nature of the information available regarding the specific parameter in question. To give an idea of the range of methods, the probability distributions for LOCA frequency and fiberglass penetration are discussed. Also, further discussion of the method for modeling the joint distribution of multiple random parameters as implemented in CASA Grande is provided.

LOCA Frequency

A probability distribution is used to model the LOCA frequency for breaks of different sizes at different locations within the plant. The following assumptions were made in order to determine the distribution:

- It was assumed that the geometric mean aggregation of LOCA frequencies in NUREG-1829 (73) is the most appropriate set of results to use for this evaluation. The NUREG-1829 data must be fit to appropriately determine the epistemic uncertainty associated with LOCA frequency estimates. Based on an evaluation of the relative merits of the arithmetic mean and geometric mean, the geometric mean aggregation was determined to be more representative of the overall consensus of the panelists (74).
- It was assumed that the current-day LOCA frequencies are more appropriate to use for this evaluation than the end-of-plant-license frequencies. This is a reasonable assumption for the

base analysis, although the effect of using end-of-plant-license frequencies can be evaluated as a sensitivity case.

- It was assumed that breaks on non-weld locations can be excluded from the evaluation. This is a reasonable assumption since the break frequency for non-weld locations would be significantly smaller than weld locations, and would not generate significantly different quantities of debris from the weld breaks. It was also assumed that isolable breaks can be excluded from the evaluation since isolable breaks would not lead to recirculation.
- Linear-linear interpolation of top-down LOCA frequencies from NUREG-1829 was used to preserve uniform probability density between expert elicitation points provided in the tables. Uniform probability density avoids any attribution of behavior that the panel did not intend and generally shifts probability density to larger break sizes.
- It was also assumed that the bottom-up LOCA frequencies that are used to assign relative frequencies to the individual weld locations can be linearly interpolated. This does not necessarily introduce conservatism to the analysis since the bottom-up frequencies are scaled to match the top-down NUREG-1829 frequencies. However, it is a reasonable approach given an incomplete understanding of the physical behavior of the LOCA frequency curve between the established values.
- Out of 193 welds on small bore (0.75-inch and 1-inch) pipes, only 35 were modeled with 3 welds modeled on 1-inch pipes and 32 welds modeled on 0.75-inch pipes (75). It was assumed that the overall break frequency for the 193 welds can be distributed across the 35 welds (176 welds assumed to be 0.75-inch and 17 welds assumed to be 1-inch). This is a reasonable assumption since breaks of this size are generally insignificant with respect to GSI-191 phenomena. Also, since the 35 welds that were modeled are scattered around containment, it is not likely that the weld locations that were not modeled would have any significant differences with respect to the quantity of debris that would be generated or transported from the locations that were modeled.
- With exception to the small bore weld count, it was assumed that the weld count in the CAD model (75) is more accurate than the weld count in the LOCA frequency report (76) in any cases where there are deviations. This is a reasonable assumption since the CAD model includes specific references to the source drawings and is consistent with the component database (77).

The steps used in determining the probability distribution and sampling that distribution in the CASA Grande implementation are summarized as follows (12):

1. Calculate the relative weight of breaks for specific weld categories based on pipe size, weld type, applicable degradation mechanisms, etc., and distribute total LOCA frequency to each weld location based on relative weight between weld cases.
2. Identify applicable weld category and spatial coordinates for each weld location.
3. Statistically fit the NUREG-1829 frequencies (5^{th}, Median, and 95^{th}) using a bounded Johnson distribution for each size category. These fits represent the epistemic uncertainty associated with LOCA frequencies.

4. Sample epistemic uncertainty (e.g., 62nd percentile) and determine the corresponding total frequency curve based on the bounded Johnson fits (assuming linear interpolation between size categories).
5. Sample break sizes at each weld location and proceed with the GSI-191 analysis carrying the appropriate probability weight with each break scenario.

Forming probability distributions for the frequencies of LOCA pipe breaks, particularly larger breaks, presents challenges because of limited data from operating experience due to the very low probabilities of these breaks occurring. The probability distribution for LOCA frequency is informed by two sources. The first source is NUREG-1829 (78), which documents an expert elicitation of the percentiles (5th, 50th, and 95th) for breaks of six effective sizes for PWR plants without inclusion of contributions due to steam generator tube ruptures; namely, NUREG-1829 Table 7.19 is used for the current-day fleet (25 years average fleet operation). This is illustrated in Table 2.5.42.

Table 2.5.42 – NUREG-1829 PWR current-day LOCA frequencies and fitted Johnson parameters

Size (in)	NUREG-1829 Quantiles				Fitted Johnson Parameters			
	5th	Median	Mean	95th	γ	δ	ξ	λ
0.5	6.80E-05	6.30E-04	1.90E-03	7.10E-03	1.650950	5.256964E-01	4.117000E-05	1.420E-02
1.625	5.00E-06	8.90E-05	4.20E-04	1.60E-03	1.646304	4.593913E-01	2.530000E-06	3.200E-03
2[1]	3.69E-06	6.57E-05	3.10E-04	1.18E-03	1.646308	4.593851E-01	1.870000E-06	2.361E-03
3	2.10E-07	3.40E-06	1.60E-05	6.10E-05	1.646605	4.589467E-01	1.200000E-07	1.220E-04
6[1]	6.30E-08	1.08E-06	5.20E-06	1.98E-05	1.646403	4.566256E-01	3.000000E-08	3.965E-05
7	1.40E-08	3.10E-07	1.60E-06	6.10E-06	1.645739	4.487957E-01	6.023625E-09	1.220E-05
14	4.10E-10	1.20E-08	2.00E-07	5.80E-07	1.645211	3.587840E-01	2.892430E-10	1.160E-06
31	3.50E-11	1.20E-09	2.90E-08	8.10E-08	1.645072	3.343493E-01	2.636770E-11	1.600E-07

The second source is an STP-specific study (79), which allows a distribution of the overall frequency associated with a particular break size across different weld locations in the plant, using a total of 45 categories of welds. Table 2.5.43 and Table 2.5.44 illustrate the 45 categories of welds and the damage mechanisms.

[1] The quantiles are not explicitly defined in NUREG-1829 for 2-inch and 6-inch breaks. However, these values were linearly interpolated from the 1-5/8-inch, 3-inch, and 7-inch break categories (60).

Table 2.5.43 – Definition of Major Piping System Component Cases

Case	Description	Weld Type	Damage Mechanism (DM)	Comment
1	RCS Hot Leg Excl. SG Inlet	B-F	PWSCC, D&C	Design basis LOCA location; B-F weld has higher failure rate but located inside Rx cavity
		B-J	TF, D&C	
2	RCS Cold Leg	B-F	PWSCC, D&C	Lower temperatures and different pipe sizes relative to hot leg
		B-J	D&C	
3	RCS Hot Leg SG Inlet	B-F	PWSCC, D&C	This case defined to address S/G Inlet nozzle-to-safe-end weld that has unusual failure count distribution[1]
4	PZR Surge Line	B-F	PWSCC, TF, D&C	Includes surge line from branch connections and nozzles to pressurizer safe end; entire surge line subjected to thermal transients during startup and shutdown
		B-J, BC	TF, D&C	
5	PZR Medium Bore Piping	B-F	PWSCC, TF, D&C	This includes pressurizer spray, and relief valve piping excluding the pressurizer surge line; B-F welds at STP in this category have weld overlays[2]
		B-J, BC	TF, D&C	
6	Class 1 Small Bore Piping	B-J	TF, D&C, TGSCC, VF	This is all the class 1 piping of size 2" and less and inside isolation valves
7	Class 1 Medium Bore SIR Piping	B-J	TF, D&C, IGSCC	Safety injection and residual heat removal (RHR) systems in standby during normal operation; Class 1 is inside the isolation valves
8	Class 1 Medium Bore CVCS Piping	B-J, BC	TF, D&C, TGSCC, VF	CVCS Piping with injection and letdown flow during normal operation

B-F	ASME XI Category B-F welds (bimetallic)
B-J	ASME XI Category B-J welds (single metal)
BC	Branch connection welds, B-J welds used at branch connections
CVCS	Chemical, Volume, and Control System
D&C	Design and Construction Defects
IGSCC	Intergranular Stress Corrosion Cracking
PWSCC	Primary Water Stress Corrosion Cracking
PZR	Pressurizer
RCS	Reactor Coolant System
SIR	Safety Injection and Recirculation Systems
TF	Thermal Fatigue, including that due to thermal transients (TT) and thermal stratification (TASC)
VF	Vibration Fatigue

Notes:
[1] An unusually high incidence of failures of this component was observed at japanese plants following Steam Generator replacements. Until it can be ruled out for STP it is included in this study. [2] NOC-AE-06002099 (January 30, 2007): Inspection and Mitigation of Alloy 82/182 Pressurizer Butt Welds, South Texas Nuclear Operating Company.

Table 2.5.44 – Definition of Specific Component Categories

System Case	System	Component Case	Weld Type	Applicable DM	STP Total No. of Welds	Pipe Size (in.)	DEGB Size (in.)
1	RC Hot Leg	1A	B-F	SC, D&C	4	29	41.0
		1B	B-J	D&C	11	29	41.0
		1C	B-J	TF, D&C	1	29	41.0
2	RC SG Inlet	2	B-F	SC, D&C	4	29	41.0
3	RC Cold Leg	3A	B-F	SC, D&C	4	27.5	38.9
		3B	B-J		4	31	43.8
		3C	B-J	D&C	12	27.5	38.9
		3D	B-J		24	31	43.8
4	RC Surge	4A	B-F	SC, TF, D&C	1	16	22.6
		4B	B-J	TF, D&C	7	16	22.6
		4C	BC		2	16	22.6
		4D	B-J		6	2.5	3.5
5	PZR	5A	B-J	TF, D&C	29	6	8.5
		5B	B-J		14	3	4.2
		5C	B-J	D&C	53	4	5.7
		5D	B-J		4	3	4.2
		5E	B-J		29	6	8.5
		5F	B-F	SC, TF, D&C	0	6	8.5
		5G	B-F	SC, D&C	0	6	8.5
		5H	B-F	D&C (Weld Overlay)	4	6	8.5
		5I	BC	D&C	2	4	5.7
		5J	B-J	TF, D&C	2	2	2.8
6	Small Bore	6A	B-J	VF, SC, D&C	16	2	2.8
		6B	B-J		193	1	1.4
7	SIR Lines Excl. Accumulator	7A	B-J	TF, D&C	21	12	17.0
		7B	B-J		9	8	11.3
		7C	B-J	SC, TF, D&C	3	8	11.3

		7D	B-J	SC, D&C	3	12	17.0
		7E	B-J, BC	D&C	57	12	17.0
		7F	B-J		30	10	14.1
		7G	B-J, BC		42	8	11.3
		7H	B-J		23	6	8.5
		7I	BC		5	4	5.7
		7J	BC		9	3	4.2
		7K	BC		10	2	2.8
		7L	B-J		0	1.5	2.1
	SIR Accumulator Lines	7M	B-J	SC, D&C	0	12	17.0
		7N	B-J	TF, D&C	35	12	17.0
		7O	B-J, BC	D&C	15	12	17.0
8	CVCS	8A	B-J	TF, VF, D&C	10	2	2.8
		8B	B-J		19	4	5.7
		8C	B-J	VF, D&C	47	2	2.8
		8D	B-J		6	4	5.7
		8E	BC	TF, D&C	4	4	5.7
		8F	BC	D&C	1	4	5.7
				Total	775		

This allows a joint distribution to be formed across break size and weld location that distinguishes different weld types of the same size based on degradation mechanisms, while maintaining consistency with NUREG-1829 for the fleet-wide quantiles. While NUREG-1829 uses six effective break sizes, a continuum of break sizes is modeled using a linear interpolation between the neighboring break sizes for the NUREG-1829 quantiles. This is equivalent to assuming that a uniform distribution governs the break size between, e.g., the NUREG-1829 sizes of a 7-inch and a 14-inch break. Table 2.5.45 through Table 2.5.52 show the relative frequencies of breaks in various weld locations based on specific DMs for categories of welds.

Table 2.5.45 – Relative frequencies vs. break size for hot leg, SG inlet, and cold leg welds (Categories 1A through 3B)

Category	1A		1B		1C		2		3A		3B	
System	Hot Leg		Hot Leg		Hot Leg		SG Inlet		Cold Leg		Cold Leg	
Pipe Size (in)	29		29		29		29		27.5		31	
DEGB (in)	41.01		41.01		41.01		41.01		38.89		43.84	
Weld Type	B-F		B-J		B-J		B-F		B-F		B-F	
DM	SC, D&C		D&C		TF, D&C		SC, D&C		SC, D&C		SC, D&C	
No. Welds	4		11		1		4		4		4	
	Break Size, X (in)	**F(LOCA≥X)**	**Break Size, X (in)**	**F(LOCA≥X)**	**Break Size, X (in)**	**F(LOCA≥X)**	**Break Size, X (in)**	**F(LOCA≥X)**	**Break Size, X (in)**	**F(LOCA≥X)**	**Break Size, X (in)**	**F(LOCA≥X)**
	0.50	4.02E-07	0.50	1.95E-09	0.50	1.25E-08	0.50	1.98E-06	0.50	1.51E-07	0.50	1.51E-07
	1.50	9.25E-08	1.50	4.49E-10	1.50	2.87E-09	1.50	4.59E-07	1.50	3.43E-08	1.50	3.43E-08
	2.00	6.92E-08	2.00	3.36E-10	2.00	2.15E-09	2.00	3.45E-07	2.00	2.38E-08	2.00	2.38E-08
	3.00	4.61E-08	3.00	2.24E-10	3.00	1.43E-09	3.00	2.31E-07	3.00	1.42E-08	3.00	1.42E-08
	4.00	3.19E-08	4.00	1.55E-10	4.00	9.90E-10	4.00	1.60E-07	4.00	9.49E-09	4.00	9.49E-09
	6.00	1.89E-08	6.00	9.19E-11	6.00	5.89E-10	6.00	9.52E-08	6.00	5.39E-09	6.00	5.39E-09
	6.75	1.61E-08	6.75	7.83E-11	6.75	5.01E-10	6.75	8.12E-08	6.75	4.53E-09	6.75	4.53E-09
	14.00	7.01E-09	14.00	3.40E-11	14.00	2.18E-10	14.00	3.35E-08	14.00	2.01E-09	14.00	2.01E-09
	20.00	3.70E-09	20.00	1.80E-11	20.00	1.15E-10	20.00	1.81E-08	20.00	1.15E-09	20.00	1.15E-09
	29.00	1.90E-09	29.00	9.24E-12	29.00	5.92E-11	29.00	9.57E-09	27.50	6.96E-10	27.50	6.96E-10
	31.50	1.64E-09	31.50	7.97E-12	31.50	5.11E-11	31.50	8.30E-09	31.50	5.63E-10	31.50	5.63E-10
	41.01	1.04E-09	41.01	5.03E-12	41.01	3.22E-11	41.01	5.24E-09	38.89	4.12E-10	43.80	3.38E-10

Table 2.5.46 – Relative frequencies vs. break size for cold leg and surge line welds (Categories 3C through 4D)

Category	3C		3D		4A		4B		4C		4D	
System	Cold Leg		Cold Leg		Surge Line		Surge Line		Surge Line		Surge Line	
Pipe Size (in)	27.5		31		16		16		16		2.5	
DEGB (in)	38.89		43.84		22.63		22.63		22.63		3.54	
Weld Type	B-J		B-J		B-F		B-J		BC		B-J	
DM	D&C		D&C		SC, TF, D&C		TF, D&C		TF, D&C		TF, D&C	
No. Welds	12		24		1		7		2		6	
	Break Size, X (in)	**F(LOCA≥X)**	**Break Size, X (in)**	**F(LOCA≥X)**	**Break Size, X (in)**	**F(LOCA≥X)**	**Break Size, X (in)**	**F(LOCA≥X)**	**Break Size, X (in)**	**F(LOCA≥X)**	**Break Size, X (in)**	**F(LOCA≥X)**
	0.50	2.79E-09	0.50	2.79E-09	0.50	9.75E-06	0.50	7.44E-08	0.50	1.21E-07	0.50	7.44E-08
	1.50	6.33E-10	1.50	6.33E-10	1.50	3.30E-06	1.50	2.52E-08	1.50	4.11E-08	1.50	2.52E-08
	2.00	4.39E-10	2.00	4.39E-10	2.00	2.43E-06	2.00	1.85E-08	2.00	3.02E-08	2.00	1.85E-08
	3.00	2.62E-10	3.00	2.62E-10	3.00	1.58E-06	3.00	1.20E-08	3.00	1.97E-08	3.00	1.20E-08
	4.00	1.75E-10	4.00	1.75E-10	4.00	1.03E-06	4.00	7.82E-09	4.00	1.28E-08	3.54	9.42E-09
	6.00	9.95E-11	6.00	9.95E-11	6.00	5.58E-07	6.00	4.26E-09	6.00	6.94E-09		
	6.75	8.36E-11	6.75	8.36E-11	6.75	4.68E-07	6.75	3.57E-09	6.75	5.82E-09		
	14.00	3.70E-11	14.00	3.70E-11	14.00	1.18E-07	14.00	9.03E-10	14.00	1.47E-09		
	20.00	2.11E-11	20.00	2.11E-11	16.00	9.19E-08	16.00	7.02E-10	16.00	1.15E-09		
	27.50	1.28E-11	27.50	1.28E-11	20.00	6.14E-08	20.00	4.69E-10	20.00	7.65E-10		
	31.50	1.04E-11	31.50	1.04E-11	22.63	4.77E-08	22.63	3.64E-10	22.63	5.93E-10		
	38.89	7.60E-12	43.80	6.23E-12								

Table 2.5.47 – Relative frequencies vs. break size for pressurizer line welds (Categories 5A through 5F)

Category	5A		5B		5C		5D		5E		5F	
System	Pressurizer		Pressurizer		Pressurizer		Pressurizer		Pressurizer		Pressurizer	
Pipe Size (in)	6		3		4		3		6		6	
DEGB (in)	8.49		4.24		5.66		4.24		8.49		8.49	
Weld Type	B-J		B-J		B-J		B-J		B-J		B-F	
DM	TF, D&C		TF, D&C		D&C		D&C		D&C		SC, TF, D&C	
No. Welds	29		14		53		4		29		0	
	Break Size, X (in)	**F(LOCA≥X)**	**Break Size, X (in)**	**F(LOCA≥X)**	**Break Size, X (in)**	**F(LOCA≥X)**	**Break Size, X (in)**	**F(LOCA≥X)**	**Break Size, X (in)**	**F(LOCA≥X)**	**Break Size, X (in)**	**F(LOCA≥X)**
	0.50	4.59E-08	0.50	4.59E-08	0.50	1.72E-08	0.50	1.72E-08	0.50	1.72E-08	0.50	5.09E-06
	0.75	2.76E-08	0.75	2.76E-08	0.75	1.03E-08	0.75	1.03E-08	0.75	1.03E-08	0.75	3.06E-06
	1.00	1.96E-08	1.00	1.96E-08	1.00	7.33E-09	1.00	7.33E-09	1.00	7.33E-09	1.00	2.17E-06
	1.50	1.24E-08	1.50	1.24E-08	1.50	4.64E-09	1.50	4.64E-09	1.50	4.64E-09	1.50	1.38E-06
	2.00	6.64E-09	2.00	6.64E-09	2.00	2.49E-09	2.00	2.49E-09	2.00	2.49E-09	2.00	7.36E-07
	3.00	2.75E-09	3.00	2.75E-09	3.00	1.03E-09	3.00	1.03E-09	3.00	1.03E-09	3.00	3.05E-07
	4.24	1.30E-09	4.24	1.30E-09	4.24	4.87E-10	4.24	4.87E-10	4.24	4.87E-10	4.24	1.44E-07
	5.66	6.26E-10			5.66	2.34E-10			5.66	2.34E-10	5.66	6.94E-08
	6.00	5.47E-10							6.00	2.05E-10	6.00	6.06E-08
	6.75	4.16E-10							6.75	1.56E-10	6.75	4.61E-08
	8.49	2.64E-10							8.49	9.89E-11	8.49	2.93E-08

Table 2.5.48 – Relative frequencies vs. break size for pressurizer and small bore line welds (Categories 5F through 6B)

Category	5G		5H		5I		5J		6A		6B	
System	Pressurizer		Pressurizer		Pressurizer		Pressurizer		Small Bore		Small Bore	
Pipe Size (in)	6		6		4		2		2		1	
DEGB (in)	8.49		8.49		5.66		2.83		2.83		1.41	
Weld Type	B-F		B-F		BC		B-J		B-J		B-J	
DM	SC, D&C		D&C (Weld Overlay)		D&C		TF, D&C		VF, SC, D&C		VF, SC, D&C	
No. Welds	0		4		2		2		16		193	
	Break Size, X (in)	**F(LOCA≥X)**	**Break Size, X (in)**	**F(LOCA≥X)**	**Break Size, X (in)**	**F(LOCA≥X)**	**Break Size, X (in)**	**F(LOCA≥X)**	**Break Size, X (in)**	**F(LOCA≥X)**	**Break Size, X (in)**	**F(LOCA≥X)**
	0.50	5.01E-06	0.50	1.74E-08	0.50	1.72E-08	0.50	4.59E-08	0.50	1.22E-06	0.50	1.22E-06
	0.75	3.01E-06	0.75	1.05E-08	0.75	1.03E-08	0.75	2.76E-08	0.75	7.18E-07	0.75	7.18E-07
	1.00	2.13E-06	1.00	7.42E-09	1.00	7.33E-09	1.00	1.96E-08	1.00	5.00E-07	1.00	5.00E-07
	1.50	1.35E-06	1.50	4.70E-09	1.50	4.64E-09	1.50	1.24E-08	1.40	3.30E-07	1.40	3.30E-07
	2.00	7.24E-07	2.00	2.52E-09	2.00	2.49E-09	2.00	6.64E-09	1.50	3.08E-07		
	3.00	3.00E-07	3.00	1.04E-09	3.00	1.03E-09	2.83	3.13E-09	1.99	1.75E-07		
	4.24	1.42E-07	4.24	4.94E-10	4.24	4.87E-10			2.00	1.73E-07		
	5.66	6.83E-08	5.66	2.37E-10	5.66	2.34E-10			2.80	8.66E-08		
	6.00	5.96E-08	6.00	2.07E-10								
	6.75	4.54E-08	6.75	1.58E-10								
	8.49	2.88E-08	8.49	1.00E-10								

Table 2.5.49 – Relative frequencies vs. break size for safety injection and recirculation line welds (Categories 7A through 7F)

Category	7A		7B		7C		7D		7E		7F	
System	SIR		SIR		SIR		SIR		SIR		SIR	
Pipe Size (in)	12		8		8		12		12		10	
DEGB (in)	16.97		11.31		11.31		16.97		16.97		14.14	
Weld Type	B-J		B-J		B-J		B-J		BC, B-J		B-J	
DM	TF, D&C		TF, D&C		SC, TF, D&C		SC, D&C		D&C		D&C	
No. Welds	21		9		3		3		57		30	
	Break Size, X (in)	**F(LOCA≥X)**	**Break Size, X (in)**	**F(LOCA≥X)**	**Break Size, X (in)**	**F(LOCA≥X)**	**Break Size, X (in)**	**F(LOCA≥X)**	**Break Size, X (in)**	**F(LOCA≥X)**	**Break Size, X (in)**	**F(LOCA≥X)**
	0.50	2.78E-06	0.50	2.78E-06	0.50	3.10E-06	0.50	3.54E-07	0.50	1.14E-08	0.50	1.14E-08
	0.75	1.67E-06	0.75	1.67E-06	0.75	1.86E-06	0.75	2.12E-07	0.75	6.84E-09	0.75	6.84E-09
	1.00	1.18E-06	1.00	1.18E-06	1.00	1.32E-06	1.00	1.51E-07	1.00	4.85E-09	1.00	4.85E-09
	1.50	7.48E-07	1.50	7.48E-07	1.50	8.34E-07	1.50	9.54E-08	1.50	3.07E-09	1.50	3.07E-09
	2.00	4.01E-07	2.00	4.01E-07	2.00	4.48E-07	2.00	5.12E-08	2.00	1.65E-09	2.00	1.65E-09
	2.83	1.67E-07	2.83	1.67E-07	2.83	1.86E-07	2.83	2.13E-08	2.83	6.85E-10	2.83	6.85E-10
	4.00	8.50E-08	4.00	8.50E-08	4.00	9.48E-08	4.00	1.08E-08	4.00	3.49E-10	4.00	3.49E-10
	4.24	7.41E-08	4.24	7.41E-08	4.24	8.26E-08	4.24	9.45E-09	4.24	3.04E-10	4.24	3.04E-10
	5.66	3.79E-08	5.66	3.79E-08	5.66	4.23E-08	5.66	4.84E-09	5.66	1.56E-10	5.66	1.56E-10
	6.00	3.31E-08	6.00	3.31E-08	6.00	3.70E-08	6.00	4.23E-09	6.00	1.36E-10	6.00	1.36E-10
	6.75	2.52E-08	6.75	2.52E-08	6.75	2.81E-08	6.75	3.22E-09	6.75	1.04E-10	6.75	1.04E-10
	7.20	2.22E-08	7.20	2.22E-08	7.20	2.48E-08	7.20	2.83E-09	7.20	9.12E-11	7.20	9.12E-11
	8.49	1.60E-08	8.49	1.60E-08	8.49	1.79E-08	8.49	2.04E-09	8.49	6.58E-11	8.49	6.58E-11
	10.00	1.16E-08	10.00	1.16E-08	10.00	1.29E-08	10.00	1.47E-09	10.00	4.75E-11	10.00	4.75E-11
	11.31	9.11E-09	11.31	9.11E-09	11.31	1.02E-08	11.31	1.16E-09	11.31	3.74E-11	11.31	3.74E-11
	14.14	5.93E-09					14.14	7.56E-10	14.14	2.44E-11	14.14	2.44E-11
	16.97	4.05E-09					16.97	5.16E-10	16.97	1.66E-11		

Table 2.5.50 – Relative frequencies vs. break size for safety injection and recirculation line welds (Categories 7F through 7L)

Category	7G		7H		7I		7J		7K		7L	
System	SIR		SIR		SIR		SIR		SIR		SIR	
Pipe Size (in)	8		6		4		3		2		1.5	
DEGB (in)	11.31		8.49		5.66		4.24		2.83		2.12	
Weld Type	BC, B-J		B-J		BC		BC		BC		B-J	
DM	D&C		D&C		D&C		D&C		D&C		D&C	
No. Welds	42		23		5		9		10		0	
	Break Size, X (in)	**F(LOCA≥X)**	**Break Size, X (in)**	**F(LOCA≥X)**	**Break Size, X (in)**	**F(LOCA≥X)**	**Break Size, X (in)**	**F(LOCA≥X)**	**Break Size, X (in)**	**F(LOCA≥X)**	**Break Size, X (in)**	**F(LOCA≥X)**
	0.50	1.14E-08	0.50	1.14E-08	0.50	1.14E-08	0.50	1.14E-08	0.50	1.14E-08	0.50	1.14E-08
	0.75	6.84E-09	0.75	6.84E-09	0.75	6.84E-09	0.75	6.84E-09	0.75	6.84E-09	0.75	6.84E-09
	1.00	4.85E-09	1.00	4.85E-09	1.00	4.85E-09	1.00	4.85E-09	1.00	4.85E-09	1.00	4.85E-09
	1.50	3.07E-09	1.50	3.07E-09	1.50	3.07E-09	1.50	3.07E-09	1.50	3.07E-09	1.50	3.07E-09
	2.00	1.65E-09	2.00	1.65E-09	2.00	1.65E-09	2.00	1.65E-09	2.00	1.65E-09	2.00	1.65E-09
	2.83	6.85E-10	2.83	6.85E-10	2.83	6.85E-10	2.83	6.85E-10	2.83	6.85E-10		
	4.00	3.49E-10	4.00	3.49E-10	4.00	3.49E-10	4.00	3.49E-10				
	4.24	3.04E-10	4.24	3.04E-10	4.24	3.04E-10	4.24	3.04E-10				
	5.66	1.56E-10	5.66	1.56E-10	5.66	1.56E-10						
	6.00	1.36E-10	6.00	1.36E-10								
	6.75	1.04E-10	6.75	1.04E-10								
	7.20	9.12E-11	7.20	9.12E-11								
	8.49	6.58E-11	8.49	6.58E-11								
	10.00	4.75E-11										
	11.31	3.74E-11										

Table 2.5.51 – Relative frequencies vs. break size for accumulator injection and CVCS line welds (Categories 7M through 8C)

Category	7M		7N		7O		8A		8B		8C	
System	ACC		ACC		ACC		CVCS		CVCS		CVCS	
Pipe Size (in)	12		12		12		2		4		2	
DEGB (in)	16.97		16.97		16.97		2.83		5.66		2.83	
Weld Type	B-J		B-J		BC, B-J		B-J		B-J		B-J	
DM	SC, D&C		TF, D&C		D&C		TF, VF, D&C		TF, VF, D&C		VF, D&C	
No. Welds	0		35		15		10		19		47	
	Break Size, X (in)	**F(LOCA≥X)**	**Break Size, X (in)**	**F(LOCA≥X)**	**Break Size, X (in)**	**F(LOCA≥X)**	**Break Size, X (in)**	**F(LOCA≥X)**	**Break Size, X (in)**	**F(LOCA≥X)**	**Break Size, X (in)**	**F(LOCA≥X)**
	0.50	3.54E-07	0.50	5.18E-08	0.50	6.26E-09	0.50	4.28E-08	0.50	4.28E-08	0.50	1.87E-08
	0.75	2.12E-07	0.75	3.11E-08	0.75	3.75E-09	0.75	2.57E-08	0.75	2.57E-08	0.75	1.12E-08
	1.00	1.51E-07	1.00	2.21E-08	1.00	2.66E-09	1.00	1.82E-08	1.00	1.82E-08	1.00	7.97E-09
	1.50	9.54E-08	1.50	1.40E-08	1.50	1.69E-09	1.50	1.15E-08	1.50	1.15E-08	1.50	5.04E-09
	2.00	5.12E-08	2.00	7.49E-09	2.00	9.04E-10	2.00	6.03E-09	2.00	6.03E-09	2.00	2.64E-09
	2.83	2.13E-08	2.83	3.12E-09	2.83	3.76E-10	3.00	2.42E-09	3.00	2.42E-09	3.00	1.06E-09
	4.00	1.08E-08	4.00	1.67E-09	4.00	2.02E-10			4.00	1.26E-09		
	4.24	9.45E-09	5.66	7.09E-10	5.66	8.55E-11			5.66	5.77E-10		
	5.66	4.84E-09	6.00	6.19E-10	6.00	7.47E-11						
	6.00	4.23E-09	6.80	4.71E-10	6.80	5.69E-11						
	6.75	3.22E-09	7.20	4.14E-10	7.20	5.00E-11						
	7.20	2.83E-09	10.00	2.16E-10	10.00	2.61E-11						
	8.49	2.04E-09	14.14	1.11E-10	14.14	1.34E-11						
	10.00	1.47E-09	16.97	7.56E-11	16.97	9.12E-12						
	11.31	1.16E-09										
	14.14	7.56E-10										
	16.97	5.16E-10										

Table 2.5.52 – Relative frequencies vs. break size for CVCS line welds (Categories 8D through 8F)

Category	8D		8E		8F	
System	CVCS		CVCS		CVCS	
Pipe Size (in)	4		4		4	
DEGB (in)	5.66		5.66		5.66	
Weld Type	B-J		BC		BC	
DM	VF, D&C		TF, D&C		D&C	
No. Welds	6		4		1	
	Break Size, X (in)	**F(LOCA≥X)**	**Break Size, X (in)**	**F(LOCA≥X)**	**Break Size, X (in)**	**F(LOCA≥X)**
	0.50	1.87E-08	0.50	7.98E-08	0.50	1.87E-08
	0.75	1.12E-08	0.75	4.79E-08	0.75	1.12E-08
	1.00	7.97E-09	1.00	3.40E-08	1.00	7.97E-09
	1.50	5.04E-09	1.50	2.15E-08	1.50	5.04E-09
	2.00	2.64E-09	2.00	1.12E-08	2.00	2.64E-09
	3.00	1.06E-09	3.00	4.51E-09	3.00	1.06E-09
	4.00	5.49E-10	4.00	2.34E-09	4.00	5.49E-10
	5.66	2.52E-10	5.66	1.08E-09	5.66	2.52E-10

In summary, conditional probabilities are formed using the STP-specific study (79). These give the probabilities that the break comes from each relevant weld category given the observation of a break of a specific size. The parameters were chosen from the class of bounded Johnson distributions to minimize the sum of the squared deviations of the fit distributions from the NUREG-1829 percentiles. To ensure that the tails of the break-size distribution are adequately sampled, a nonuniform Latin hypercube sampling procedure (80) was used in the CASA Grande implementation.

Fiberglass Debris Penetration

A model of the filtration function of the ECCS sump strainers was used, and the parameters of that model are given in Section 2.2.29 of (12). The following assumptions were made regarding fiberglass penetration of the strainer (12):

- It was assumed that the debris beds on the strainers would not be disrupted after the debris initially accumulates. This is a reasonable assumption since the strainers are not located in the immediate vicinity of any potential breaks where the break flow could impinge the strainers and shear off a portion of the debris.
- It was assumed that debris that penetrates the strainers would be uniformly distributed in the flow and would transport proportional to the flow split to the SI pumps vs. CS pumps (γ) and the flow split to the core vs. bypass paths (λ). This is a reasonable assumption since the fiber that penetrates the strainer would be very fine and would easily transport with the flow.
- It was assumed that all debris that penetrates the strainer and transports through the core would be trapped on the core (i.e., 100% filtration efficiency). This is a conservative assumption since it maximizes the debris load on the core.
- It was assumed that all debris that penetrates the strainer and bypasses the core (either through the containment sprays or directly out the break) would immediately be transported back to the containment pool. This is a conservative assumption since it neglects potential hold-up of debris in various locations and neglects the time that it would take for debris to transport through the systems and wash back to the pool.

To construct the empirical envelope for the filtration function, the following three steps were carried out:

1. Data from each experiment at ARL was used to fit the parameters of the equations of the mass-transport theory described in Section 5.9 of (72). These equations predict, as a function of time, the mass accumulated on the strainer, the mass that has passed through the strainer, and the mass remaining in the pool given the rate of flow, the flow fraction captured by the filters, and the masses of debris and the timing of their introduction. Parameters of the mass-transport theory equations that most closely match the data were found using a constrained weighted least-squares procedure detailed in (60).
2. The parameters obtained in Step 1 were used to construct both filtration as a function of time and the mass-on-the-strainer as a function of time at discretized time steps. Time was then

"eliminated" to obtain what is labeled a data series for each experiment, specifying filtration efficiency as a function of mass on the strainer.

3. Steps 1 and 2 are repeated for each of the experiments, and the results yield multiple data series indicating the variability seen across the experiments. Taking these data, an empirical envelope was formed for filtration as a function of mass on the strainer by finding three functions: First, a least-squares fit was used to find a central fit to the multiple data series from Step 2, optimizing the parameters of Equation 14 [(12), Section 2.2.33]. This yields the parameters in the "Center" row of Table 2.2.32 in (12). The second function is also of the form of Equation 14 but majorizes the data while having minimum area under the function. The third function is again of the form of Equation 14 but minorizes the data and has maximum area under the function. These latter two functions correspond to the parameters in the "Upper" and "Lower" rows of Table 2.2.32 in (12).

The analysis that was used to develop the model is based on a mass-transport theory described in Section 5.9 of (12) with the statistical fitting procedure detailed in (60). The approach is summarized below.

Following a break in RCS piping, some of the fiberglass insulation debris from nearby piping and equipment would be transported to the ECCS sumps, where it would accumulate on the sump strainers. In addition some of the fine debris would pass through, or penetrate, the strainers. Debris can pass through a strainer directly or via shedding from the accumulated fiber bed on the strainer. The filtration efficiency of a strainer increases towards one as mass accumulates on the strainer. Test data from prototype strainer module experiments performed at Alden Research Laboratory (ARL) in October 2012 provide measurements of mass that passed through the strainer with specified time resolution (61). Table 2.5.53 illustrates the results from the ARL testing:

Table 2.5.53 – Significant Parameters and Total Penetration Results

Test	Flow Rate, gpm	Debris Batches	Debris Introduced, g	Penetration, g
1	353	1	1088.72	190.87
2	353	1	1088.67	220.89
3	353	1	1088.63	180.1
4	353	10	1088.85	179.07
5	353	4	4354.71	222.65
6	82.1	4	4354.53	277.93
7	217.5	4	4354.54	319.25

A combination of 100% capture filter bags and isokinetic grab samples were used to gather data regarding the change in penetration as a function of time. Table 2.5.54 displays the number of pool turnovers (PTOs) and time from the first debris batch addition to the removal of the specified filter bag set from the test tank for Tests 1 through 3, and Table 2.5.55 displays each filter bag set weight for Tests 1 through Test 3.

Table 2.5.54 – Tests 1-3 Time and PTO when filter bag set was removed from the test tank

	Time [and PTO] when Filter Bag Set was Removed, min [PTO]			
Test	1st	2nd	3rd	4th
1	26.7 [11.3]	40.2 [17.1]	90.2 [38.3]	N/A
2	24.5 [10.4]	38.3 [16.3]	88.2 [37.5]	136.7 [58.1]
3	22.2 [9.4]	35.7 [15.2]	84.0 [35.7]	133.5 [56.8]

Table 2.5.55 – Tests 1-3 filter bag set weights

	Filter Bag Set Weight, g			
Test	1st	2nd	3rd	4th
1	178.84	4.08	7.34	N/A
2	190.12	4.02	11.51	14.56
3	168.53	4.88	3.77	2.13

Table 2.5.56 displays the number of PTO and time from the first debris batch addition to the removal of the specified filter bag from the test tank for Test 4, and Table 2.5.57 displays each filter bag weight for Test 4.

Table 2.5.56 – Test 4 time and PTO when filter bag set was removed from the test tank

	Time [and PTO] when Filter Bag Set was Removed, min [PTO]						
Test	1st	2nd	3rd	4th	5th	6th	7th
4	16.2 [3.9]	32.8 [14.0]	48.8 [20.8]	65.5 [27.9]	83.0 [35.3]	100.0 [42.5]	117.2 [49.8]

	Time [and PTO] when Filter Bag Set was Removed, min [PTO]					
Test	8th	9th	10th	11th	12th	13th
4	132.8 [56.5]	149.7 [63.7]	166.8 [71.0]	179.5 [76.3]	227.8 [96.9]	276.3 [117.5]

Table 2.5.57 – Test 4 filter bag set weights

	Filter Bag Set Weight, g						
Test	1st	2nd	3rd	4th	5th	6th	7th
4	37.81	32.00	28.77	22.94	13.52	12.37	9.27

	Filter Bag Set Weight, g					
Test	8th	9th	10th	11th	12th	13th
4	6.89	5.44	4.80	1.49	1.78	1.26

Table 2.5.58 displays the number of PTO and time from the first debris batch addition to the removal of the specified filter bags from the test tank for Test 5 through Test 7, and Table 2.5.59 displays each filter bag weight for Test 5 through Test 7.

Table 2.5.58 – Tests 5-7 time and PTO when filter bag set was removed from the test tank

	Time [and PTO] when Filter Bag Set was Removed, min [PTO]						
Test	1st	2nd	3rd	4th	5th	6th	7th
5	21.8 [9.3]	45.5 [19.4]	68.8 [29.3]	91.8 [44.7]	105.0 [44.7]	153.0 [65.1]	201.5 [85.7]
6	76.3 [7.6]	147.3 [14.6]	209.7 [20.7]	271.3 [26.8]	323.2 [32.0]	N/A	N/A
7	29.5 [7.7]	61.0 [16.0]	93.7 [24.6]	126.3 [33.1]	147.3 [38.6]	223.7 [58.6]	302.7 [79.3]

Table 2.5.59 – Tests 5-7 filter bag set weights

	Each Filter Bag Set Weight, g						
Test	1st	2nd	3rd	4th	5th	6th	7th
5	170.25	23.86	10.56	9.54	2.8	1.91	1.65
6	199.04	33.12	21.15	14.76	9.46	N/A	N/A
7	218.57	33.69	21.88	19.19	7.45	7.41	3.66

Table 2.5.60 displays the number of PTO and the time from the first debris batch addition to the completion of the grab samples, and Table 2.5.61 displays the concentration of the grab samples.

Table 2.5.60 – Time and PTO when each grab sample was completed

	Grab Sample Time [and PTO] After the First Debris Batch Addition, min [PTO]							
Test	1st	2nd	3rd	4th	5th	6th	7th	8th
1	1.8 [0.8]	5.7 [2.4]	8.7 [3.7]	12.2 [5.2]	17.2 [7.3]	34.2 [14.5]	66.3 [28.2]	N/A
2	1.5 [0.6]	4.5 [1.9]	7.8 [3.3]	10.8 [4.6]	15.2 [6.5]	32.3 [13.8]	62.8 [26.7]	112.5 [47.9]
3	1.8 [0.8]	5.0 [2.1]	7.8 [3.3]	12.2 [5.2]	15.7 [6.7]	27.8 [11.8]	56.8 [24.2]	107.5 [45.7]
4	1.5 [0.6]	4.5 [1.9]	8.3 [3.5]	19.2 [8.2]	22.3 [9.5]	26.7 [11.3]	35.3 [15.0]	38.5 [16.4]
5	1.3 [0.6]	4.3 [1.8]	7.7 [3.3]	24.7 [10.5]	27.7 [11.8]	30.5 [13.0]	48.8 [20.8]	51.5 [21.9]
6	5.7 [0.6]	16.0 [1.6]	26.5 [2.6]	59.8 [5.9]	70.0 [6.9]	83.3 [8.2]	93.7 [9.3]	103.8 [10.3]
7	2.5 [0.7]	7.3 [1.9]	11.5 [3.0]	15.7 [4.1]	20.2 [5.3]	33.0 [8.7]	37.0 [9.7]	41.5 [10.9]

	Grab Sample Time [and PTO] After the First Debris Batch Addition, min [PTO]							
Test	9th	10th	11th	12th	13th	14th	15th	16th
4	41.8 [17.8]	51.8 [22.0]	54.8 [23.3]	58.7 [25.0]	68.5 [29.1]	71.5 [30.4]	74.5 [31.7]	85.8 [36.5]
5	55.0 [23.4]	72.2 [30.7]	75.3 [32.0]	78.5 [33.4]	98.3 [41.8]	125.2 [53.2]	178.8 [76.1]	N/A
6	154.7 [15.3]	164.7 [16.3]	175.5 [17.4]	217.3 [21.5]	227.8 [22.5]	237.7 [23.5]	301.2 [29.8]	N/A
7	65.7 [17.2]	70.0 [18.3]	74.0 [19.4]	97.8 [25.6]	101.8 [26.7]	106.7 [28.0]	140.7 [36.9]	N/A

	Grab Sample Concentration, mg/L							
Test	17th	18th	19th	20th	21st	22nd	23rd	24th
4	2.52	1.38	0.90	3.15	1.00	1.10	1.29	0.72

	Grab Sample Concentration, mg/L					
Test	25th	26th	27th	28th	29th	30th
4	0.81	1.29	0.61	0.70	1.21	1.00

Table 2.5.61 – Grab sample concentration

	Grab Sample Concentration, mg/L							
Test	1st	2nd	3rd	4th	5th	6th	7th	8th
1	1.29	26.06	13.96	4.62	2.13	1.33	1.42	N/A
2	2.74	27.28	11.28	6.87	2.14	1.37	1.17	3.23
3	8.90	23.89	8.34	4.34	2.15	1.49	0.82	0.90
4	0.70	5.36	1.09	0.91	3.27	1.11	1.31	3.39
5	4.21	21.97	9.53	2.53	3.18	3.66	2.47	3.90
6	5.64	1.22	0.86	1.24	1.45	1.17	1.39	1.52
7	1.00	1.63	2.25	1.15	2.25	0.87	1.85	8.45

	Grab Sample Concentration, mg/L							
Test	9th	10th	11th	12th	13th	14th	15th	16th
4	1.39	2.54	11.97	1.00	1.19	1.85	0.90	2.23
5	2.35	1.87	3.22	3.39	1.83	2.19	0.61	N/A
6	1.53	1.44	1.32	1.70	1.66	1.73	0.91	N/A
7	1.99	4.03	4.43	1.92	3.13	3.28	1.63	N/A

	Grab Sample Concentration, mg/L							
Test	17th	18th	19th	20th	21st	22nd	23rd	24th
4	2.52	1.38	0.90	3.15	1.00	1.10	1.29	0.72

	Grab Sample Concentration, mg/L					
Test	25th	26th	27th	28th	29th	30th
4	0.81	1.29	0.61	0.70	1.21	1.00

The filtration efficiency of the strainer was modeled as a function of the mass on the strainer using the empirical filtration function shown below (12).

$$f(M^S) = \begin{cases} mM^S + b & if\ 0 \le M^S \le M_c \\ f(M_c) + (1 - f(M_c))\left(1 - e^{-\delta(M^S - M_c)}\right) & if\ M^S > M_c \end{cases}$$

where:

f = Filtration efficiency
M^S = Mass of fiber on strainer
m, b, M_c, δ = Fitted filtration parameters

The parameters of this function, as displayed in Table 2.5.62, were estimated using data from the ARL experiments.

Table 2.5.62 – Fitted Filtration Parameters for Test Module

	m_{test} (g^{-1})	b	δ_{test} (g^{-1})	$M_{c,test}$ (g)
Lower	0.0003391	0.656	0.001308	880
Center	0.0003263	0.689	0.001125	930
Upper	0.0003723	0.706	0.031787	790

To use the test results, it is necessary to scale the parameters back to the plant conditions. Parameter b (the filtration efficiency at clean strainer conditions) is dimensionless. However, m, δ, and M_c have to be scaled proportional to the scaled strainer area. Given a test module area of 91.44 ft^2 and a strainer area of 1,818.5 ft^2 per train, the test parameters can be scaled to the plant conditions using the following equations. Table 2.5.63 shows the adjusted parameters.

$$m_{strainer} = m_{test} \cdot \frac{A_{module}}{A_{strainer}} = m_{test} \cdot \frac{91.44ft^2}{1{,}818.5ft^2}$$

$$\delta_{strainer} = \delta_{test} \cdot \frac{A_{module}}{A_{strainer}} = \delta_{test} \cdot \frac{91.44ft^2}{1{,}818.5ft^2}$$

$$M_{c,strainer} = M_{c,test} \cdot \frac{A_{strainer}}{A_{module}} = M_{c,test} \cdot \frac{1{,}818.5ft^2}{91.44ft^2}$$

Table 2.5.63 – Fitted Filtration Parameters for each ECCS Strainer

	m (lb_m^{-1})	b	δ (lb_m^{-1})	M_c (lb_m)
Lower	0.007741	0.656	0.02968	38.5
Center	0.007449	0.689	0.02511	40.7
Upper	0.008499	0.706	0.7259	34.6

The shedding coefficients determined from the testing (results of Tests 5-7) are shown in Table 2.5.64 (60).

Table 2.5.64 – Fitted Shedding Parameters

	ν	η (min^{-1})
Minimum	0.0096	0.0082
Average	0.0152	0.0313
Maximum	0.0196	0.0546

Rather than simply developing point estimates of the parameters of the filtration efficiency function and using the resulting point estimate of the filtration function, the experimental data was used to form an empirical envelope for the filtration efficiency. Then, when executing a computer simulation in CASA Grande, using a uniform random variable, repeated samples were taken of the filtration efficiency function from the empirical envelope, maintaining the same functional form of the filtration equation.

The differential rate of change for each debris type in the pool (assuming a homogenous mixing volume) can be described using the following equation (81):

$$\frac{dm_n}{dt} = S_n - f_n \frac{Q}{V} m_n - \gamma\lambda g_n (1 - f_n) \frac{Q}{V} m_n + s_n - \gamma\lambda g_n s_n$$

where all of the properties can be time-dependent and have the following definitions:

m_n = Mass of debris type n suspended in the pool
t = Time
f_n = Filtration efficiency for debris type n at the strainer
Q = Volumetric flow rate passing through strainers
V = Total volume of the pool
S_n = Source rate for initial introduction of debris type n
s_n = Shedding rate for debris type n from existing bed
g_n = Filtration efficiency for debris type n at the core
γ = Fraction of the total flow going to the SI pumps
λ = Fraction of SI flow going to the core

Based on the previous equation, the total quantity of debris that accumulates on the strainer or the core can be described by the following equations (81):

$$M_n^S(t) = \int_0^t \left[f_n(t')m_n(t')\frac{Q(t')}{V(t')} - s_n(t')\right]dt'$$

$$M_n^C(t) = \int_0^t \gamma(t')\lambda(t')g_n(t')\left[\left(1 - f_n(t')\right)\frac{Q(t')}{V(t')}m_n(t') + s_n(t')\right]dt'$$

where:

M_n^S = Cumulative mass of debris type n on the strainer
M_n^C = Cumulative mass of debris type n on the core
t' = Dummy integration variable where t' ≤ t denotes all times from the start to t of interest

These equations can be determined using the following analytical solution, where the subscript n has been dropped for simplification:

$$m(t_i) = \frac{S(t_{i-1})}{H(t_{i-1})} \cdot \left[1 - e^{-H(t_{i-1})\cdot\Delta t_{i-1}}\right] + m(t_{i-1}) \cdot e^{-H(t_{i-1})\cdot\Delta t_{i-1}}$$

$$M_j^S(t_i) = M_j^S(t_{i-1}) + f_j(t_{i-1}) \cdot h_j(t_{i-1}) \cdot m(t_{i-1}) \cdot \Delta t_{i-1} - s_j(t_{i-1}) \cdot \Delta t_{i-1}$$

$$M_j^C(t_i) = M_j^C(t_{i-1}) + \Delta t_{i-1} \cdot \sum_{j=1}^{N}\left[s_j(t_{i-1}) + \left(1 - f_j(t_{i-1})\right) \cdot h_j(t_{i-1}) \cdot m(t_{i-1})\right] \cdot \gamma_j(t_{i-1}) \cdot \lambda(t_{i-1}) \cdot g(t_{i-1})$$

$$S(t_{i-1}) = \sum S_k(t_{i-1}) + \sum_{j=1}^{N}\left[s_j(t_{i-1}) \cdot \left(1 - \gamma_j(t_{i-1}) \cdot \lambda(t_{i-1}) \cdot g(t_{i-1})\right)\right]$$

$$H(t_{i-1}) = \sum_{j=1}^{N} h_j(t_{i-1}) \cdot \left[\frac{\gamma_j(t_{i-1}) \cdot \lambda(t_{i-1}) \cdot g(t_{i-1})}{1 - \gamma_j(t_{i-1}) \cdot \lambda(t_{i-1}) \cdot g(t_{i-1})} + f_j(t_{i-1})\right] \cdot \left[1 - \gamma_j(t_{i-1}) \cdot \lambda(t_{i-1}) \cdot g(t_{i-1})\right]$$

$$h_j(t_{i-1}) = \frac{Q_j(t_{i-1})}{V(t_{i-1})}$$

$$\Delta t_{i-1} = t_i - t_{i-1}$$

where:

t_i = End of specific time step interval
t_{i-1} = Beginning of specific time step interval
N = Number of ECCS strainers
Subscript j = Variables specific to a given ECCS strainer
S_k = Source rate for initial introduction of fiber type k

Each of these equations can be solved by explicit forward integration assuming that the integrands are known at the beginning of each time step and that they remain constant during each time step. Variables such as the source rate of debris to the pool (S), the strainer flow rate (Q), the pool volume (V), the SI and CS flow split (γ), and the SI flow vs. boil-off flow split (λ) are defined in the analysis. The filtration efficiency for the core (g) is conservatively assumed to be 100% (i.e. all debris that transports to the core is trapped). Therefore, the primary unknowns are the filtration efficiency at the strainer (f) and the shedding rate (s).

The shedding rate can be defined as a function of time as described in the following equation (81):

$$s_n(t) = \nu_n \eta_n e^{-\eta_n t} \int_0^t f_n(t') \frac{Q(t')}{V(t')} m_n(t') e^{\eta_n t'} dt'$$

where:

ν_n = Fraction of debris type n that is "sheddable" (i.e. able to pass through a debris bed)
η_n = Time constant associated with the shedding process

Similar to the analytical solution above, this equation can be solved as follows where the subscript n has been dropped for simplification:

$$m_j^{sh}(t_i) = m_j^{sh}(t_{i-1}) \cdot e^{-\eta \cdot \Delta t_{i-1}} + \frac{\nu}{\eta} \cdot f_j(t_{i-1}) \cdot h_j(t_{i-1}) \cdot m(t_{i-1}) \left[1 - e^{-\eta \cdot \Delta t_{i-1}}\right]$$

$$s_j(t_i) = \eta \cdot m_j^{sh}(t_i)$$

where:

m_j^{sh} = Mass of sheddable debris in the bed

Modeling Dependencies

Multiple parameters are random in the analysis, and hence a joint distribution governs the associated random vector. This means that the corresponding dependence structure should be described. There are two main strategies for dealing with the challenge of handling multi-variate uncertainties for CASA

Grande input parameters. These strategies involve: (i) appropriate dimension reduction by modeling "perfect correlations" and (ii) appropriate modeling of conditional independence.

As an example of dimension reduction, consider the uncertainty associated with LOCA exceedance frequencies for a 2-inch break and for a 6-inch break. Let Λ_2 denote the exceedance frequency for a 2-inch break with (cumulative) distribution function F_2, and let Λ_6 and F_6 denote the analogous quantities for a 6-inch break. Here, F_2 and F_6 are fit as described above and described in more detail in Section 5.3 of (12) and in (82).

The random variables Λ_2 and Λ_6 were not modeled as being independent. (If one were to do so then it would be possible, in simulating observations from these distributions, that the 6-inch exceedance frequency would be greater than the 2-inch frequency.) Instead, dependence using dimension reduction was modeled as follows: Let $U \sim U(0, 1)$ be a uniform random variable on the interval (0, 1). Then using the standard simulation technique called inversion, $\Lambda_2 = F_2^{-1}(U)$ has distribution F_2 and $\Lambda_6 = F_6^{-1}(U)$ has distribution F_6. The dimension is reduced by assuming a perfect correlation via the bivariate random vector $(F_2^{-1}(U), F_6^{-1}(U))$, where the *same* uniform random variable is used in both expressions. In this way, if the 2-inch frequency, Λ_2, is at the 62nd percentile (via U = 0.62) of the distribution F_2 then Λ_6 is at the 62nd percentile of F_6. This type of dimension reduction is employed for modeling break sizes in CASA Grande.

Appropriate modeling of conditional independence is the second main strategy for handling multivariate uncertainty, and this approach is used pervasively in the analysis. As a first example, the timing of key plant response actions are, strictly speaking, random variables. However, these are determined in a conditional manner as described in Section 2.2.1 of (12). For a break smaller than 2-inches, the accumulators would not inject, and the sprays would not be initiated. Similarly, the timing for switchover to recirculation depends on the volume of water in the RWST, the total ECCS and CSS flow rate, and the break size. Operating procedures are further conditioned on the number of operating CS pumps (again, see Section 2.2.1 of (12)). The pool water level is discussed in Section 2.2.6 of (12) and this depends on the size of the break and on the elevation of the break. The pool temperature profiles depend on the size of the break, as described in Section 2.2.6 of (12).

Item 5.b: Defense-in-Depth

See discussion in Volume 1 Section 2.1 and Appendix C (Enclosure 4-1).

Item 5.c: Radioactivity Barrier Safety Margin

See discussion in Volume 1 Section 2.2 and Appendix C (Enclosure 4-1).

Item 5.d: Uncertainty

There are a large number of input parameters that are used in the risk-informed evaluation, and technically, almost every input parameter has a probability distribution and a given level of uncertainty associated with it. For some input variables, a best-estimate value may be adequate for a realistic analysis. However, some input variables require probability distributions. Figure 2.5.53 shows an illustration of a probability distribution for water volume. Depending on the specific analysis, either the calculated minimum or calculated maximum water volume would be used as an input for a deterministic evaluation. For a risk-informed evaluation, the input probability distribution is sampled to determine the actual impact on the results with an appropriate probability weight carried through the analysis for the extreme conditions associated with the minimum and maximum values. In this project, most of the input variables have potential sources of uncertainty and variability. In some cases, the parameters were treated as random variables and in other cases as point estimates. These decisions were made based on the availability of data for uncertainty analysis (i.e., development of distributions), and the available consensus on the values assigned to specific factors (e.g., for some values, there is a high level of confidence by the industry and the NRC). The decisions on the selection of factors as random variables versus point estimates were made for STP conditions. However, these decisions may be different for other plants. For the factors that have been chosen to be random variables, the distributions were developed based on the available data. Conservatism has been considered in the development of distributions to fill the data gaps and to secure the reliability of the ultimate estimate of risk. This means that the distribution developed for each factor may not depict all sources of uncertainty, but still ensures the reliability of estimated risk by considering certain conservative assumptions. Based on considering some of the uncertainties, modeling physical phenomena, and a few conservatism assumptions, the ultimate estimated risk in this project has a high level of confidence. However, there are opportunities for other plants to reach more realistic risk by reducing conservatisms (e.g., by developing more data to cover additional sources of uncertainties). The risk-informed methodology in this project is a first of its kind, and when more data is available and implemented within the methodology, it would consequently lead to a more realistic (i.e., less conservative) estimate of risk.

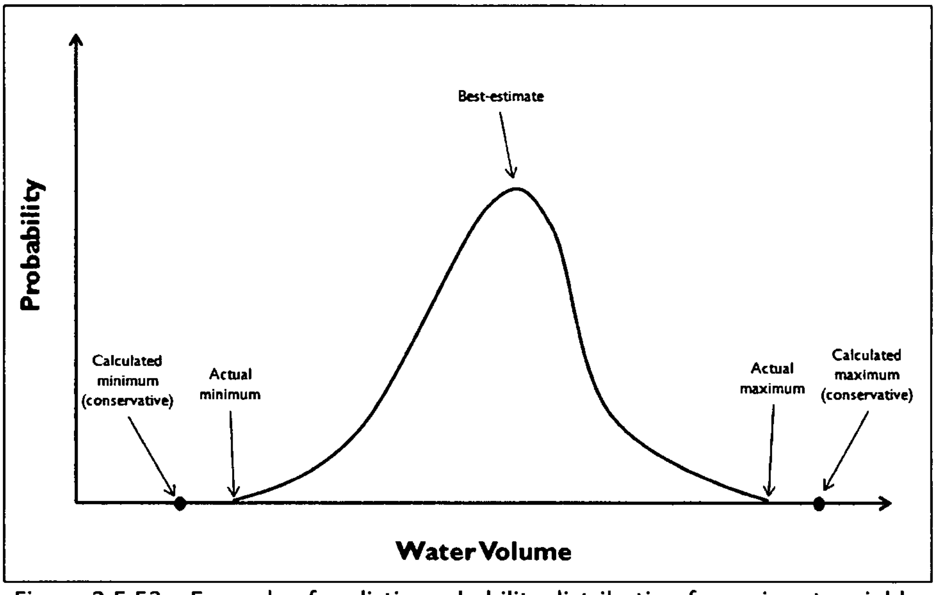

Figure 2.5.53 – Example of realistic probability distribution for an input variable

In addition to using realistic inputs, it is also important to perform a time-dependent evaluation to capture the time-dependent factors and events that are significant to GSI-191. This includes time-dependent failure for unqualified coatings, time-dependent transport of debris to the strainers, time-dependent corrosion and subsequent precipitation of chemical products, time-dependent operator actions such as securing pumps or switching over to hot leg injection, etc.

Some specific examples of how the probability distributions are developed have been provided in the response to Item 5.a.16. A summary of the input parameters used in the STP risk-informed GSI-191 evaluation is shown in Table 2.5.65. This table indicates whether a distribution or a fixed value (or values) were used in the evaluation, along with references to the Volume 3 sections (12) and original source documents.

Table 2.5.65 – Input parameter summary

Input Parameter	Distribution(s) or Fixed Value(s)	Dependencies	Enclosure 4-3 Volume 3 Section(s)	Source Reference(s)
Time to recirculation	Fixed values	Break size	Section 2.2.1	(32)
Time to secure containment spray	Fixed value	None	Section 2.2.1	(83; 84)
Time to hot leg switchover	Distribution	None	Section 2.2.1	(85; 86)
Containment geometry	Fixed values	None	Section 2.2.2, Section 5.2	(47)
Break size and frequency	Distributions	Break location	Section 2.2.3, Section 5.3	(82; 79; 47; 77)
Pool volume	Distributions	Break size	Section 2.2.5	(87)
Pool area	Fixed value	None	Section 2.2.5	(87)
Pool temperature	Fixed values	Break size	Section 2.2.6	(32)
Containment pressure	Fixed values	Pool temperature	Assumption 1.c	None
Operating pumps	Fixed values	None	Section 2.2.4, Section 2.2.7, Section 5.1	(88)
Low head safety injection flow rate	Fixed values	Break size, pumps running	Section 2.2.8	(89; 32)
High head safety injection flow rate	Fixed values	Break size, pumps running	Section 2.2.8	(89; 32)
Containment spray flow rate	Distributions	Pumps running	Section 2.2.8	(89; 90)
Qualified coatings quantity	Fixed values	None	Section 2.2.9	(10)
Unqualified coatings quantity	Fixed values	None	Section 2.2.10	(7)
Unqualified coatings failure time	Fixed values	None	Section 2.2.10	(7)
Crud quantity	Fixed value	None	Section 2.2.11	(45)
Latent debris quantity	Fixed values	None	Section 2.2.12	(36)
Miscellaneous debris quantity	Fixed value	None	Section 2.2.13	(36)
Miscellaneous debris failure time	Fixed value	None	Assumption 4.b	None
Insulation ZOI size	Fixed values	Break size, insulation location	Section 2.2.14	(91; 56)
Fiberglass size distribution	Fixed values	Break size, insulation location	Section 2.2.15	(92)
Debris characteristics	Fixed values	None	Section 2.2.16	(36; 10; 7; 45)
Chemical product formation time	Fixed values	Pool temperature	Assumption 5.a, Section 5.6.3	(25)

Input Parameter	Distribution(s) or Fixed Value(s)	Dependencies	Enclosure 4-3 Volume 3 Section(s)	Source Reference(s)
Blowdown transport	Distributions	Break location, debris size	Section 2.2.17	(13)
Washdown transport	Distributions	Sprays initiated, debris size	Section 2.2.18	(13)
Pool fill transport	Fixed values	Break location, debris size	Section 2.2.19	(13)
Recirculation transport	Fixed values	Break size, break location, debris type, debris size	Section 2.2.20	(13)
Fiberglass spray erosion	Fixed value	Sprays initiated	Section 2.2.21	(13)
Fiberglass pool erosion	Distribution	None	Section 2.2.21	(13; 18)
Fiberglass pool erosion time	Fixed values	None	Section 2.2.21 Assumption 6.g	(13; 18)
Transport time	Fixed values	Sump flow rate, pool volume, failure time	Section 5.5.8	(13)
Strainer geometry	Fixed values	None	Section 2.2.22	(93; 94; 95; 96; 97; 98)
Geometric strainer loading	Fixed values	Fiber quantity	Section 5.6.2	(93; 94; 95)
Clean strainer head loss	Fixed value	None	Section 2.2.23, Section 5.6.1	(58)
Thin-bed thickness	Fixed value	None	Assumption 7.c	None
Conventional head loss bump-up	Fixed value	None	Section 5.6.2	None
Chemical head loss bump-up	Distributions	Break size	Section 5.6.3	(25)
Pump NPSH required	Fixed values	Void fraction	Section 2.2.24, Section 5.6.5	(99)
Pump NPSH available	Fixed values	Pool temperature, pump flow rate, pool level, containment pressure	Section 5.6.5	(99)
Strainer structural margin	Fixed value	None	Section 2.2.25	(100; 101)
Containment relative humidity	Fixed value	None	Assumption 8.e	None
Pump gas void limits	Fixed value	None	Section 2.2.28	(102)
Fiber filtration parameters	Distributions	None	Section 2.2.29, Section 5.8	(60)
Fiber shedding parameters	Distributions	None	Section 2.2.29, Section 5.8	(60)
Boil off flow rate	Fixed values	None	Section 2.2.30, Section 5.10.3	(103; 104)
Number of fuel assemblies	Fixed value	None	Section 2.2.31	(103)
Core blockage fiber limits	Fixed values	Break location, injection path	Section 2.2.31, Section 5.10.5	(63)
Boron precipitation fiber limits	Fixed values	Break location, injection path	Section 5.11.2	(71)

The fixed values listed in the previous table do not require additional detail to assess the treatment of uncertainty. This is because of the previously discussed factors (results are not heavily dependent on the variation of the parameter value, or the range of parameter values is close enough that a best estimate value is adequate to provide realistic results). The values listed as having a distribution associated with them are described below.

Time to Hot Leg Switchover

Switchover to hot leg injection is started 5.5 hours after the beginning of the event (85; 86). It was assumed that switchover to hot leg injection would occur between 5.75 and 6 hours after the start of the event. This is a reasonably assumption since according to plant personnel, switchover for both trains can be completed within 15 minutes.

Break Size and Frequency

See discussion for Item 5.a.16.

Pool Volume

The volume of the recirculation pool during mitigation of a LOCA is documented in a plant-specific calculation (87). The following discussion documents the methods, basis, and results for the distribution used to define the pool volume.

Method: The basic methodology used for the STP post LOCA water volume analysis is shown below:

1. The range of water inventory associated with injection from the RWST was developed based on operating procedures and plant data. The injection volume was constructed as the difference of the initial and final volume in the RWST. The injection mass was developed by applying accurate densities to the volumetric values. The range of this inventory is significant and substantially affects subsequent evaluations; therefore, this input required the development of probability distributions.
2. The water inventory attributed to the RCS was evaluated based on operating procedures and design inputs. The volume and state of the inventory at hot-full power operating conditions was evaluated to determine the best estimate RCS volume and mass. The method of developing the RCS water inventory input allowed for a representative best estimate value.
3. The SI accumulator water inventory was derived through analysis of the technical specifications for volume, temperature and pressure. Due to the tight range between the minimum and maximum values, it has been determined that a best estimate value is adequate for all postulated break conditions.
4. The total water in containment was developed as the sum of the RWST, RCS, and SI accumulator water inventories. Due to the variation of the RWST, the total water in containment is presented as a probability distribution.
5. The active water in containment value was determined as the difference between the total water in containment and any inactive cavities. The amount of inventory designated as inactive

depends on the break size. Due to the variation of the RWST injection inventory, the active water in containment is presented as a probability distribution.

6. The pool volume was established by subtracting any hold-up volumes from the active water in containment. The applicable amount of hold-up volume varies based on break size, break elevation, containment spray activation, containment spray flow rate, break flow rate, and pool temperature. To account for all of these variables, a function was derived to define the pool volume in containment.

Basis: The following is a detailed description of how the methodology referred to above was used to develop the appropriate input to the risk-informed evaluation.

RWST Distribution

The RWST is the largest source of water available for post-LOCA mitigation: therefore, it is the largest source of variance between minimum and maximum values. For this reason, a best-estimate value may not accurately represent the actual amount of water injected from the RWST. Therefore, a probability distribution for the RWST inventory was formulated to fully encompass the range of injection volume/mass.

The following figure illustrates the level alarms and volume capacities of the RWST that were used to evaluate the minimum and maximum RWST values:

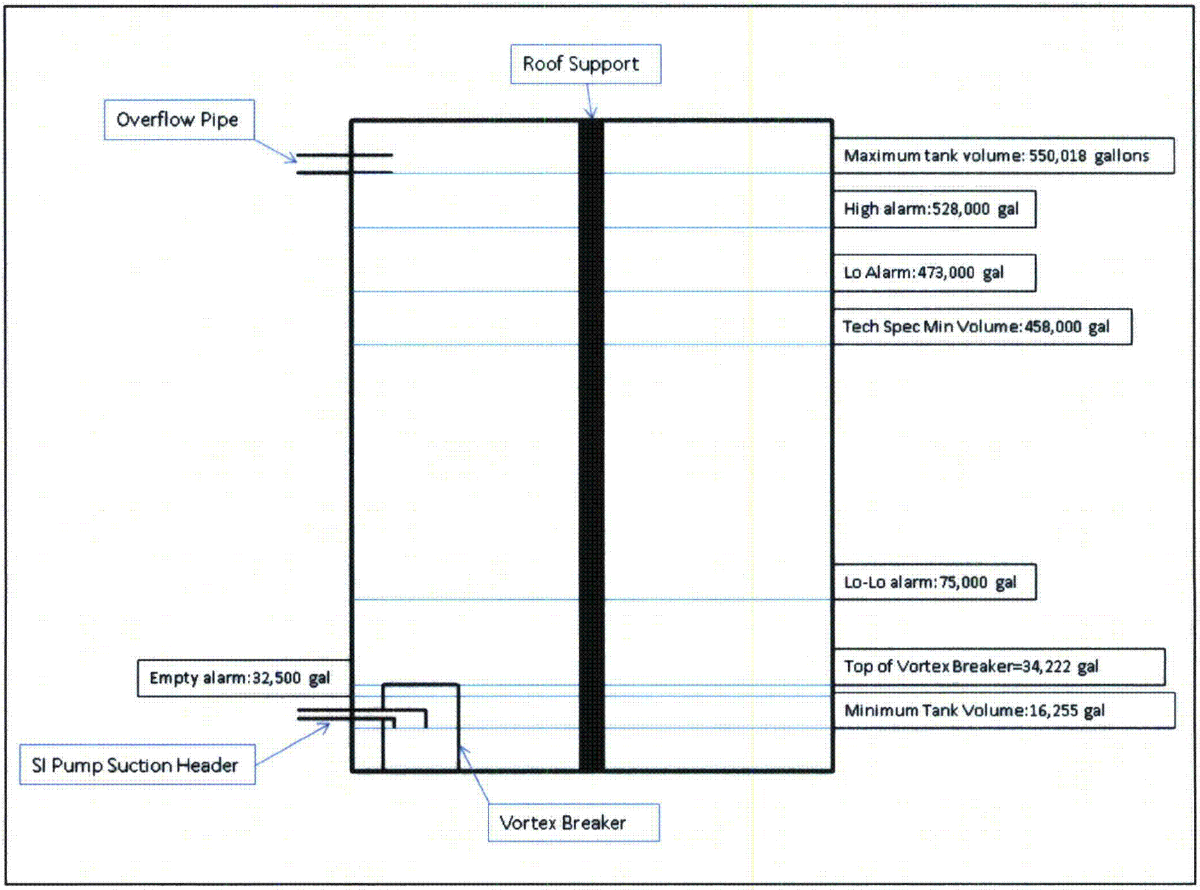

Figure 2.5.54 – RWST Water Levels and Alarms

The initial maximum injection volume is the volume corresponding to the Hi alarm. The minimum volume in the tank is the volume at the top of the vortex breaker. This is a suitable volume because the switchover must be completed before the water level drops below this to avoid possibly excessive air entrainment. The actual maximum RWST injection volume is calculated as follows:

$$V_{RWST}(Act.Max) = V_{initial}(Max) - V_{final}(\text{Min})$$

$$V_{RWST}(Act.Max) = (528{,}000 - 34{,}222)gal = 493{,}778\ gal = 66{,}009\ ft^3$$

This value is converted to mass using the density of water at the minimum acceptable temperature during normal operating conditions: 50 ^{0}F.

$$M_{RWST}(Act.Max) = V_{RWST}(Act.Max) * \rho$$

$$M_{RWST}(Act.Max) = \frac{493{,}778\ gal}{7.4805 \frac{gal}{ft^3}} * (62.414 \frac{lbm}{ft^3}) = 4{,}119{,}866\ lbm$$

The actual minimum injection volume was formulated by evaluating the input parameters of the RWST. The initial minimum volume in the tank was set at the Lo alarm. The maximum final volume in the tank was evaluated at the volume corresponding to the Lo-Lo alarm: this is due to operating mandates (105). Although there is automatic valve realignment where all of the valves to the containment sumps are opened, the procedures require a manual action to close the valves to the RWST (106) (105). This would result in possibly pulling flow from both locations. However, if the containment pressure of the RCB is higher than 5 psig (which it normally would be for large and medium breaks), the containment pressure would be greater than the RWST pressure and would cause the RWST check valves to close (106) (105). Therefore, no adjustment to the Lo-Lo alarm volume was made, and it was used as the maximum final volume in the tank. The actual minimum injection volume was calculated as follows:

$$V_{RWST}(Act. Min) = V_{initial}(Min) - V_{final}(Max)$$

$$V_{RWST}(Act. Min) = (473{,}000 - 75{,}000)gal = 398{,}000\ gal = 53{,}205\ ft^3$$

This value is converted to mass using the density of water at the maximum acceptable temperature during normal operation: 104 ^{0}F.

$$M_{RWST}(Act. Min) = V_{RWST}(Act. Min) * \rho$$

$$M_{RWST}(Act. Min) = \frac{398{,}000\ gal}{7.4805 \frac{gal}{ft^3}} * \left(61.944 \frac{lbm}{ft^3}\right) = 3{,}295{,}730\ lbm$$

With the minimum and maximum values established, the probability distribution of injection volume from the RWST was established using operating data on the water level in the RWST during normal operation (See Figure 2.5.55). The volume of water left in the tank was set at the volume associated with the Lo-Lo alarm (for the same reason as discussed in the actual minimum volume calculation). The probability distribution of RWST injection volume uses a trapezoidal distribution: this is used to fully encompass the operating data and the minimum and maximum values. The top of the trapezoidal distribution encompasses the 25th and 75th percentile values, while the bottom of the trapezoidal distribution is bounded by the actual minimum and maximum injection values.

Figure 2.5.55 – RWST Operating Data

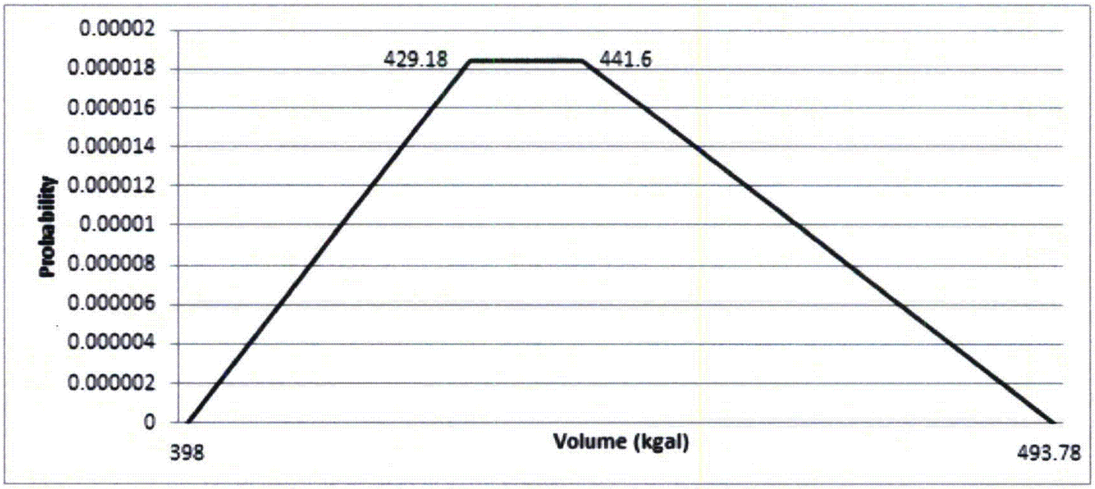

Figure 2.5.56 – RWST Injection Volume Probability Curve

The probability distribution is characterized by five input values:

- a= the minimum value bounding the bottom left portion of the trapezoid
- b= the 25th percentile value bounding the top left portion of the trapezoid
- c= the 75th percentile value bounding the top right portion of the trapezoid
- d= the maximum value bounding the bottom right portion of the trapezoid
- h= the probability of the top portion of the trapezoid

The following table illustrates the five input values for the RWST injection volume probability curve:

Table 2.5.66 – RWST Volume Probability Function Inputs

Input	RWST Volume Function
a	398,000
b	429,179
c	441,596
d	493,778
h	0.000018485

The RWST injection mass probability curve follows the same trapezoidal pattern as the volume probability distribution. To apply this to a mass distribution, the 25th and 75th percentile values were converted to mass values with the average temperature; 77 ^{0}F temperature corresponding to a density of 62.28 lbm/ft^{3}.

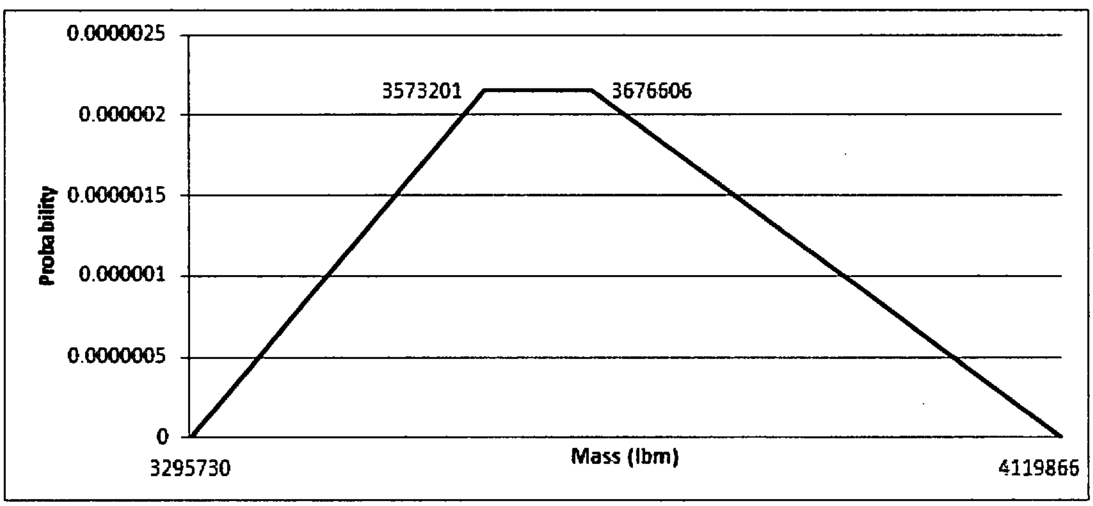

Figure 2.5.57 – RWST Injection Mass Probability Curve

The inputs for the RWST injection mass distribution are illustrated in the following table:

Table 2.5.67 – RWST Mass Probability Function Inputs

Input	RWST Volume Function	RWST Mass Function
a	398,000	3,295,730
b	429,179	3,573,201
c	441,596	3,676,606
d	493,778	4,119,866
h	0.000018485	0.000002156

RCS and SI Accumulator Fixed Values

The RCS and SI accumulator volumes are significantly small than the RWST injection volume, and the range between minimum and maximum values is small. Therefore, fixed values were used as a best estimate volume for these water sources. The RCS was evaluated at the volume associated with hot-full power operation because the plant is in full power production mode for the majority of the year (the only exceptions are for refueling outages. The best-estimate value of RCS volume is documented as 14,044 ft^3. The best estimate RCS mass is 612,644 lbm. The best estimate of the volume in the SI accumulators was calculated using operating data over a nearly two year span. The average water level for each of the three accumulators was summed yielding a total injection volume of 3,711 ft^3. The mass of the accumulators was calculated with the average temperature and average absolute pressure to define the density of the water inventory. The best estimate mass was calculated as 231,334 lbm.

Total Mass in Containment Distribution

The total mass in containment probability distribution was formulated using the trapezoidal distribution for the RWST mass, and adding the best estimate mass values of the RCS and SI accumulators. This distribution may be converted to volume using the time dependent pool temperature profiles formulated using thermal-hydraulic modeling.

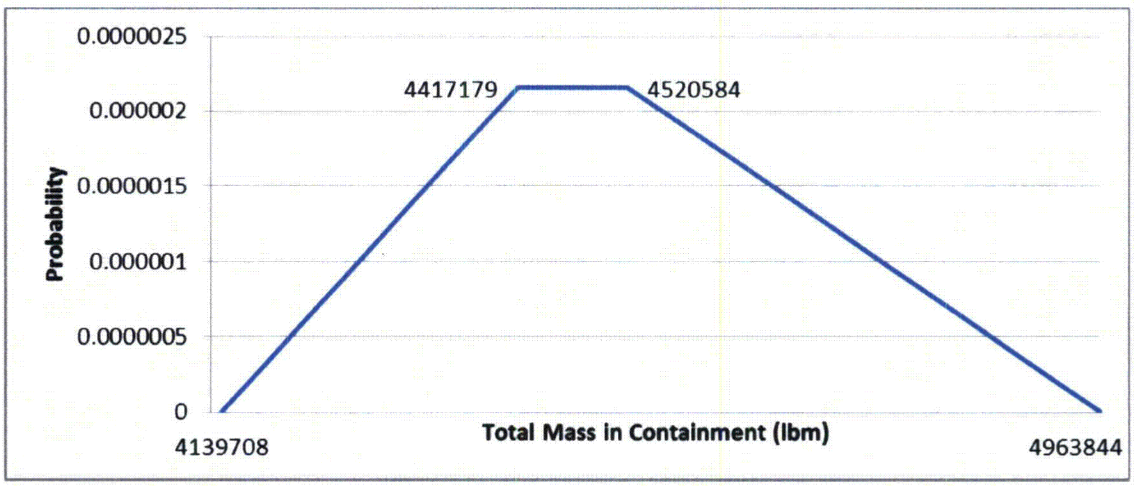

Figure 2.5.58 – Total Mass in Containment Probability Curve

The inputs for the total mass in containment probability curve are documented in the following table:

Table 2.5.68 – Total Mass in Containment Probability Function Inputs

Input	RWST Volume Function	Total Mass Function
a	398,000	4,139,708
b	429,179	4,417,179
c	441,596	4,520,584
d	493,778	4,963,844
h	0.000018485	0.000002156

Active Water in Containment Distribution

The active water in containment is defined as the total water in containment minus any inactive cavities. The inactive cavities would remove water from the recirculation inventory; the water in these cavities is effectively stagnant. Through engineering analysis of the containment building, it was determined that there are no inactive cavities for an MBLOCA and an LBLOCA. Therefore, the active water in containment would be the same as the total water in containment for these break conditions.

For an SBLOCA, the SI accumulators are an inactive cavity. During normal operating conditions, there are a series of check valves isolating the SI accumulators from the RCS. Depressurization of the RCS below the nitrogen pressure head of the accumulators causes injection into the core (105). For an MBLOCA and an LBLOCA, this depressurization of the RCS would occur. Therefore, there needs to be no adjustment to the active water in containment as all of the accumulators would inject their inventory to the reactor core for immediate cooling. An SBLOCA may not result in rapid full depressurization of the RCS below the nitrogen pressure head of the accumulators. In addition, before the long-term depressurization of the RCS, the SI accumulators may be isolated (107). Therefore, it is reasonable to assume that the accumulators would not inject to the reactor core for the SBLOCA condition. The total water in containment was reduced by the value of the SI accumulators to form the active water in containment for an SBLOCA.

The probability distribution of the active water in containment uses the trapezoidal distribution.

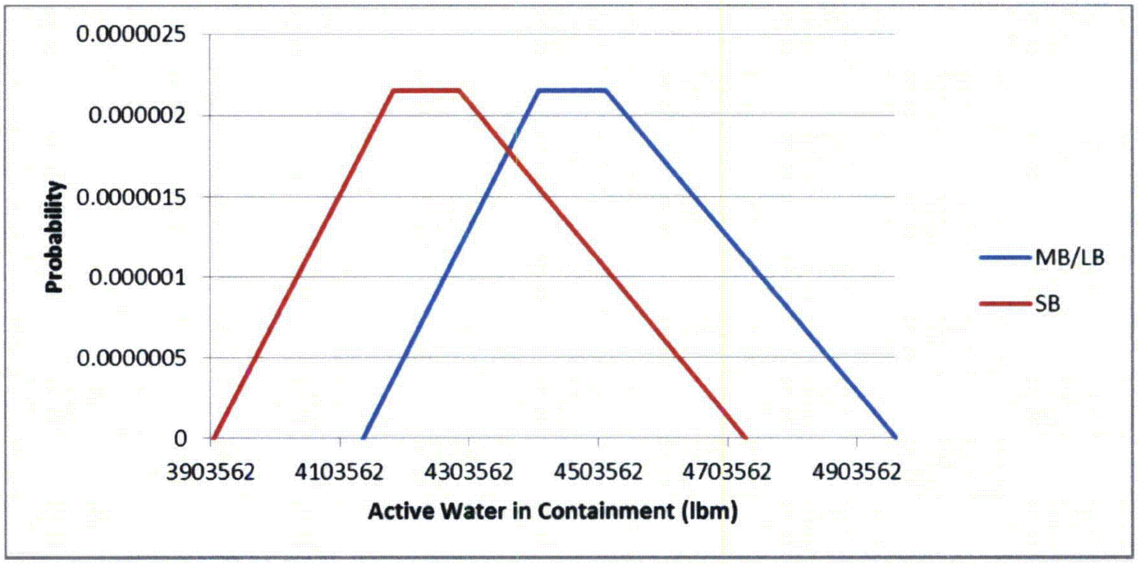

Figure 2.5.59 – Active Water in Containment Probability Curve

The inputs for the active water in containment probability curve are documented in the following table:

Table 2.5.69 – Active Water in Containment Probability Function Inputs

Input	RWST Volume Function	AWC Function-SBLOCA	AWC Function-MBLOCA	AWC Function-LBLOCA
a	398,000	3,908,374	4,139,708	4,139,708
b	429,179	4,185,845	4,417,179	4,417,179
c	441,596	4,289,250	4,520,584	4,520,584
d	493,778	4,732,510	4,963,844	4,963,844
h	0.000018485	0.000002156	0.000002156	0.000002156

The active water in containment is the basis for the base pool volume in containment. A value from this distribution is sampled as the base volume from which transitory hold-up volumes were subtracted. These transitory hold-up volumes include the inventory held up in the RCS, containment spray falling through containment, vapor in the atmosphere, etc. These values are a function of break size, flow rates, pool temperature, etc.

The minimum and maximum values were taken for bounding conditions for small, medium, and large breaks as shown in the following table (87).

Table 2.5.70 – Range of water volumes implemented in CASA Grande

Break Size	Minimum Volume (ft^3)	Maximum Volume (ft^3)
LBLOCA	45,201	69,263
MBLOCA	39,533	69,444
SBLOCA	43,464	61,993

Containment Spray Flow Rate

If containment sprays are initiated, the flow rate is not dependent on the size of the break. However, it would vary depending on the number of trains in operation. The maximum spray flow rate for a single train is 2,600 gpm. If all three trains are operating, the maximum flow rate is approximately 2,060 gpm per train (40). If two trains are operating, the maximum flow rate is approximately 2,350 gpm per train (41). The minimum probable CS flow rates are approximately 1,657 gpm per train for three train operation and 1,932 gpm per train for two train operation (41). The minimum spray flow rate for one train operation was not available in STP documentation, but was assumed to be 80% of the maximum flow rate consistent with the range of flow rates for two and three train operation. This is a reasonable assumption since the minimum spray flow rate for two train operation is 82% of the maximum spray flow rate for the two train operation, and the minimum spray flow rate for three train operation is 80% of the maximum spray flow rate for three train operation. This gives a minimum spray flow rate of 2,080 gpm for single train operation. Table 2.5.71 provides a summary of the range of containment spray flow rates.

Table 2.5.71 – Containment Spray Flow Rate Information

Number of Operating Spray Pumps	Minimum Spray Flow per Train (gpm)	Maximum Spray Flow per Train (gpm)
One Train	2,080	2,600
Two Trains	1,932	2,350
Three Trains	1,657	2,060

Blowdown Transport

See discussion for Item 5.a.2.

Washdown Transport

See discussion for Item 5.a.3.

Chemical Head Loss Bump-up

See Discussion for Item 5.a.11

Fiber Filtration Parameters

See Discussion for Item 5.a.16

Fiber Shedding Parameters

See Discussion for Item 5.a.16

3 REFERENCES

1. **NOC-AE-13002954.** *South Texas Project, Units 1 and 2, Docket Nos. STN 50-498 and STN 50-499, STP Pilot Submittal and Request for Exemption for a Risk-Informed Approach to Resolve Generic Safety Issue (GSI)-191.* : January 31, 2013.
2. **AE-NOC-13002417.** *South Texas Project, Units 1 and 2 – Supplemental Information Needed for Acceptance of Requested Licensing Action RE: Request for Exemption for a Risk-Informed Approach to Resolve Generic Safety Issue 191 (TAC NOs. MF0613 and MF0614).* : April 1, 2013.
3. **1011753.** *Design Basis Accident Testing of Pressurized Water Reactor Unqualified Original Equipment Manufacturer Coatings.* Final Report : September 2005.
4. **Carboline Testing Project #03471.** *General Electric-BWR Group LOCA Test Project.* Revision 0 : April 1998.
5. **ALION-REP-LAB-TXU-4464-02.** *TXU Paint Chip Characterization.* Revision 0 : October 2007.
6. **ALION-REP-LAB-2352-225.** *Test Report of Unqualified Alkyd Coatings Bench Top Testing.* Revision 0 : February 2008.
7. **ALION-CAL-STP-8511-06.** *STP Unqualified Coatings Debris Generation.* Revision 2 : November 26, 2012.
8. **Internal Letter from BWR Owners' Group Projects.** *BWR Owners' Group Containment Coatings Committee Meeting Report.* September 1998 : Revision 0.
9. **BWR Owners' Group.** *Utility Resolution Guide for ECCS Suction Strainer Blockage: Volume 4.* October 1998 : Revision 0.
10. **ALION-CAL-STP-8511-03.** *STP Qualified Coatings Debris Generation.* Revision 0 : August 10, 2012.
11. **South Texas Project Calculation 9AC5002#1.** *Quantification of Unqualified Coatings Inside Reactor Containment Building Unit 1.* s.l. : Revision 6.
12. **STP-RIGSI191-V03.** *South Texas Project Risk-Informed GSI-191 Evaluation, Volume 3, CASA Grande Analysis.* Revision 2E DRAFT : October 31, 2013.
13. **ALION-CAL-STP-8511-08.** *Risk-Informed GSI-191 Debris Transport Calculation.* Revision 2 : January 21, 2013.
14. **NUREG/CR-6369, Volume 2.** *Drywell Debris Transport Study: Experimental Work.* : September 1999.
15. **Letter from John Boska (NRC) to Entergy Nuclear Operations, Inc.** *Indian Point Nuclear Generating Unit Nos. 2 and 3 - Report on Results of Staff Audit of Corrective Actions to Address Generic Letter 2004-02 (TAC Nos. MC4689 and MC4690).* : July 29, 2008.
16. **NUREG/CR-6369, Volume 2.** *Drywell Debris Transport Study: Experimental Work.* September 1999.

17. **Letter from Thomas Hiltz (NRC) to Richard Rosenblum (Southern California Edison Company).** *San Onofre Nuclear Generating Station, Units 2 and 3 - Report on Results of Staff Audit of Corrective Actions to Address Generic Letter 2004-02 (TAC Nos. MC4714 and MC4715).* : May 16, 2007.

18. **ALION-REP-ALION-I006-04.** *Erosion Testing of Small Pieces of Low Density Fiberglass Debris - Test Report.* Revision 1 : November 7, 2011.

19. **Adrien, Nicolas G.** *Computational Hydraulics and Hydrolody, an Illustrated Dictionary.* CRC Press : p. 134, 2004.

20. **NUREG/CR-6772.** *GSI-191: Separate Effects Characterization of Debris Transport in Water.* 2002.

21. **NEI PWR Sump Performance Task Force Report NEI 04-07.** *Pressurized Water Reactor Sump Performance Evaluation Methodology.* Revision 0 : December 2004.

22. **Schlumberger.** *Log Interpretation Principle/Applications.* Schlumberger Educational Services : s.n., 1987.

23. **Baumeister, Theodore.** *Mark's Mechanical Engineers' Handbook.* McGraw-Hill Book Company Inc. : 1958, Sixth Edition.

24. **Foote, G.B., and DuToit, P.S.** *Terminal Velocity of Raindrops Aloft.* J. Appl. Meteor, 8 : pp. 249-253, 1969.

25. **CHLE-016.** *Calculated Material Release.* Revision 1 : January 10, 2013.

26. **WCAP-16530-NP.** *Evaluation of Post-Accident Chemical Effects in Containment Sump Fluids to Support GSI-191.* Revision 0 : February 2006.

27. **Office of Nuclear Reactor Regulation.** *Final Safety Evaluation by the Office of Nuclear Reactor Regulation Topical Report WCAP-16530-NP "Evaluation of Post-Accident Chemical Effects in Containment Sump Fluids to Support GSI-191" Pressurized Water Reactor Owners Group Project No. 694.* : December 21, 2007.

28. **Lane, A.E., et al.** *Evaluation of Post-Accident Chemical Effects in Containment Sump Fluids to Support GSI-191.* Pittsburge, PA : Westinghouse Electric Company, 2006.

29. **Gustafsson, J.P.** *Visual MINTEQ. www.lwr.kth.se/English/OurSoftware/vminteq/index.html.* 2010 : s.n.

30. **UNM.** *CHLE-016 T2 LBLOCA Test Report.* 2013 : s.n.

31. **CHLE-012.** *T1 MBLOCA Test Report.* Revision 3 : January 9, 2013.

32. **Texas A&M University Department of Nuclear Engineering.** *Sump Temperature Sensitivity Analysis.* Revision 2.0 : January 2013.

33. **CHLE-014.** *T2 LBLOCA Test Report.* Revision 1 : January 12, 2013.

34. **CHLE-006.** *STP Materials Calculation.* Revision 1 : August 15, 2012.

35. **NUREG/CR-6914, Volume 1.** *Integrated Chemical Effects Test Project: Consolidated Data Report.* : December 2006.

36. **ALION-CAL-STPEGS-2916-002.** *GSI 191 Containment Recirculation Sump Evaluation: Debris Generation.* Revision 3 : October 20, 2008.

37. **OG-07-129.** *Pressurized Water Reactor Owners Group Responses to the NRC Second Set of Requests for Additional Information (RAI's) on WCAP-16530, "Evaluation of Chemical Effects in Containment Sump Fluids to Support GSI-191".* s.l. : April 3, 2007.

38. **OG-07-408.** *Responses to NRC Requests for Clarification Regarding WCAP-16530, "Evaluation of Chemical Effects in Containment Sump Fluids to Support GSI-191" (PA-SEE-0275).* : September 12, 2007.

39. **Office of Nuclear Reactor Regulation.** *Evaluation of Chemical Effects Phenomena Identification and Ranking Table Results.* : March 2011.

40. **CHLE-005.** *Determination of the Initial Pool Chemistry for the CHLE Test.* Revision 1 : August 13, 2012.

41. **CHLE-018.** *Bench-Scale Test Results of Effect of pH and Temperature on Aluminum Corrosion and Silicon Dissolution.* Revision 0 : DRAFT.

42. **CHLE-011.** *Test 2: Medium Break LOCA Tank Test Parameter Summary.* Revision 1 : October 30, 2012.

43. **CHLE-013.** *T2: Large Break LOCA Tank Test Parameter Summary.* Revision 2 : January 23, 2013.

44. **ML120440060.** *STP Post-Meeting Notes for January 26-27, 2012 Public Meeting.* : February 6, 2012.

45. **ALION-CAL-STP-8511-07.** *STP Crud Debris Generation.* Revision 0 : November 12, 2012.

46. **0PRP07-ZR-0004.** *Shielding.* Revision 19 : March 8, 2012.

47. **ALION-SUM-WEST-2916-01.** *CAD Model Summary: South Texas Reactor Building CAD Model for Use in GSI-191 Analyses.* Revision 3 : November 27, 2012.

48. **NUREG/CR-6914, Volume 3.** *Integrated Chemical Effects Test Project: Test #2 Data Report.* : December 2006.

49. **Letter from Balwant Singal (NRC) to STP Nuclear Operating Company.** *Summary of September 6, 2012, Pre-Licensing Public Meeting with STP Nuclear Operating Company Held via Conference Call to Discuss the Proposed Risk-Informed Approach to the Resolution of GSI-191, "Assessment of Debris Accumulation on PWR Sump Performance".* : October 4, 2012.

50. **CR 03-9542.** : June 30, 2003.

51. **CR 08-5448.** : April 4, 2008.

52. **0415-0100086WN (CN-SEE-1-08-66).** *South Texas Project LOCADM.* Revision A : December 9, 2008.

53. **ALION-CAL-STP-008511-02.** *STP Cold Volume Analysis.* Revision 0 : May 17, 2012.

54. **NUREG/CR-6224.** *Parametric Study of the Potential for BWR ECCS Strainer Blockage Due to LOCA Generated Debris.* : October 1995.

55. **ALION-REP-STP-8511-02.** *South Texas Vertical Loop Head Loss Testing Report.* Revision 1 : January 24, 2013.

56. **NEI 04-07 Volume 2.** *Safety Evaluation by the Office of Nuclear Reactor Regulation Related to NRC Generic Letter 2004-02, Nuclear Energy Institute Guidance Report "Pressurized Water Reactor Sump Performance Evaluation Methodology".* Revision 0 : December 2004.

57. **ALION-REP-STP-8511-02.** *South Texas Vertical Loop Head Loss Testing Report.* Revision 1 : January 24, 2013.

58. **66-9088089-000.** *South Texas Project Test Report for ECCS Strainer Testing.* Revision 0 : August 29, 2008.

59. **CHLE-010.** *CHLE Tank Test Results for Blended and NEI Fiber Beds with Aluminum Addition.* Revision 2 : August 19, 2012.

60. **University of Texas at Austin.** *Filtration as a Function of Debris Mass on the Strainer: Fitting a Parametric Physics-Based Model.* s.l. : June 5, 2013.

61. **ALION-REP-STP-8511-03.** *South Texas Penetration Test Report.* Revision 1 : January 24, 2013.

62. **Texas A&M University, Department of Nuclear Engineering.** *Core Blockage Thermal-Hydraulic Analysis.* Revision 2.1 : January 2013.

63. **WCAP-16793-NP.** *Evaluation of Long-Term Cooling Considering Particulate, Fibrous and Chemical Debris in the Recirculating Fluid".* Revision 2 : October 2011.

64. **Letter from Sheldon Stuchell (NRR) to Anthony Nowinowski (PWROG).** *Draft Safety Evaluation for Pressurized Water Reactor Owners Group Topical Report WCAP-16793-NP, Revision 2, "Evaluation of Long-Term Core Cooling Considering Particulate Fibrous and Chemical Debris in the Recirculating Fluid" (TAC No. ME1234).* : January 29, 2013.

65. **Texas A&M University, Department of Nuclear Engineering.** *RELAP5 Model Input Deck Certification.* Revision 3.0 : August 1, 2011.

66. **Texas A&M Department of Nuclear Engineering.** *MELCOR Input Deck Certification: South Texas.*

67. **Texas A&M, Department of Nuclear Engineering.** *6 Inch Cold Leg Break Scenario 30-Day Containment Response.*

68. —. *15 Inch Cold Leg Break Scenario 30-Day Containment Response .*

69. **WCAP-17047-NP.** *Phenomena Identification and Ranking Tables (PIRT) for Un-Buffered/Buffered Boric Acid Mixing/Transport and Precipitation Modes in a Reactor Vessel During Post-LOCA Conditions.* Revision 0 : May 2009.

70. **SEC-LIS-3908-C4.** *Hot Leg Switchover Analysis to Support RSG Program.* Revision 0 : July 16, 1997.

71. **Letter from Sher Bahadur (NRC) to Anthony Nowinowski (PWROG).** *Final Safety Evaluation for Pressurized Water Reactor Owners Group Topical Report WCAP-16793-NP, Revision 2, "Evaluation of Long-Term Cooling Considering Particulate Fibrous and Chemical Debris in the Recirculating Fluid" (TAC No. ME1234).* : April 8, 2013.

72. **STPEGS UFSAR.** *Chapter 6.3: Emergency Core Cooling System.* Revision 15.

73. **NUREG-1829.** *Estimating Loss-of-Coolant Accident (LOCA) Frequencies Through the Elicitation Process.* : April 2008.

74. **University of Texas at Austin.** *Means of Aggregation and NUREG-1829: Geometric and Arithmetic Means.* : June 13, 2013.

75. **ALION-SUM-WEST-2916-01.** *CAD Model Summary: South Texas Reactor Building CAD Model for Use in GSI-191 Analyses.* Revision 3 : November 27, 2012.

76. **KNF Consulting Services LLC, and Scandpower Risk Management Inc.** *Development of LOCA Initiating Event Frequencies for South Texas Project GSI-191 Final Report for 2011 Work Scope.* : September 2011.

77. **Scandpower.** *Risk Informed GSI-191 Resolution LOCA Frequency Component Database.* Revision 2 : October 21, 2011.

78. **NUREG-1829.** *Estimating Loss-of-Coolant Accident (LOCA) Frequencies through the Elicitation Process.* : April 2008.

79. **KNF Consulting Services LLC, and Scandpower Risk Management Inc.** *Development of LOCA Initiating Event Frequencies for South Texas Project GSI-191 Final Report for 2011 Work Scope.* : September 2011.

80. **University of Texas at Austin.** *A Framework for Uncertainty Quantification: Methods, Strategies, and an Illustrative Example.* : January 21, 2013.

81. **LA-UR-13-20079.** *Parametric Model of Debris Penetration Through Sump Strainers with Concurrent Filtration and Shedding.* : January 2013.

82. **University of Texas at Austin.** *Modeling and Sampling LOCA Frequency and Break Size for STP GSI-191 Resolution.* : January 23, 2013.

83. **0POP05-EO-ES11.** *SI Termination.* Revision 14 : May 13, 2010.

84. **Email from Tim Sande (Alion) to Kerry Howe (UNM) and Ernie Kee (STP).** *Best-Estimate Time for Spray Operation.* : February 23, 2012.

85. **0POP05-EO-EO10.** *Loss of Reactor or Secondary Coolant.* Revision 20 : April 28, 2011.

86. **0POP05-EO-ES14.** *Transfer to Hot Leg Recirculation.* Revision 7 : July 1, 2008.

87. **ALION-CAL-STP-8511-01.** *STP Post LOCA Water Volume Analysis.* Revision 1 : September 20, 2012.

88. **STP-2699325-O-03.** *Subject: On the Frequency of Success States Involving Different Numbers of Pumps Operating.* : December 18, 2012.

89. **MC-6220.** *SI & CS Pump NPSH.* Revision 4 : February 5, 2002.

90. **5N109MB01024.** *Design Basis Document Containment Spray.* Revision 3 : November 17, 2004.

91. **NEI 04-07 Volume 1.** *Pressurized Water Reactor Sump Performance Evaluation Methodology.* Revision 0 : December 2004.

92. **ALION-REP-ALION-2806-01.** *Insulation Debris Size Distribution for Use in GSI-191 Resolution.* Revision 4 : May 20, 2009.

93. **SFS-STP-PA-7101.** *South Texas Project Units 1 & 2 Sure-Flow Strainer Module Details.* Revision 5 : September 5, 2006.

94. **TDI-6005-01.** *SFS Surface Area, Flow and Volume Calculations.* Revision 1 : August 31, 2006.

95. **SFS-STP-GA-00.** *South Texas Project Units 1 & 2 Sure-Flow Strainer General Arrangement.* Revision 4 : August 25, 2006.

96. **SFS-STP-PA-7103.** *South Texas Project Units 1 & 2 Sure-Flow Strainer Sections and Details.* Revision 2 : August 4, 2006.

97. **2F369PSI0572 Sheets 3, 4 & 6.** *Safety Injection 'SI'.*

98. **5L019PS0004.** *Specification for Criteria for Piping Design and Installation.* Revision 23 : s.n.

99. **ALION-CAL-STP-8511-05.** *STP Net Positive Suction Head Margin.* Revision 0 : November 19, 2012.

100. **EC-PCI-STP-6005-1001.** *AES Document No. PCI-5473-S01 Rev 2 "Structural Evaluation of Strainers for Containment Emergency Sumps".* Revision 2 : January 7, 2010.

101. **EC-PCI-STP-6005-1004.** *AES Document No. PCI-5473-S03 Rev 0 "Structural Evaluation of Strainers for Containment Emergency Sumps for Long Term Post LOCA Case".* Revision 0 : January 7, 2010.

102. **Regulatory Guide 1.82.** *Water Sources for Long-Term Recirculation Cooling Following a Loss-of-Coolant Accident.* Revision 4 : March 2012.

103. **5N079NB01000 (WCAP-12381).** *STPNOC Design Basis Document Accident Analysis.* Revision 15 : July 29, 2009.

104. **Technical Specifications Section 1.27.** *Rated Thermal Power.* Unit 1 Amendment No. 154; Unit 2 Amendment No. 142 : s.n.

105. **South Texas Project Electric Generating Station.** *STPEGS UFSAR-6.3-ECCS.* s.l. : Revision 15.

106. —. *0POP05-EO-ES13 Transfer to Cold Leg Recirculation.* July 2008 : Revision 10.

107. **WES010-Calc-001.** *South Texas Project Pos-LOCA containment Water Level Calculation.* Revision 0 : November 2008.

108. **CHLE-012.** *T1 MBLOCA Test Report.* Revision 2 : December 19, 2012.

ENCLOSURE 6

Changes to

June 19, 2013 Submittal

Enclosure 6

Changes to June 19, 2013 Submittal

In STPNOC's October 3, 2013 letter to the NRC (ML 13295A222) identifying errors in the STPNOC June 19, 2013 licensing submittal (ML131750250), STPNOC stated that the supplement would include a description of the changes required to resolve the differences that were identified between the CASA Grande analysis and the description in Enclosure 4-3 of the June 19th application. This enclosure provides that information.

Identified Discrepancies in Documentation of STP Risk-Informed Resolution Submittal (Reference 3 in the cover letter)

STP elected to systematically identify and disposition all discrepancies that are found through the following two-step process: (1) line-by-line comparison of all numeric input in the CASA Grande input files to the tabular information provided in Enclosure 4-3 (also referred to as Volume 3), and (2) subject-matter-expert review of the Volume 3 modeling assumptions with CASA Grande implementation. This quality assurance review may reveal the following generic types of discrepancies:

a) Intentional CASA Grande input that conservatively increased the reported quantitative risk relative to Volume 3 descriptions,
b) Modeling approaches in Volume 3 that are not fully implemented in CASA Grande,
c) Modeling approaches in CASA Grande that are not precisely described in Volume 3,
d) Errors in CASA Grande input caused by misinterpretation of information or mistaken transcription,
e) Errors in Volume 3 tabular data caused by misinterpretation of information or mistaken transcription,
f) Errors in CASA Grande model implementation,
g) Errors in Volume 3 model description,

All identified discrepancies were logged and dispositioned prior to risk requantification using a staged evaluation process.

Description of Review Process

Comparison of Volume 3 documentation to the CASA Grande input was conducted in two phases:

1) <u>Initial screening</u> by two staff engineers to note any observations of perceived inconsistencies. This review was conducted over the entire input section of Volume 3 (Section 2.2); some observations were duplicated for completeness; some observations were resolved by information found later in the document; however, a master list of

observations was compiled without deleting any items for confirmation and resolution in Phase II.

2) Committee review of all initial observations and the entirety of Volume 3 to confirm actual findings and add new findings. This review was conducted over a 5-day period over which all review actions were recorded and tracked for the purpose of final disposition. Technical discussions of each initial observation revealed additional action items that were recorded, and assessed for disposition. Every item was recorded and will be tracked to final resolution. The systematic review was conducted from two perspectives:

    a. Sequentially walking through Volume 3 and verifying input values and implementation in CASA Grande
    b. Sequentially walking through CASA Grande and verifying model descriptions and implementation in Volume 3.

    Limited confirmation of numeric values between Volume 3 and source references (engineering calculations and precursor analysis reports) revealed one transcription error. Because of this finding, all numeric input adopted in Volume 3 were reviewed with source references. Deeper levels of confirmation will not be pursued unless specific items are identified.

Objectives of the review included:

1) Identifying all actual inconsistencies between Volume 3 documentation and CASA Grande input files
2) Confirming the validity of actual conflicts
3) Assessing the options for changing either Volume 3 documentation or CASA Grande input to achieve agreement between documentation and model. The following logic was applied:
    a. Correcting any confirmed errors
    b. Addressing any identified non-conservative approaches
    c. Minimizing changes to CASA Grande input with a preference toward correcting Volume 3 for accuracy and preserving existing conservatism in quantitative input.

Discrepancy Matrix

Table 1 below documents *all* observations that were recorded during the QA comparison. Of particular interest are the last two columns on the right – "Final Disposition" and "Rank". "Final Disposition" provides a description of changes that were made and "Rank" explains whether (1) a change was recommended for CASA Grande input, (2) a change was recommended for documentation in Volume 3, or (3) no change was recommended for either Volume 3 and CASA Grande input. All potential impacts from Rank Level 1 are expected to be small, but do require modification of CASA Grande input with subsequent re-quantification. Note that all reference locations in the following table are for the June 19, 2013 submittal since that is document that was reviewed.

Table 1: Disposition matrix documenting all observed issues, discrepancies and questions noted during the QA review.

<table>
<tr><th>Item</th><th>Section and Page Number</th><th>Volume 3 Values</th><th>CASA GRANDE Values</th><th>Final Disposition</th><th>Rank</th></tr>
<tr><td>1</td><td>Section 5.1
Pg. 107
Table 5.1.1</td><td>Plant Failure States Quantified<table><tr><td>3</td><td>HHSI</td></tr><tr><td>1</td><td>LHSI</td></tr><tr><td>3</td><td>CS</td></tr></table>Working Pumps
(2 LHSI failed)</td><td>Plant Failure States Quantified<table><tr><td>1</td><td>HHSI</td></tr><tr><td>3</td><td>LHSI</td></tr><tr><td>3</td><td>CS</td></tr></table>Working Pumps
(2 HHSI failed)</td><td>Change CASA Grande input. No change to Volume 3.</td><td>1</td></tr>
<tr><td>2</td><td>Section 2.2.9
Pg. 54 - 57</td><td>Break-size dependent SI pump flows.</td><td>Run out pump flows used for SI pumps, all breaks, all Cases.</td><td>Assign appropriate flow ranges in CASA input by S,M,L for each failure case

Preserve correlation between LHSI and HHSI flow.

Editorial changes to Volume 3</td><td>1</td></tr>
<tr><td>3</td><td>Section 2.2.9
Pg. 57
Table 2.2.13</td><td>Train-dependent CS pump flows.</td><td>Range used for CS pumps, all breaks, all Cases.</td><td>Assign appropriate flow ranges in CASA Grande input by failure Case.

No change to Volume 3</td><td>1</td></tr>
</table>

Item	Section and Page Number	Volume 3 Values	CASA GRANDE Values	Final Disposition	Rank
4	Section 2.2.11 Pgs. 59-61	Distributions defined for unqualified coatings failure fractions.	Approximate mean values used	Editorial Change to Volume 3 to note use of 100% failure fractions. Implemented 100% failure fractions in CASA Grande	1
5	Section 3 Pg. 85 Assumption 7.b	Treated small pieces of Low Density Fiber Glass (LDFG) as 0.5-inch cubes and large pieces as 1 inch cubes for the purpose of head loss calculations. This is non-conservative since it neglects flow through the pieces (Item 6).	CASA Grande input was consistent with the Volume 3 description.	Revise Volume 3 to treat fiber pieces as individual fibers. Rerun CASA Grande	1
6	Section 5.7.2 Pg. 195 Table 5.7.2 Table 5.7.3	Surface area-to-volume ratio for small and large LDFG was based off the 0.5 inch and 1 inch cubes for small and large LDFG respectively (Item5).	CASA Grande input was consistent with the Volume 3 description	Revise Volume 3 to treat fiber pieces as individual fibers. Rerun CASA Grande	1
7	Section 3 Pg. 85 Assumption 6.f	Unqualified coatings in upper containment are assumed to be washed to the pool immediately after failure if sprays are on.	Total fraction of coatings that transport are assumed to reach the pool at a constant rate.	Editorial change to Volume 3.	2

Item	Section and Page Number	Volume 3 Values	CASA GRANDE Values	Final Disposition	Rank
8	Section 2.2.1 Pg. 37	Point value was described in Volume 3 for time to turn off spray pumps	Break-size dependent distribution with same mean was used in CASA Grande.	Editorial Change to Volume 3.	2
9	Section 5.3 Pgs. 130-165	Volume 3 describes weld break frequency methodology.	CASA Grande implemented a slightly different methodology in the interpolation scheme from what was described.	Editorial changes to Volume 3.	2
10	Section 2.2.7 Pg. 54 Figure 2.2.3	Volume 3 plot of temperature transient did not show temperature values prior to start of recirculation.	Linear temperature profile was implemented for initial transient.	Editorial changes to Volume 3.	2
11	Section 2.2.10 Pg. 58 Table 2.2.14 Section 5.4.4	Volume 3 provides break size-dependent qualified coatings debris quantities.	CASA Grande used the maximum qualified coatings quantities.	Editorial change to Volume 3.	2
12	Section 2.2.11 Pg. 62 Table 2.2.19	Table in Volume 3 specifies time-dependent unqualified coatings failure fractions over 30 days.	CASA Grande incorporated a constant failure rate for unqualified coatings (equal to the average failure rate in the first 48 hours from Volume 3).	Editorial change to Volume 3.	2
13	Section 2.2.17 Pg. 65 Table 2.2.23	Range given for microscopic density of crud.	Conservative low value of microscopic density was used in CASA Grande.	Editorial change to Volume 3.	2

Item	Section and Page Number	Volume 3 Values	CASA GRANDE Values	Final Disposition	Rank
14	Section 2.2.17 Pg. 65 Table 2.2.23	Range given for unqualified coatings particulate size in Volume 3.	NEI 04-07 values were adopted in CASA Grande (10 μm).	Editorial change to Volume 3.	2
15	Sections 2.2.21-2.2.25 Pgs. 66-71	Volume 3 provides debris-dependent and break-dependent transport fractions including ranges for several transport parameters.	Fixed debris-dependent transport fractions were used for all breaks in CASA Grande.	Editorial change to Volume 3.	2
16	Section 2.2.21 Pg. 67 Table 2.2.24	Volume 3 describes blowdown transport fractions for every compartment.	The blowdown transport fractions of the steam generator compartment were used.	Editorial change to Volume 3.	2
17	Section 2.2.22 Pg. 68 Table 2.2.25	Range was supplied for small Low Density Fiber Glass washdown in Volume 3.	Conservative value from was used.	Editorial change to Volume 3.	2
18	Section 2.2.22 Pg. 68 Table 2.2.26	Pool fill fractions were provided for breaks inside and outside of the secondary shield wall.	Only pool transport fractions inside of the secondary shield wall were used.	Editorial change to Volume 3.	2
19	Section 2.2.24 Pg. 69 Table 2.2.27	Volume 3 describes recirculation transport fractions for every compartment.	The recirculation transport fractions of the steam generator compartment were used.	Editorial change to Volume 3.	2
20	Section 2.2.26 Pg. 71	Strainer height value was taken from plant drawings.	Conservative larger value was used.	Editorial change to Volume 3 to note unintended conservatism in CASA Grande.	2

Item	Section and Page Number	Volume 3 Values	CASA GRANDE Values	Final Disposition	Rank
21	Section 5.7.1 Pg. 191	Velocity dependent clean strainer head loss.	Maximum clean strainer head loss was used.	Editorial change to Volume 3.	2
22	Section 2.2.28 Pg. 74	Most conservative pump elevation shown.	Actual elevations for all three pumps used.	Editorial change to Volume 3.	2
23	Section 2.2.33 Pg. 76 Table 2.2.32	Shedding parameters are specified with a scaling factor.	Same values used in CASA Grande without scaling factor.	Editorial change to Volume 3.	2
24	Section 3 Pg. 79	Hot-leg injection switchover time specified as point value.	CASA Grande used range for hot-leg switchover with same mean.	Editorial change to Volume 3.	2
25	Missing From Section 2.2	Description of computational time step not described in Volume 3.	User specified time step sets scenario resolution.	Editorial change to Volume 3.	2
26	Missing From Section 2.2	Description of strainer debris-loading table not described in Volume 3.	Strainer loading table implemented for time-dependent accumulation.	Editorial change to Volume 3.	2
27	Section 3 Pg. 87 Assumption 8.i	Gas void fraction was incorrectly described as being split between pumps.	Gas void fraction at the strainer was applied to all pumps.	Editorial change to Volume 3.	2
28	Section 5.7.3 Pg. 200	Volume 3 states that the end points of the chemical bump-up distribution are always included in the sample design.	Tail end point not captured in every sample set.	Editorial change to Volume 3.	2
29	Section 3 Assumption 11.c	Boron precipitation was assumed not to occur for small breaks.	Boron precipitation was not precluded for small breaks (although it was not observed).	Editorial change to Volume 3.	2

Item	Section and Page Number	Volume 3 Values	CASA GRANDE Values	Final Disposition	Rank
30	Section 5.6.6 Pg. 176	Reference to erosion timing.	Erosion treated as occurring prior to recirculation.	Editorial change to Volume 3.	2
31	Section 4.2 Pg.102 Figure 4.2.4	NPSH available equation in Figure 4.2.4 incorrectly excluded containment pressure.	Containment pressure was correctly included in NPSH available model.	Editorial change to Volume 3.	2
32	Section 5.3.4 Pg. 164	Equation 34 describing number of medium breaks sampled incorrectly used a range of 6 to 4 inches.	CASA Grande correctly used a range of 6 to 2 inches in this equation.	Editorial change to Volume 3.	2
33	Section 5.6.7 Pg. 179-180 Figures 5.6.3 and 5.6.4	Example transport logic tree fractions did not match actual transport fractions in CASA Grande	Bounding transport fractions associated with a steam generator compartment break were used in CASA Grande	Editorial change to Volume 3.	2
34	Section 5.7 Pg. 189	Velocity dependent clean strainer head loss	Maximum clean strainer head loss was used.	Editorial change to Volume 3 (same as Item 21).	2
35	Appendix 1	Input file only provided for one CASA Grande case.	A total of 10 cases were run.	Editorial change to Volume 3	2
36	Section 5.7.2 Pg. 195	A value of 6 μm was listed as the epoxy fines diameter, which is inconsistent with the input value of 6 mil (see Table 2.2.23).	CASA Grande used 6 μm in all cases.	Editorial change to Volume 3 to describe conservatism.	2

Item	Section and Page Number	Volume 3 Values	CASA GRANDE Values	Final Disposition	Rank
37	Global	A minor error was discovered in the DEGB total SI flow rate in Table 2.2.12 (last entry) Due to this error, all Volume 3 input values were re-reviewed for accuracy.	Changed entry to correct value	Editorial change to Volume 3 to correct error in Table 2.2.12. Review identified no additional errors.	2
38	Section 5.7.5 Pgs. 208-209 Equations 59-64	Implicit formulas presented for NPSH friction factor calculations.	An explicit form of the friction factor equation was used.	Editorial change to Volume 3.	2
39	Section 5.8.1 Pg. 210	Volume 3 describes Froude number equation for vortex formation.	CASA Grande did not explicitly evaluate vortex formation.	Editorial change to Volume 3.	2
40	Section 5.8.2 Pg. 211	Method for determining saturation pressure is not described.	Two different functions are available in CASA Grande to determine saturation pressure: Steam tables and an equation that fits the steam tables.	Editorial change to Volume 3 to describe source reference for steam properties. Adopt NIST tables for all evaluations	2
41	Section 5.7.2 Pg. 194 Equation 50	Equation 50 as written in Revision 1 describes the conventional formula for calculating composite specific surface area.	Linear mass weighting was used in CASA Grande. Adequate margin is provided by the addition of 5 times added head loss	Editorial change to Volume 3 for consistency.	2

Item	Section and Page Number	Volume 3 Values	CASA GRANDE Values	Final Disposition	Rank
42	Section 2.2.1 Pg. 37	Volume 3 does not explicitly state a time that sprays are secured for an SBLOCA since the sprays are assumed never to initiate.	CASA Grande implemented time range for securing containment sprays for an SBLOCA, but sprays were never initiated.	No action required.	3
43	Section 5.7.2 Pg. 192 Equation 44	Volume 3 (Rev 1) Eq. 44 for primary head loss correlation contains a typo. Leading coefficient of second term should be 0.66 rather than 0.65	CASA Grande used proper formulas.	Editorial change to Volume 3.	2
44	Section 5.7.2 Pg. 193 Equation 46	Volume 3 (Rev 1) Eq. 46 for mixture solidity contains a typo. Last factor should be c/c_0 rather than c alone	CASA Grande used proper formulas.	Editorial change to Volume 3.	2
45	Section 5.7.2 Pg. 193 Equation 48	Volume 3 (Rev 1) Eq. 48 for compression contains a inconsistent explanation. The constant K should equal 2.4 lbm/ft3 for fiberglass rather than being defined as 1.0 with no units	CASA Grande used proper formulas.	Editorial change to Volume 3.	2
46	Section 2.2.3 Pg. 39 Table 2.2.2	Lamda value was rounded to four significant figures.	Lambda value included 7 significant figures.	No action required.	3

Item	Section and Page Number	Volume 3 Values	CASA GRANDE Values	Final Disposition	Rank
47	Section 2.2.15 Pg. 58 Table 2.2.15	Volume 3 itemizes upper, lower and reactor cavity failed coatings distributions	CASA Grande accounts for spatial location of unqualified coatings via transport equations.	No action required.	3
48	Section 2.2.13 Pg. 63 Table 2.2.21	Latent fiber given as a mass.	Mass was correctly converted to volume.	No action required.	3
49	Section 2.2.14 Pg. 63	Surface area of miscellaneous debris is 100 ft^2.	Verified surface area of miscellaneous debris is 100 ft^2.	No action required.	3
50	Section 2.2.15 Pg. 64	ZOI of 2D for Transco RMI. RMI assumed to be negligible.	ZOI of 1D for Transco RMI. RMI not explicitly evaluated.	No action required.	3
51	Section 2.2.25 Pg. 71	Erosion fraction for fiberglass was listed as "below 10%" because source report is proprietary.	Value below 10% was used in CASA Grande.	No action required.	3
52	Section 2.2.28 Pg. 74	NPSH required is 12 ft.	NPSH required is 12 ft.	No action required.	3
53	Section 2.2.31 Pg. 74	Froude numbers for bubble transport are provided to support analysis in Section 5.8.3.	CASA Grande did not explicitly evaluate bubble transport.	No action required.	3
54	Section 2.2.34 Pg. 76	Decay heat generation rate is provided as an input for calculating boil off rates in Section 5.11.3.	Boil off rates matching the values in Section 5.11.3 were used.	No action required.	3

Item	Section and Page Number	Volume 3 Values	CASA GRANDE Values	Final Disposition	Rank
55	Section 2.2.35 Pg. 77	A core blockage acceptance criterion of 15 g/FA is provided. Additional acceptance criteria are provided in Section 5.11.5 and 5.12.2.	Appropriate acceptance criteria are used in CASA Grande.	No action required.	3
56	Missing From Section 2.2	Earliest time for chemical product formation is not specifically described, but is dependent on temperature.	Time for chemical product formation is bounded by temperature dependence.	No action required.	3
57	Missing From Section 2.2	Temperature dependence of chemical product formation is described in Section 5.7.3.	Temperature dependence is consistent with Volume 3.	No action required.	3
58	Repeat of previous issue regarding debris transport fractions	N/A	N/A	No action required.	3
59	Section 5.4.1 Pg. 166	Hemispherical ZOI is constrained along axis of pipe.	Hemispherical ZOI is constrained along axis of pipe.	No action required.	3
60	Section 5.4.5 Pg. 171	Equations describing unqualified coatings failure are consistent	Equations describing unqualified coatings failure are consistent	No action required.	3
61	Missing From Section 2.2	Chemical bump-up factor described in Section 5.7.3.	Chemical bump-up factor that was implemented is consistent with Volume 3.	No action required.	3

Item	Section and Page Number	Volume 3 Values	CASA GRANDE Values	Final Disposition	Rank
62	Section 2.2.3 Pg. 40 Table 2.2.3	Subcontractor KNF reported potential over conservatism in “bottom up” assignment of weld count.	Over conservatism was used in CASA Grande input.	No action required.	3

Additional Changes in this submittal (i.e., Supplement 1 to the June 19, 2013 application):

Supplement 1 includes changes to each of the enclosures with the exception of Enclosure 1. Each enclosure lists the changes at the front of the enclosure. The types of changes are described below.

1. Where Enclosure 4-3 corrections affected other enclosures in the license application
    a. Revised input to the PRA quantification (i.e., Enclosure 4-2)
    b. The changes to Enclosure 4-3 involved renumbering several of the sections and there were specific references to the revised sections elsewhere in the licensing submittal. Those complementary changes have been incorporated.
2. The revised changes in CDF and LERF that resulted from the PRA requantification associated with correcting CASA Grande are presented in Enclosure 4-2, and those values were revised where they appear in the cover letter and other enclosures.
3. Information that was primarily presented in a particular enclosure was in a number of cases repeated in another enclosure. To minimize the chance of having conflicting information, repeated information was deleted from several locations and the primary presentation referenced instead (e.g., the detailed description of the PRA was removed from the Enclosure 3 License Amendment Request because it is primarily presented in Enclosure 4-1).
4. The UFSAR changes that implement the proposed license amendment are included in Enclosure 3 for NRC approval. A clarification is added that 10CFR50.59 will be the change control process for those UFSAR sections. The table in proposed UFSAR Appendix 6A was revised to delete Aluminum as a parameter based on the revision to Enclosure 4-3 and the associated Appendix 6A references were updated.
5. The proposed approval date for this licensing submittal was changed from December 2014 to June 2015 in the cover letter and where it appears in the licensing enclosures. The time for review and approval is requested in recognition this is a pilot project application.